Recognition of Butyrophilin-family Members by gamma-delta T Cells

Marc Rigau Cortal

ORCID ID:

0000-0001-5978-1073

from Navata, Catalonia, Spain

Submitted in total fulfilment of the requirements of the joint degree of
Doctor of Philosophy (PhD)
of the Medical Faculty
The Rheinische Friedrich-Wilhelms-Universität Bonn
and
The Department of Microbiology and Immunology
The University of Melbourne

Bonn/Melbourne, 2021

Performed and approved by the Medical Faculty of the Rheinischen Friedrich-Wilhelms-Universität Bonn and The University of Melbourne

Supervisors:
Prof *Dale I. Godfrey* (Melbourne)
Prof Dr med *Christian Kurts* (Bonn)

Co-supervisor:
Dr *Adam P. Uldrich* (Melbourne)

Date of submission: 15th November 2020
Date of the oral examination: 21st May 2021

Director of the Institute of Experimental Immunology (Bonn, Germany):
Prof Dr med *Christian Kurts*

Director of the Peter Doherty Institute in Melbourne (Melbourne, Australia):
Prof *Sharon Lewin*

Contents

Glossary V

Abbreviations VII

List of Tables XV

List of Figures XVII

Declaration XXIII

Preface XXV

Acknowledgements XXVII

List of Publications XXXI

1 Introduction 1

1.1 The Immune System . . . 1

1.1.1 Adaptive T Cells . . . 2

1.1.2 Innate-like T Cells . . . 3

1.1.3 T-cell Recognition of Non-peptidic Antigens . . . 4

1.2 The Biology of $\gamma\delta$ T Cells . . . 12

1.2.1 Human and Mouse Diversification of $\gamma\delta$ T cells . . . 14

1.2.2 Roles of $\gamma\delta$ T Cells in Innate and Adaptive Immunity . . . 16

1.2.3 Emerging Role of $\gamma\delta$ T Cells in Infectious Diseases . . . 17

1.2.4 Cancer Immunotherapy with $\gamma\delta$ T Cells . . . 20

1.3 Ligand Recognition by $\gamma\delta$ T Cells . . . 22

1.3.1 Soluble Antigens . . . 22

1.3.2 MHC-Peptide Presentation to $\gamma\delta$ T-cells . . . 24

1.3.3 CD1 and Lipid Complexes . . . 25

1.3.4 Stress-induced Surface Ligands . . . 25

1.3.5 Butyrophilin-Like Epithelial Proteins . . . 26

1.4 The Phosphoantigen-reactive $\gamma\delta$TCR . . . 27
1.4.1 General Structure . . . 28
1.4.2 Evolutionary Background . . . 28
1.4.3 Comprehensive Alanine-Scanning Mutagenic Screens . . . 28
1.5 The Family of Butyrophilin Molecules . . . 29
1.5.1 Genetic Organisation . . . 31
1.5.2 Genetic Polymorphisms and Implications in Diseases . . . 33
1.5.3 The Importance of the Intracellular B30.2 Domain . . . 35
1.5.4 Regulation of T-cell Responses . . . 38
1.6 Aims of the Thesis . . . 42

2 Material and Methods **45**
2.1 Cell Cultures . . . 45
2.1.1 Human Samples . . . 45
2.1.2 Isolation of $\gamma\delta$ T cells and Expansion . . . 45
2.1.3 Functional $\gamma\delta$ T-Cell Assays . . . 46
2.1.4 Flow Cytometry . . . 46
2.1.5 Detection of Förster Resonance Energy Transfer . . . 47
2.1.6 Jurkat-Reporter T-Cell Assays . . . 47
2.1.7 Plate-Bound Assays . . . 48
2.1.8 Tumour Cell Viability . . . 49
2.2 Genetically Engineered Proteins . . . 49
2.2.1 Production of Tetramers . . . 49
2.2.2 Production of Recombinant Antibodies . . . 49
2.2.3 Expression of Extracellular Domain Protein Constructs . . . 52
2.2.4 Transfection of Full-length Protein Constructs . . . 52
2.3 Whole-genome Knockout Genetic Screen . . . 53
2.4 Biochemical Analysis . . . 54
2.4.1 Isothermal Titration Calorimetry . . . 54
2.4.2 Surface Plasmon Resonance . . . 54
2.5 Organoid Cell Clulture . . . 55
2.5.1 Human-surgical Samples . . . 55
2.5.2 In-vitro Organoid Cultures . . . 55
2.5.3 Organoid Disaggregation for Flow Cytometry . . . 56
2.6 Statistic Analyses . . . 56

3 BTN2A1 Is a Ligand for the Vγ9 Domain of $\gamma\delta$ T-cells 57
3.1 Introduction . . . 57
3.2 Phenotyping Tumour Cell Lines and $\gamma\delta$TCR-ligand Screen . . . 58
3.3 A Genetic Screen Identifies BTN2A1 as a Vγ9Vδ2-TCR Ligand . . . 60
3.4 Validation of *BTN2A1*-Candidate Gene . . . 63
3.4.1 The Vγ9Vδ2-TCR Affinity Depends on BTN2A1 . . . 63
3.4.2 Antagonist Antibodies Obstruct $\gamma\delta$TCR Ligand-recognition . . . 64
3.4.3 The Vγ9 Domain Binds to BTN2A1 . . . 68
3.5 BTN2A1 Is Essential to Phosphoantigen-induced $\gamma\delta$ T-cell Responses 68
3.5.1 Antibodies Impede Drug-induced V$\delta2^+$ T-cell Responses . . . 71
3.5.2 Drug-induced $\gamma\delta$ T-cell Responses Relay on BTN2A1 . . . 73
3.5.3 Antibodies Modify the Immune Response to HMBPP . . . 74
3.6 Discussion . . . 76

4 BTN2A1 and BTN3A1 Associate to Form a Functional Antigen-presenting Complex 83
4.1 Introduction . . . 83
4.2 Dual BTN2A1/3A1 Expression Induces Phosphoantigen Responses . . . 84
4.3 BTN2A1/3A1 Ectodomains Trigger $\gamma\delta$ T-Cell Responses . . . 85
4.4 Membrane Association between BTN2A1/3A1 Proteins . . . 90
4.4.1 BTN2A1 and BTN3A1 Co-localise in Microscope Imaging . . . 96
4.4.2 BTN2A1/3A Associate Independently from Phosphoantigen . . . 96
4.4.3 Antibodies Impair Association of the BTN2A1/3A Complex . . . 98
4.5 The Intracellular BTN2A1 Domain Has a Functional Role . . . 100
4.6 The BTN2A1 Enhances CD1-restricted $\gamma\delta$ T-Cell Responses . . . 106
4.7 Discussion . . . 110

5 How Vγ9Vδ2 T Cells Recognise a Dual-ligand and their Antitumoral Future Perspectives 115
5.1 Introduction . . . 115
5.2 The Vγ9Vδ2 TCR Recognises a Dual-ligand . . . 116
5.2.1 Vγ9 Germline-regions Have a BTN2A1 Footprint . . . 116
5.2.2 Responses to Phosphoantigens Requires a Second Ligand . . . 117
5.2.3 Agonist 20.1 Activity Depends on BTN2A1 . . . 121
5.3 Varying Strengths of $\gamma\delta$ T-cell Responses . . . 122
5.4 Antitumour Vγ9Vδ2 T-cell Responses . . . 127
5.5 The $\gamma\delta$ T cells in the Tumour Microenvironment . . . 127
5.5.1 Detection of BTN2A1 and BTN3A in Renal Carcinoma Cells . . . 129

5.5.2 Consolidation of Air-liquid Interface Organoid Cultures 130
5.5.3 Infiltrated $\gamma\delta$ T-cells in the Tumour Microenvironment 130
5.6 Clonotype Sequencing Paired with Single-cell Transcriptome 133
5.7 Discussion 134

6 Overall Discussion **139**
6.1 BTN2A1 Is a Ligand for the Vγ9 Domain of $\gamma\delta$ T Cells 141
6.2 The BTN2A1-BTN3A1 Functional Complex 143
6.3 Phosphoantigen-reactive $\gamma\delta$ T-cells Recognise a Dual-ligand 144
6.4 The Biological Implication of the Vγ9Vδ2 T-cells in Kidney Organoids . 145
6.5 The Scenario of Vγ9Vδ2 T Cells in the Clinic 146
6.6 Concluding Remarks 148
6.7 Future Work 153

Bibliography **155**

Curriculum Vitae **183**

A Generation, Titration, and Validation of Reagents **187**
A.1 Production of Soluble Vγ9Vδ2 TCR and BTN Fluorescent Probes . . . 187
A.2 Prevention from Secondary Antibody Cross-reactivity 187
A.3 Generation of Monoclonal Antibodies 190
A.3.1 Cloning and Elution Profiles of anti-BTN3A Antibodies 190
A.3.2 Generation of anti-BTN2A1 Monoclonal Antibodies 195
A.4 Validation of CRISPR/Cas9-mediated Knockout Cell Lines 196
A.5 Assessment of Förster Resonance Energy Transfer 198
A.5.1 Monoclonal Antibody Fluorophore Experiments 198
A.5.2 Intracellular Fluorescent Protein Constructs 199
A.6 Site-directed Mutagenesis 199
A.6.1 Alanine Scanning Method of the G115 T-Cell Receptor 204
A.6.2 Generating a Truncated BTN2A1 Protein 204
A.7 Transcript Expression of BTN Molecules 204
A.8 Glycosylation Effects on BTN2A1 204

B Data Collection **211**
B.1 Collection of Raw Datasets 211
B.2 Commercial Antibody List 211
B.3 Record of Mycoplasma Tests 211

Glossary

A

Amine-to-sulfhydryl succinimidyl 4-(N-maleimidomethyl)cyclohexane-1-carboxylate is a water-soluble heterobifunctional protein crosslinker that contains an amine reactive Sulfo-NHS ester on one end to increase water solubility, and a maleimide functional group that can be utilised to react specifically with cysteines or sulfhydryl groups. 46, 52

Autoimmune regulator (AIRE) is a transcription factor expressed by medullary thymic epithelial cells and promotes promiscuous expression of genes that are otherwise specific to individual peripheral tissues. Peptides derived from these tissue-specific antigens are presented by these thymic epithelial cells to developing $\alpha\beta$ T cells, and any T cells with high-affinity TCRs may be clonally deleted as a means of central tolerance. 17

C

Checkpoint refers to molecules that act as gatekeepers and regulate the antigen recognition by T-cells in the process of immune response. 31, 34, 42, 148

Chimeric antigen receptor T cells are genetically engineered to produce an artificial T-cell receptor for use in immunotherapy in order to redirect cytotoxic specific responses towards tumour cells. 22

CRISPR/Cas9 technology is based on a RNA-guided Cas9 nuclease from the microbial adaptive immune system that cleaves double-stranded DNA of clustered regularly interspaced short palindromic repeats (CRISPR) following a protospacer adjacent motif sequence. Selected single-guide RNAs are adapted for used in molecular genome engineering. This allows molecular biologists to alter desired DNA sequences and modify gene function. 53, 57

G

Genetic screen aka mutagenesis screen, is a laboratory technique used to create and detect a mutant organism. It identifies the function of an unknown gene

introducing general mutations into a population of cells and then compare the mutant to the control population expecting to detect critical differences in their phenotypes. 60

I

Immune synapse defines the molecular interactions underlying regulation of the immune response that takes place in a nano-scale gap between T cells and any antigen-presenting cell. 1, 17

P

Polymerase chain reaction is a fast and inexpensive technique used to amplify small segments of DNA composed in three steps: denaturation of template, primer annealing, and extension of the target sequences by the polymerase from the 3'-end along the template strands. 45, 48, 53, 204, 205, 211

S

Secondary lymphoid tissues are sites where lymphocytes interact with each other and non-lymphoid cells to generate immune responses to antigens. These include the spleen, lymph nodes, and mucosa-associated lymphoid tissues (MALT). 16

Single nucleotide polymorphisms pronounced "snips", are the most common type of genetic variation among people, each representing a single nucleotide difference in the genome. 33, 34, 35

V

V(D)J recombination is the mechanism of genetic recombination that occurs in developing lymphocytes during the early stages of T and B cell maturation. It involves somatic recombination and results in the highly diverse repertoire of immunoglobulin antibodies and T cell receptors found in B cells and T cells, respectively. This process is a defining feature of the adaptive immune system and worth being recognised for the 1987 Nobel Price to Tonegawa Susumu. 12

Abbreviations

Symbols

α-GalCer α-galactosylceramide. 7, 23, 25, 47, 60, 63, 95, 104, 189, 213
K_D dissociation constant at equilibrium. 36, 54, 125
5-OP-RU 5-(2-oxopropylideneamino)-6-D-ribitylaminouracil. 6
5-OE-RU 5-(2-oxoethylideneamino)-6-D-ribitylaminouracil. 6
6-FP 6-formylpterin. 5
786-O hypertriploid renal cell carcinoma. 127, 129

A

ACHN renal cell adenocarcinoma. 127
ADCC antibody-dependent cellular cytotoxicity. 19, 22
A-I apolipoprotein A-I. 7, 23
Ac-6-FP acetyl-6-formylpterin. 5
ALI air-liquid interface. 55, 129, 130, 137, 146
APC antigen-presenting cell. 1, 46
APC allophycocyanin. 68
Apppl triphosphoric acid 1-adenosin-5-yl ester 3-(3-methylbut-3-enyl) ester. 8

B

B2G β2-glycoprotein. 23, 25
B2M β_2-microglobulin. 26
B30.2 PRY/SPRY. XX, XXV, 31, 35, 36, 37, 38, 39, 41, 42, 50, 54, 57, 83, 84, 86, 90, 93, 96, 100, 102, 103, 104, 105, 112, 113, 114, 123, 125, 127, 140, 143, 145, 149, 150
BCG *Mycobacterium bovis* Bacille Calmette-Guérin. 18
BTLA B and T lymphocyte attenuator. 41
BTN butyrophilin. XX, XXV, 28, 29, 31, 32, 33, 34, 35, 37, 38, 40, 41, 42, 43, 47, 48, 52, 54, 58, 59, 62, 64, 79, 83, 84, 85, 86, 89, 90, 91, 96, 99, 100, 101, 102,

110, 112, 114, 123, 125, 130, 135, 137, 138, 139, 140, 141, 142, 143, 144, 145, 148, 150, 151, 153, 187, 188, 199, 200, 202, 207, 211

BTNL butyrophilin-like. XX, 26, 27, 31, 32, 33, 41, 83

C

C1R Epstein-Barr virus transformed lymphoblastoid. 58, 59, 73, 75, 79, 81, 122

CA9 carbonic anhydrase IX. 132, 145

Caki-1 clear renal cell carcinoma. 129

CAR-T chimeric antigen receptor T. 147

CCL5/RANTES chemokine (C-C motif) ligand 5. 23

CD1 MHC-like lipid-presenting molecule. XX, 4, 6, 7, 14, 25, 42, 47, 83, 106, 114, 149

CD19 B-lymphocyte surface antigen B4. 22, 147

CD25 IL-2 receptor subunit α. 71, 72, 73, 74, 75, 84, 85, 88, 92, 102, 106, 107, 108, 110, 111, 126, 127, 133, 210, 214, 216

CD27 TNF-receptor of memory cells. 21

CD28 T-cell co-stimulatory receptor. 2, 18, 23, 45, 74, 75, 76, 78, 88, 89, 92, 109, 111, 147, 214

CD3 signalling glycoprotein component. 45, 46, 48, 64, 66, 67, 68, 69, 72, 74, 75, 76, 78, 88, 89, 92, 107, 109, 111, 204, 210, 214, 215, 216

CD4 co-receptor of MHC class II. 2, 3, 12, 19, 25, 35, 38, 216

CD45 leucocyte common antigen and cell activation assistant tyrosine phosphatase receptor type-C. 20, 23, 41, 132, 133, 137, 216

CD69 early transmembrane C-Type lectin activation marker. 47, 48, 106, 109, 118, 120, 121, 122, 123, 124, 126, 127, 133, 215, 216

CD8 co-receptor of MHC class I. 2, 7, 12, 19, 23, 24, 38, 132, 216

CD80 co-stimulatory molecule B7-1. 17

CD86 co-stimulatory molecule B7-2. 17

CDR complementarity-determining region. XX, 23, 24, 25, 26, 27, 28, 29, 50, 80, 115, 117, 144, 149, 154

CFP cyan fluorescent protein. 47, 96, 100

CHO-K1 Chinese hamster ovary K1. 84, 86, 94, 95

CL cardiolipin. 23, 25

CMV cytomegalovirus. 18, 20

CSL Commonwealth Serum Laboratories Limited. XXV, XXVII, 54, 58, 77, 78, 195, 211

CTLA-4 cytotoxic T-lymphocyte-associated protein 4. 34, 38, 148

CXCL13 CXC chemokine ligand-13. 16
CXCR5 CXC chemokine receptor-5. 16, 19

D

Daudi Burkitt's lymphoma Daudi. 59
DC dendritic cell. 6, 16, 17, 25, 33, 34, 148, 149, 204, 209
DC-SIGN DC-specific intercellular adhesion molecule-3-grabbing nonintegrin. 34
DETC dendritic epidermal T cell. 15, 16, 17, 26, 33, 38, 140
DMAPP dimethylallyl pyrophosphate. 8, 10
DTT 1,4-dithiothreitol. 195

E

EAE autoimmune encephalomyelitis. 38
EBV Epstein-Barr virus. 20, 23, 26
EC_{50} half maximal effective concentration. 13, 136
EcIF1 *Escherichia coli* translation initiation factor. 23, 24
EDTA ethylenediaminetetraacetic acid. 54, 56
ELISA enzyme-linked immunosorbent assay. XXV
Eomes eomesodermin. 4
EPCR endothelial protein C receptor. 23
ERMAP erythroblast membrane associated protein. 32, 33
ESAT-6 early-secreted antigenic target 6-kDa protein. 22

F

F_1-ATPase F_1-adenosine triphosphatase. 7, 23, 142
FACS fluorescence-activated cell sorting. 57
FBS foetal bovine serum. 46
FDR false discovery rate. 54, 60, 61
Foxp3 forkhead family transcription factor Foxp3. 2
FPPS farnesyl pyrophosphate synthase. 8, 9, 10, 139
FRET Förster resonance energy transfer. 47, 58, 59, 64, 65, 68, 69, 79, 90, 93, 94, 95, 96, 98, 99, 100, 101, 102, 103, 105, 111, 112, 113, 143, 145, 198, 199, 201, 202, 203, 213

G

GATA3 GATA binding protein 3. 3, 4
GFP green fluorescent protein. 47, 48, 53, 93, 95, 100, 105, 118, 199, 204

GM-CSF granulocyte-macrophage colony-stimulating factor. 71, 73, 81, 85
GvHD graft versus host disease. 4, 21, 147

H

HARS histidyl-tRNA synthetase. 14, 23, 24
HEK-293T human embryonic kidney 293. 48, 53, 58, 59, 64, 66, 73, 75, 79, 80, 81, 116, 118, 188, 220, 222
HGSC high-grade serous epithelial ovarian cancer. 34
HIV human immunodeficiency virus. 18, 19, 20
HLA human leukocyte antigen. 96, 97
HMBPP (E)-4-hydroxy-3-methyl-but-2-enyl pyrophosphate. 8, 11, 18, 35, 37, 40, 46, 47, 50, 54, 74, 75, 76, 77, 78, 81, 83, 93, 95, 98, 99, 100, 112, 113, 117, 120, 122, 123, 124, 125, 126, 135, 136, 144, 153, 154
HSP heat shock protein. 23, 24
HSV herpes simplex virus. 23
HV4 hypervariable region 4. 27, 115, 135

I

ICAM-1 intercellular adhesion molecule 1. 16, 21
IFN-γ interferon-γ. 2, 4, 18, 21, 23, 26, 38, 46, 71, 73, 75, 76, 81, 85, 110, 115, 127
Ig immunoglobulin. XXV, 2, 16, 19, 28, 29, 31, 34, 35, 36, 38, 39, 57, 85, 111, 148
IL-6 interleukin 6. 76
IL-8 interleukin 8. 73, 76, 85
IL-9 interleukin 9. 71, 76, 85
IL-15 interleukin 15. 18, 45
IL-21 interleukin 21. 16
IL-10 interleukin 10. 16, 38, 71, 73, 76, 85
IL-17A interleukin 17A. 4, 14, 24, 26, 71, 76, 85, 115
IL-13 interleukin 13. 4, 71, 76, 85
IL-4 interleukin 4. 2, 16, 71, 76, 85
IL-5 interleukin 5. 2, 4
IL-2 interleukin 2. 2, 16, 18, 20, 23, 38, 45, 46, 71, 89
iNKT invariant natural killer T cell. 7
IPP isopentenyl pyrophosphate. 8, 10, 11, 21, 35, 47, 54, 83, 113, 123, 124, 125, 126, 136
ITAM immunoreceptor tyrosine-based activation motif. 2
ITC isothermal titration calorimetry. 36, 54, 100, 123, 125

J

JRT3-T3.5 leukemic T-cell lymphoblast non-β chain. 117, 124, 126
Jurkat 76.2 T-cell leukaemia Jurkat 76.2. 58, 59, 79

K

K562 human erythroleukemia. 22, 23, 58, 59, 60, 61, 62, 63, 64, 66, 73, 74, 75, 79, 80, 81, 117, 120, 122, 123, 127, 141, 142, 147, 219

L

LLO listeriolysin. 22, 23
LM-MEL Ludwig Melbourne-MELanoma. 58, 59, 79
LRRC4/NGL-2 leucine rich repeat containing 4/Netrin-G ligand-2. 34

M

MACS magnetic-activated cell sorting. 45
MAIT mucosal-associated invariant T cells. XX, 1, 3, 4, 5, 6
MEG-01 human megakaryoblastic leukaemia. 58, 59
MHC major histocompatibility complex. XX, 2, 3, 4, 14, 17, 24, 25, 28, 31, 42, 57, 80, 84, 139, 140, 142, 147, 151
MIC MHC class I chain-related. 3, 7, 21, 25, 26
moDC monocyte-derived macrophages. 19
MOG myelin oligodendrocyte glycoprotein. 32, 33, 34, 35, 38
MOLT-4 human T lymphoblast from acute lymphoblastic leukemia. 59
MR1 MHC-related protein 1. 4, 5, 6, 14
MRP5 multidrug resistance-associated protein 5. 12

N

NIH/3T3 mouse fibroblast NIH-3T3. 47, 84, 86, 94, 95, 99, 106
NK natural killer cell. 7
NKG2D natural killer group 2 member D. 7, 17, 19, 21, 26, 111, 137, 146, 147
NKT natural killer T cells. 1, 3, 4, 7, 25

O

ONJCRI Olivia Newton-John Cancer Research Institute. XXV, XXVII, 58

P

PBMC peripheral blood mononuclear cells. 22, 45, 46, 68, 71, 126, 134
PBS phosphate buffered saline. 46, 48, 49, 51, 54, 56, 125
PD1 programmed cell death protein 1. 41, 148
PD-L1 programmed cell death-ligand 1. 31, 38, 41, 148
PDO patient-derived organoids. XXI, 43, 55, 130, 146
PE R-phycoerythrin. 14, 23, 24, 45, 46, 47, 48, 49, 52, 58, 59, 68, 79, 90, 93, 94, 95, 98, 199, 201, 202
PILRβ paired immunoglobulin-like type 2 receptor β. 84, 85, 86, 90, 93, 100, 102, 104, 105, 112, 113
PLZF promyelocytic leukemia zinc finger. 3
PMA phorbol myristate acetate. 90, 214
PPD purified protein derivative. 22, 23

R

RAG recombination-activating gene. 12
Raji Burkitt's lymphoma of the left maxilla. 58, 59
RAMOS Burkitt's lymphoma negative for Epstein-Barr virus. 58, 59, 90, 93
RhoB Ras homolog gene family, member B. 41, 143, 151
RORγt RAR-related orphan receptor γ. 4, 26
RPMI-8226 multiple myeloma. 58, 59, 90, 93

S

SDS-PAGE sodium dodecyl sulfate poly-acrylamide gel electrophoresis. 51, 195
SE *Staphylococcal* enterotoxins. 24
SKW-3 T-cell chronic lymphocytic leukaemia. 58, 59
SPR surface plasmon resonance. XXV, 36, 54, 80
SPRY sequence repeat of the splA/ryanodine receptor. 35, 114

T

T-bet T-box transcription factor TBX21. 4
TCR T-cell receptor. XX, XXV, 1, 2, 3, 4, 7, 8, 12, 14, 21, 22, 23, 24, 25, 26, 27, 28, 29, 30, 31, 37, 38, 41, 42, 47, 48, 50, 53, 57, 59, 60, 61, 63, 64, 66, 67, 68, 69, 70, 71, 75, 79, 80, 89, 90, 93, 94, 95, 100, 102, 104, 106, 107, 110, 111, 112, 113, 114, 115, 116, 117, 121, 122, 130, 134, 135, 136, 139, 140, 142, 143, 144, 145, 147, 148, 149, 150, 151, 187, 188, 204, 209, 210, 211, 213
Tfh T follicular helper. 2, 19
Th T helper. 2, 3, 21, 38, 85, 115, 147

THP-1 human monocytic. 58, 59, 79, 90, 93
TLR toll-like receptor. 22, 35
TNF tumour necrosis factor. 2
TNF-α tumour necrosis factor-α. 12, 21, 71, 73, 75, 76, 81, 85, 127
Treg regulatory T-cell. 2
TRIM tripartite motif. 35
TT tetanus toxin. 23, 25

U

ULBP UL16-binding protein. 3, 7, 21, 23, 26
UPS universal primer site. 134

V

VSV vesicular stomatitis virus. 19

Y

YFP yellow fluorescent protein. 47, 96, 100

List of Tables

1.1 Registered bisphosphonate drugs 9
1.2 Genomic TCR gene loci 14
1.3 Localisation of predominant $\gamma\delta$TCRs 15
1.4 Recognition of tumour types by Vγ9Vδ2 T cells 20
1.5 Scope of $\gamma\delta$ T cell ligands in humans 23
1.6 Scope of $\gamma\delta$ T cell ligands in mouse 23
1.7 Summary of mutated $\gamma\delta$TCR residues 30
1.8 Expression profile and function of BTN members 33
1.9 Interactions between phosphoantigens and BTN3A proteins 36

2.1 HMBPP-reactive TCR CDR3 sequences 50
2.2 Molecular mass and extraction coefficients 50
2.3 Extracellular domain sequences of BTN molecules 52

3.1 Gene-wise top-ranked genes 62
3.2 Statistic table for antibody treatment in drug stimulated PBMC 71
3.3 Statistic table for Vδ2 T cell response 75
3.4 Turkey-adjusted p-values of antibody functional activities 75

4.1 Differential activation effect between V$\delta2^+$ and total $\gamma\delta$ T cells 88

A.1 Antibody cloning sequences 191
A.2 Primers for PCR and site-directed mutagenesis 205
A.3 Primers for BTN and reference genes selected for real-time qPCR . . . 209

B.1 Details of antibodies and reagents used in this work 216
B.2 Collection of mycoplasma-free verified cell line tests 217

List of Figures

1.1 Major antigen-presentation modes to T cells 5
1.2 Chemical structure and composition of phosphoantigens 9
1.3 Metabolism of isoprenoids 10
1.4 Structure of bisphosphonates 10
1.5 Bioactivity of diverse phosphorylated compounds 13
1.6 Molecular structure of a $\gamma\delta$TCR 31
1.7 Evolutionary tree of B7-superfamily genes 32
1.8 The human BTN-genetic cluster 32
1.9 Molecular model of the BTN3A1 intracellular B30.2 domain 37
1.10 Structure of human BTN3A ectodomains 40

3.1 Surface expression of BTN molecules in tumour cell lines 59
3.2 Ligand screen using six different Vγ9Vδ2 TCR clonotypes 60
3.3 Genome-wide negative selection screen 61
3.4 *BTN*-knockout melanoma lines lose affinity for Vγ9Vδ2 TCR clonotypes 63
3.5 Reexpressing *BTN2A1* in *BTN*-deprived cells restored $\gamma\delta$TCR bond . . 65
3.6 Antibodies change Vγ9Vδ2 TCR affinity to tumour cell lines 66
3.7 Specific antibodies modify BTN2A1 affinity for $\gamma\delta$TCR 67
3.8 Tetramerised BTN2A1 probe binds uniquely to the Vγ9 domain 69
3.9 Biomolecular interaction analysis between Vγ9 domain and BTN2A1 . 70
3.10 Antibody treatment abrogates drug-induced V$\delta2^+$ T-cell response . . . 72
3.11 V$\delta2^+$ T-cell response to drug stimulated tumour cells 74
3.12 Functional BTN2A1 antibodies modulate immune responses 77
3.13 Modulating the function of Vγ9Vδ2 T cells with antibody treatment . . . 78

4.1 Purified V$\delta2^+$ T cells respond to BTN2A1 and BTN3A1 complexes . . 86
4.2 Cytokine production in response to rodent BTN-transfected cells 87
4.3 Purified V$\delta2^+$ T cells response to immobilised BTN ectodomains . . . 91
4.4 Normalised V$\delta2^+$ T-cell response to immobilised protein 92
4.5 Association between BTN2A1 and BTN3A proteins 93

4.6 The Vγ9Vδ2 TCR binds to human BTN2A1 transfected rodent cells . . 94
4.7 Human BTN-transfected rodent cells - summary 95
4.8 Microscopy co-localisation of BTN2A1 and BTN3A1 97
4.9 Co-localisation of BTN2A1 and BTN3A1 in microscopy imaging 98
4.10 Intracellular BTN2A1/3A1 domains associate regardless of antigen . . 99
4.11 Functional antibodies alter BTN2A1 and BTN3A1 arrangement 101
4.12 The BTN2A1 B30.2 intracellular domain needed to join BTN3A1 103
4.13 Truncated BTN2A1 B30.2 domain affects Vγ9Vδ2 TCR bound 104
4.14 Truncated BTN2A1 alters the association with BTN3A1 and TCR affinity 105
4.15 Immune $\gamma\delta$ T-cell response to truncated BTN2A1 and BTN3A1 107
4.16 Predicted $\gamma\delta$ T-cell responses to truncated BTN2A1 and BTN3A1 . . . 108
4.17 The BTN2A1 enhances T-cell responses to CD1c/d molecules 109

5.1 Alanine scan identifies Vγ9Vδ2 TCR reactive sites 118
5.2 Reactive sites in the G115 surface molecular model 119
5.3 Molecular representation of the BTN2A1 reactive site 119
5.4 Alanine G115 mutants impair JRT3-T3.5 reactivity to K562 cells 120
5.5 Agonist 20.1 functional activity depends on BTN2A1 122
5.6 Jurkat-reporter cells with a Vγ9Vδ2 TCR response to phosphoantigens 124
5.7 Isothermal titration calorimetry between B30.2 and phosphoantigen . . 125
5.8 Titration response to phosphoantigens 126
5.9 Antitumoural activity of Vγ9Vδ2 T cells 128
5.10 Expression of BTN family members in renal carcinoma cells 129
5.11 Schematic representation for preparation of PDO-ALI cultures 131
5.12 Visual look of carcinogenic organoid samples 131
5.13 Population of lymphocytes in renal tumour samples 132
5.14 Tumour infiltrating lymphocytes in renal carcinoma organoids 133
5.15 Schematic clonotype paired transcriptome sequencing scheme 134

6.1 Presentation of phosphoantigens to $\gamma\delta$ T cells 150
6.2 Theoretical phosphoantigen-presentation complex models 152

A.1 Construction of soluble tetramers 188
A.2 Titration of tetramer TCR-6 189
A.3 Primary and secondary antibody unspecificity control 189
A.4 Gels of in-house produced antibodies 195
A.5 Antibody elution profiles 196
A.6 Anti-BTN2A1 cross-reactivity profile 197

A.7 Validated melanoma CRISPR/Cas9 Knockout lines 198
A.8 Generation of intracellular fluorescent tagged proteins 200
A.9 Best antibody pair for FRET analysis 201
A.10 Association of BTN2A1 and BTN3A on rodent cells 202
A.11 Antibodies disrupt FRET between BTNs expressed on murine cells . . 203
A.12 Efficiency of TCR transfection 206
A.13 Transcription profile of BTN molecules 207
A.14 Electrophoresis gel of real-time qPCR 208
A.15 Deglycosylated BTN2A1 binds monocyte-derived DCs 209
A.16 The intracellular domain of BTN2A1 is important for $\gamma\delta$ T-cell response 210

B.1 Transfection efficiency of CD1-molecules in mouse fibroblasts 212
B.2 BTN phenotypic profile and $\gamma\delta$TCR scan across human tumour lines . 213
B.3 Purified Vδ2^{+} T-cell responses to immobilised BTN ectodomains . . . 214
B.4 The BTN2A1-Vγ9 enhances $\gamma\delta$ T-cell CD1c/d-reactivity 215

Abstract

Human gamma-delta ($\gamma\delta$) T cells can respond rapidly with cytotoxic responses to pathogenic infections and malignant cells. Although they are found at low numbers in peripheral blood, these might expand and constitute up to half of the total circulating T cells after infection. Most systemic $\gamma\delta$ T cells expressed a recombined heterodimeric T-cell receptor (TCR) with genes of the variable (V) γ9 and δ2 loci, termed Vγ9Vδ2 T cells. Opposed to conventional $\alpha\beta$ T cells that recognise processed peptides on major histocompatibility complex (MHC) class I and II and elicit delayed adaptive responses, $\gamma\delta$ T cells are innate-like T cells that recognise non-peptidic antigens akin to mucosal-associated invariant T (MAIT) or MHC-like lipid-presenting molecule (CD1)-restricted T cells which recognise vitamin-B derivates or lipids, respectively. The most interesting feature of Vγ9Vδ2 T cells is that they recognise phosphorylated antigens (aka *phosphoantigens*) which are essential for life including bacteria and particularly abundant in cancer cells. Little is known how $\gamma\delta$ T cells recognise phosphoantigens, even though, a few putative ligands have been described.

Butyrophilins (BTNs) are a family of transmembrane molecules capable of regulating the immune activity of innate-like $\gamma\delta$ T cells. They dimerise to constitute complexes, some of which may interact with germline-encoding regions of the $\gamma\delta$ T cell receptors in murine or human species. For instance, mouse butyrophilin-like (BTNL) molecules shape the V$\gamma7^+$ $\gamma\delta$ T-cell compartment in the intestine, while human BTNL counterparts selectively activate V$\gamma4^+$ $\gamma\delta$ T cells of the colon. Here, tetrameric $\gamma\delta$TCR clonotype probes are used for a genetic screen to identify a previously unknown molecular ligand essential for recognition of phosphorylated antigens by $\gamma\delta$ T cells. This screen identifies BTN2A1 and subsequent experiments elucidate this protein contacts with the Vγ9 domain irrespective of the Vδ recombined segment and is essential to confer reactivity to phosphoantigens together with BTN3A1. Thus, BTN2A1 and BTN3A1 constitute a functional complex of which we found both intracellular domains are critically important in maintaining an active conformation. Whereas internal BTN3A1 PRY/SPRY (B30.2) motif senses the antigen, the BTN2A1 intracellular domain appears fundamental to retain association of the complex. Mutagenic alanine screens reveal a dual-ligand binding site for the Vγ9Vδ2 TCR, where conserved residues of the Vγ9 domain bind to BTN2A1 and several residues located at the complementarity-determining regions (CDRs) might react to a putative molecule of the BTN3A family. Thus, this work proposes a phosphoantigen-reactive $\gamma\delta$ T cells recognise a dual-ligand binding complex where BTN2A1 contacts the Vγ9 domain and BTN3A1 is a phosphoantigen sensor molecule that plausibly induces the molecular

switch necessary to induce immune responses.

Lastly, the influence of tumour infiltrated phosphoantigen-reactive $\gamma\delta$ T cells in renal carcinogenic tumour patient-derived organoids (PDO) samples is examined and their relevance in healing disease assessed in comparison to previous clinical studies. These results are of vital importance to better understand the potential of $\gamma\delta$ T cells in prospective medical applications.

Declaration

The work presented in this thesis was conducted at the University of Melbourne (Australia) and the Rheinische Friedrich-Wilhelms-Universität Bonn (Germany), in the laboratories of Prof *Dale I. Godfrey* (Peter Doherty Institute for Infection and Immunity) and Prof der med *Christian Kurts* (Institute of Experimental Immunology), respectively.

This research work was founded by the Bonn-Melbourne Research and Graduate School Immunosciences IRTG2168.

In this declaration, I certify that:

(i) the thesis comprises only my original work towards the PhD except where indicated in the Preface;

(ii) due acknowledgement has been made in the text to all other material used;

(iii) the thesis is less than 100,000 words in length, exclusive of tables, maps, bibliographies, and appendices.

Preface

In accordance with the regulations of the University of Melbourne, I acknowledge that components of the work presented in this thesis were performed alongside the following collaborators with of the work per chapter indicated in brackets:

- Prior to enrolment in the degree, Dr Adam Uldrich and Zheng Ruan produced the $\gamma\delta$TCR monomer protein clones defined in Table 2.1 (Chapter 2).
- Zheng Ruan assisted in the generation of genetic cloning of BTN members, site-directed mutagenesis, production of BTN2A1 and BTN3A1 protein extracellular (immunoglobulin (Ig)V-IgC) and intracellular (B30.2) domains, and help to construct some Jurkat-reporter cell lines. Together with Adam Uldrich also generated site-directed mutagenesis and cloning of the G115 Vγ9Vδ2 TCR pMIG constructs (Chapter 2).
- Dr Adam P. Uldrich contributed to antibody labelling of 2.2.2 (Chapter 2).
- Dr Nicholas A. Gherardin generated the human MR1 protein tetramers loaded with 5-OP-RU substrate and contributed to isolate and expand $\gamma\delta$ T cells from random donors.
- Commonwealth Serum Laboratories Limited (CSL) generated the panel of monoclonal antibodies against BTN2A1 as described in Sec. A.3.2 and respective enzyme-linked immunosorbent assay (ELISA) in Fig. A.6 b (Chapter 2); and performed the surface plasmon resonance (SPR) depicted in Fig. 3.9 (Chapter 3).
- Dr Andreas Behren, from the Olivia Newton-John Cancer Research Institute (ONJCRI), Australia, supplied melanoma cell lines LM-MEL-19, 34, -36, -42, -46, -53, -62, -75 (Behren et al., 2013) and together with his team made LM-MEL-62 and LM-MEL-75 CRISPR/Cas9 knockout lines for *BTN2A1* and *BTN3A1* (Chapter 3).

- Dr Tom Fulford, from the University of Melbourne, Department of Microbiology and Immunology, Godfrey laboratory, Australia, contributed to establish Jurkat-reporter cell lines (Chapter 2).
- Dr Darryl N. Johnson, from the University of Melbourne, Department of Microbiology and Immunology, Godfrey laboratory, Australia, performed microscopy images of Sec. 4.4.1 (Chapter 4).
- Dr Hamish McWilliam and Prof José Villadangos, from the University of Melbourne, Department of Microbiology and Immunology, Villadangos laboratory, Australia, provided the genomic library GeCKOv2 and gave technical advice for the genetic screen (Chapter 3).
- Dra Sonia Leonardelli, from the University of Bonn, Institute of Clinical Chemistry and Clinical Pharmacology, Hölzel laboratory, Bonn, contributed to the microscopy image in Fig. 5.13 (Chapter 5).

Acknowledgements

Throughout the progress of this dissertation, I received a considerable amount of support and assistance that contributed to the fluent and successful development of this work.

First and foremost, I would like to thank Dr Adam P. Uldrich for his time and excellent teaching of fundamental laboratory techniques necessary to perform this project. His broad expertise and deep understanding of the $\gamma\delta$ T-cell biology contributed greatly as well as were vital in developing this piece of work. Adam's critical opinion directly impacted my learning curve and influenced me in questioning previous misconceptions on the basic understanding of phosphoantigen-presentation mechanisms to $\gamma\delta$ T cells. Indeed, his opinions were the most influencing in helping me develop this project. These also leveraged both reasoning and critical thinking, which eventually lead to a breakthrough hypothesis later yielding to a more extensive collaborative high-standing research article in *Science*. His advice immensely helped in advancing experimental work and establishing the methodology that was essential in resolving current research problems in the field of $\gamma\delta$ T cells. After long hours of debates trying to resolve complex questions also brought us a close friendship, which I am incredibly thankful for him sharing personal experiences and tips about sightseeing sea creatures around the Mornington Peninsula.

I would also like to thank my two supervisors, Prof Dale I. Godfrey and Prof Dr med Christian Kurts, for hosting me in their research teams. They also provided valuable guidance throughout my studies and endless tools that were essential to develop experiments without constraints towards the right direction of the project and complete this dissertation successfully.

Moreover, I would like to express my sincere gratitude to Prof Jonathan Cebon and Dr Andreas Behren from the ONJCRI and CSL for taking me, as part of the Bonn-Melbourne Research and Graduate School Immunosciences IRTG2168, on board of their previous collaborative project. This agreement granted our access to use a privileged comprehensive antibody panel against the BTN2A1 crucial for revealing its functional role in cancer and promoting outstanding collaborative research. This

same partnership allowed us to experiment with a batch of melanoma cell lines and the study the role of BTN2A1 protein in the biology of cancer. Eventually, our three-party cooperation yielded to excellent research teamwork with a myriad of forthcoming research projects in the next years.

I want to acknowledge my colleagues and secretary team of the Bonn-Melbourne Research and Graduate School for their interesting questions during our project presentation meetings, supportive chats, and discussions over these long-lasting bureaucracy procedures required to fulfil the requirements from a dual degree combined between Universities of two different countries. Especially, I want to express my sincere thanks to Patrick Günther and Ioanna Gemünd for their interest and time-sharing on their view over different protocol methodologies for planning future work on single-cell sequencing methods. Also, I want to thank Marie-Sophie Philipp, my co-Boomerang partner, for her friendship and introducing me to the daily-life routine during my arrival at the Institute of Experimental Immunology of the University of Bonn, Germany.

I wish to show my gratitude to Michael Hölze and Marieta Toma, for having me in their laboratory facilities, sharing equipment, and introducing the idea of working with patient-derived organoid cultures. I sincerely thank their team members, who got me involved and taught the basics for growing patient-derived organoid cultures. Also, I acknowledge Marc Beyer for his open discussions about sequencing $\gamma\delta$ T-cell protocols and willingness to host me in developing further prospect applications that arouse from this dissertation.

My honest thanks also go to my fellow labmates from the Godfrey laboratory, especially Dr Michael Souter, Dr Nicholas Gherardin, and Shihan Tony Li, and others who provided me easy access to purified lymphocytes from buffy coats. That drastically shortened the time needed to acquire a supply of primary cells vital to undertook research experiments for this project. Also, I thank all members in our lab for their interesting exchanging opinions that implicated critical thinking during my understanding of the immune system. Likewise, I am incredibly grateful to Tom Fulford. He provided immediate support and helped to accelerate some of the post-review experiments required for our successful co-author contribution to a publication arising from the work of this dissertation. Moreover, I would like to express my appreciation to Marcin Cirula and Scott J. Reddiex (Godfrey lab) and Moritz Blankart (Kurts lab) for my first introduction to the laboratory and constant supply for research reagents and access to instrumentation in the department facilities. Particularly, Marcin Cirula and Scott J. Reddiex that together with Darryl N. Johnson, shared interesting stories and knowledge about the Australian culture and provided exciting travel tips that came handy while exploring the wonderful yet, unexplored Australian's outback country.

Besides my advisors, I would like to thank the rest of my thesis internal committee at the University of Melbourne Prof Katherine Kedzierska and Dr Lucy Sullivan, for their insightful comments and encouragement in improving my research writing skills from various perspectives. Also, I acknowledge all staff members of the University of Melbourne flow cytometry facility, who performed some of the cell sorting experiments, including Dr Alexis Perez Gonzalez, who gave useful advice in understanding advanced features in different flow cytometry instruments.

And last but not least, I would like to give special thanks to my parents, Mariàngels and Jaume, and sister Judit, for supporting my career and raising my strength during hard times. I want to dedicate this work to my family, who have always shared love and encouraged me to my goals. Additionally, I wish to thank Laura for her care and staying in contact despite the long-distance relationship in the course of developing this project.

Moreover, I would like to give special tribute to the Catalan people who are fighting, during the time of performing this work and years before, for the freedom of expression and sustenance of the Catalan culture, that like any other is a must to maintain global diversity and show respect for the land, traditions, and cultural heritage of others.

Finally, I want to acknowledge to anyone I have forgotten and was instrumental in this project.

List of Publications

- Adam P. Uldrich, Marc Rigau, Dale I. Godfrey. Immune recognition of phosphoantigen–butyrophilin molecular complexes by $\gamma\delta$ T cells. *Immunological Reviews*, Oct 2020. doi: 10.1111/imr.12923.

- Marc Rigau, Simone Ostrouska, Thomas S. Fulford, Darryl N. Johnson, Katherine Woods, Zheng Ruan, Hamish E. McWilliam, Christopher Hudson, Candani Tutuka, Adam K. Wheatley, Stephen J. Kent, Jose A. Villadangos, Bhupinder Pal, Andrew Hammet, Anne M. Verhagen, Gino Vairo, Eugene Maraskovsky, Con Panousis, Nicholas A. Gherardin, Jonathan Cebon, Dale I. Godfrey, Andreas Behren, Adam P. Uldrich. Butyrophilin molecules govern $\gamma\delta$ T cell reactivity against phosphoantigens. *The Journal of Immunology*, May 2020. Annual Meeting Abstracts, the American Association of Immunologists.

- Marc Rigau, Simone Ostrouska, Thomas S. Fulford, Darryl N. Johnson, Katherine Woods, Zheng Ruan, Hamish E. McWilliam, Christopher Hudson, Candani Tutuka, Adam K. Wheatley, Stephen J. Kent, Jose A. Villadangos, Bhupinder Pal, Andrew Hammet, Anne M. Verhagen, Gino Vairo, Eugene Maraskovsky, Con Panousis, Nicholas A. Gherardin, Jonathan Cebon, Dale I. Godfrey, Andreas Behren, Adam P. Uldrich. Butyrophilin 2A1 is essential for phosphoantigen reactivity by $\gamma\delta$ T cells. *Science*, Jan 2020. doi: 10.1126/science.aay5516.

- Andreas Behren, Jonathan Cebon, Marc Rigau, Thomas S. Fulford, Dale I. Godfrey, Andrew Hammet, Simone Ostrouska, Con Panousis, Adam P. Uldrich. *International Patent* Method of inhibiting or activating gamma delta T cells. Number WO 2020/257871 A1, Dec 2020.

Chapter 1

Introduction

1.1 The Immune System

The immune system consists of a complex defence biological system that protects the individual from diseases. It relies on two principal well-organised immunologic networks known as the innate and adaptive immunity. Innate immunity prevails in all living organisms and provides a nonspecific-host defence and physical barriers. In the event of encountering an infectious pathogen or substance, innate cells respond with a rapid secretion of inflammatory cytokines and cytolytic soluble agents to heal infection or corresponding tissue disruption. However, during speciation, jawed vertebrate organisms evolved a higher hierarchy of orchestrated responses that adapted specificity to antigens from virtually any source. Adapted immunity creates immunological memory after infection as a result of developing an army of adaptive cells. Acquiring these specific antigen responses depends on the phagocytic activity of professional antigen-presenting cells (APCs) of the innate system, which engulfs and process foreign antigen. Processed antigens are then presented mediating an *immune synapse* to specialised TCRs expressed by a group of adaptive lymphocyte cells. This process activates clonal expansion of cytotoxic T-cells with targeted responses of which clones with the highest antigenic affinity proliferate the most as a result of natural selection. Hence, the immune response builds a mature specialised cellular orchestrated defence that protects the organism from disease and future encounters with the infectious pathogen. However, recent advances show a burgeoning family of T lymphocytes that includes MAIT, natural killer T cells (NKT), and $\gamma\delta$ T cells empowered with traits from both innate and adaptive systems. These appear to have crucial roles in healing pathogenic infections, tissue-homeostasis, and tumour immunosurveillance (Godfrey et al., 2015).

1.1.1 Adaptive T Cells

Canonical T cells form their antigen-specific TCR expressing genes of the α and β loci. The function of this $\alpha\beta$TCR is to recognise peptide antigens presented by polymorphic MHC class I and II molecules. Antigen-presenting molecules of the MHC class II are on the surface of professional presenting cells and mostly prime T helper (Th) cells with co-receptor of MHC class II (CD4), which promotes their migration to lymph nodes and licensing cytotoxic T lymphocytes expressing the co-receptor of MHC class I (CD8) for a robust, targeted effector response. All T-lymphocytes receive three-signalling stimuli for their activation. First, a TCR/CD3 complex engagement that initiates the immunoreceptor tyrosine-based activation motif (ITAM) phosphorylation and following distinct biochemical pathways that activates specific genetic, transcriptional machinery. Second, co-stimulatory signals form T-cell co-stimulatory receptor (CD28) necessary to promote survival and enhanced stimuli. Third, they receive multiple cytokine signals which determine the type of immune response along self-secretion of interleukin 2 (IL-2) T-cell survival signalling. Effector cytotoxic T lymphocytes lyse infected or abnormal cells that present the antigenic target loaded on MHC class I molecules. A clonal expansion these cytotoxic $CD8^+$ T cells generate a pool of diverse effector clonotypes but also some long-lasting, highly specific, and sustained long-term memory T-cell subsets which respond rapidly in the event of a repeated infection (Ratajczak et al., 2018). Another lineage-committed subset called regulatory T-cells (Tregs), best identified by the expression of forkhead family transcription factor Foxp3 (Foxp3), are fundamental to maintain self-tolerance and control the immune response (Fontenot and Rudensky, 2005).

Typical immune responses derived from Th cells are differentiated mainly by secretion of type 1 or 2 cytokines, each associated with the clearance of distinct pathogens or tissue dysregulation. There are, however, other classes of defined immune response profiles and Th lymphocyte subclasses such as the Th17, Th22, or T follicular helper (Tfh) cells commonly associated with a distinct cytokine release or functions like the development of B-cell humoral immunity in the lymph node germinal centres. Major Th1 responses are characterised for the production of interferon-γ (IFN-γ) and tumour necrosis factor (TNF) secretion and specify to eliminate microbial and viral infections. Th2 responses are associated with extracellular infections and allergy. Th2 responses secrete interleukin 5 (IL-5) that stimulates eosinophils for a rapid clearance of parasites and induces eosinophils through interleukin 4 (IL-4) which cause B-cell isotype switch to Ig class E. The Th17 pro-inflammatory response usually has important roles in protecting physical barrier sites with the clearance of mucosal-associated

pathogens.

1.1.2 Innate-like T Cells

Innate-like T cells such as MAIT, NKT, and $\gamma\delta$ T cells express adaptive TCR receptors despite eliciting rapid innate-like immune responses. These cells have invariant or semi-invariant TCRs that can be shared among different individuals and are characterised to recognise selective non-peptide antigens presented by non-classic monoclonal MHC molecules. Innate-like T cells are capable of regulating immune responses, activate adaptive immunity, and evoke rapid cytotoxic activity by themselves. Activated innate-like T cells not only may result in a clonal expansion and cytotoxic activity, but they can also prime $\alpha\beta$ Th cells to broaden the immune response. Hence, innate-like T cells are considered an independent immune cellular component that bridges the innate and adaptive systems.

Innate-like T cells comprise a small TCR repertoire that recognises evolutionary conserved non-peptide immunogens, opposed to the vast diversity of conventional $\alpha\beta$ T cell clonotypes in which each recognises a unique antigenic epitope (Lepore et al., 2018). Importantly, these conserved receptors have unique functions and manifest emerging roles in the immune response against infectious diseases and cancer (Godfrey et al., 2018). Innate-like T cells can also detect a wide range of stress-induced biomarkers such as MHC class I chain-related (MIC) or UL16-binding protein (ULBP) molecules arising from cellular distress. Discrete populations of innate-like T cells are located in exposed organs and preferably present tissue-specific tropism for physical barrier tissues such as the skin, liver, or mucosa and epithelia of the intestine and lung tissues. In contrast, many others circulate in peripheral blood and lymph nodes (Fan and Rudensky, 2016).

Most innate-like T cells establish their response profile identities during thymic development, contrary to $\alpha\beta$ T cells that acquire their specification after experiencing antigen presentation in the periphery. Although as early thymocytes they commit to the dominant pathway of *Notch* signalling, this route is later repressed for the differentiation of the innate-like T cell fate (Cherrier et al., 2012; Rothenberg, 2019). Most of innate-like lymphocyte responses are frequently classified similar to $CD4^+$ Th cell groups, but innate-like T-cell effector functions are distinctively determined by induction of master transcription factors like promyelocytic leukemia zinc finger (PLZF) and GATA binding protein 3 (GATA3) that regulate their thymic differentiation and innate-like T-cell responses (Kreslavsky et al., 2009; Savage et al., 2008). Selected transcription factors continue to promote lineage-defining factors that de-

termine the type immune response and cytokine release assigning a set of different effector functions. For instance, T-box transcription factor TBX21 (T-bet) (Szabo et al., 2000) often co-expresses with eomesodermin (Eomes) (Zhang et al., 2018) to promote the development and functional differentiation of Th1-like responses and IFN-γ production, whereas they repress the opposed Th2 phenotype. The Th2 response is driven by the continuous expression of GATA3 and produces IL-5 and interleukin 13 (IL-13) among other cytokines that have a role against helminth infections and induce allergic reactions (Yagi et al., 2014). Distinctively, pro-inflammatory cytokines like interleukin 17A (IL-17A) are associated with the nuclear receptor RAR-related orphan receptor γ (RORγt) to regulate their identity (Ivanov et al., 2006).

Mature innate-like T cells preferentially migrate to non-lymphoid tissues to provide a defence against pathogenic intruders. They are particularly important at exposed barrier surfaces colonised by pathogens and play crucial roles in innate immune responses to either parasite or viral infections across various mucosal tissues (Godfrey et al., 2015; Khairallah et al., 2018). Innate-like T cell features include the ability to recognise distinct antigens and respond immediately eliciting direct targeted cytotoxicity right form the anatomical sites they reside (Vantourout and Hayday, 2013). Harnessing these cells is also of interest to prevent chronic inflammatory diseases, metabolic disorders, or even cancer (Chien et al., 2014; Gentles et al., 2015). Their potential is currently being developed in the clinic to benefit from their innate-like immunity and MHC-unrestricted characteristics, of which the later is decisive to avoid acute graft versus host disease (GvHD) in immunotherapeutic treatments (Godfrey et al., 2018; Sebestyen et al., 2020).

1.1.3 T-cell Recognition of Non-peptidic Antigens

Four main classes of antigens that activate T cells can be classified according to their chemical structure and composition: peptides, lipids, vitamin-B derivates, and small phosphorylated metabolites (Fig. 1.1). Usually, these immunogens are bound to cell-surface proteins to form an antigen-presenting complex that is recognised by antigen-specific TCRs. Canonical $\alpha\beta$ T cells recognise MHC class I or II bond to peptide fragments. However, unconventional innate-like T cells are known for recognising non-peptide antigens that are presented by largely monomorphic non-classic MHC molecules. Examples of these are CD1-restricted $\alpha\beta$ T cells or NKT cells responding to lipid-based compounds presented by CD1 isoforms or MAIT cells that recognise vitamin-B derivates loaded on MHC-related protein 1 (MR1) molecules (Adams and Luoma, 2013; Godfrey et al., 2015; Lepore et al., 2018). Small phosphorylated

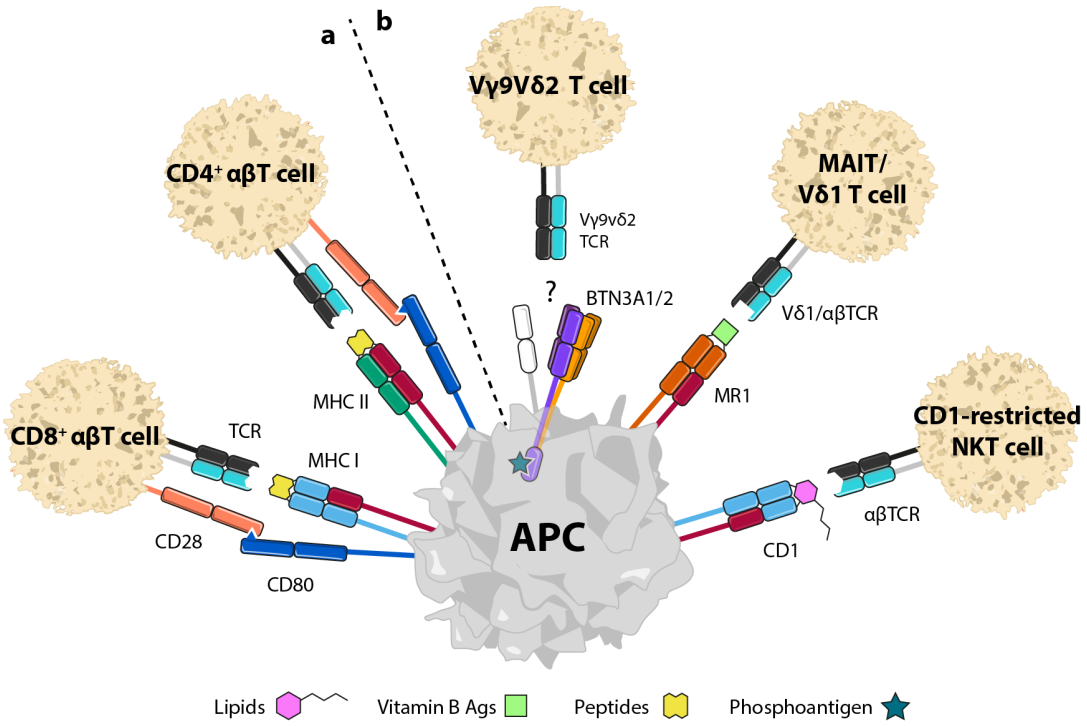

Figure 1.1: *Schematic diagram on the four current major antigen classes and their associated antigen-presenting molecules required for presentation to (a) conventional T cells and (b) unconventional innate-like T cells.*

metabolites, also termed phosphoantigens, uniquely activate $\gamma\delta$ T cells of the Vγ9Vδ2 subset (Brenner et al., 1986; Hata et al., 1988; Hayday et al., 1985; Kabelitz et al., 1991; Morita et al., 1999; Tanaka et al., 1995). Unconventional innate-like T cells arouse interest because of their predisposition to recognise unusual metabolic-related antigens that indicate the presence of many microbial infections or transformed cells like cancer (Godfrey et al., 2015; Kabelitz et al., 2004; Lança et al., 2010; Lepore et al., 2018; Morita et al., 1999).

Vitamin-B Derivates

A subset of MAIT and several $\gamma\delta$ T cells respond to transient metabolites generated in the synthesis of riboflavin when these are associated with cell-surface MR1 antigen-presenting complexes (Harriff et al., 2018; Le Nours et al., 2019). These antigens are mostly biosynthetic precursors of vitamin B_9 (folic acid) or vitamin B_2 (riboflavin) found in a range of bacteria, yeast, and plants, but not mammalian organisms. Such a metabolic exclusion probably contributes to the human defence system in discriminating self from non-self vitamin B derivates. All these compounds share similar chemistry with a bicyclic structure and ribityl tail but their antigenicity varies greatly from non-stimulatory antigen 6-formylpterin (6-FP) or acetyl-6-formylpterin (Ac-6-FP)

(Corbett et al., 2014; Eckle et al., 2014; Kjer-Nielsen et al., 2012) to potent metabolite activators of MAIT cells derived from the riboflavin metabolism (Corbett et al., 2014).

The refolding capability between the antigen and MR1 is what mostly determines the stimulating potential of these complexes to MR1-reactive T cells (Mak et al., 2017). Precursor elements of microbial vitamin derivates can diffuse in mucosal barriers and enter the cells to form adducts with compounds of other metabolic pathways. These form unstable metabolites 5-(2-oxoethylideneamino)-6-D-ribitylaminouracil (5-OE-RU) and 5-(2-oxopropylideneamino)-6-D-ribitylaminouracil (5-OP-RU) without the need of enzymatic reactions and became trapped by MR1 in a reversible covalent Schiff-base bond complex (Corbett et al., 2014). Unlike others, the antigen presentation process of MR1 does not constitutively present self-ligands or antigenic metabolites. MR1 is sequestered in the endoplasmic reticulum until merging vesicles with riboflavin derivate metabolites contact and bind to the MR1 antigen-binding groove. Presenting complexes migrate to the surface membrane but only those that remain stable reach the cell-surface for presentation (McWilliam et al., 2016). Although some of these complexes degrade in the process, during their transition towards the surface can recycle back and load new antigenic material. Thus, the success rate of antigen-presenting complexes that reach the surface increases despite being tightly regulated by the antigen affinity and availability (McWilliam et al., 2016).

Lipid Antigens

CD1 family members have distinct antigen-binding pockets that evolved to bind chemically to a range of lipid-based substrates. These substrates vary in the nature of their head groups (glycolipid, phospholipid, or ganglioside) which results in distinct binding efficiencies and discriminates their interaction between CD1 isoforms (Cotton et al., 2018; de Jong et al., 2014; Gadola et al., 2002; Zajonc et al., 2005). This evolutionary isomorphism might result from selective pressure that selected structurally conserved antigen moieties according to the antigen type they interact the most. The lipid acyl chain largely determines the orientation of its head group and loading efficiently in the CD1 binding groove. These grooves vary drastically in size and shape between different CD1 isoforms, and it is mostly reflected in how they accommodate the lipid tails. Each of these isoforms has a distinct expression pattern. CD1a is highly expressed on dendritic cell (DC) and Langerhans cells; CD1b is restricted to myeloid DCs of lymphoid organs; and CD1c is on B cells. However, CD1d is broadly distributed on many cell types, including monocytes, macrophages, B cells and epithelial cells.

The structure of these CD1 isoforms also varies in their cytoplasmic domain, which has unique motives responsible for trafficking across different endosomal compart-

ments (Mori et al., 2016). Isoform CD1a recycles in early endosomes, CD1b and CD1d are restricted to late endosomal vesicles, and CD1c can recycle in either early or late endosomes. The ability of these four isoforms to distinctively recycle in different endosomal compartments symbolise they individually survey a specific cellular compartment in which lipids with different characteristics accumulate.

Some polyclonal T cells recognise and react to CD1a isoform loaded with apolar skin oils, although the CD1a is usually loaded with ubiquitous inhibitory membrane lipid compounds that present a polar head group (de Jong et al., 2014). NKT and other CD1-restricted T cells with a semi-invariant antigen receptor recognise CD1a, -b, or -c isoforms loaded with a variety of lipid antigens (Borg et al., 2007; Spada et al., 2000). Instead, a less common type of invariant natural killer T cell (iNKT) responds more selectively to glycolipids like α-galactosylceramide (α-GalCer) presented only by the CD1d isoform (Bendelac et al., 1994), although some iNKT with diverse $\alpha\beta$ TCR and Vγ1Vδ1$^+$ T cells are also reactive to neuroendocrine glycolipid sulfatide (Jahng et al., 2004; Luoma et al., 2013; Miyamoto et al., 2001). INKT and Vδ1$^+$ $\gamma\delta$ T cells react a CD1d-α-GalCer complex too, albeit their affinity differs (Uldrich et al., 2013).

Stress-induced Molecular Ligands

Most cells have mechanisms to alert the immune system from cellular stress or malfunction. Under such conditions, they express stress-induced molecular markers that are recognised by non-TCR like the C-type lectin-like natural killer group 2 member D (NKG2D) receptor expressed by $\gamma\delta$ T cells, natural killer cell (NK), and several CD8 T cells. NKG2D recognises MIC-A and -B and six members of the ULBP family (Groh et al., 1998; Zingoni et al., 2018), and it can promote co-stimulatory and functional responses that are regulated by different biochemical mechanisms (Das et al., 2001a; Rincon-Orozco et al., 2005; Zhang et al., 2006). MIC molecules are also recognised by the Vδ1$^+$ TCR even though the affinity is much lower; thus, causing a competition of mutual exclusion (Bauer et al., 1999; Xu et al., 2011; Zhang et al., 2006). Other stress-related molecules have been identified, including a mitochondrial ATP synthase complex F_1-adenosine triphosphatase (F_1-ATPase) that is overexpressed during an active cell division of tumour cells. The Vγ9Vδ2 T subset particularly responds to F_1-ATPase in the addition of apolipoprotein A-I (A-I) (Scotet et al., 2005).

Phosphorylated Antigens

Phosphoantigens are low-molecular-weight molecular intermediates that are specifically recognised by Vγ9Vδ2 T cells in a in a TCR-dependent manner (Espinosa et al., 2001; Morita et al., 1999; Pfeffer et al., 1990). These metabolites are ubiquitously present in all living cells and regarded indispensable precursors of the isoprenoid synthesis that yields to cholesterol, vitamin K, coenzyme Q10, and steroid hormones needed for diverse cellular functions and growth. Their source varies among organisms that use distinct metabolic routes. *Eukarya*, *archaea*, *fungi*, and the cytosol and mitochondria organelles of plants use the *mevalonate* pathway to synthesise isoprenoid compounds, whereas chloroplasts and most *eubacteria* and *apicomplexia* parasites have a mevalonate-independent, aka *non-mevalonate* or 2-C-methyl-D-erythritol 4-phosphate/1-deoxy-D-xylulose 5-phosphate (MEP/DOXP) pathway that supports the production of isoprenoids (see Fig. 1.3) (Goldstein and Brown, 1990; Rohmer, 1999). Although the chemical core of phosphoantigens can vary, they conserve two or more phosphoantigen groups located at the distal end of their organic oligo-carbon skeleton and are generally below 500 Da (Fig. 1.2).

Eukaryotic cells convert the mevalonate into two isopentenyl pyrophosphate (IPP) molecules that are subsequently catalysed by the farnesyl pyrophosphate synthase (FPPS) to yield dimethylallyl pyrophosphate (DMAPP), both metabolites known to activate $\gamma\delta$ T cells (Fig. 1.3). Other forms of eukaryotic phosphoantigens like G3P or triphosphoric acid 1-adenosin-5-yl ester 3-(3-methylbut-3-enyl) ester (ApppI) also exist and stimulate Vγ9Vδ2 T cells, although they are required at much higher doses (Sandstrom et al., 2014; Vantourout et al., 2009). In cancer, however, the demand for cholesterol and related compounds needed for growth increases this metabolic rate, and so does the presence of phosphoantigens that accumulate in their cytoplasm. This sudden increment of phosphoantigens is sensed by antigen-presenting molecules and cause activation of Vγ9Vδ2 T cells (Gober et al., 2003; Goldstein and Brown, 1990). Other methods of pharmacological interest to externally induce the presence of phosphoantigens in eukaryotic cells is the use of synthetic FPPS inhibitors such as the amino-bisphosphonate drugs, which are described in Table. 1.1 and Figure. 1.4b (Benzaïd et al., 2011; Russell et al., 1999). These drugs have been widely used to treat osteoporosis and bone metastases before observing their incidentally indirect effects enhancing phosphoantigen-derived immune responses from Vγ9Vδ2 T cells.

Most bacteria use the non-mevalonate pathway to yield end-substrates IPP and DMAPP, which then incorporate to the synthesise of isoprenoid and derivates. A particularity of this metabolism is that produces (E)-4-hydroxy-3-methyl-but-2-enyl py-

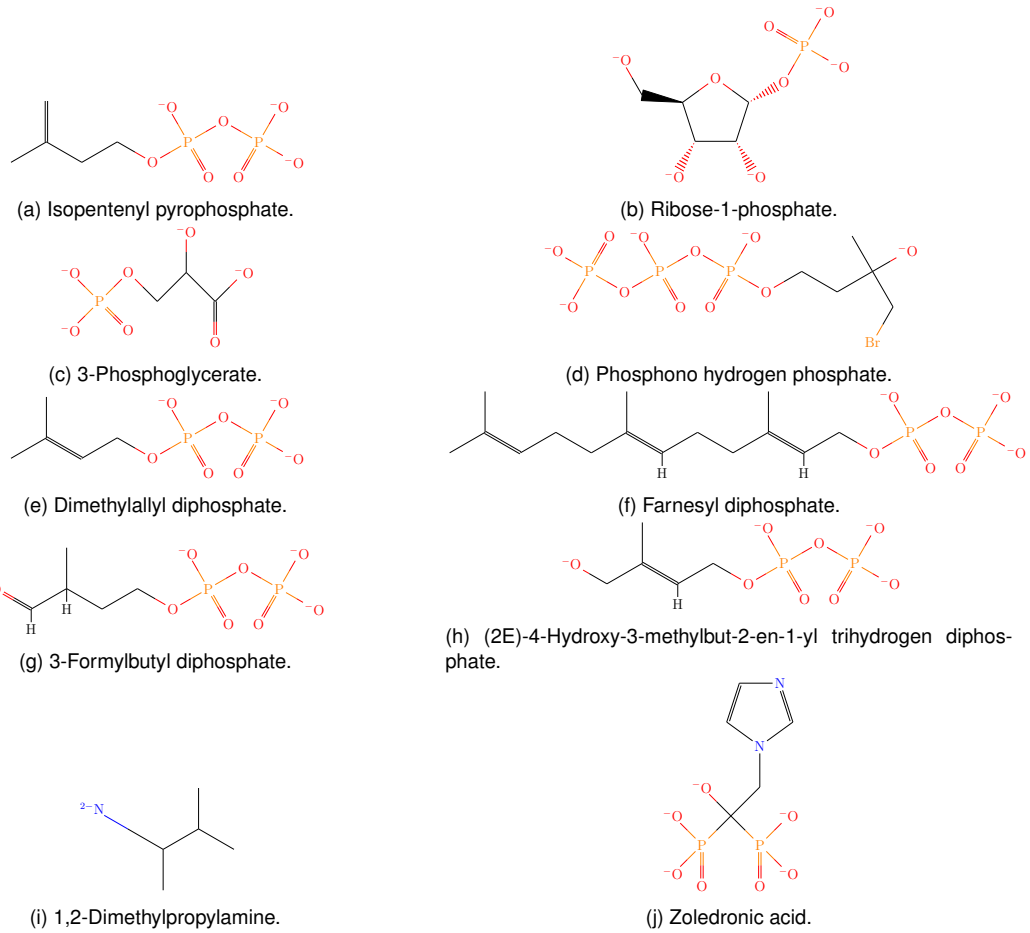

(a) Isopentenyl pyrophosphate.

(b) Ribose-1-phosphate.

(c) 3-Phosphoglycerate.

(d) Phosphono hydrogen phosphate.

(e) Dimethylallyl diphosphate.

(f) Farnesyl diphosphate.

(g) 3-Formylbutyl diphosphate.

(h) (2E)-4-Hydroxy-3-methylbut-2-en-1-yl trihydrogen diphosphate.

(i) 1,2-Dimethylpropylamine.

(j) Zoledronic acid.

Figure 1.2: *Chemical composition of (a-f) endogenous and (g-h) microbial phosphoantigen, (i) alkene, and (j) aminobisphospohante zoledronate drug compounds that stimulate Vγ9Vδ2 T cells.*

Table 1.1: *Registered bisphosphonates and they respective capacity to inhibit recombinant human FPPS at 0.1* µM *10* min *dose, by Dunford et al. (2001). Only nitrogen-containing bisphosphonates target specifically the enzyme FPPS of the mevalonate pathway. R1 and R2 indicate adaptations from a carbo-pyrophosphate scaffold group in Fig. 1.4b. Nitrogen containing (NBS) and non-nitrogen containing (NNBP) groups.*

Generation	*Name*	*R1*	*R2*	*Inhibition (%)*	*Type*
First	Clodronate	C	Cl	5	NNBP
Early	Etidronate	OH	CH_3	10	NNBP
Second	Tiludronate	H	$CH_2-S-\text{phenyl}-Cl$	10	NNBP
Second	Pamidronate	OH	$CH_2CH_2NH_2$	40	NBS
Second	Alendronate	OH	$(CH_2)_3NH_2$	60	NBS
Third	Ibandronate	OH	$CH_2CH_2N(CH_3)(\text{pentyl})$	78	NBS
Third	Incadronate	H	$C_8H_{19}NNa_2O_7P_2$	80	NBS
Third	Risedronate	OH	$CH_2-3-\text{pyridine}$	95	NBS
Third	Minodronate	OH	$CH_2-2-\text{imidazo}-\text{pyridinyl}$	100	NBS
Third	Zoledronate	OH	$CH_2-(\text{imidazole})$	100	NBS

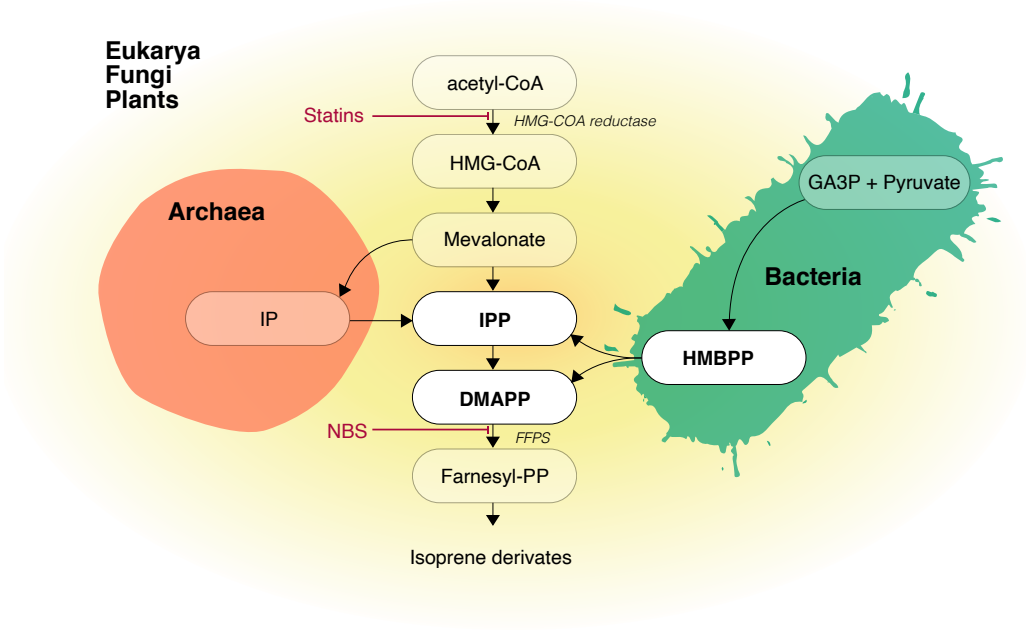

Figure 1.3: *Isoprene biosynthesis in eukaryotic organisms rely on the mevalonate metabolic pathway, whilst most bacteria use an alternative biosynthetic pathway independent of mevalonate metabolites. Statins inhibit HMB-CoA reductase and stop the eukaryotic isoprene synthesis. Aminobisphosphontates (NBS) inhibit FPPS resulting in an accumulation of prenyl pyrophosphates such as IPP and DMAPP.*

(a) Pyrophosphat (b) Bisphosphonat

Figure 1.4: *Bisphosphonates are considered analogs of the pyrophosphate. The replacement of the oxygen pyrophosphate linker for a carbon atom attached to two radical groups confers a stable solute that is able to bind into the binding pocket of the FPPS enzyme to inhibit its functional activity.*

rophosphate (HMBPP), a natural intermediate that is the most potent known activator of $\gamma\delta$ T cells (Morita et al., 2000; Puan et al., 2007). The HMBPP microbial phosphoantigen is found in many bacteria including pathogenic stains of *Escherichia coli*, *Yersinia enterocolitica*, *Mycobacterium tuberculosis*, and in also in malaria parasites among other infectious pathogens (Eisenreich et al., 2004; Morita et al., 2000; Puan et al., 2007). However, its potency in vitro is about 10,000-fold when compared to IPP or amino-bisphosphoante drugs (Fig. 1.5) (Rhodes et al., 2015). Nonetheless, other microbial compounds apart from this major microbial product are the mycobacterial antigens TUBag with identical molecular weight and chemical composition that reach similar potency to stimulate $\gamma\delta$ T cells (Feurle et al., 2002; Morita et al., 1999). Bacterial species lack the non-mevalonate pathway and use the classical mevalonate pathway instead, such as *Streptococcus*, *Staphylococcus*, and *Borrelia*, do not produce HMBPP nor are able to activate Vγ9Vδ2 T cells specifically. Besides, following the immense potential of these microbial antigens, many HMBPP-related synthetic substances are recently being synthesised in the laboratory to use as drug compounds, some of which are in clinical trials (Bennouna et al., 2010; Boëdec et al., 2008; Hsiao et al., 2014; Kilcollins et al., 2016; Okuno et al., 2020)

Phosphoantigens usually accumulate in infected or metabolically distressed cells to activate Vγ9Vδ2 T cells. All these share a pyrophosphate or triphosphate nucleotide moiety linked through the terminal phosphate to a short alkyl chain normally containing five carbons (Espinosa et al., 2001; Morita et al., 2001) Composition seems to vary the potential to stimulate Vγ9Vδ2 T cells (Table. 1.5). The group of *Mycobacteria tuberculosis* antigen species (TUBags) have a formyl-alkyl diphosphate core which weakens their stimulatory capacity in comparison to HMBPP, like that of *Escherichia coli* (Zhang et al., 2006). But, spacial conformation between isomers should reflect the stimulatory potential by a marginal difference only (Boëdec et al., 2008). Some structures that contain monoethyl phosphate, 2,3-diphosphoglyceric acid, β-D-ribosyl phosphate, xylose-1-phosphate, and glycerol-3 phosphoric acid, differ more drastically and so require much higher concentrations for triggering immune responses by $\gamma\delta$ T cells. However, many of these can be modified synthetically at the phosphodiester bond linking the alkyl chain to its proximal phosphate of eukaryotic phosphoantigens by a phosphatase-resistant phosphonate bond (Zgani et al., 2004). This simple modification leads to compounds with increased bioactivity. Though the opposed effect is observed increasing their allylic or alkyl side chains (Zgani et al., 2004).

It has been hypothesised that phosphoantigens move through the cells' plasma membrane via transmembrane transporters or inside-out mechanism by a transmembrane transfer protein whose activity is either ATP-dependent or driven by the con-

centration gradient, instead of a passive transport given their low molecular masses. Transporter multidrug resistance-associated protein 5 (MRP5) can have a role as inhibitors of this unidirectional transmembrane protein prevent activation of Vγ9Vδ2 T cells, whereas its enforced expression in Burkitt's lymphoma Daudi cell line induces tumour necrosis factor-α (TNF-α) secretion akin applying amino-bisphosphonate drug zoledronate (Kistowska, 2009). Given the fact that other studies suggest phosphoantigens interact intracellularly (Salim et al., 2017), the role of these transporters is more likely to be involved in increasing a secondary co-stimulatory signal transduction factors. Noteworthy, similar transmembrane transporters internalise microbial phosphoantigens into professional accessory cells.

1.2 The Biology of $\gamma\delta$ T Cells

Most $\gamma\delta$ T cells are double negative (CD4$^-$ CD8$^-$) innate-like lymphocytes that generate antigen-specific TCR receptors via recombination-activating genes (RAGs) and somatic V(D)J recombination of the γ and δ gene loci in the thymus (Brenner et al., 1986; Hayday et al., 1985; Pereira et al., 2012). These combinatory repertoires offer a rage of combinatory possibilities that depends on the species evolutionary background (Table. 1.2). Despite the number of γ/δ V(D)J recombination segments is more limited than those expressed by $\alpha\beta$ T cells, they possess vital roles in the immune system since birth and co-operate with other immune cells to contribute in the host immune defence. Occasionally, human Vδ regions can rearrange with Jα-Cα to form a productive TCR α chain, which can then pair with a TCRβ chain and give rise to a hybrid (δ)/$\alpha\beta$TCR (Pellicci et al., 2014). The recombining process of the $\gamma\delta$TCR can sometimes present multiple D segments in tandem and theoretically, comprise a higher level of diversity than $\alpha\beta$ T cells, albeit this fact is not observed in practice(Hata et al., 1988).

During the maturation process of $\gamma\delta$ T cells, thymic epithelia may express cell-surface markers like Skint-1 and -2, in mice, to promote function differentiation and pre-commit $\gamma\delta$ T-cell identities (Jandke et al., 2020; Turchinovich and Hayday, 2011). These and other specific functional $\gamma\delta$ T-cell profiles usually associate with the type of $\gamma\delta$TCR they use and tend to home tissue-specific localisations (Table. 1.3). Although $\gamma\delta$ T cells represent between 0.5–10 % of total circulating lymphocytes in adult humans and mice (Cairo et al., 2010; Parker et al., 1990), they are predominantly more abundant within preferential anatomical epithelial tissues or mucosal sites (Hayday, 2009; Vantourout and Hayday, 2013). The human $\gamma\delta$ T cell repertoire is mainly differentiated by the expression of their Vδ2 gene segment. The vast majority of them

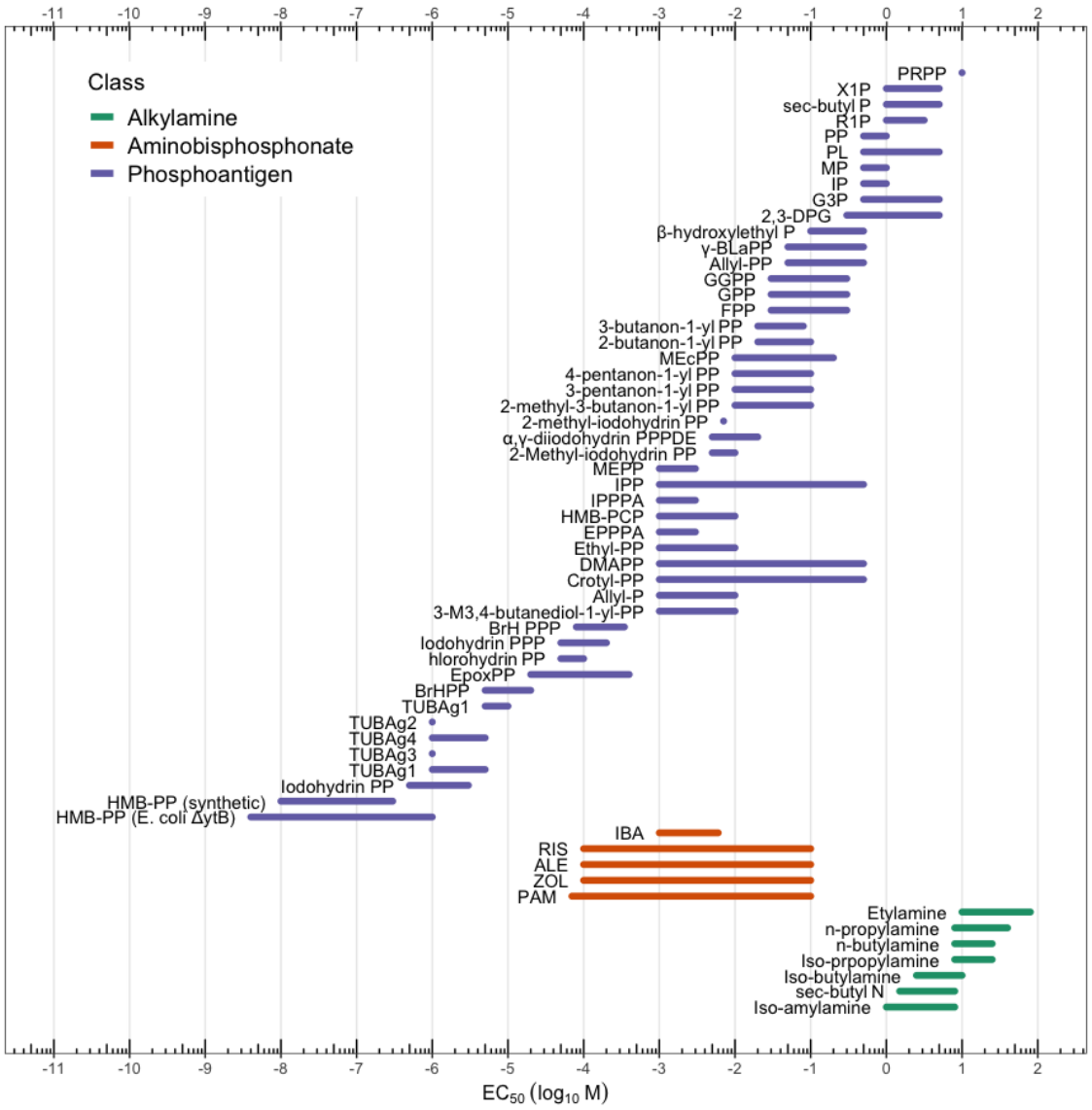

Figure 1.5: *Collection of data depicting a conservative estimate of half maximal effective concentration (EC_{50}) range for various substances activating human Vγ9Vδ2 T cells. Data rendered from the literature (Belmant et al., 2000; Bukowski et al., 1999; Constant et al., 1995; Das et al., 2001b; Espinosa et al., 2001; Gennaro, 1997; Gossman and Oldfield, 2002; Häcker et al., 1992; Morita et al., 2000; Poquet et al., 1996; Tanaka et al., 1996; Wang et al., 2003)*

Table 1.2: *Genomic V(D)J and C gene loci that following recombination processes form a double chain TCR in human or mouse. Pseudogenes and subgroups may exist (Allison and Garboczi, 2002; Lefranc et al., 2015).*

$\gamma\delta$	*Human*	*Mouse*	$\alpha\beta$	*Human*	*Mouse*
Cδ	1	1	Cα	1	1
Vδ	3	11	Vα	41	23
Dδ	3	2	Dα	-	-
Jδ	4	2	Jα	61	61
Cγ	3	4	Cβ	2	2
Vγ	11	7	Vβ	30	31
Dγ	-	-	Dβ	2	2
Jγ	5	4	Jβ	14	14

are Vδ2$^+$ and mostly pair with the Vγ9. Contrary, in anatomical sites like the skin or intestine, the non-Vδ2$^+$ phenotype predominates with a Vδ1 or Vδ3 paired with diverse γ chains (Deusch et al., 1991; Ebert et al., 2006; Toulon et al., 2009). Notably, peripheral blood Vγ9Vδ2 T cells are found in human, other primates, and more recently described in the alpaca (Fichtner et al., 2020), but they are absent in rodents (Karunakaran et al., 2014).

The $\gamma\delta$TCR generally recognise antigens by non-classic MHC antigen-presenting molecules like CD1 or MR1, and probably other unknown ligands (Benveniste et al., 2018; Gu et al., 2018; Le Nours et al., 2019; Uldrich et al., 2013). They can also respond to the presence of soluble antigens like histidyl-tRNA synthetase (HARS) in humans or algae protein R-phycoerythrin (PE) in both human and mouse species (Zeng et al., 2012). Recognition of soluble antigen seems to allow $\gamma\delta$ T cells to self-activate and induce a rapid response with production of IL-17A before developing adaptive immunity (Bruder et al., 2012; Zeng et al., 2012). However, a generally observed pattern in primate $\gamma\delta$ T cells is their ability to respond rapidly and generate immune responses upon stimulation with phosphoantigens.

1.2.1 Human and Mouse Diversification of $\gamma\delta$ T cells

In early human development, the non-Vδ2$^+$ T-cell phenotype dominates the population consisting mostly of the Vδ1$^+$ paired to diverse γ chains (Rosa et al., 2004). They contribute to the first line of defence in blood, epithelial tissues, and mucosa lining surfaces. These, mostly naive non-Vδ2 cells, recognise diverse microbial antigens before the adaptive system acquires specific and memory immunity following

Table 1.3: *Predominant recombined $\gamma\delta$ TCR variants across tissue-specialised localisation in adult human and mouse species.*

Species	*Tissue location*	*Predominant subset*	*Reference*
Human	Dermis	Vδ1	(Toulon et al., 2009)
	Gut epithelia	Vδ1Vγ4, Vδ1 and Vδ3	(Deusch et al., 1991)
	Liver	Vδ1 and Vδ3	(Bonneville et al., 2010)
	Peripheral blood	Vγ9Vδ2	(Deusch et al., 1991)
	Spleen	Vδ1	(Bonneville et al., 2010)
	Thymus	Vδ1	(Bonneville et al., 2010)
Mouse	Adult thymus	Diverse	(Itohara et al., 1990)
	Epidermis	Vγ5Vδ1 (DETC)	(O'Brien and Born, 2015)
	Gut epithelia	Vγ7Vδ4, Vγ7Vδ5 and Vγ7Vδ6	(Itohara et al., 1990)
	Peripheral blood	Vγ4	(Itohara et al., 1990)
	Liver	Vγ1Vδ6.3, Vγ4 and Vγ6	(Gerber et al., 1999)
	Lung epithelia	Vγ4 (adult) and Vγ6 (natal)	(Sim et al., 1994)
	Lymph nodes	Vγ4 and diverse	(Itohara et al., 1990)
	Mouth tissue/ meninge	Vγ6	(Itohara et al., 1990)
	Spleen	Vγ1 and Vγ4	(Gerber et al., 1999)
	Utero-vaginal epithelia	Vγ6Vδ1	(Itohara et al., 1990)

experiences with antigens. The other main group of $\gamma\delta$ T cells consisting of the V$\delta2^+$ phenotype remains behind at lower frequencies during a natal stage until they expand quickly during the first year of life in peripheral blood reasonably from resulting multiple encounters with antigen (Parker et al., 1990; Rosa et al., 2004).

Mouse $\gamma\delta$ T cells are generated throughout a strict developmentally programme that goes in waves of phenotypic maturation driven by the expression of the γ-chain segment (Carding and Egan, 2002; Heilig and Tonegawa, 1986). Each murine $\gamma\delta$ T cell that expresses a unique Vγ-gene segment leave the thymus at a defined time points during foetal development. These egress the thymus and migrate to preferential epithelial tissues where remain differentiated and provide tissue-specific protection. The murine $\gamma\delta$ T-cell development begins fortnight pre-birth with the dendritic epidermal T cell (DETC) Vγ5Vδ1 phenotype (O'Brien and Born, 2015). Those with the expression of the Vγ6 gene segment recombined with a diverse repertoire of δ-chains preferentially migrate to the uterus, lung, and tongue tissues (Itohara et al., 1990). The Vγ4 phenotype migrates to lymphatic nodes, spleen, blood, and a few to the lungs (Sim et al., 1994). Instead, some V$\gamma7^+$ murine lymphocytes mature independently from the thymus and prevail in intestinal intra-epithelial tissues (Carding and Egan, 2002).

1.2.2 Roles of $\gamma\delta$ T Cells in Innate and Adaptive Immunity

A distinct feature of the $\gamma\delta$ T cells is to bridge innate and adaptive immunity by engaging cellular *cross-talks* with other immune cell types (Brandes et al., 2009; Girard et al., 2020; Meuter et al., 2010).

Humoral Immunity

Mouse $\gamma\delta$ T cells can mediate B-cell antibody class switching in $\alpha\beta$-deprived mice (Wen et al., 1996). Similarly, the production of IgG1 and IgE is also possible from a murine DETC subset, albeit in a NKG2D-dependent signalling (Strid et al., 2011). Indeed, human $\gamma\delta$ T cells also influence the adaptive immune response after their activation through interaction with peripheral DC (Banchereau and Steinman, 1998; Eberl et al., 2004; Girard et al., 2020) or B cells in reactive secondary lymphoid tissues (Caccamo et al., 2006). Following in-vitro phosphoantigen stimulation, human Vγ9Vδ2 T-cells can produce IL-2, IL-4, and interleukin 10 (IL-10) and upregulate CXC chemokine receptor-5 (CXCR5) during the three first days post-stimulation, albeit then the expression of CXCR5consistently decreases (Caccamo et al., 2006). These activated Vγ9Vδ2 T cells also expressed co-stimulatory molecules ICOS and CD40L, and unless they were blocked, production of IgM, IgG, and IgA antibodies was detected in the supernatant of B-cells isolated from the tonsil of the same individual (Caccamo et al., 2006). Human phosphoantigen-stimulated peripheral blood Vγ9Vδ2 T cells receiving interleukin 21 (IL-21) signals also reported to generate CXC chemokine ligand-13 (CXCL13), a B-cell chemoattractant, which emphasises the capacity of these major Vγ9Vδ2 T-cell subset to influence on hormonal immunity (Vermijlen et al., 2007). These adaptations might be necessary in adults but predominantly vital during early developmental stages, when the organism prepares its defence against intruding pathogens and copes with a myriad of environmental challenges with an undeveloped adaptive immunity.

Priming $\alpha\beta$ T Cells

A few reports have shown that human $\gamma\delta$ T cells can take afferent roles equivalent to tissue-associated DCs or macrophages after phagocytosis processes and actively migrate to lymph nodes to prime adaptive immunity. Phosphoantigen-induced Vγ9Vδ2 T cells were observed to up-take soluble antigens and subsequently upregulated antigen-presenting markers such as CD40 and intercellular adhesion molecule 1 (ICAM-1) and CCR7, among many other chemokine receptors (CXCR3, CCR1, CCR2 and CCR5) that promote migration to lymph nodes (Brandes et al., 2005). Also, $\gamma\delta$

T cells can process microbial antigens and upregulate transcription of MHC class II genes along with both co-stimulatory molecule B7-1 (CD80) and co-stimulatory molecule B7-2 (CD86) receptors usually linked to immune synapse (Brandes et al., 2009). At one occasion and under the presence of high antigen loads, Vγ9Vδ2 T cells have been able to present antigen, and prime naive $\alpha\beta$ T cells with comparable efficiently to DCs or monocytes, but their antigen-presenting activity decreased when the presence these products were low; thus, limiting their sensibility threshold (Brandes et al., 2005; Moser and Eberl, 2011).

Mouse DETC afferent roles are rare, and only surveillance of the basal and apical epidermis near the squamous keratinocyte tight junctions are observed in some tissues. These cells seem to be able to engage in a steady-state, and TCR-dependent manner cell clusters in the skin, where the immune synapse might take place (Chodaczek et al., 2012). Such activity is independent form co-stimulatory NKG2D receptor and could be mediated through the integrin αEβ7 (aka CD103) complex, a typical membrane protein in professional antigen-presenting DCs (Chodaczek et al., 2012). Foetal murine DETC were also described in the thymus to play a role in medullary epithelial Skint1-expressing cells and autoimmune regulator during the $\alpha\beta$ T-cell thymic selection (Hayday and Tigelaar, 2003).

1.2.3 Emerging Role of $\gamma\delta$ T Cells in Infectious Diseases

Many reported bacteria and parasite infective species promt clonal expansion of peripheral blood $\gamma\delta$ T cells (Eberl et al., 2003; Morita et al., 2000, 2007). Intracellular bacterial infections may realise microbial phosphoantigen compounds after they infect cells or are phagocyted by immune cells. Extracellular pathogens, on the other hand, could potentially leave a trace of diffusion phosphoantigen molecules that might be later integrated by antigen-presenting cells throughout their membranes. Some other hypotheses state that cellular transmembrane transport-related proteins could promote antigen intake.

Tuberculosis

Vγ9Vδ2 T cells protect against live *Mycobacterium tuberculosis* and can contain the disease (Li et al., 1996). During acute and chronic phases of the infection, they display different pattern responses and promote the activity of several adaptive $\alpha\beta$ T cells (Boom et al., 1992; Brandes et al., 2005; Kabelitz et al., 1991). In the active states of the disease, Vγ9Vδ2 T cells can proliferate and expand to constitute as much as 65–90 % of total peripheral blood $\gamma\delta$ T cells and form activation clusters at the site

of infection (Chen et al., 2008). The healing potential of Vγ9Vδ2 T cells was demonstrated in primate cynomolgus macaques (*M. fascicularis*). The study demonstrated a major Vγ9Vδ2 T cell clonal expansion response reduces the microbial burden and attenuates tuberculosis lesions caused in the lung tissue (Chen et al., 2013). These Vγ9Vδ2 immune responses diverged into effector populations capable of producing anti-TB cytokines IFN-γ, perforin and granulysin, reducing growth of intracellular bacteria. Importantly, Vγ9Vδ2 T cells undertook clonal expansion and enhanced further pulmonary responses driven by peptide-specific Th1-like $\alpha\beta$ T cells, which constituted increased resistance to tuberculosis (Chen et al., 2013).

Concerning to animal trials with th most common and primarily used *Mycobacterium bovis* Bacille Calmette-Guérin (BCG) vaccine, phosphoantigen-specific Vγ9Vδ2 T cells have shown to actively expand and acquire a memory-type response in post-vaccinated macaques, just days after intravenous infection (Shen et al., 2002). More recently, this population represented one of the primary T-cell subsets to expand during the first two weeks post-inoculation(Darrah et al., 2020).

Malaria

Human peripheral blood Vγ9Vδ2 T cells control the development of *Plasmodium sp.* infection at its merozoite stage. Although they provide continuous surveillance with an increased population in patients suffering from malaria, the protective mechanism is unknown (Zaidi et al., 2017). This parasite produces HMBPP (Emami et al., 2017), which might maintain activated Vγ9Vδ2 T cells in circulation and prolonged secretion of granzymes (Costa et al., 2011). The role of co-stimulatory receptor CD28 might also enhance the effectiveness of these lymphocytes response along a IL-2 and interleukin 15 (IL-15) signal survival loop. Strategies to achieve long-term protection attenuated whole-parasite malaria vaccines shed light in conferring durable immunity and maintain elevated numbers of circulating Vγ9Vδ2 T cells for enhanced and preserved immunosurveillance. More recent advances show an in-vivo stimulation after a three-dose regimen vaccination increased the relative number of Vγ9Vδ2 T cells up to one-third of total T cells in peripheral blood (Lyke et al., 2017).

Viral Infections

Some evidence suggests that $\gamma\delta$ T cells have a role in response to viral infections by lysing virally infected cells such as in influenza, human immunodeficiency virus (HIV), and cytomegalovirus (CMV). Although immediate cytolytic activities often characterise $\gamma\delta$ T cells, there is growing evidence they can take other roles in triggering adaptive

and humoral responses when needed (Chen et al., 2018; Maloy et al., 1998). In-vivo expanded $\gamma\delta$ T cells using amino-bisphosphonate drugs can enhance immune responses against viral infections (Li et al., 2013; Poccia et al., 2009; Tu et al., 2014). This expanding method is becoming more common due to the relatively abundant Vγ9Vδ2 T cells in human blood and facilitates to obtain large numbers of them in vitro with the use of phosphoantigens, which is gaining an important role against viral protection.

Studies show that phosphoantigen-expanded $\gamma\delta$ T cells lyse influenza-infected monocyte-derived macrophages (moDC) (Qin et al., 2009) and lung alveolar epithelial cells (Li et al., 2013) to inhibit viral replication. These cells required cell-to-cell contact and NKG2D and their response was mediated by Fas-Fas ligand and perforin-granzyme B pathways. The importance of $\gamma\delta$ T cells in the influenza infection also highlights their synergy with $\alpha\beta$ Tfh cells and humoral response, where they enhance the potential of CXCR5$^+$ CD4 Tfh to induce B-cell IgM and IgG production subsequent to virus-specific infection in humanised mice (Chen et al., 2018). The relation between $\gamma\delta$ T cells and the humoral response has also been observed in murine vesicular stomatitis virus (VSV)-infected models (Maloy et al., 1998). Another study in a mouse model demonstrated the capacity of human Vγ9Vδ2 T cells to be expanded (8-fold) in vivo and cleared the viral infection of one strain (H1N1), but not another (H5N1) (Tu et al., 2014). Together, these reports demonstrate that $\gamma\delta$ T cells respond to some viral influenza strains, and using expanding phosphoantigen-reactive $\gamma\delta$ T cells can offer a more comprehensive immune response to control the disease.

Both Vγ9Vδ2 and Vδ1 T cell subsets seem to respond against HIV infection although in a case-scenario which each associate with the early infection or chronic stage of the disease, respectively (Li et al., 2008). In an early stage, the virus stresses cells and might demand to increase the mevalonate pathway to produce cholesterol-related compounds, indirectly causing an abrupt accumulation of intracellular phosphoantigens and eventual Vγ9Vδ2 T-cell expansion (van 't Wout et al., 2005). During these high viral loads, Vγ9Vδ2 cells also associated with an abundance of circulating CD4$^+$ T cells (Li et al., 2008), suggesting there could be a relation between the two cell types as observed in later influenza-related studies (Chen et al., 2018). However, in the chronic state, the population of Vγ9Vδ2 cells decreases, while Vδ1 T cells take over along CD8$^+$ T cells (Cocchi et al., 1995). Whereas it seems that Vγ9Vδ2 T cells lose their potential in the chronic state, an unusual CD16$^+$ Vδ2$^+$ T cell subset could dominate the infection with antibody-dependent cellular cytotoxicity (ADCC) degranulation against viral-infected cells to control the disease (He et al., 2013). Besides, an HIV-infected cohort were reported to transiently manage infection increasing the

Table 1.4: *The population of Vγ9Vδ2 T cells directly recognise a series of cancer cells types and hold the potential to eradicate the tumour.*

Cancer type	*Reference*
Breast Cancer	(Dhar and Chiplunkar, 2010; Janssen et al., 2020)
Colorectal carcinoma	(Bouet-Toussaint et al., 2008; Corvaisier et al., 2005)
Hepatocellular carcinoma	(Bouet-Toussaint et al., 2008)
Lung	(Kang et al., 2009)
Lymphoma	(Lança et al., 2010)
Multiple myeloma	(Kunzmann et al., 2000)
Melanoma	(Cordova et al., 2012; Corvaisier et al., 2005; Toia et al., 2016)
Prostate	(Petrovics et al., 2005)
Renal cell carcinoma	(Viey et al., 2005)

Vγ9Vδ2 T-cell numbers following treatment with amino-bisphosphonate zoledronate drug and IL-2 (Poccia et al., 2009).

Unlike influenza and HIV infections, the $\gamma\delta$ T cell anti-viral role in CMV seems to be controlled by the V$\delta2^-$ subset. Their functions could be relevant for immunosuppressed organ CMV-seropositive recipients, where virtually all V$\delta2^-$ T cells exhibit a cytotoxic memory effector phenotype (Pitard et al., 2008). Trials with polyclonal V$\delta2^-$ T cell lines from CMV-seropositive healthy donors lysed CMV-infected targets in all cases and could be further expanded to treat transplantation recipients. This effector memory V$\delta2^-$ T cell activity seems to be CMV-specific response as they do not react to Epstein-Barr virus (EBV) (Knight et al., 2010).

1.2.4 Cancer Immunotherapy with $\gamma\delta$ T Cells

Patients with an abundance of $\gamma\delta$ T cells in blood cancer or solid tumours represented the most favourable prognostic according to a study with a large dataset (Gentles et al., 2015). This work demonstrates excellent potential for $\gamma\delta$ T cells in future immunotherapeutic uses. However, not all clinical trials have been showing promising outcomes (Godfrey et al., 2018). Table. 1.4 shows some reports which used Vγ9Vδ2 T cells were examined for their efficiency in cancer therapy, discussed herein.

Human blood Vγ9Vδ2 T cells infiltrate in tumour sites and can actively be involved in tumour immunosurveillance in different cancer types (Table 1.4). Their presence in melanoma sites correlates with an absence of metastasis; thus, they contribute to preventing the dissemination of the disease and immunosurveillance roles (Cordova et al., 2012). Moreover, they are associated with lower mortality and relapse rates (Toia et al., 2016). In vitro phosphoantigen-expand $\gamma\delta$ T-cells generates leucocyte

common antigen and cell activation assistant tyrosine phosphatase receptor type-C (CD45)$^+$ TNF-receptor of memory cells (CD27)$^-$ effector memory Vγ9Vδ2 T cells which often secrete Th1-like cytokines capable of reducing malignant cells as shown in melanoma (Cordova et al., 2012), hepatocellular carcinoma (Bouet-Toussaint et al., 2008), colorectal carcinoma (Bouet-Toussaint et al., 2008; Corvaisier et al., 2005), and renal tumour cells (Viey et al., 2005). Although $\gamma\delta$ T cells respond rapidly to phosphoantigen-induced stimulus, the uptake of amino-bisphosphonate drugs in tumour cell lines varies and does not seem to be productive in lymphoma, myeloid leukaemia, or mammary carcinoma cell lines, which show relative resistance. Instead, renal cell carcinoma cells are more susceptible to amino-bisphosphonate zoledronate drug, and its use enhanced the antitumoural Vγ9Vδ2 T cell response (Idrees et al., 2013). Of note, amino-bisphosphonate drugs in peripheral blood may be absorbed by neutrophils and mitigate or produce adverse effects in long-term or elevated doses, effects of which should be taken under consideration (Kalyan et al., 2014).

Elevated levels of infiltrated Vγ9Vδ2 T cells with a functional memory phenotype were found in subjects with renal cell carcinoma (Viey et al., 2005). After in vitro phosphoantigen challenge, these primary cells appear to elicit selective cytolysis to autologous renal tumour cells but not healthy renal cells in a TCR- and NKG2D-dependent manner (Viey et al., 2005). Similarly, Vγ9Vδ2 T cells relay on TCR and NKG2D signalling to induced TNF-α and IFN-γ secretion against allogeneic colon carcinoma and melanoma cell lines (Corvaisier et al., 2005). Their antitumor response against the colon cell lines is dependent on IPP production and ICAM-1 by the target cells (Corvaisier et al., 2005). Additionally, TCR-dependent Vγ9Vδ2 T-cell antitumor activity against hepatocellular and colorectal carcinoma established cell lines were enhanced by NKG2D co-stimulation (Bouet-Toussaint et al., 2008). These tumour targets presented surface levels of both stress-related markers MICA and ULBP, which indicates the $\gamma\delta$ T-cell response could be driven not only by a single cellular signal but multiple signal-inducer tumour-related ligands.

Blood cancer clinical trials with Vγ9Vδ2 T-cell infusions show promising outcomes. Clinical trials that transfused $\gamma\delta$ T cells into patients who had leukaemia improved their recovery and survival rates as demonstrated in an eight-year follow-up study (Godder et al., 2007). Infusing $\gamma\delta$ T cells to augment the level of host $\gamma\delta$ T-cells has no noticeable effect in acute GvHD (Godder et al., 2007). This intrinsic biological attribute in Vγ9Vδ2 and other innate-like T cells to recognise malignant cells without causing GvHD makes them principle allies for future immunotherapeutic treatments.

Engineering $\gamma\delta$ T cells for cancer immunotherapeutic treatments is underway. Gründer et al. (2012) recombined V segments in Vγ9Vδ2 TCRs to increase receptor

affinity for their molecular ligands on target cancer cells. Deniger et al. (2013) have propagated polyclonal $\gamma\delta$ T cells and rendered them bispecific through the expression of a B-lymphocyte surface antigen B4 (CD19)-specific chimeric antigen receptor T cells to increase specificity against B lymphoma cancers. These CD19-specific chimeric antigen receptor T cells $\gamma\delta$ T cells have demonstrated efficacy in killing a myelogenous leukaemia human erythroleukemia (K562) cell line and mice leukaemia xenografts without expressing any symptoms of alloreactivity.

Novel approaches using bispecific antibodies are in the pipeline and already being tested in ovarian cancer tumour-infiltrating lymphocytes conjugating a receptor with an IgG1-Fc domain to facilitate recognising an unknown ubiquitous antigen present in the tumour and mediating killing via ADCC. This Fc region would bind to the CD16, a FcRIII that upregulates on any $\gamma\delta$ T cell. Whether the response favours antitumour or pro-tumour angiogenic responses and the control over these responses is yet to be seen.

1.3 Ligand Recognition by $\gamma\delta$ T Cells

Human and mouse species have a different $\gamma\delta$ T cell repertoire, within each notably has different TCR usage, function, and distribution. The composition of their $\gamma\delta$TCR and patterns of tissue homing mostly determines the nature of the antigen they recognise, here summarised in Table. 1.5 and 1.6 with a summary of the most relevant literature.

1.3.1 Soluble Antigens

$\gamma\delta$ T cells recognise a few soluble peptide antigens that originate from microbes (Guo et al., 1995; Rust et al., 1990). The purified protein derivative (PPD) from *Mycobacterial tuberculosis* causes auto-reactivity in both human and murine non-Vδ2 $\gamma\delta$ T cells that use of diverse recombinant-TCR J segments to fine-tune the affinity for this antigen. A soluble virulent peptide early-secreted antigenic target 6-kDa protein (ESAT-6) can also trigger an aggressive $\gamma\delta$ T cell independent-response, albeit its interaction is likely to occur via toll-like receptor (TLR) instead of being driven by TCR recognition (Li and Wu, 2008; Pathak et al., 2007). Also, peptide fragments from *Listeria monocytogenes* like the listeriolysin (LLO) peptide 470-508, which shares high degree of homology with other gram-positive bacterial toxins, stimulates $\gamma\delta$ T cell proliferation from several isolated human peripheral blood mononuclear cells (PBMC) extracts (Guo et al., 1995).

Table 1.5: *Reported γδ T cell ligands (humans) and associated responses*

TCR	Ligand	Response	Comments	Reference
Vγ1Vδ1	Soluble PE	Pro-inflammatory IL-17	Essential function of the CDR3δ region.	(Zeng et al., 2012)
Vγ1Vδ2	Cytosolic protein EcIF1	Up-regulates IL-2R	TCR-dependent reactivity to rhabdomyosarcoma cells.	(Wiendl et al., 2002)
Vγ1.2Vδ8	HSV type I	MHC-independent	Recognises unprocessed glycoprotein in the absence of APC	(Sciammas et al., 1994)
Vγ1,3Vδ2	HARS and derivate proteins; EcIF1	Up-regulates IL-2R	Reactivity to myoblasts and TE671 rhabdomyosarcoma cells in a CDR3-dependent way.	(Bruder et al., 2012)
Vγ2,3,8,9Vδ1; Vδ3; Vγ4Vδ5	CMV-infected fibroblasts, unrestricted to MHC, MICA, or NKG2D	Cytolysis, TNF-α, Fas.	$V\delta2^-$ limited to CXCR4 and CCR9 compared to $V\delta2^+$ with specially high CCR5. Anti-CMV-reactive $V\delta2^-$ T cells also recognise intestinal tumour epithelial cells.	(Halary et al., 2005)
Vγ4Vδ1	BTNL3/8	Up-regulates IL-2R	Intestine specific.	(Di Marco Barros et al., 2016)
Vγ4/8Vδ1	MART-1/GP100-HLA-A*02	Cytolytic	Solved crystal structure; $CD8^+$ cells.	(Benveniste et al., 2018)
Vγ4Vδ5	CMV → EPCR	Up-regulates CCR9 chemokine.	Clone LES TCR binds EPCR directly.	(Willcox et al., 2012)
Vγ5Vδ1	CD1d-α-GalCer	Clonotype expansion	Solved crystal structure.	(Uldrich et al., 2013)
Vγ8Vδ3	Annexin A2	Clonotype expansion	Membrane annexin A2 is an oxidative stress signal.	(Marlin et al., 2017)
Vγ9Vδ2	Phosphoantigen BTN3A1 dependent.	Th1 response IFN-γ, TNF-α.	Requires cell-cell contact.	(Morita et al., 1999; Wang and Morita, 2015)
Vγ9Vδ2	Malaria irradiated sporozoites.	Th1 response IFN-γ, TNF-α, granulysin.	Vγ9Vδ2 cells populate up to 10–30 % PBMC.	(Deroost and Langhorne, 2018)
Vγ9Vδ2	F_1-ATPase-A-I	Clonotype expansion	G115 and AS/F_1-ATPase interaction.	(Scotet et al., 2005)
Vγ9Vδ2	Tumour cell lines	Cytolysis, IFN-γ, up-regulates IL-2R.	Tumour xenografts in mice including Daudi (B-lymphoblastoma), RPMI8226/S, OPM2, LME1 (multiple myelomas), K562 (myelogenous leukemia); and solid line Saos2 (osteosarcoma), MZ1851RC (renal carcinoma), SCC9, Fadu (head and neck cancer), MDA-MB231, MCF7,BT549 (breast cancers). Combinatorial-γδTCR-chain exchange increase avidity.	(Fisch et al., 1990; Gründer et al., 2012)
Vγ9Vδ2	Bacteria alkylamines	Clonotype expansion	Memory T cells capable of responding	(Bukowski et al., 1999)
Vγ9Vδ2	Ovarian carcinoma protein extract	Cytolytic, IL-2, IL-12	Independent of CDR3δ L97	(Xi et al., 2010)
Vγ9Vδ2 Vδ1	EBV → ULBP4	Th1 response IFN-γ, TNF-α.	Vδ1 from colon and Vγ9Vδ2 from ovarian and colon carcinoma respond to ULBP4 plate bound.	(Kong et al., 2009)
Vδ1	CD1d-sulfatide	Th1 response IFN-γ, TNF-α.	Germline residues contact CD1d; CDR3δ the antigen.	(Luoma et al., 2013)
Vδ1	APC-dependent HSP70/72	Clonotype expansion	Knocked down *HSP60/70* confirms specificity.	(Zhang et al., 2005)
Vδ2	MutS homologue 2 (hMSH2)	Cytolytic, IFN-γ.	hMSH2 induced in EBV infection, also a NKG2D ligand.	(Daï et al., 2012)
Vδ1	Stress-induced CD1c, independent of MICA.	Prolifereation, IL-2R, cytolysis, IFN-γ, TNF-α, granulysin.	Absent NKR-P1A, CD28, and CD4. Unsure response is due to CD1c-reactive or -self lipid complex.	(Spada et al., 2000)
Vδ1	MICA/MICB	Cytolysis	NKG2D is required for full activation phenotype.	(Groh et al., 1998; Kong et al., 2009; Wu et al., 2002)
γδ T cells	LLO (470-508)	Clonotype expansion	αβ T cells respond too.	(Guo et al., 1995)
γδ T cells	TT	Proliferation, cytolytic, IFN-γ.	TT can induce pAgs.	(Kozbor et al., 1989, 1990)

Table 1.6: *Reported γδ T cell ligands (mouse) and associated responses*

TCR	Ligand	Response	Comments	Reference
Vγ1	Polypeptide $Glu^{50}Tyr^{50}$-MHC class Qa-1	Production IL-2	TCR-dependent contact ($CD4^-$ $CD8^-$).	(Vidović et al., 1989)
Vγ1	APC-dependent HSP60	Possible autoimmunity.	Auto-reactivity.	(Belles et al., 1999)
Vγ1Vδ6	*Mycobacterium* PPD MHC-unrestricted	Production IL-2	TCR-dependent.	(Happ et al., 1989)
Vγ1Vδ6	*M. tuberculosis* B2G MHC-unrestricted	Production IL-2	TCR-dependent.	(Born et al., 2003)
Vγ1Vδ6	CL MHC-unrestricted	Production IL-2	TCR-dependent.	(Born et al., 2003)
Vγ1Vδ-diverse	Soluble insulin peptide (B:9-23)	Self-reactivity	Response is independent of APCs; disease-associated.	(Zhang et al., 2010)
Spleen Vγ1, Vγ4; intestine Vγ7	Soluble PE	Pro-inflammatory IL-17 ↑CD44 ↓CD62L	Affinity to Vγ chains differs from human. Activated cells do not proliferate, rather acquire an adaptive phenotype.	(Zeng et al., 2012)
Spleen Vγ1, Vγ4; intestine Vγ7	Stress-induced H2-T10 and H2-T22	Up-regulates IL-2R	Solved crystal structure. CDR3 motif derived from germline-encoded residues.	(Adams et al., 2008; Crowley et al., 2000; Shin et al., 2005)
Vγ2Vδ8	Soluble HSV-1 GP1	Th1 response IFN-γ.	Auto-reactivity and related to autoimmune diseases.	(Johnson et al., 1992; Sciammas and Bluestone, 1998)
Vγ3	CD1d-CL	Th1 IFN-γ and CCL5/RANTES.	Solved crystal structure.	(Dieudé et al., 2011)
Vγ5Vδ1	Keratinocytes MHC-unrestricted	Production IL-2	TCR-dependent reactivity.	(Havran et al., 1991)
Vγ5Vδ1 (DETC)	Skint-1	Egr3, T-bet, CD45RB	*Skint-1* is not evolutionary conserved among species.	(Boyden et al., 2008)
Vγ5Vδ1 (DETC)	MHC class II I-Ad	Cytolysis	Cross-reacts to multiple I-E alleles.	(Matis et al., 1989)
Vγ5Vδ1 (DETC)	MHC class II I-Eb,k,s; not d	Cytolysis	Epitope lying outside the peptide-binding groove.	(Matis et al., 1989)
Vγ7	Btnl1/6	Up-regulates IL-15β	Promoted weak activation of $V\gamma7^+$ IELs.	(Di Marco Barros et al., 2016)

A minor group of $\gamma\delta$ T cells respond to bacterial substrate *Staphylococcal* enterotoxins (SE) A and E in two separate mechanisms (Rust et al., 1990). One is driven by the subset of blood $\gamma\delta$ T cells composed of a Vγ9 paired with Vδ1 or Vδ3 segments and appears to be mediated by MHC class II presenting molecules similarly to how $\alpha\beta$ T cells recognise these and other SE variants. In this setting, cytolysis occurs without T-cell proliferation. The determining factor regarded as conferring this TCR-specific affinity is believed to be a disulphide link to a C region (Rust et al., 1990). The other mechanism responds to SE without the Vγ9 domain, but is antibody-dependent and controlled by Fcγ membrane receptors. Unlike the former, responses emerging from these Fcγ receptors induced cell proliferation (Rust and Koning, 1993).

Some non-Vγ2 cells combined with diverse Vγ domains respond to soluble algae-derived protein PE and are capable of inducing rapid IL-17A production (Zeng et al., 2012). This interaction relays mainly from both γ and δ CDR3 loops despite residues of the germline encoding CDR1/2 regions could also play a relevant role (Zeng et al., 2012). Likewise, the $\gamma\delta$ T cells use the CDR3 loops to recognise soluble HARS and related proteins like *Escherichia coli* translation initiation factor (EcIF1) from the translational apparatus (Bruder et al., 2012). This $\gamma\delta$TCR response derives from an autoimmune muscle lesion isolated T-cell line M88 (Vγ1.3Vδ2) and reveals an intriguing link between T and B cell responses in autoimmune myositis due to the manner they recognise soluble antigens.

1.3.2 MHC-Peptide Presentation to $\gamma\delta$ T-cells

Although its is generally assumed that $\gamma\delta$ T cells are MHC-unrestricted, several studies report a few peptide fragments being presented by MHC molecules. Vidović et al. (1989) show an isolated murine relatively invariant cell-surface MHC class I allotype Qa-1 presents a synthetic co-polymer (poly[Glu^{50} Tyr^{50}]) to Vγ1^{+} cells in a TCR-dependent faishon. Peptides like conserved housekeeping heat shock protein (HSP) can bind to murine Qa-1b antigen-presenting molecules and activate mouse $\gamma\delta$ T cells (Imani and Soloski, 1991). Only a few of these shock proteins are reported to stimulate tissue-resident distinct groups of non-Vδ2 T cells such as Vγ1 paired mostly with Vδ6. Specifically, HSP-60, HSP-70, and HSP-72 can be targets for human $\gamma\delta$ T cells as their presence on the cell-surface membranes in transformed cells cause the expansion of $\gamma\delta$ T cells among other cellular types (Belles et al., 1999; Zhang et al., 2005). Besides, a mouse $\gamma\delta$ T cell clone recognises a processed insulin peptide in dependency of accessory cells (Zhang et al., 2010).

Besides the standard criteria, several $\gamma\delta$ T cells with expression of CD8 have been

reported to recognise tetanus toxin (TT) in a self-MHC-restricted manner, specifically the HLA-DR4 allotype (Kozbor et al., 1989). Similarly, others found $CD4^+$ $\gamma\delta$ T cells respond to MHC class II when mixed with DCs (Takamizawa et al., 1995). Lastly, Benveniste et al. (2018) describe the structure of a melanoma-associated antigen bound onto HLA-A presenting molecule and its direct interaction to a $\gamma\delta$TCR (Benveniste et al., 2018). Altogether, these studies and others (Happ et al., 1989; Matis et al., 1989), broaden the understanding that $\gamma\delta$ T cell reactivity could not only be restricted to mononuclear MHC-unrestricted molecules, but they may also present a few unusual specificities to several distinct alleles from MHC molecules.

1.3.3 CD1 and Lipid Complexes

Human $\gamma\delta$ T cells can recognise lipid molecules in complex with some CD1 isoforms as NKT cells do. There are human tissue $V\delta1^+$ $\gamma\delta$TCR clones that react to CD1c independent from the presence of foreign lipid or glycolipid antigenic compounds and respond by secreting inflammatory cytokines, perforin, and granulysin lysing CD1c-bearing targets in a TCR-dependent manner (Spada et al., 2000). Sequencing of the CDR3 regions revealed substantially different lengths and diversity within these isolated CD1c-reactive $\gamma\delta$ T-cell clonotypes (Spada et al., 2000). $\gamma\delta$ T cells may also recognise endogenous lipid-derivates from infected cells that result from damaged mitochondria. Damaged cells release cardiolipin (CL) and β2-glycoprotein (B2G), and they both are potential candidates to stimulate $V\gamma6V\delta1^+$ T cells in dependency of accessory cells (Born et al., 2003). Besides, group II CD1d associates with sulfatide or α-GalCer to engage activation of $V\delta1$ paired to diverse γ chains. In this recognition, the TCR germline encoding residues dominated interactions for the contact to CD1d, while the CDR3γ loop might represent the principal determinant for antigen specificity (Luoma et al., 2013; Uldrich et al., 2013).

1.3.4 Stress-induced Surface Ligands

There are numerous stress-induced protein ligands recognised by $\gamma\delta$ T cells. Many of these stress-related surface structures are conserved and structurally related to MHC class molecules. In humans, $V\delta1^+$ T cells can recognise MIC genes A and B expressed in intestinal epithelial stressed cells (Groh et al., 1998; Xu et al., 2011). However, insights on its respective sequencing of $V\delta1^+$ T cell clonotypes revealed the γ chain might not be significantly relevant but necessary to hold a functional conformational $\gamma\delta$TCR structure that is reactive to the MIC stress-ligand molecular markers (Groh et al., 1998; Kong et al., 2009; Wu et al., 2002).

Similarly, two closely homologous MHC-Ib antigens T10 and T22 are ligands of the murine $\gamma\delta$ T cell repertoire with detailed molecular interactions solved (Adams et al., 2008; Wingren et al., 2000). These are stress-ligands by themselves as cannot present peptides due to an alteration of their α1/α2 domains akin to human MIC members. These variations rely on three amino acid deletion within the α1 domain and 13-residue deletion in α2 of the α-helical region (Bonneville et al., 1989; Ito et al., 1990) plus four substitutions of the eight amino acids that are essential to bind peptide fragments (Soloski et al., 1989). T22-reactive $\gamma\delta$ T-cells may express various segments of the γ chain (Vγ1 and Vγ4 from spleen and Vγ7 from intra-epithelia compartment), which indicate the Vγ usage is more reflective of the tissue origin than of the antigen specificity for this ligand (Shin et al., 2005). In this regard, a molecular structural study shows the top surface domains hold interaction with murine $\gamma\delta$TCR where the CDR3δ loop holds sufficient to recognise these T10 and T22 ligands (Adams et al., 2008). More recently, a human Vγ8Vδ3 TCR clone showed reactivity to annexin A2 in a glioblastoma cell line (Marlin et al., 2017).

Human $\gamma\delta$ T cells recognise ULBP4, one of its six human members. All related isoforms are independent of β_2-microglobulin (B2M) and frequently expressed in tumours, virally-infected cells, or selective normal tissues, and are inducible by increased retinoid acid and cellular stress. Intriguingly, reactivity to these ligands is limited to $\gamma\delta$ T cells of the Vγ9Vδ2 linage isolated both from colonic and ovarian tumours of EBV-infected cells; and they respond with IFN-γ secretion and granule release to clear their targets (Kong et al., 2009). Other members of the ULBP family would be recognised by other subsets of $\gamma\delta$ T cells, although recognition seems to be driven by NKG2D receptor than $\gamma\delta$TCR-dependent ligand recognition.

1.3.5 Butyrophilin-Like Epithelial Proteins

BTNL proteins are present on the surface of many vertebrate epithelial cells, and their interactions with immune receptors may decide the fate of specific $\gamma\delta$ T cell subsets. Murine Btnl-relatives *Skint-1* and *Skint-2* can infer on the development and maturation of progenitor mouse DETC (Boyden et al., 2008; Jandke et al., 2020). Early-stage thymocytes exit the thymus to encounter epithelial cells that express the Skint-1/2 ligands. Upon contact, they selectively engage naive T cells for maturation onto the *Egr3*-mediated pathway and IFN-γ production. However, in their absence, naive T cells mature into the Vγ6Vδ1 lineage under the regulation of Sox13 and RORγt routes, defining this subset as IL-17A-producing cells (Turchinovich and Hayday, 2011). Genetic evidence of the functional relevance of mouse Skint-1/2 proteins with the inter-

action and docking mode to Vγ5Vδ1 TCR has been recently elucidated (Jandke et al., 2020).

Several mouse BTNL proteins determine the function of specific $\gamma\delta$ T cell subsets. Mouse *Btnl1* can mediate epithelial regulation of $\gamma\delta$ T cells in the intestinal epithelial tissue with an intrinsic effect on the development of intestinal epithelial Vγ7 lymphocytes. In the lack of *Btnl1* expression, the presence of V$\delta4^+$ T cells is favoured over the V$\gamma7^+$ phenotype in the intestine (Bas et al., 2011). However, *Btnl1* is preferably expressed and retained in the endoplasmic reticulum unless Btnl6 is present. Together, Btnl1 and Btnl6 heterodimerise facilitating the complex migration to the surface membrane, which results in differentiation and maturation of intraepithelial murine V$\gamma7^+$ lymphocytes (Di Marco Barros et al., 2016; Vantourout et al., 2018).

Intriguingly, similar events occur in humans, where epithelial expression of *BTNL3* and *BTNL8* in intestinal epithelial cells is mostly restricted to the gut. The two BTNL proteins are also required for differentiation and residence of V$\gamma4^+$ T cells into the primary colonic intraepithelial tissue. The two human BTNL3 and BTNL8 share homology and form heterodimers at the cell surface (Di Marco Barros et al., 2016). Mutation analysis and contacts between the human BTNL heterodimer and its respective TCR engagement denote interactions that are largely uninfluenced by the δ chain, but mostly driven by concordant Vγ4 chain (Melandri et al., 2018). Such interactions take place between the Vγ4 domain and the IgV domain of BTNL3 which are mainly determined by CDR2γ and hypervariable region 4 (HV4), two Vγ subregions closely contiguous in their tertiary space structure (Willcox et al., 2019).

1.4 The Phosphoantigen-reactive $\gamma\delta$TCR

Only Vγ9Vδ2 T cells with limited diverse junctional sequences respond to phosphoantigens (Bukowski et al., 1998; Miyagawa et al., 2001; Tanaka et al., 1995). Thus, a distinctive feature of phosphoantigen-reactive $\gamma\delta$ T cells is the expression of the Vγ9Vδ2 TCR, whose γ-chains show a Vγ9-JP rearrangement paired with Vδ2 domain (Davodeau et al., 1993). These cells are regarded as semi-invariant, with largely invariant, JγP region in the Vγ9JPVδ2 TCR. Its CDR has a public immunodominant CDR3γ motif that pair with a Vδ2 TCR-δ chain with diversity at the CDR3δ region in terms of length and composition (Davodeau et al., 1993; Gründer et al., 2012). The first Vγ9Vδ2 TCR structure was solved by Allison et al. (2001) and colleagues in 2001. However, the phosphoantigen presentation mechanism and the putative respective molecular ligand it recognises remains a mystery.

1.4.1 General Structure

$\gamma\delta$ T cells arouse in jaw vertebrates and bear semi-invariant receptors (Adams et al., 2015). The $\gamma\delta$TCR structure is fairly different from $\alpha\beta$TCRs. During ontogeny, the $\gamma\delta$ gene loci organisation has been conserved, where usually adopts two D segments specific of the δ gene and one J segment for each δ and γ genes (Davodeau et al., 1993). Thus, the $\gamma\delta$TCR is characterised for having one long and one short CDR3, whereas those CDR3 in the $\alpha\beta$TCRs have similar length (Rock et al., 1994). This feature makes the antigen-binding sites more closely related to Ig than $\alpha\beta$TCRs (Wong et al., 2019). Also, the $\gamma\delta$ TCR can recognise soluble antigens (Zeng et al., 2012), which would give them a similar function to antibodies.

The $\gamma\delta$TCR have other notable differences compared to $\alpha\beta$TCRs. The constant regions swing out from each other in a pronounced acute angle that folds the whole structure in more compact shape (Allison et al., 2001). Moreover, and perhaps the least relevant, is the V domain joints to the C region in an atypical hinge folding in an acute torsion that allows the TCR structure to twist into itself (Allison and Garboczi, 2002).

1.4.2 Evolutionary Background

In contrast to more evolutionary conserved and constrained $\alpha\beta$TCR that recognises MHC molecules, $\gamma\delta$TCRs are more evolutionarily labile and have adaptive immune and innate immune functions that differ even within the same class of vertebrates species (Adams et al., 2015). Strong concomitant conservation suggests that the Vγ9 and Vδ2 gene segments have co-evolved together with a genetic cluster of BTN genes in placental mammals (Karunakaran et al., 2014). However, this co-evolution does not appear valid for rodent or lagomorphs, which lack all these genes.

1.4.3 Comprehensive Alanine-Scanning Mutagenic Screens

Multiple mutagenic screens have been carried out to assign essential functions to specific amino acids that constitute the phosphoantigen-reactive Vγ9Vδ2 TCR. Mutagenic alanine-screens have been the gold standard to determine the contribution of a specific residue to the stability or function of a given protein.

The Vγ9Vδ2 TCR crystal structure was solved in a prototypical G115 clone (Allison et al., 2001). At that time, the authors identified a positively charged pocket in between the two CDR3 of the γ and δ chains consisting of two positively charged lysines (γK108 and γK109) and one hydrophobic leucine (δL97) as opposed to the γ chain

(Allison and Garboczi, 2002). Subsequent alanine-screens consolidated these three conserved residues important for reactivity to phosphoantigens, plus an additional CDR2δ positive arginine (δR51). Highlighting that a change for an opposed negative glutamic acid charge (γK109E) obstructed a normal response, while substitution of lysine to alanine (γK109A) weakened its biological activity (Yamashita et al., 2003). Hydrophobic residue valine, leucine, or isoleucine substitutions at position 97 at the CDR3δ renders poor Vγ9Vδ2 TCR responses to phosphoantigen stimuli (Nishimura et al., 2004).

More mutagenic analyses causing a three amino acid deletion (δTDK113$-$115*del*) and single alanine substitutions (δL97A, δF109A, and δV115A) revealed residues at the hydrophobic core of the δ chain heavily weakened $\gamma\delta$ T-cell responsiveness. However, such a result could be a consequence of impairing the folding of the structure as a whole and subsequent functionality (Gründer et al., 2012). Addition of alanine residues from the CDR3δ 97 position did not appear to affect the functionality of the antigen-specific receptor, meaning that plausibly these clones allow incorporation of five to seven residues that increments their variable γ or δ CDR3 length without altering antigen specificity but modelling functional avidity for the ligand. The extend of these residues might be limited due to the leucine 97 at the δ chain retains a defined critical spatial location. Likewise, the CDR3γ comprises a vital role for the amino acid γA102 conferring crucial reactivity to the ligand as the incorporation of two subsequent alanines in this sites does not alter reactivity. In support of this hypothesis, the IMGT database records the most cited functional CDR3 clonotypes varying in a range of five to seven amino acids only (Gründer et al., 2012; Lefranc et al., 2003). Amino acid comparisons between Vγ9Vδ2 reactive clones show a series of relatively non-conservative residues between the 102–104 positions of the CDR3γ changes the structure and ligand affinity of this loop (Gründer et al., 2012). A collection of reported mutation screens in Vγ9Vδ2 TCR is represented in Figure 1.6 for a comprehensive overview of those site-directed mutations collected in Table 1.7.

1.5 The Family of Butyrophilin Molecules

The family of BTN molecules collectively regulate $\gamma\delta$ T-cell functions of vertebrate immune systems (Abeler-Dörner et al., 2012; Arnett and Viney, 2014; Di Marco Barros et al., 2016; Rhodes et al., 2016). However, the first *BTN* was identified in mouse (*Btn1a1*) and described as necessary for secretion of milk-lipid droplets in mammary glands of mice, denoting its *butter*-like name (Ogg et al., 2004). Their members are composed of Ig-like surface transmembrane type I proteins similar to traditional co-

Table 1.7: *Summary of mutagenic analysis in two $\gamma\delta$TCR clones G115 and DG.SF13 in response to phosphorylated antigens. All residue positions are noted according to Kabat (1991). (*) the mutation hinters correct TCR surface expression on reporter cells. Data obtained from (Gründer et al., 2012; Wang et al., 2010; Xi et al., 2010; Yamashita et al., 2003)*

Chain	*Region*	*Residue*	*Position*	*Incorporation*	*Impairs response*	*Clone*
δ	CDR1	E	28	A	Abrogate	DG.SF13
		I	30	E	Irrelevant	DG.SF13
		I	30	E	Weakens	DG.SF13
		N	32	A	Weakens	DG.SF13
	CDR2	R	51	A	Abrogate	DG.SF13
		R	51	E	Abrogate	Purified
		E	52	A	Abrogate	DG.SF13
		E	52	A	Abrogate	DG.SF13
	CDR3	L	97	A	Abrogate	Purified
		L	97	S	Abrogate	Purified
		L	97	A	Weakens	G115
		L	97	D/E/I/S	Abrogate	OT10
		G	98	–	Abrogate	$G115_{LM0}$
		G	98	A	Abrogate	$G115_{LM1}$
		G	98–101	A_4	Weakens	$G115_{LM4}$
		G	98–109	A_{12}	Weakens	$G115_{LM12}$
		TDK	104–106	–	*	G115
		L	107	A	*	G115
		I	108	A	Weakens	G115
		F	109	A	*	G115
	J1	V	115	A	*	G115
γ	CDR1	T	29	A	Abrogate	DG.SF13
		I	30	E	Irrelevant	DG.SF13
		T	33	A	Irrelevant	DG.SF13
		S	34	A	Irrelevant	DG.SF13
	CDR2	Y	54	A	Abrogate	DG.SF13
		T	57	A	Abrogate	DG.SF13
		R	59	A	Irrelevant	DG.SF13
		K	60	A	Irrelevant	DG.SF13
	CDR3	W	100	GN	Abrogate	DG.SF13
		E	102	A	Abrogate	G115
		Q	103	A	Abrogate	G115
		Q	104	A	Abrogate	G115
		–	104	A	Irrelevant	$G115_{LM2}$
		K	108	E	Abrogate	DG.SF13
		K	108	A	Weakens	DG.SF13
		K	109	E	Abrogate	DG.SF13
		K	109	A	Irrelevant	Purified
		–	103–104	A_2	Irrelevant	$G115_{LM3}$

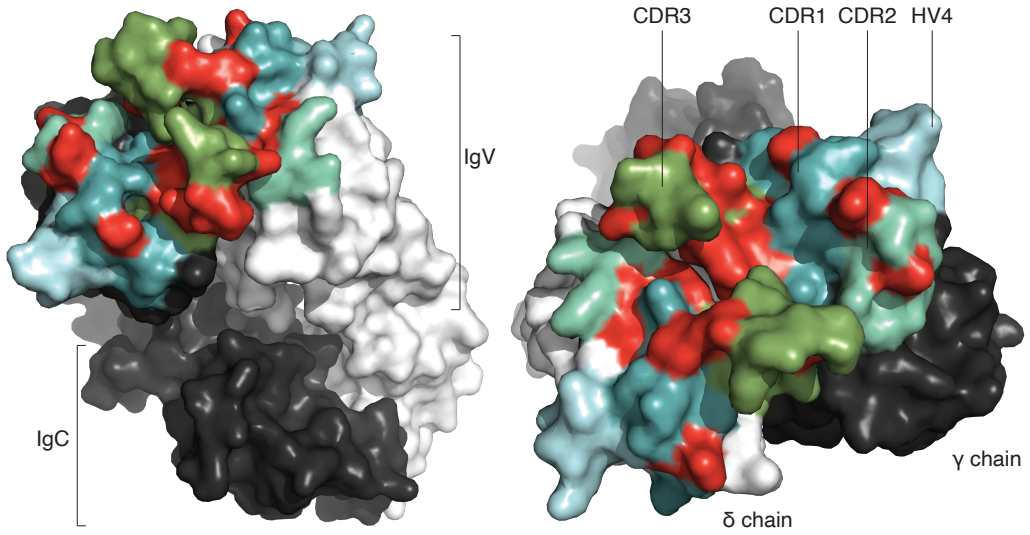

Figure 1.6: *Molecular structure of a human Vγ9Vδ2 TCR in side and top views (left and right, respectively) for the prototype $\gamma\delta$TCR G115 model showing its γ and δ chains (black and white, respectively) and their hypervariable domains (tones of green), with reported mutation sites that abrogate reactivity to phosphorylated antigens (red). Created in PyMOL, RCSB PDB entry 1HXM.*

stimulating factors of the B7 superfamily cell-surface molecules or concurrent prime-class checkpoint inhibitor targets like the programmed cell death-ligand 1 (PD-L1) (Butte et al., 2007; Rhodes et al., 2001). Their structure usually consists of extracellular IgV and IgC folded domains connected to a single transmembrane span with an intracellular carboxyl-terminal B30.2 domain (Arnett et al., 2009; Palakodeti et al., 2012).

1.5.1 Genetic Organisation

In the human genome, the *BTN* family mostly consists of two genetic groups: one *BTN* cluster located at the extended MHC region in the chromosome 6p22.1 and mostly shared among primates (Rhodes et al., 2001); and another in the chromosome 5q35 whose members diverged more across species and are named homolog *BTNL* genes (Fig. 1.7). The *BTN* cluster contains seven genes within three subfamily groups. The second and third groups have genetic sequences that share approximately 50 % amino acid identity and they contain three members each that probably resulted from evolutionary tandem duplication events (Fig. 1.8) (Rhodes et al., 2001). These are named *BTNA1*; *BTN2A1*, *BTN2A2*, *BTN2A3* (pseudogene); and *BTN3A1*, *BTN3A2*, and *BTN3A3*. All these genes acquired mutations and changed during evolutionary processes with an important genetic variation when species diversified from

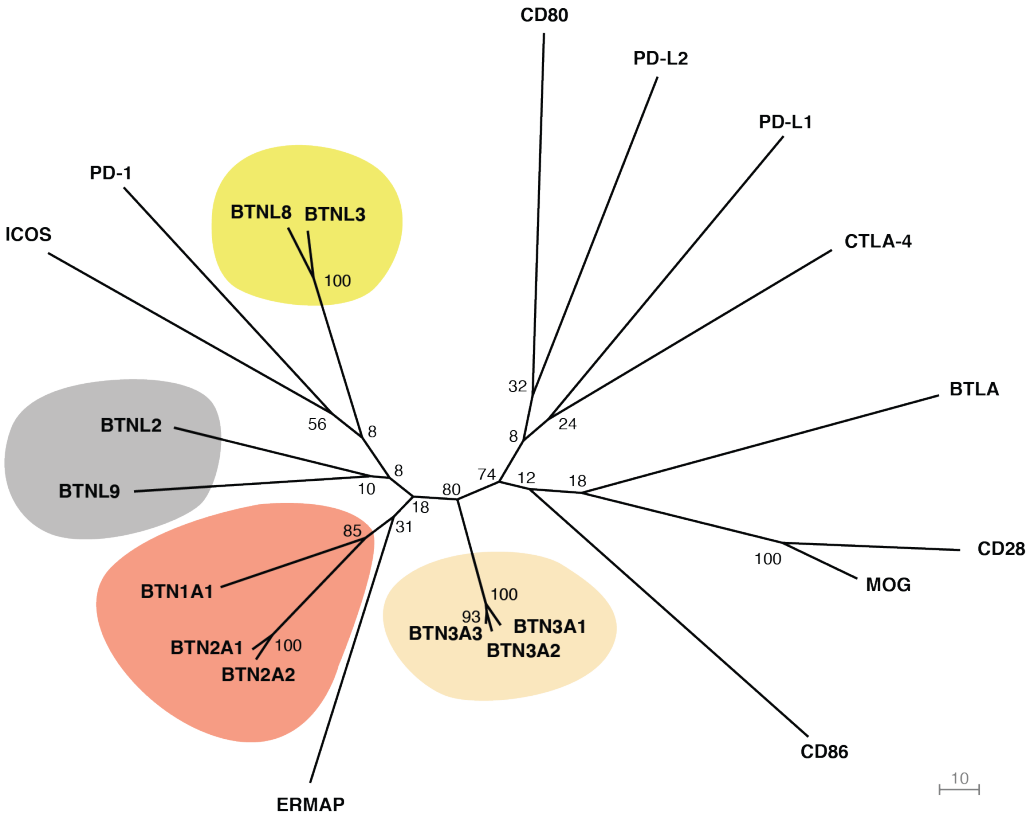

Figure 1.7: *Genetic evolutionary tree of human major immunoregulatory proteins of the B7-immunoglobulin superfamily molecules. Scale indicates expected number of changes per nucleotide and node percentage of confidence. Analysed by the maximum likelihood neighbour joining method and general time reversible substitution model in CLC Main Workbench.*

primates and rodents (Afrache et al., 2017; Karunakaran et al., 2014). This explains why most primates share gene members of the BTN cluster but mouse and hamster species only conserved *Btn1a1* and *Btn2a2*.

In the human genome there are only four *BTNL2*, *3*, *8*, and *9* genes, whereas the mouse genome has seven members named *Btnl1*, *2*, *4*, *5*, *6*, *7*, and *9*. Note the human *BTNL2* lies within the BTN cluster, opposed to *BTNL3*, *8*, and *9* relatives that are situated in the chromosome 5q35. Human and mouse species share ortholog genes *erythroblast membrane associated protein (ERMAP)* and *myelin oligodendrocyte glycoprotein (MOG)* considered within and akin to *BTNL* genes. Mice species

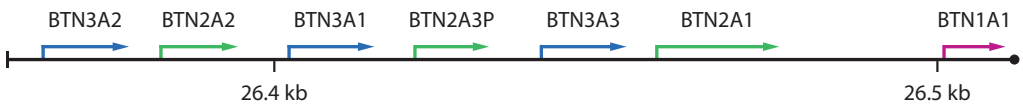

Figure 1.8: *Distribution of the main BTN gene cluster in the human chromosome 6p22.1.*

Table 1.8: *Collected details for the expression and functional relations of BTN family members in human and mouse species. Protein expression patterns are a mix of detected protein expression profiles in the indicated reference and are inferred from detecting a high message RNA expression in quantitative analysis performed in Arnett et al. (2009).*

Human sp.	*Mouse sp.*	*Protein expression profile*	*Recognised by*	*Associated to*	*Reference*
BTN1A1	Btn1a1	Mouse mammary glands, thymic stromal cells and B cells	Human activated T cells and macrophages	Mouse regulation of milk-droplet secretion, inhibitor of T cell activation	(Smith et al., 2010)
BTN2A1	–	Umbilical vein endothelial cells, intestinal epithelial cells and immune cell expression	DC-SIGN (expressed by DC and monocytes)	Associated to metabolic syndrome, dyslipidaemia, myocardial infarction and chronic kidney disease, Th2 diabetes	(Hiramatsu et al., 2011; Horibe et al., 2014; Malcherek et al., 2007; Yoshida et al., 2011a,b)
BTN2A2	Btn2a2	Dendritic cells, monocytes, B cells and thymic epithelial cells	Activated T cells	Inhibits T cell activation	(Sarter et al., 2016; Smith et al., 2010)
BTN3A1	–	Stressed cells, malignant cells and broad immune and tissue cell expression	B cells and Vγ9Vδ2 T cells	Phosphoantigen reactivity	(Harly et al., 2012)
BTN3A2	–	Malignant cells and broad immune and tissue cell expression	Vγ9Vδ2 T cells	Phosphoantigen reactivity, Type 1 diabetes, ovarian cancer.	(Le Page et al., 2012; Vantourout et al., 2018; Viken et al., 2009)
BTN3A3	–	Broad immune and tissue cell expression	Tumour-associated macrophages LSECtin	Ovarian (-associated) and breast cancer	(Liu et al., 2019; Peedicayil et al., 2010)
BTN5 (ERMAP)	Btn5 (ERMAP)	Erytrocytes, bone marrow, spleen	Scianna antigens	Scianna blood antigen system	(Wagner et al., 2003; Ye et al., 2000)
–	Btnl1	Intestinal epithelial cells and macrophages	Vγ7 T cells, activated B cells and dendritic cells	Modulator of intestinal Vγ7 T cell	(Bas et al., 2011; Di Marco Barros et al., 2016; Yamazaki et al., 2010)
BTNL2	Btnl2	Brain, heart, kidney, liver, pancreas, ovary, small intestine, colon, testis, thymus, leukocytes, lymph node, spleen, macrophages	T cells, B cells and vascular endothelium	Deactivation of T cells, sarcoidosis polygenic immune disorder, allergy (IgE)	(Arnett et al., 2007; Konno et al., 2009; Valentonyte et al., 2005)
BTNL3	–	Intestine epithelia, liver, lung, bone marrow, spleen, neutrophils	Intestinal Vγ4 T cells	Modulator of intestinal Vγ4 T cell	(Di Marco Barros et al., 2016)
–	Btnl4	Intestinal epithelial cells	Unknown	Unknown	(Bas et al., 2011)
–	Btnl5	Unknown	Unknown	Unknown	
–	Btnl6	Intestinal epithelial cells	Intestine Vγ7 T cells	Modulator of intestinal Vγ7 T cell	(Bas et al., 2011; Di Marco Barros et al., 2016)
–	Btnl7	Unknown	Unknown	Unknown	
BTNL8	–	Intestine epithelia, spleen, bone marrow, neutrophils, eosinophils	Intestinal Vγ4 T cells	Modulator of intestinal Vγ4 T cell	(Di Marco Barros et al., 2016)
BTNL9	Btnl9	Adipose tissue, lung, thymus, spleen, heart, B cells	Activated T cells, B cells, DC and macrophages	Unknown	(Arnett et al., 2009)
BTNL11 (MOG)	Btnl11 (MOG)	Oligodendrocytes of the central nervous system	DC-SIGN of mycroglia and DC	Integrity to the myelin sheath, MHC-associated multiple sclerosis	(García-Vallejo et al., 2014; Liñares et al., 2003)
–	Skint1	Thymic epithelial cells	Vγ5Vδ1 DETC	Thymic maturation of DETC	(Boyden et al., 2008)
–	Skint2	Broad expression in lymphoid and non-lymphoid tissues	Activated T cells and antigen-presenting cells	InhibitsT cell activation	(Yang et al., 2007)

also have an additional group of *BTNL* genes named *Skint*, which diversifies within eleven derivates, whereas primates have only *SKINT-1*, and it is a pseudogene (Mohamed et al., 2015). The family of BTN genes has just been studied from the last two decades and their functions have only began to be revealed, most of the present knowledge summarised in Table. 1.8.

1.5.2 Genetic Polymorphisms and Implications in Diseases

Several genetic studies associate BTNL2 polymorphisms to immune-related diseases including sarcoidosis (enlargement of lymph nodes), renal granuloma, and susceptibility to tuberculosis (Lin et al., 2015; Möller et al., 2007; Nishimura et al., 2019; Valentonyte et al., 2005). Most of them relate to a specific single nucleotide polymorphism (G→A, rs2076530) associated with sarcoidosis, thereby causing an enlargement of lymph nodes and often granulomas. This mutation truncates the BTNL2

protein leaving it without an IgC domain and transmembrane helix, preventing the formation of homodimers (Valentonyte et al., 2005). As a result, BTNL2 is unable to fold properly or migrate to the cell-surface membrane (Valentonyte et al., 2005). This has consequences associated with decreased inflammatory T-cell activity (Valentonyte et al., 2005). Besides, BTNL2 has some structural similarities to cytotoxic T-lymphocyte-associated protein 4 (CTLA-4), a common target of immune checkpoint drugs that inhibits T-cell responses (Arnett et al., 2007). Together, these studies highlight the relation of BTNL2 with immune disorders and T-cell regulation.

Polymorphisms in BTN2A1 are mostly known to affect an Asian population of Japanese individuals in diseases such as diabetes mellitus, myocardial infarction, and chronic kidney disease (Hiramatsu et al., 2011; Horibe et al., 2014; Yoshida et al., 2011a,b). Both BTN2A1 and BTN2A2 paralog genes have a high polymorphic diversity at their IgV domains (Afrache et al., 2017). At present, little is known about BTN2A1 molecular interactions but that binds DC-specific intercellular adhesion molecule-3-grabbing nonintegrin (DC-SIGN) lectin, expressed in monocytes and DCs. Although this bond depends on protein glycosylation, reversed attempts to detect BTN2A1 on cells using a DC-SIGN probe failed (Malcherek et al., 2007). DC-SIGN on brain microglia or DCs also interacts with BTN-homolog MOG to control innate immune homeostasis (García-Vallejo et al., 2014). Such interaction is in a glycosylated-dependent manner too (García-Vallejo et al., 2014).

More recently, a comprehensively high-throughput for the detection of receptor-ligand interactions of the extracellular protein network in human membrane-expressed proteins, highlighted the interaction of BTN2A1 with FAM187B (Verschueren et al., 2020). Among others, the study defined several more interactions with members of the BTN3A subfamily with proteins such as CDH9, LRRC4B/C, ST14, TGOLN2, and VSIG8. Although the function of most of these BTN ligands is still unknown, the LRRC4/NGL-2 has been reported to have multiple roles in the biological processes of gliomas (Li et al., 2014). This suppresses glioma cell growth, angiogenesis, and invasion through signalling regulation networks (Li et al., 2014), and maybe, it involves BTN immune regulation and $\gamma\delta$ T cells (Rhodes et al., 2016).

Association studies in humans show that there is certain polymorphism between the BTN3A subfamily genes, albeit marked by extreme homogenisation of the IgV sequences (Afrache et al., 2017). Some evidence of single nucleotide polymorphisms relates BTN3A2 to being susceptibile of developing diseases like type 1 diabetes (Afrache et al., 2017), akin to BTN2A1 and type 2 diabetes (Hiramatsu et al., 2011). Also, there is data that indicates BTN3A2 is associated with longer overall survival and lower risk of high-grade serous epithelial ovarian cancer (HGSC) disease progression

(Le Page et al., 2012). Epithelial *BTN3A2* expression significantly modulates the intratumoral infiltration of immune cells by attracting higher density of infiltrating T cells, particularly CD4+ cells (Le Page et al., 2012). Lastly, single nucleotide polymorphisms in MOG, BTN2A1, and BTN3A3 were all associated with rubella virus-specific cellular immunity following vaccination (Kennedy et al., 2014), suggesting they could play some roles in adaptive immunity.

1.5.3 The Importance of the Intracellular B30.2 Domain

All BTNs have an intracellular B30.2 domain except for BTN3A2 and BTNL2 (Arnett et al., 2007; Rhodes et al., 2001). This domain mostly consists in a sequence repeat of the splA/ryanodine receptor (SPRY) with a N-terminus PRY region (Rhodes et al., 2005). However, it is also conserved in many more proteins, especially, those encoded by tripartite motif (TRIM) genes (D'Cruz et al., 2013; Perfetto et al., 2013), suggesting natural selection could have maintained it as a component of immune system. The B30.2 domain covers a wide range of functions and acts similar to pattern-recognition receptors like TLR or nucleotide-binding oligomerisation domains (NOD)-like receptor proteins that are involved in the immune defence system (Rhodes et al., 2005). Moreover, B30.2 cleaves pyrin and inhibit IL-1β production via the NF-κB pathway, a transcription factor responsible for both the innate and adaptive immune response (Chae et al., 2008).

The BTN1A1 B30.2 has implications in mammary epithelial cells during lactation (Robenek et al., 2006). It binds to *xanthine oxidoreductase*, an enzyme associated with the production of milk fat globules, and both stabilise at the apical cell membrane (Jeong et al., 2009). This involves BTN1A1 in an enzymatic reaction in which oxygen reactive species intended for immunomodulatory and antimicrobial maternal functions are produced (Jeong et al., 2009).

The BTN3A1 has been identified as a key player in inducing phosphoantigen activation of $\gamma\delta$ T cells with a critical antigen-sensitive role for B30.2 (Sandstrom et al., 2014). Thus, most recent reports relate the B30.2 of BTN3A1 with reactivity to phosphoantigens and part of the antigen-presenting complex that activates Vγ9Vδ2 T cells by promoting an 'inside-out' triggering mechanism (Gu et al., 2018; Sandstrom et al., 2014; Wang and Morita, 2015; Yang et al., 2019). Structural data supports that BTN3A1 B30.2 binds directly to microbial HMBPP and endogenous IPP phosphoantigens alike, despite previous work also reported phosphoantigens could bind to its IgV ectodomain (Table. 1.9) (Sandstrom et al., 2014; Vavassori et al., 2013; Wang and Morita, 2015). Nonetheless, these two phosphoantigen species have a

Table 1.9: *Affinity interactions between phosphoantigens and the BTN3A1 IgV or intracellular domain B30.2 vary on the nature of the ligand. Affinities were estimated by calculating K_D values in an isothermal titration calorimetry (ITC) (or SPR in Vavassori et al. (2013)) experiments considering one-to-one stoichiometry in all cases.*

Protein domain	*Ligand*	*Source*	K_D (µM)	*Reference*
BTN3A1 IgV	IPP	Eukaryota	69.9	(Vavassori et al., 2013)
BTN3A1 IgV	HMBPP	Microbial	3.06	(Vavassori et al., 2013)
BTN3A1 B30.2	IPP	Eukaryota	490	(Sandstrom et al., 2014, Suppl.)
BTN3A1 B30.2	EtPP	Synthetic	280	(Sandstrom et al., 2014, Suppl.)
BTN3A1 B30.2	HDMAPP	Microbial	0.92	(Sandstrom et al., 2014, Suppl.)
BTN3A3 B30.2	HDMAPP	Microbial	Unreported	(Sandstrom et al., 2014, Suppl.)
BTN3A1 B30.2	HDMAPP	Microbial	3.3	(Yang et al., 2019)
BTN3A3 B30.2^{R351H}	HDMAPP	Microbial	2.3	(Yang et al., 2019)
BTN3A1 B30.2	cHDMAPP	Synthetic	0.51	(Sandstrom et al., 2014, Suppl.)

distinct affinity for B30.2, where the former dissociation constant at equilibrium (K_D) is magnitudes higher than the later, corresponding to what is observed in dose-based $\gamma\delta$ T-cell in-vitro stimulating assays. The interaction of phosphoantigen with B30.2 depends on a positively charged inner pocked and heavily relays on histidine 351 (H351) (Sandstrom et al., 2014; Yang et al., 2019). Although BTN3A1 and BTN3A3 are very similar and share over 80 % amino acid identity, BTN3A3 B30.2 domain does not bind phosphoantigens due to the absence of H351. Yet, inserting H351 in BTN3A3 can reverse this condition and confer BTN3A3 affinity for phosphoantigens (Sandstrom et al., 2014).

Six polar residues that constitute four turns surrounding the edges around the B30.2 pocket of BTN3A1 have positive charges and potentially improve the affinity for phosphoantigens (Fig. 1.9 a) (Wang and Morita, 2015). Furthermore, three areas of the B30.2 domain are dynamic and can move prominently following phosphoantigen bound, which could result in a global protein shift from a putative *V-shape* resting state into a functional *head-to-tail* dimer conformation (Gu et al., 2017; Palakodeti et al., 2012). These are defined as two systematic groups enclosed between 393–397 and 410–419 positions named *apo* and *pocket* segments, respectively (Fig. 1.9 b) (Gu et al., 2017). Molecular simulations predict the apo segment shifts outwards, whereas the pocket segment turns inwards as indicated by the arrows in Fig. 1.9.b.

Sensing phosphoantigens and triggering the inside-out mechanism might not be the unique role of the BTN3A1 B30.2 domain, but it could also interact with other neighbouring proteins (Wang et al., 2019; Yang et al., 2019). Molecular dynamic simulations demonstrated it is possible dimer intracellular proteins cooperate in sensing phosphoantigen to enhance the efficiency of $\gamma\delta$ T-cell activation (Yang et al., 2019).

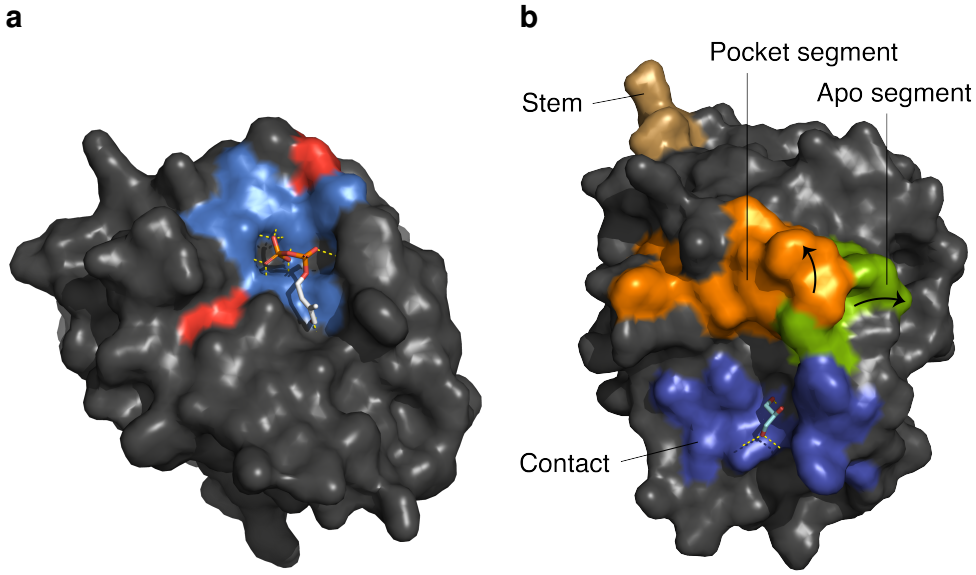

Figure 1.9: *Molecular model of the BTN3A1 intracellular B30.2 domain with a (a) basic pocket highlighting its positive (blue) or negative (red) residues and hydrogen bonds to a HMBPP metabolite (yellow dashes); (b) Functional areas when cHMBPP (cyan) is bound to the basic pocket; pocket (orange) and apo (green) segments move apart upon antigen bound and the contact area (purple) fits into a neighbouring asymmetric B30.2 unit (not shown). Steam (brown). Created in PyMOL with reference structures 5ZXK and 5HM7, respectively.*

When phosphoantigens bind B30.2 of BTN3A1 in target cells induces a $\beta \rightarrow \alpha$ conformational transition of residue H351. This change, together with other residue movements of the surrounding basic pocket, convey to the coiled-coil α-helical juxtamembrane structure with acquired configurations that increase the avidity between the extracellular domain of BTN3A1 and the Vγ9Vδ2 TCR, resulting in an immune response (Yang et al., 2019). In a soluble state, the BTN3A1 B30.2 domain forms two distinct dimers: a symmetric dimer interface in which two binding phosphoantigen pockets are located away from each other; and an asymmetric form with one phosphoantigen near the junction interface. Presumably, the H351 α-conformation is expected to cause a movement of W350 and W391 residues impacting in the symmetric dimer-interface and inducing the asymmetric configuration, which is needed for efficient Vγ9Vδ2 T-cell activation (Wang and Morita, 2015; Yang et al., 2019).

The adjacent juxtamembrane coiled helix that links the B30.2 to the BTN3A1 protein seems to contribute to transfer phosphoantigen activation of $\gamma\delta$ T cells (Peigné et al., 2017). The intracellular helices in BTN proteins form coiled-coil bonds with a characteristic empty molecular space in between the B30.2 domains of BTN dimers. Freeing space between B30.2 domains could increase the ability to sense small phosphoantigen metabolites by B30.2 domains facilitating them to navigate and reach the basic pocket of the B30.2 domain supposing these are interacting one with another.

Wang et al. (2019) proposed models of these helical structures and suggest a secondary protein is likely to interact with these B30.2 domains once phosphoantigens are bound. However, it is yet unexplored whether this might be a contiguous B30.2 domain of the neighbouring BTN or a third party protein member is involved.

1.5.4 Regulation of T-cell Responses

First relation of the BTN molecules involved in immune regulatory events were described in mouse models. Btn1a1 and Btn2a2 bound to activated T cells to inhibit proliferation of $CD4^+$ and $CD8^+$ lymphocytes along with respective metabolism and IFN-γ and IL-2 cytokine secretion (Smith et al., 2010). These demonstrate their potential to regulate immune responses and a possible co-inhibitory role to balance the immune response following activation similar to that of B7 family molecules such as PD-L1 or CTLA-4. In mice species this could also be implicated in regulating maternal T-cell function in the mammary gland during the budding process of milk fat globules from mammary epithelial cells of the lactating tissue (Kumar et al., 1985). Similarly, Btn1a1 and MOG could be competing for the same ligand on T cells. Btn1a1 was observed to suppresses Th1-like cytokines and increased production of IL-10 in autoimmune encephalomyelitis (EAE)-induced mice by immunisation of MOG, a multiple sclerosis autoantigen (Mañá et al., 2004). Likewise, administration of Btn1a1 IgV peptide prevented encephalitis resulting from a severe inflammatory T-cell response to MOG (Stefferl et al., 2000). That indicates Btn1a1 and MOG homolog proteins must share part of their respective functional domains as both compete for the same ligand while conveying opposed functions.

BTNs, as well as their relative members, tend to dimerise by their Ig ectodomains and jointly acquire functionality to regulate T cells in specific anatomical compartments (Di Marco Barros et al., 2016). Mouse thymic epithelial cells co-express *Skint-1* and *Skint-2* for differentiation and maturation of DETCs (Jandke et al., 2020). Similarly, Btnl1 requires the presence of Btnl6 for migration to the cell's plasma membrane, and jointly induce TCR-dependent responses specifically in intestinal $V\gamma7^+$ T cells. These observations are akin to human intestinal epithelial cells of the colon, although humans use BTNL3 and BTNL8 to induce $V\gamma4^+$ T cells (Di Marco Barros et al., 2016). Moreover, the BTNL3/8 heterodimer intracellular organisation seems to indirectly regulate the expression of BTNL9 (Aigner et al., 2013), despite this has no involvement in intestine epithelial cell functions nor it has been reported to dimerise with other BTNs members (Arnett et al., 2009).

The mechanism by which phosphoantigens activate $V\gamma9V\delta2$ T cells can be al-

tered by specific antibodies against the BTN3A subfamily members (aka CD277), suggesting this mechanism relies on a cell-to-cell contact. Targeting non-susceptible cells with antibody 20.1 mimics the effect of phosphoantigens and activates Vγ9Vδ2 T cells. Contrary, the antibody 103.2 inhibits this effect and abrogates phosphoantigen-induced $\gamma\delta$ T-cell responses completely. None of these antibodies discriminate between BTN3A members that share almost identical amino acid composition (Fig. 1.10 a), but whereas 20.1 can cross-link multiple members by binding on their side IgV domains, the 103.2 seems to obstruct the upper IgV domains of BTN3As (Palakodeti et al., 2012). It has also been shown that the agonist 20.1 stimulates a selective range of clonotypes and generally activates around 40 % of donor-derived polyclonal Vγ9Vδ2 T cells (Starick et al., 2017).

Members of the BTN3A subfamily dimerise, even in solution, in two alternative structural conformations each hold by weak chemical contacts such as hydrogen bonds and van der Waals contacts (Fig. 1.10 b) (Palakodeti et al., 2012). One forms V-shape structures with IgV domains pulled away from the membrane and is hold by IgC domains contacting each another on facing symmetric parallel β-sheets involving D120, D124, and T203 residues. The alternative form structures in a head-to-tail conformation and integrates residues from the A and D strands of the IgC domain linking the IgV domain of the other. Of the two possible structures, the V-shape seems to prevail in the form of BTN3A1/2 dimers, as trapping this structure by induced IgC disulphide bonds (D124/S207C) diminishes its immunogenic proprieties either in the presence of phosphoantigen or an agonist 20.1 (Gu et al., 2017). This V-shape structure could represent the resting state of these heterodimers, and when phosphoantigens are bond to BTN3A1 B30.2 the dimer shifts into the alternative head-to-tail conformation and activates $\gamma\delta$ T cells (Gu et al., 2018).

BTN3A1 has been regarded as the hallmark molecule that senses phosphoantigens and activate Vγ9Vδ2 T cells (Gu et al., 2018; Willcox and Willcox, 2019). However, there has been a debate on whether phosphoantigen binds to BTN3A1 intracellular B30.2 or extracellular IgV domains (Sandstrom et al., 2014; Vavassori et al., 2013; Wang and Morita, 2015). Phosphoantigen interactions with either domain have been reported (Table. 1.9). The hypothesis where phosphoantigen binds to IgV postulates a model analog to classical recognition of antigen-molecular complexes (Vavassori et al., 2013). The other model was supported by crystallographic studies and describes a novel antigen-presentation mode in which BTN3A1 senses the phosphoantigen metabolites internally, by its B30.2 domain, and subsequent structural conformational changes transmitted towards its ectodomains is what activates Vγ9Vδ2 T cells (Gu et al., 2018; Sandstrom et al., 2014; Wang and Morita, 2015). Even though

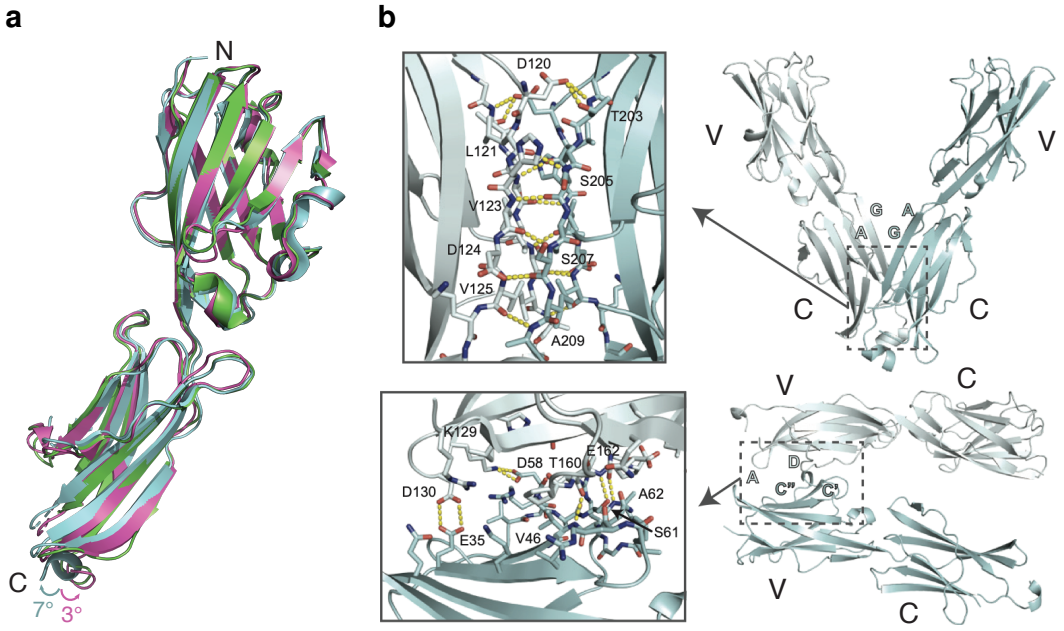

Figure 1.10: *Human BTN3A ectodomains shares 95 % amino acid identity (a) superposed with indicated angle shift from BTN3A1 (green), BTN3A2 (slate), and BTN3A3 (pink) with carboxyl (C) or amino (N) terminal groups, in PyMOL; and (b) adapted supplementary figure form Palakodeti et al. (2012) denoting two observed configurations for BTN3 crystal structures indicating constant (C) and variable (V) domains.*

the first molecular interpretation in support of the second model was challenged by the absence of electron density in the HMBPP-analog side chain, which defines the non-diphosphate part that determines the activity to phosphoantigens, this was later revised and widely accepted (Wang and Morita, 2015; Yang et al., 2019). The second model has been more accepted than the former and now supported by several crystallographic studies (Sandstrom et al., 2014; Wang and Morita, 2015; Yang et al., 2019). Even though BTN3A1 senses phosphoantigens and is necessary (Sandstrom et al., 2014; Vavassori et al., 2013), yet not sufficient to stimulate Vγ9Vδ2 T cells (Riaño et al., 2014). Stimulating them with mouse or hamster BTN3A1-transfected cells plus agonist 20.1 is neither enough to induce activation, unless inserting the entire human chromosome 6 (Riaño et al., 2014; Riaño, 2016). All these indications suggest there is at least a second protein ligand involved in this presentation mechanism which is absent in rodent species and contained within the human chromosome 6.

BTN3A1 heterodimerise in the endoplasmic reticulum with BTN3A2 else BTN3A3, regardless of phosphoantigens, and this is a necessary condition for correct BTN3A1 expression on the cell-surface (Vantourout et al., 2018). This phenomena is also observed across the family of BTN molecules, nevertheless. Mouse Btnl1 and Btnl6 are regulated under similar mechanism, where Btnl1 is retained in the cytoplasm un-

less Btnl6 is present (Jandke et al., 2020). Soluble BTN3A proteins homodimerise themselves too (Palakodeti et al., 2012; Vantourout et al., 2018), although most commonly they are functionally active in form of heterodimers such as Skint1/2, Btnl1/6, BTNL3/8, or BTN3A1/2-3 (Di Marco Barros et al., 2016; Jandke et al., 2020; Melandri et al., 2018; Vantourout et al., 2018). Presentation of phosphoantigens is thus controlled by BTN3A1 and co-expression of either BTN3A2 or BTN3A3 members that transmit activation signals to human Vγ9Vδ2 T cells. Additionally, there are two membrane associated proteins Ras homolog gene family, member B (RhoB) and periplakin that appear to confer stability of the BTN3A1/2-3 membrane complex and the cytoskeleton scaffold (Laplagne et al., 2020; Rhodes et al., 2015; Sebestyen et al., 2016). Periplakin relates to cross-linking the complex together with the plasma membrane and its interaction is dependent on membrane-proximal di-leucine motif located upstream of the BTN3A1 B30.2 cytoplasmic tail excusively, as neither BTN2A2 nor BTN3A3 have this motif (Rhodes et al., 2015). Similarly, GTPase activity of RhoB seems another vital factor linked to the plasmic membrane adhession necessary for complete phosphoantigen-induced responses by $\gamma\delta$ T cells (Laplagne et al., 2020). Intracellular GTPase activity of RhoB is likely a critical mediator that regulates aspects of intracellular actin dynamics, apart from other essential cellular related functions (Vega and Ridley, 2018). Considering the number of proteins involved and their interactions, it would be reasonably to believe in the formation of a BTN-based clustering and membrane-adhered factors to constitute a complex raft that uses an inside-out signalling mechanism involving structural changes of BTN3A1 to confer reactivity by $\gamma\delta$ T cells (Gu et al., 2018).

Surface expression of BTN3A proteins is considered ubiquitous in somatic cells, and corresponding genetic expression remarkably rich across the majority of cancer profiles including blood and solid tumours alike (Gentles et al., 2015; Verschueren et al., 2020, PRECOG). Detection of circulating programmed cell death protein 1 (PD1), PD-L1, pan-BTN3As, BTN3A1 and B and T lymphocyte attenuator (BTLA) proteins in plasma samples detected with respective antibodies is associated with patients suffering from pancreatic adenocarcinoma, meaning detection of these proteins in blood screens could predict tumour diagnosis (Bian et al., 2019). $\gamma\delta$ T cells infiltrate most human tumours and their potential often ignored (Legut et al., 2015). Knowing their activation can be elicited by BTN and BTNL molecules is essential for the advance of immunotherapy and understanding their implications in both $\alpha\beta$ and $\gamma\delta$ T cell responses. The latest study to date reports that BTN3A1 inhibits tumour-reactive $\alpha\beta$ TCR activation by preventing segregation of N-glycosylated CD45 from the immune synapse (Payne et al., 2020). Alternative agonist 20.1 functions to stimulate circulat-

ing Vγ9Vδ2 T cells, while antagonist 103.2 or CTX-2026 BTN3A-specific antibodies can elicit coordinated restoration of infiltrated $\alpha\beta$ T-cell effector functions against cancer cells, abrogating malignant progression (Harly et al., 2012; Payne et al., 2020). These encouraging results mimic immune checkpoint therapy and pave the way for enhanced $\gamma\delta$ T cell innate and adaptive functions using BTN regulatory molecules as the main immunotherapeutic target.

1.6 Aims of the Thesis

This thesis aims to advance the understanding in the activation mechanism of Vγ9Vδ2 T cells by phosphoantigens and provide an insight into the relationship between these cells and molecules of the BTN family.

The underlying mechanism in the activation of $\gamma\delta$ T cells by phosphoantigens has been a crucial question since their discovery and the identity of the ligands recognised by the $\gamma\delta$TCR a mystery, yet essential to resolve to understand better the function of the Vγ9Vδ2 T-cell subset. Seminal investigations describe phosphoantigen-presentation is MHC-unrestricted and molecules of the BTN family are required (Harly et al., 2012; Sandstrom et al., 2014; Vavassori et al., 2013). It is assumed that phosphoantigen-dependent activation of $\gamma\delta$ T cells depends on BTN3A1, an immunoglobulin-like molecule. However, additional proteins located in the same cluster are indispensable for its function (Harly et al., 2012; Riaño et al., 2014; Sandstrom et al., 2014). Although phosphoantigens interact to a basic inner pocket located at the BTN3A1 B30.2 domain involving a global structural change (Sandstrom et al., 2014; Wang et al., 2019), the full activation mechanism has not been described nor the direct $\gamma\delta$TCR ligand identified.

Accordingly, the aims of this thesis are:

- Identify the molecular ligand that directly binds to the phosphoantigen-reactive $\gamma\delta$ TCR and determine its affinity.
- Investigate the role of BTN3A1 in $\gamma\delta$TCR-dependent recognition of phosphoantigens.
- Study the role of BTN family molecules and phosphoantigens in the context of inducing $\gamma\delta$ T-cell immune responses.
- Explore the co-stimulatory propriety of the new ligand in conjunction with members of the CD1 family of lipid-presenting molecules in activating $\gamma\delta$ T-cells.

- Decipher which residues are implicated in recognition of phosphoantigens by the Vγ9Vδ2 TCR.

- Evaluate the cytolytic capacity of $\gamma\delta$ T-cells and the role of BTN in cancer therapy using BTN-knockout lines and assessing the viability of tumour cells in vitro.

Moreover, the progression of cancer disease seems to associate to a reduced number of infiltrating Vγ9Vδ2 T cells in tumour sites and correlates with lower mortality and relapse rates (Toia et al., 2016). Some tumour cells are susceptible to amino-bisphosphonate drug treatments, including several renal cell carcinoma cell lines such as ACHN or 786-O that show increased antitumoural effector functions by $\gamma\delta$ T cells (Idrees et al., 2013). This phosphoantigen-reactive $\gamma\delta$ T cell responses are consistent with previous reports where $\gamma\delta$ T cells selectively lyse renal cell carcinoma resistant to conventional treatments (Viey et al., 2005). Herein, this work grows PDO cultures from kidney biopsies to study the prevalence of phosphoantigen-reactive $\gamma\delta$ T cells infiltrated within the renal tumour microenvironment.

- Culture 3D-organoid cultures to study the role of phosphoantigen-reactive $\gamma\delta$ T cells in the tumour environment of renal carcinomas.

Finally, this thesis aims to set the basis for identifying single-cell $\gamma\delta$TCR clonotypes and link this information to their respective transcriptomes after receiving different stimuli such as phosphoantigens, antibodies, or amino-bisphosphonate drugs (Tu et al., 2019). For this reason, it sets the framework to advance future work on:

- Single-cell $\gamma\delta$ T-cell 5'-clonotyping paired with a massive parallel transcriptome analysis from donor-purified $\gamma\delta$ T cells.

Chapter 2

Material and Methods

2.1 Cell Cultures

2.1.1 Human Samples

Healthy donor blood derived human PBMC were obtained from the Australian Red Cross Blood Service under ethics approval 17-08VIC-16 or 16-12VIC-03, with ethics approval from University of Melbourne Human Ethics Sub-Committee (1035100), and isolated via density gradient centrifugation (Ficoll-Paque PLUS GE Health care) followed by lysis of red blood cells (ACK buffer, produced in-house). Established cell lines were routinely verified for *Mycoplasma sp* either with the MycoAlert (Lonza) or PCR (Venor®GeM Classic, Minerva Biolabs) tests (Sec. B.3).

2.1.2 Isolation of $\gamma\delta$ T cells and Expansion

Donor-derived $\gamma\delta$ T cells were enriched by magnetic-activated cell sorting (MACS) using PE-Cy7-conjugated anti-$\gamma\delta$TCR followed by anti-phycoerythrin-mediated magnetic bead purification (Miltenyi Biotec). After enrichment, the signalling glycoprotein component (CD3)$^+$ Vδ2$^+$ $\gamma\delta$ T cells were further purified in a cell sorter Aria III (BD). These enriched $\gamma\delta$ T cells were subsequently stimulated in vitro for 48 h in a plate-bound anti-CD3ϵ (OKT3, 10 µg ml^{-1}, Bio-X-Cell), soluble anti-CD28 (CD28.2, 1 µg ml^{-1}, BD Pharmingen), phytohemagglutinin (0.5 µg ml^{-1}, Sigma-Aldrich), IL-15 (50 ng ml^{-1}), and recombinant human IL-2 (100 U/ml, PeproTech), and maintained with IL-2 and IL-15 for 14–21 days. Cells were cultured in complete medium consisting of a 50:50 (v/v) mixture of RPMI-1640 and AIM-V (Invitrogen) supplemented with 10 % (v/v) FCS (JRH Biosciences), penicillin (100 U/ml), streptomycin (100 µg ml^{-1}), Glutamax (2 mM), sodium pyruvate (1 mM), nonessential amino acids (0.1 mM), and HEPES buffer (15 mM), pH 7.2–7.5 (all from Invitrogen Life Technologies), plus 50 µM 2-mercaptoethanol (Sigma-Aldrich).

2.1.3 Functional $\gamma\delta$ T-Cell Assays

Fresh PBMC (2×10^6) were cultured in 24-well plates in the presence or absence of zoledronate (4 µM, Sigma) and purified monoclonal antibodies against BTN2A1, BTN3A1, or isotype control IgG1κ (MOPC-21, BioLegend) (10 µg ml^{-1}). After 24 h CD3ϵ^+ $\gamma\delta$TCR V$\delta2^\pm$ T cell activation was assessed by flow cytometry and cytokine production was determined by cytometric bead array according to manufacturer's instructions (BD). For the assays in supplementary figure 7, PBMC were cultured in 24 well plates and blocked for 30 min with monoclonal antibodies against BTN2A1, BTN3A1, or isotype control (10 µg ml^{-1}). Cells were then stimulated for 18 h with combinations of HMBPP (0.5 ng ml^{-1}, Sigma), zoledronate (4 µM, Sigma) and CEF (1 µg ml^{-1}, Miltenyi Biotec) in addition to IL-2 (25 U ml^{-1}, Miltenyi Biotec) and Golgiplug protein transport inhibitor (BD Biosciences). Cells were surface-stained and then fixed and permeabilized using Foxp3/Transcription Factor Staining Buffer Set (Invitrogen) according to the manufacturer's protocol followed by staining with anti-IFN-γ (Biolegend). For coculture assays, purified and in vitro-expanded $\gamma\delta$ T cells (5×10^5) were incubated in 96-well plates with antigen-presenting cells (3×10^5) for 24 h $\pm$ zoledronate (4 µM), and $\gamma\delta$ T cell activation was determined by flow cytometry as above. Alternatively, 4×10^4 primary $\gamma\delta$ T cells purified from PBMC donors using a $\gamma\delta$ T cell magnetic bead isolation kit (Miltenyi Biotec) were cultured at a two-to-one ratio with either wild-type LM-MEL-62 or *BTN2A1*$^{-/-}$ as antigen-presenting cells in the presence of zoledronate (1 µM) for 2 days. Non-adherent cells were subsequently washed and cultured in fresh plates without APC for an additional 7 days in media plus 100 U ml^{-1} IL-2. V$\delta2^+$ $\gamma\delta$ T cells were then enumerated by flow cytometry.

2.1.4 Flow Cytometry

Human cells were pelleted at 400g, washed, and incubated at 4 ℃ with phosphate buffered saline (PBS) containing 2 % foetal bovine serum (FBS) and human Fc receptor block (Miltenyi Biotec). Mouse Fc receptors were instead blocked with anti-CD16/CD32 (clone 2.4G2, produced in-house). Cells were then incubated with 7-aminoactinomycin D (7-AAD, Sigma) or LIVE/DEAD viability markers (ThermoFisher) plus antibodies (Table. B.1). BTN2A1 and BTN3A were detected using monoclonal antibodies generated in-house (Sec. A.3). Anti-BTN2A1 monoclonal antibodies or matched isotype control (clone IgG2a, produced in house —here, aka BM4) were conjugated to AF647 via amine coupling (ThermoFisher), and anti-BTN3A (clone 103.2) was conjugated to PE (Prozyme) using sulfo-SMCC heterobifunctional crosslinker. In some experiments, unconjugated anti-BTN2A1 monoclonal antibody was detected

using goat anti-mouse polyclonal secondary antibody BV421 or PE (BD-Pharmingen), with a subsequent blocking step (5 % normal mouse serum). Cells were also stained with tetrameric Vγ9Vδ2 TCR, BTN2A1 or mouse CD1d–α-GalCer ectodomains (produced in house), or equivalent amounts of streptavidin conjugate alone (BD). Each reagent was titrated to determine the optimal dilution factor. All data was acquired on an LSRFortessa™ II, FACSCanto (BD), or CytoFLEX LX (Beckman Coulter), and analysed with FACSDiva and FlowJo (BD) software. All samples were gated to exclude unstable events, doublets and dead cells using time, forward scatter area versus height, and viability dye parameters, respectively

2.1.5 Detection of Förster Resonance Energy Transfer

Cells were stained with PE-conjugated anti-BTN3A1 (donor) and AF647-conjugated BTN2A1 (acceptor) for detection of Förster resonance energy transfer (FRET) between BTN2A1 and BTN3A1 extracellular domains. The FRET signal was detected in a compensated yellow 670/30 channel. Each cyan fluorescent protein (CFP) (mTurquoise2, donor) or yellow fluorescent protein (YFP) (mVenus, acceptor) constructs contained either a long (used for BTN3A1 and BTNL3) or short (used for BTN2A1 and BTNL8) flexible amino-terminal sequence linker synthesised artificially (ThermoFisher). These were cloned into the carboxyl-terminus of full-length BTN constructs between an in-frame MfeI site introduced by site-directed mutagenesis and a 3' SalI site that removed the pMIG IRES-green fluorescent protein (GFP) motif. The CFP fluorescent signal was detected in a violet 450/50 channel and the YFP in the yellow 585/15. The FRET was detected in the violet 530/30 channel from which CFP and YFP spillover had been removed by compensation. The frequency of cells identified in a FRET positive signal were examined on gated CFP$^+$ and YFP$^+$ mouse fibroblast NIH-3T3 (NIH/3T3) cells for dual-transfectants or CFP$^+$ or YFP$^+$ for respective single-transfectants.

2.1.6 Jurkat-Reporter T-Cell Assays

Antigen-presenting cell lines LM-MEL-62 or LM-MEL-75 were seeded at 2.5×10^4 cells per well in a 96-well plate and incubated overnight. Then 2×10^4 G115 mutant $\gamma\delta$TCR-expressing Jurkat-reporter cell line J.RT3-T3.5 (ATCC® TIB-153™) were added in the presence or absence of zoledronate, HMBPP, or IPP. Early transmembrane C-Type lectin activation marker (CD69) expression was measured the next day by flow cytometry on GFP$^+$ Jurkat cells. A panel of nineteen single-residue alanine mutants, each within in the Vγ9 or Vδ2 domains of G115 were generated by site-directed mu-

tagenesis using the primers listed in Table. A.2. Primers (IDT) were phosphorylated (PNK, NEB) followed by twenty-five cycles of PCR using KAPA HiFi master mix (KAPA Biosystems) and the wild-type G115 in pMIG as a template. Respective PCR products were digested with DpnI (NEB) and ligated with T4 DNA ligase (NEB). Construct sequences were verified by Sanger sequencing prior to transfections. To examine the capacity of G115 mutants to bind to BTN2A1 tetramer, human embryonic kidney 293 (HEK-293T) cells were transfected with individual γ- or δ-chain mutants, plus the corresponding wild-type δ- or γ- chain, respectively, as well as a pMIG constructs encoding 2A-linked human CD3$\gamma\delta\epsilon\tau$, at a one-to-three ratio with FuGENE® HD (Promega) in OptiMEM™ (Gibco, ThermoFisher). From 48 h post-transfection, HEK-293T cells were resuspended by pipetting, and stained for CD3ϵ expression and PE-labelled BTN2A1 tetramer or control PE-conjugated streptavidin. The median fluorescence intensity of BTN2A1-tetramer fluorescent probe interacting with mutant G115 TCRs was examined on gated CD3$^+$ GFP$^+$ HEK-293T cells by flow cytometry. The capacity of G115 mutants to respond to phosphoantigen stimulation was assessed by transducing JRT3-T3.5 cells with G115 mutant TCRs. Log-expanding PE cells were transfected with each particular γ- or δ-chain mutant plus the corresponding wild-type δ- or γ-chain, respectively, along with human CD3, pVSV(-G), and pEQ-Pam3(-E), and mixed at a one-to-three ratio with FuGENE® HD in OptiMEM™. After 24 h, all viral supernatants were collected and filtered through a 0.45-µm CA syringe filter membrane and incubated with JRT3-T3.5 cells for 12 h. This process was repeated twice a day for four days. CD3$^+$ and GFP$^+$ JRT3-T3.5 cells were purified by FACS (BD FACSAria™ III) and examined for their capacity to respond to phosphorylated antigens presented by wild-type LM-MEL-75 antigen-presenting cells as described above. To measure G115 $\gamma\delta$TCR-expressing JRT3-T3.5 cell reactivity to anti-BTN3A1 (clone 20.1) monoclonal antibody, 2.5×10^4 LM-MEL-75 melanoma cells were pre-incubated with functional grade 20.1 (10 µg ml^{-1}, Biolegend), or matched isotype control for 30 min at room temperature and later plated in a flat-bottom 96-well plate. Once antigen-presenting cells had adhered, 2.5×10^4 JRT3-T3.5 cells were added making a final antibody concentration of 5 µg ml^{-1}. After 24 h coculture the level of CD69 activation marker on CD3$^+$ and GFP$^+$ gated Jurkat cells was determined by flow cytometry.

2.1.7 Plate-Bound Assays

Either single or combined purified in-house BTN protein products or antibody controls were added into 96-well standard polystyrene cell culture plates with 50 µl sterile-PBS solution and incubated for 2 h at 37 ℃ to coat the underling surface. The remaining

protein in solution was rinsed three times with sterile-PBS. Each well was immediately covered with a solution of $\gamma\delta$ T-cell media containing either donor-purified Vδ2 T cells or Jurkat-reporter cells. After an overnight incubation at 37 ℃ and 5 % CO_2 the cells were harvested and respective activation markers analysed in a flow cytometer.

2.1.8 Tumour Cell Viability

Tumour cells (2.5×10^4) were stained with CellTrace™ Violet (ThermoFisher) for long-term single-cell labelling and seeded in 96-well flat bottom plates with $\gamma\delta$ T-cell media in the presence or absence of zoledronate (4 µM). After 4 h, purified Vγ9Vδ2 T cells were added in ratios of one-to-none, -one, -five, and in the next two days all cells were harvested and enumerated in a LSRFortessa™ II.

2.2 Genetically Engineered Proteins

2.2.1 Production of Tetramers

Soluble monomers were designed and produced in-house according to Sec. A.1 to increase the stability and avidity for specific ligands of laboratory self-constructed synthetic biological probes. The yield was quantified by measuring their absorbance at 280 nm wavelength read in a NanoDrop™ (Thermo Fisher) instrument, and respective values were divided by their corresponding extinction coefficient value (Table 2.2). Table 2.1 show the amino acid characteristics for six $\gamma\delta$TCR clones.

Each monomer was tetramerised by adding four times the monomer's volume to streptavidin-conjugated in PE across three rounds to achieve maximum efficiency. This mixture was incubated in the dark at room temperature to ensure the maximum binding capacity of its four reactive binding sites. The final concentration was regarded as the maximum load of monomer added in the reaction. All solutions were diluted in TBS pH 8 Tris 10 mM 150 mM NaCl.

2.2.2 Production of Recombinant Antibodies

Monoclonal antibodies clones 20.1 and 103.2 against membrane proteins of the BTN3 family were produced in a mammalian cell culture followed by purification steps and conjugation to a fluorescent fluorophore. Variable sequences were synthesised (ThermoFisher) including restriction enzyme sites for AgeI/SalI in the heavy and AgeI/BsiWI in the light chains were codon optimised for expression in human cell cultures (Table. A.1). DNA was digested along with a high copy number Kanamycin-resistance

Table 2.1: *Paired γ- and δ-chain sequences of CDR3 from selected HMBPP-reactive TCR from a single cell sort and the prototypical clone G115.*

Clone	*TRDV*	*TRDD*	*TRDJ*	*CDR3δ*	*TRGV*	*TRGJ*	*CDR3γ*
3	V2*03	D3	J1	CACDPVQVTGGYKVDKLIF	V9	JP	CALWEVHELGKKIKVF
4	V2*03	D3	J1	CACDTVQRLGDRPTDKLIF	V9	JP	CALWEVQELGKKIKVF
5	V2*03	D3	J1	CACDGILGDSHTDKLIF	V9	JP	CALWELAELGKKIKVF
6	V2*03	D2+3	J1	CACDPLLGSERLGDTGIDKLIF	V9	JP	CALWESQELGKKIKVF
7	V2*02	D3	J1	CACDRVLGDTRWTDKLIF	V9	JP	CALWEVHELGKKIKVF
8	V2*02	D2+3	J1	CACDPISYAGGYPPLYTDKLIF	V9	JP	CALWEVQELGKKIKVF
G115	V2	D3	J1	CACDTLGMGGEYTDKLIF	V9	JP	CALWEAQQELGKKIKVF

Table 2.2: *Compound chemical details of common reagents used in the lab and related information for protein expression and quantification.*

Expression system	*Species*	*Protein*	*Molecular mass (kDa)*	*Mass attenuation coefficient ($g^2\,cm^{-1}$)*
HEK-293S.GnTI	Human	BTN2A1 IgV-IgC	27.7	1.180
Expi293.GnTI$^-$	Human	BTN2A1 IgV-IgC	27.7	1.180
Expi293	Human	BTN2A1 B30.2	23.6	1.270
HEK-293S.GnTI	Human	BTN3A1 IgV-IgC	53.9	1.270
Expi293.GnTI$^-$	Human	BTN3A1 IgV-IgC	53.9	1.270
Expi293	Human	BTN3A1 B30.2	22.9	1.910
HEK-293S.GnTI	Mouse	CD1d	45.0	NA
DH5-Alpha	Human	hMR1-5-OP-RU	43.0	2.070
HEK-293S.GnTI	Human	TCR-3	67.4	0.940
HEK-293S.GnTI	Human	TCR-4	67.4	0.918
HEK-293S.GnTI	Human	TCR-5	67.1	0.921
HEK-293S.GnTI	Human	TCR-6	67.8	0.912
HEK-293S.GnTI	Human	TCR-7	67.5	0.998
HEK-293S.GnTI	Human	TCR-8	67.7	0.978

in DH5alpha mammalian vector pCMV containing an IGHV signal peptide and mouse IgG1 constant regions. Resulting products were run in an electrophoresis gel with 1.5 % agarose and TBE buffer; resulting bands excised and purified in an UltraClean® 15 DNA Purification Kit (Qiagen) (Fig. A.4 a). An insert ratio of one-to-three was deduced effective considering their relative molar ratios. Conversions were made as (see Promega online tool)

$$\mu\text{g DNA} \times \frac{10^6 \text{ pg}}{1 \text{ µg}} \times \frac{\text{pmol}}{660 \text{ pg}} \times \frac{1}{\text{N}} = \text{pmol DNA}, \tag{2.1}$$

where N is the number of nucleotides and 660 pg pmol^{-1} is the average molecular mass of a nucleotide pair. The quantity of insert used was calculated accordingly to

$$\text{ng of insert} = \text{ng of vector} \times \frac{\text{kb of insert}}{\text{kb of vector}}, \tag{2.2}$$

where the light chain is 330 bp, heavy chain 360 bp, and plasmids 800 bp. The insert and plasmid were ligated accordingly with an overnight 4 ℃ incubation with a T4 ligase (New England Biolabs) and 2× buffer (Promega). Ligated plasmids were transformed into competent *E. coli* DH5-Alpha cultures and cultured in a 30 µg ml^{-1} kanamycin agar plates. Next day, the bacterial culture was grown in 10 ml lysogeny broth overnight and plasmid DNA isolated in a miniprep classic kit (Zymo Research). Samples were amplified and sequenced with forward (1012 Fwd) and reverse (1012 Rev2) primers for verification. Confirmed colonies were amplified in a low-endotoxin PureYield™ maxiprep system (Zymo Research) for a larger yield and sequences were verified in all cases by alignment on CLC Main Workbench (Qiagen). Resulting light and heavy chain constructs of respective antibodies were jointly expressed in a transient Expi293 cell expression system (Thermo Fisher) according to Vazquez-Lombardi et al. (2017, Steps 19–29).

Filtered cell culture supernatants were purified in an immobilised protein G HP column (GE Lifesciences) using an automated Äkta pure system, where buffer *A* contained comercial endotoxin-free PBS (Gibco) and *B* a 0.2 µm filtered elution glycine-HCl 0.1 M pH 2.7 buffer. Eluted antibodies were collected in 1 M Tris pH 9.2 to neutralise the acidic pH of the elution buffer at a final 7.8 pH solution (Fig. A.5). Fractions containing the antibodies were concentrated in Vivaspin concentrator tubes (GE Lifesciences) and final antibody concentration recorded at A280 (10 µm) in a NanoDrop™ Lite (Thermo Fisher) instrument. Finally, the quality of concentrated antibodies were validated under reduced and non-reduced conditions sodium dodecyl sulfate polyacrylamide gel electrophoresis (SDS-PAGE) (Fig. A.4 b).

Table 2.3: *Extracellular domain (EC) amino acid sequences of BTN2A1 and BTN3A1 members for cloning in pHLsec vectors, including a start codon and secretory leader sequence from pHLsec (olive green), an AgeI cloning site (orange), a flexible linker (cyan), an Avi-Tag where biotin is attached to the K residue (purple), a Hexa-His tag (blue), an XhoI cloning site (red), and an internal KpnI cloning site for alternative constructs with C-terminal BirA-tag proteins (midnight blue).*

Construct	*Amino acid final product sequence*
BTN2A1$_{EC}$	MPALLSLVSLLSVLLMGCVAETGQFIVVGPTDPILATVGENTTLRCHLSPEKNAEDMEVRWFRSQFSPAV FVYKGGRERTEEQMEEYRGRTTFVSKDISRGSVALVIHNITAQENGTYRCYFQEGRSYDEAILHLVVAG LGSKPLISMRGHEDGGIRLECISRGWYPKPLTVWRDPYGGVAPALKEVSMPDADGLFMVTTAVIIRDKS VRNMSCSINNTLLGQKKESVIFIPESFMPSVSGTGSGSGGLNDIFEAQKIEWHEHHHHHH
BTN3A1$_{EC}$	MPALLSLVSLLSVLLMGCVAETGQFSVLGPSGPILAMVGEDADLPCHLFPTMSAETMELKWVSSSLRQV VNVYADGKEVEDRQSAPYRGRTSILRDGITAGKAALRIHNVTASDSGKYLCYFQDGDFYEKALVELKVA ALGSDLHVDVKGYKDGGIHLECRSTGWYPQPQIQWSNNKGENIPTVEAPVVADGVGLYAVAASVIMRG SSGEGVSCTIRSSLLGLEKTASISIADPFFRSAQGTGSGSGGLNDIFEAQKIEWHEHHHHHH

A partition of the 103.2 antibody clone was labelled to PE fluorophore according to an in-house conjugation protocol which used a sulfo-SMCC heterobifunctional crosslinker bound to PE (Prozyme) at its free-reactive amino-sulfhydryl group and to the antibody at the maleimide functional group.

Antibody Labeling

Antibody clone 103.2 was labelled to PE fluorophore according to an in-house conjugation protocol based on a sulfo-SMCC water-soluble heterobifunctional protein cross-linker with PE at the amino-sulfhydryl side and the antibody to the maleimide side. Antibodies against the BTN2A1 and respective isotype control (IgG2a/BM4) were instead conjugated to AF647 with a conjugation antibody labelling kit (Thermo Fisher) following the manufacturer instructions.

2.2.3 Expression of Extracellular Domain Protein Constructs

Genetic sequences encoding for extracellular domains of two BTN molecules were optimised for expression in mammalian system in pHLsec vectors and included both enzyme restriction sites and protein tags for recovery and post-processing the product produced. Table 2.3 show the amino acid codes respective of the BTN2A1 and BTN3A1 extracellular protein products with highlighted additional sequences for post-production processes.

2.2.4 Transfection of Full-length Protein Constructs

Codon-optimised gene sequences for *BTN2A1*, *BTN2A2*, *BTN3A1*, *BTN3A2*, *BTNL3* and *BTNL8* (all isoforms 1) were cloned into pMIG II mammalian expression vector

(a gift from D. Vignali, Addgene plasmid # 52107) and verified by Sanger sequencing. Mouse NIH-3T3, hamster CHO-K1, human LM-MEL-62 cells were seeded the day before and transfected using FuGene HD® or Viafect™ in OptiMEM according to manufacturers' instructions. After 48 h (72 h with LM-MEL-62 cells) to enable gene expression, cells were tested for GFP and gene expression and subsequently used in phenotyping or functional assays. All transfection efficiencies were evaluated previously to the experiments (Sec. A.5.1 and A.6).

2.3 Whole-genome Knockout Genetic Screen

The knockout screen was based on the CRISPR/Cas9 technology and performed as described in Joung et al. (2017). Briefly, a pooled lentiviral human gRNA knockout library containing six gRNA per gene and four per microRNA (Addgene GeCKOv2 # 1000000048, a gift from F. Zhang) was transformed into Endura™ ElectroCompetent cells (Lucigen) at $>500\times$ coverage and grown in 1 L liquid Luria Broth cultures for 16 h at 37 ℃. Plasmid DNA was purified (PureLink™ gigaprep, ThermoFisher) and gRNA abundance in pre- and post-amplified libraries were validated by sequencing of PCR-amplified libraries (Illumina HiSeq, 60 10^6 reads per sample), with <0.2 % gRNA dropout. Lentiviral particles were produced by transient transfection of HEK-293T cells with the gRNA library DNA plus packaging plasmids using FuGENE® (Promega), and culture supernatant was titrated on LM-MEL-62 cells to determine the viral titre using puromycin (1 $\mu g\,mL^{-1}$, ThermoFisher). Four biological replicates of LM-MEL-62 cells (2×10^8 each) were transduced with the lentiviral library at a multiplicity of infection circa 0.3. Transduced cells were then selected with puromycin for an additional 5 d, after which Vγ9Vδ2 TCR tetramer clone 6^{low} cells were sorted from half of each replicate (circa 6×10^7), and the remaining half was used as the unsorted control. The sorted cells were re-expanded for approximately two weeks and subsequently re-sorted. This was repeated twice in order to adequately enrich for a clear Vγ9Vδ2 TCR tetramer clone 6^{low} population of LM-MEL-62 cells. Genomic DNA was then extracted as previously described in Chen et al. (2015), including an additional phenol-chloroform purification step. gRNA from 6×10^7 unsorted and 3×10^7 sorted cells was amplified from genomic DNA using PCR (33 cycles) with Pfu-based DNA polymerase (Herculase II Fusion, Agilent Technologies) and one-step primers containing index and adaptor sequences (IDT Ultramer oligos) as previously described in Joung et al. (2017). Amplicons were gel-extracted following electrophoresis (Wizard® SV Gel Clean-Up System, Promega), quantified with PicoGreen® (ThermoFisher) and sequenced using a NovaSeq (Illumina). Sample data were demultiplexed using a

combination of the forward primer stagger motifs, and the reverse 8-mer barcodes using Cutadapt (Martin, 2011) and analysed using the EdgeR software package in R (R Core Team, 2019; Robinson et al., 2009). Guides were enumerated using the processAmplicons function, allowing for a single base pair mismatch or shifted guide position. Guides with less than 0.5 counts/10^6 in at least five samples were excluded from the analysis. After dispersion estimation, differential gRNA expression between unsorted and sorted samples was determined using the exactTest function, where a false discovery rate (FDR) of $<$0.05 was considered statistically significant.

2.4 Biochemical Analysis

2.4.1 Isothermal Titration Calorimetry

ITC experiments were conducted on a MicroCal ITC200 instrument (GE Healthcare) at 25 ℃. BTN2A1 or BTN3A1 B30.2 domains were buffer-exchanged into PBS, and adjusted to a final concentration of 100 µM. HMBPP (Cayman Chemical) or IPP were adjusted to a final concentration of 1.9 and 2 mM, respectively, and serially injected into the cell in 2-µL increments following an initial 0.4-µL injection that was discarded from the analysis. Data were analysed with Microcal Origin software.

2.4.2 Surface Plasmon Resonance

In-home SPR experiments were conducted on a Biacore™ 3000 (GE Healthcare) and CSL repeats used a Biacore 8K instrument (GE Healthcare). All runs were at 25 ℃ and used 10 mM HEPES-HCl (pH 7.4), 150 mM NaCl, 3 mM ethylenediaminetetraacetic acid (EDTA), and 0.05 % Tween 20 buffer. $\gamma\delta$TCR ectodomains were directly immobilised to 260 resonance units (RU) on a Biacore sensor chip SA pre-immobilised with streptavidin. Soluble BTN proteins were serially half-diluted (200–3.125 µM) and simultaneously injected over test and control surfaces at a rate of 30 µl min^{-1}. After subtraction of data from the control flow cell (streptavidin alone) and blank injections, interactions were analysed using Biacore T200 evaluation software (GE Healthcare) and their respective K_D with R program (R Core Team, 2019).

2.5 Organoid Cell Clulture

2.5.1 Human-surgical Samples

Primary and metastatic human surgical biopsy samples from clear cell renal carcinoma tissues were obtained through the University Klinikum of Bonn (Germany), from patients undergoing surgical resection. All interventions and subsequent experiments were approved by the University of Bonn and Klinikum in accordance with the German regulations and ethical protocols with previous patient-informed consent for research.

2.5.2 In-vitro Organoid Cultures

For the preparation of air-liquid interface (ALI)-organoid plates, inserts containing a membranous bottom (PICM03050, Millicell-CM, Millipore) were inserted into tissue culture dishes as previously described in (Li et al., 2014; Ootani et al., 2009). Briefly, collagen gel matrices were prepared for trans-well inserts by mixing collagen matrix (Cellmatrix type I-A) with 10× concentrated sterile culture medium (Ham's F-12), next adding a sterile reconstitution buffer (2.2 g $NaHCO_3$ in 100 ml of 0.05 N NaOH and 200 mM HEPES). The mixture was kept at at 4 ℃ in a 8:1:1 ratio until solidifying as described in (Neal et al., 2018). A base-layer of 1 ml of reconstituted collagen solution was left to solidify at room temperature for 30 min at the bottom and later topped with the gel formation added to the insert. Human PDO culture Tumour tissues were minced in cold, washed twice in ADMEM/F12 (Invitrogen) containing 1× Normocin (InvivoGen), resuspended in 1 ml of Type I collagen gel (Trevigen), and layered on top of pre-solidified 1 ml collagen gel within a 30 mm, 0.4 mm inner trans-well to form the double dish air-liquid culture system. The trans-well containing tumour tissue and collagen was placed into an outer six-well plate culture dish containing 1 ml of medium (ADMEM/F12 supplemented with 50 % L-Wnt3A, RSPO1, Noggin-conditioned media (L-WRN, ATCC) with HEPES (1 mM, Invitrogen), Glutamax (1×, Invitrogen), Nicotinamide (10 mM, Sigma), N-Acetylcysteine (1 mM, Sigma), B-27 without vitamin A (1×, Invitrogen), A83-01 (0.5 mM, Tocris), Pen-Strep Glutamine (1×, Invitrogen), Gastrin (10 nM, Sigma), SB-202190 (10 mM, Sigma), and EGF (50 $\mathrm{ng\,ml^{-1}}$, Invitrogen) followed by replacing the plate's lid. Organoids were passaged every fortnight to a month by dissociation with 200 $\mathrm{U\,ml^{-1}}$ of collagenase IV (Worthington) at 37 ℃ for 30 min, followed by three 5 min washes with 100 % heat-inactivated FCS and replacing at a one-to-fourth split into new ALI collagen gels.

2.5.3 Organoid Disaggregation for Flow Cytometry

Organoids were recovered and dissociated from collagen gel by incubation with collagenase IV and following 0.05 % trypsin and EDTA. After cells were washed with 100 % heat-inactivated FCS and disaggregated with GentleMACS (Miltenyi Biotec) and passed through a 40 µm strainer before pelleted by centrifugation at 200 g. These pellets were next resuspended with FACS staining solution (2 % FCS in PBS) containing a 1/20 Fc-receptor blocking agent (Miltenyi Biotec) and respective antibody staining cocktail.

2.6 Statistic Analyses

Statistical significance between groups was performed using linear mixed model analysis (Bates et al., 2015; Pinheiro and Bates, 2000). In these analyses, we specified model predictors as fixed or random effects according to whether these affected equally across all samples or varied between them, such as were cells obtained from random donor sources. The output from the fix effects was used to compare between-sample estimates and respective Tukey-adjusted p-values calculated assuming an $\alpha = 0.05$ error (confidence interval $1 - \alpha$). Normal distribution of residuals has been evaluated for each statistical process. After analysis, contrasts between marginal means were reported in tables or the difference between predicted means plotted in graphs for visual comparison (Searle et al., 1980). The graphic representations highlighted confidence intervals for estimated means in blue and indicated between-sample comparisons in red arrows, where overlapping arrows meant no significance between the two groups according to the adjusted settings above-mentioned. The computation has been done using the R project statistical software according to their specific statistical R packages (Pinheiro et al., 2020; R Core Team, 2019).

Chapter 3

BTN2A1 Is a Ligand for the Vγ9 Domain of $\gamma\delta$ T-cells

3.1 Introduction

Human Vγ9Vδ2 T cells respond to phosphoantigens derived from microbial infections or tumour cells. This antigen-presentation mechanism is MHC-unrestricted and involves BTN3A1. The intracellular B30.2 domain of BTN3A1 plays a crucial role in sensing the presence of phosphoantigens and induces a structural conformational change. This molecular switch may work in conjunction with an additional proteins located at the chromosome 6 to activate the Vγ9Vδ2 T cells and cause an immune response (Harly et al., 2012; Riaño et al., 2014; Sandstrom et al., 2014). One of these proteins is BTN3A2 or BTN3A3 that heterodimerises with BTN3A1 and allows complex migration to the cell surface, where the two extracellular domains form a V-shape motif (Gu et al., 2017; Vantourout et al., 2018). Although the intracellular mechanisms required for $\gamma\delta$ T cell activation are unknown, there is an antagonist antibody capable to multimerise BTN3A protein and induce activation of Vγ9Vδ2 T cells irrespectively from phosphoantigen metabolites (Harly et al., 2012; Palakodeti et al., 2012).

To date, no direct ligand for the Vγ9Vδ2 TCR has been described despite multiple investigation attempts (Scotet et al., 2005; Vavassori et al., 2013; Willcox and Willcox, 2019). All studies agree the presence of BTN3A1 is a prerequisite and its intracellular B30.2 domain contains a basic pocket regarded as the phosphoantigen-binding site (Sandstrom et al., 2014; Wang and Morita, 2015; Yang et al., 2019). Interestingly, additional genes located in the human chromosome 6 (Riaño et al., 2014) are necessary despite one study considered BTN3A1 alone was sufficient to bind phosphoantigens via its extracellular IgV domain and activate $\gamma\delta$ T cells (Vavassori et al., 2013).

Here, tetramerised $\gamma\delta$TCR-fluorescent probes are used to scan putative molecular $\gamma\delta$TCR ligands across established human cancer cell lines. Cells that yield stronger affinity for these probes were selected for undertaking a genome-wide CRISPR/Cas9 knockout genetic screen with following fluorescence-activated cell sorting (FACS) for

the negative phenotype which enriched the negative population. Those cells with targeted genes incurring affinity loss for this fluorescent marker were compared to a reference population. Differential abundance in single-guide RNA reads between the two populations highlighted relevant genes presumbly responsible for that selected phenotype. The resulting top-hit gene was selected for undertaking subsequent experimental assays that validated the results form the genetic analysis. Next, biochemical interaction measures were performed to assess the receptor-ligand affinity and in vitro cell cultures with phosphoantigen challenge evidenced its relation to phosphoantigen activation by $\gamma\delta$ T cells.

3.2 Phenotyping Tumour Cell Lines and $\gamma\delta$TCR-ligand Screen

Assuming the role of BTN molecules in regulating $\gamma\delta$ T cell immune responses produced in-house anti-BTN3A antibodies (Sec. 2.2.2) were used to evaluate the prevalence of BTN3A protein members across the panel of human tumour cell lines, of which reflected the heterogeneity of most predominant cancer types. In the same line, a joined collaboration[1] was consolidated to access a panel of monoclonal antibodies against BTN2A proteins, of which those with unique specificity for BTN2A1 were used to reveal the profile of this protein at the cell surface (Sec. A.3). Antibody conjugation to PE or AF647 which targets either BTN member, enabled simultaneous staining to detect a possible FRET between these fluorophores. This procedures resulted in a twenty cell lines being characterised for their relative abundance of BTN2A1 and BTN3A family members and acquiring intuition if these proteins assembled should they realise a FRET signal (Fig. 3.1). Most Ludwig Melbourne-MELanoma (LM-MEL) cell lines, human monocytic (THP-1), HEK-293T, and K562 or human megakaryoblastic leukaemia (MEG-01) had a consistently elevated presence of BTN2A1 at their cell membranes. In contrast, multiple myeloma (RPMI-8226), Epstein-Barr virus transformed lymphoblastoid (C1R), Burkitt's lymphoma negative for Epstein-Barr virus (RAMOS) and Burkitt's lymphoma of the left maxilla (Raji), or T-cell leukaemia Jurkat 76.2 (Jurkat 76.2) and T-cell chronic lymphocytic leukaemia (SKW-3)[2] presented lower levels of detectable BTN2A1 protein at the surface membrane. Besides, BTN3A family members were found ubiquitous across all cell types. However, differentiation between BTN3A1, A2, and A3 members was undetermined due to the technical limitation of finding an antibody that discrete between their highly consolidated homogeneity. The presence of BTN2A1 using antibody RF13-231 was

[1] Tripartite collaborative agreement between the University of Melbourne, the ONJCRI, and the CSL.

[2] This cell line is likely to reflect an acute lymphoblastic leukaemia cell line KE-37 according to previous DNA fingerprint (DSMZ).

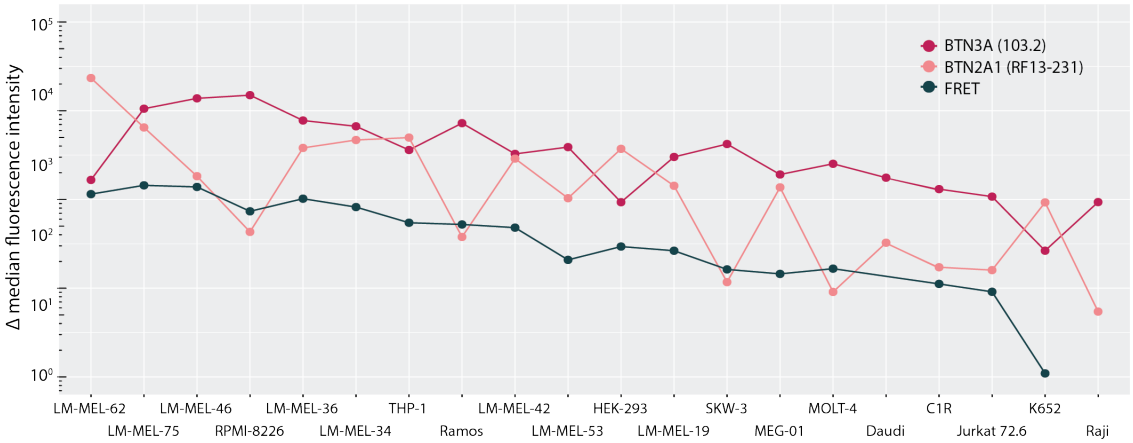

Figure 3.1: *Surface expression of BTN molecules in tumour cell lines. The y axis indicated the median fluorescence intensity differential-signal from monoclonal specific antibodies against BTN2A1 (RF13-231 in AF647), and BTN3 (103.2 in PE), or they resulting FRET detection (670/30-yellow) to respective isotype controls and averaged between two to three experiments.*

similar to BTN3A members in most LM-MEL cell lines and showed more variability in other established tumour lines such as in C1R, human T lymphoblast from acute lymphoblastic leukemia (MOLT-4), SKW-3, or Raji that its detection was minor.

Next, six selected phosphoantigen-reactive Vγ9Vδ2-TCR soluble protein clones were individually combined with streptavidin-PE conjugates to form tetramerised receptor fluorescent probes (Sec. 2.2.1). These were used to detect the presence of respective putative ligands present at the surface of the same established tumour cell lines, mentioned above. The resulting screening profile using this diverse panel of $\gamma\delta$ TCR-tetramers showed several clonotypes diversified in their affinity with putative ligands expressed on the surface of these cancer cell lines. Cones number 3 and 7 had a persistent affinity with most cancer cells followed by clones 4 and 6, whose binding affinity for these targets were similar; albeit a few exceptions like THP-1, Jurkat 76.2, and RAMOS resulted in a weak affinity or none regarding B-cell lines such as RPMI-8226, MEG-01, Burkitt's lymphoma Daudi (Daudi), Raji, and C1R. Contrary, clone 8 barely bound to any cancerous cell at all (Fig. B.2). LM-MEL-62 denoted the most outstanding affinity among every clonotype tested but clonotype number 8. This fact indicated a plausible generally accepted $\gamma\delta$ TCR-ligand recognised these tetramerised TCR-fluorescent probes. Following the top-ranked LM-MEL-62 cell line, K562 cells, HEK-293T, another melanoma LM-MEL-75, and the THP-1 cell lines were also considered potential candidates to host the same ligand.

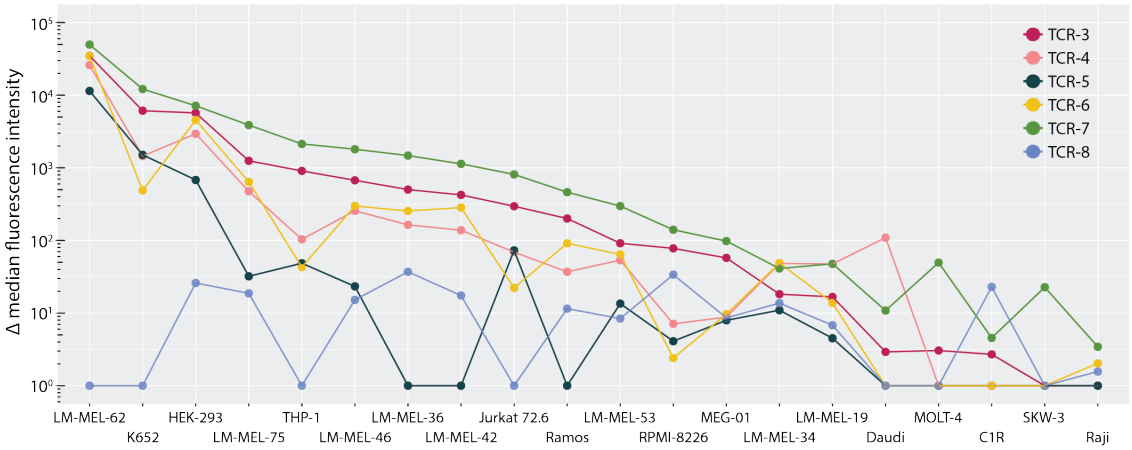

Figure 3.2: *Ligand screen using six different Vγ9Vδ2 TCR clonotypes across twenty human tumour cell lines. Human phosphoantigen-reactive Vγ9Vδ2 TCR clones are in a fluorescent tetramer form. Fluorescence signal was subtracted from a mouse CD1dα-GalCer tetramer control and averaged among two to three experiments.*

3.3 A Genetic Screen Identifies BTN2A1 as a Vγ9Vδ2-TCR Ligand

Genetic screens are genome-scale CRISPR/Cas9-knockouts in a given cell line to identify the function of an unknown gene. The strategy here consisted of mutating every protein encoding-gene in LM-MEL-62 or K562 cell lines to target putative TCR-ligands or critical modulators regarding this interaction. Screened cell populations were sorted and enriched, selecting for those stained cells that lost or incremented their fluorescent signal respective to a tetramerised TCR-6 probe detected by flow cytometry. This outcome resulted in two distinctive hits among 179 suggested genes considered within an acceptable FDR estimate regarding the LM-MEL-62 analysis for the negatively selected population, which lost the $\gamma\delta$-TCR stain. These two guiding sequences are GGCCATCCTGCACCTCGTAG corresponding to *BTN2A1*, and CGAGTAGGTCTGCTCCGCCA corresponding to *SPPL3*. Both of these genes obtained a similar p-value of 3×10^{-7} and 4×10^{-7}, respectively (Fig. 3.3 a). In contrast, the equivalent analysis for K562 cells resulted in lack of sensitivity to draw a defined outcome.

Next, given the lack of stringency supported by the *tag-wise* method to demonstrate the relevance for a gene having a role in the selected phenotype, an additional analysis was conducted to integrate the information of each sequence relative to their targeting genes. This second *gene-wise* analysis reinforced the statistical significance for BTN2A1 and SPPL3 genes respective of the two previous outstanding sequences that results form the LM-MEL-62 negative screen and expanded the parallelism between the genes they represent to a redefined p-values of 6×10^{-15} and 2×10^{-13},

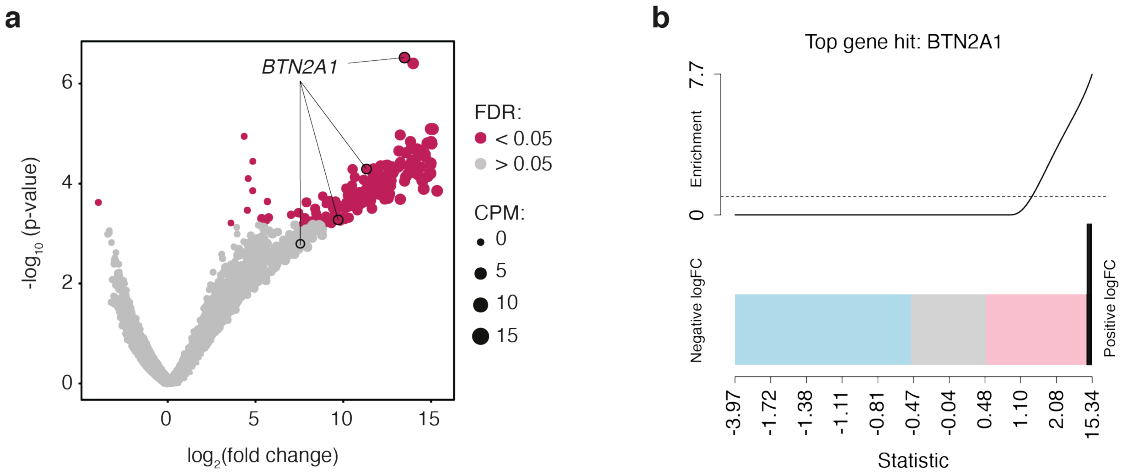

Figure 3.3: *Genome-wide negative selection screen in a melanoma LM-MEL-62 cell line. (a) Highlights those sequences with a statistical significative FDR and scaling according to normalised counts per million (CPM), and (b) shows a barcode representation for the top-ranked* BTN2A1 *gene resulting from a gene-wise analysis (Wu and Smyth, 2012). The four black vertical lines denote each* BTN2A1 *guiding sequence among others in the dataset.*

respectively (Fig. 3.3 b). Such a correlation-adjusted approach narrowed the results to twenty-eight genes considered responsible for losing affinity between the $\gamma\delta$-TCR clone 6 and its ligand on the LM-MEL-62 cell line. Thus, within a 95 % confidence interval and accounting for a readjusted FDR, the final outcome highlighted three candidate genes (*BTN2A1*, *SPPL3*, *SLC15A1*; Table 3.1). Altogether, the signal peptide peptidase-like 3 (SPPL3) becomes a popular hit for genomic screens targeting surface protein ligands, and investigations found it is responsible for regulating glycosphingolipid synthesis necessary to constitute the cell plasma membrane. It is reported without *SPPL3* the membrane becomes longer and adopts a (neo)lacto-glycosphingolipid conformation that prevents binding of receptors to membrane ligands (Jongsma et al., 2020). Herein this gene was regarded unimportant for binding to a phosphoantigen-reactive TCR and provided a more reliable assumption that the *BTN2A1* was a solely top-hit. Solute carrier family 15 member 1 (SLC15A1) is expressed at the brush border membrane of the intestinal epithelium enterocytes and mediates the uptake of tiny peptides from the lumen into the enterocytes. It has a vital role in the uptake and digestion of dietary proteins and facilitates the absorption of numerous peptidomimetic drugs. No genes became significantly relevant for the K562 gene-wise analysis matching the initial tag-wise dispersion, although each of the read counts accounting for three sequences targeting the *BTN2A1* gene were observed above their respective counts compared to the reference screen.

The analysis assessing the differential gene expression on populations enriched

Table 3.1: *Top ten ranked genes in a gene-wise analysis for each negative and positive screen. Data produced in a correlation adjusted mean rank camera gene-set test. Each gene is representative for the collection of its respective number of guide-RNAs (Guides). Direction indicates whether the number of sgRNA sequences is above (↑) or below (↓) of that in the reference screened population.*

	LM-MEL-62					K562				
	Gene	*Guides*	*Direction*	p-*value*	*FDR*	*Gene*	*Guides*	*Direction*	p-*value*	*FDR*
Negative	*BTN2A1*	4	↑	$6 \cdot 10^{-15}$	$2 \cdot 10^{-12}$	*IL1RN*	3	↑	0.014 336	0.930 498
	SPPL3	4	↑	$2 \cdot 10^{-13}$	$5 \cdot 10^{-11}$	*CA9*	3	↑	0.015 803	0.930 498
	SLC15A1	3	↑	0.000 225	0.035 7	*UGT1A*	3	↓	0.018 725	0.930 498
	CEACAM1	3	↑	0.001 129	0.100 1	*RHOXF2*	3	↓	0.021 752	0.930 498
	TTC9C	3	↑	0.001 237	0.100 1	*LIN37*	3	↓	0.025 522	0.930 498
	OSMR	4	↑	0.001 259	0.100 1	*HDAC1*	3	↓	0.033 248	0.930 498
	C11orf88	3	↑	0.001 615	0.105 8	*AKAP1*	3	↑	0.034 489	0.930 498
	CHURC1	3	↑	0.001 775	0.105 8	*OR4D1*	3	↓	0.043 159	0.930 498
	CSNK1A1L	3	↑	0.002 24	0.111 9	*RET*	3	↓	0.047 199	0.930 498
	CLK1	3	↑	0.002 346	0.111 9	*SLC6A5*	3	↓	0.057 992	0.930 498
Positive	*PCDHA*	4	↑	0.000 006	0.006 135	*PCDHA*	4	↑	0.000 002	0.001 49
	TSPY	4	↑	0.000 028	0.013 674	*TSPY*	4	↑	0.000 030	0.008 765
	UGT1A	3	↑	0.000 149	0.047 788	*UGT1A*	4	↑	0.000 07	0.013 731
	PRR20	3	↑	0.000 26	0.062 663	*URB2*	4	↓	0.000 206	0.030 165
	OR51A7	3	↓	0.000 455	0.077 804	*PCDHGA*	3	↑	0.000 471	0.055 033
	PCDHGA	3	↑	0.000 485	0.077 804	*PRR20*	3	↑	0.007 012	0.605 08
	HNRNPCL	3	↑	0.001 47	0.201 83	*HNRNPCL*	3	↑	0.007 949	0.605 08
	OR4F	3	↑	0.002 011	0.241 686	*GNB2*	3	↑	0.008 288	0.605 08
	TAPBP	3	↓	0.002 553	0.272 661	*PRND*	3	↓	0.012 652	0.818 23
	VNN1	3	↓	0.006 872	0.600 924	*SLC22A7*	3	↓	0.014 319	0.818 23

for the increased affinity of selective TCR-6 tetramer resulted without remarkable sequences or significant statistic proves that any gene enhanced the affinity for this fluorescent $\gamma\delta$-TCR probe. Nonetheless, succeeding gene-wise analysis ranked three top gene family hits *PCDHA*, *TSPY*, *UGT1A* within an acceptable FDR just below 0.05 equally matching between the LM-MEL-62 and K562 tumour line screens alike. Moreover, less relevant *PCDHGA*, *PRR20*, *HNRNPCL1* and *LOC649330* also matched across the two cell line screens with significant p-value below 0.01, albeit non-accepted FDR (Table 3.1). The *PCDHA* belongs to a large cluster of protocadherins mostly in neurone and is required in diverse neurodevelopment processes. The *TSPY* also has several members and specific of the y male chromosome, as denoted testis-specific Y-encoded proteins. Again, the *UGT1A* compresses a gene family encoding for enzyme uridine 5'-glucuronosyltransferase and functions to transfer glucuronic acid to small hydrophobic molecules. The function of these transcripts was not found to be related to the immune system or its regulation except for BTN2A1 which belongs to the BTN family molecules representing burgeoning roles in controlling and regulating the biology of $\gamma\delta$ T cells across primate and mouse species.

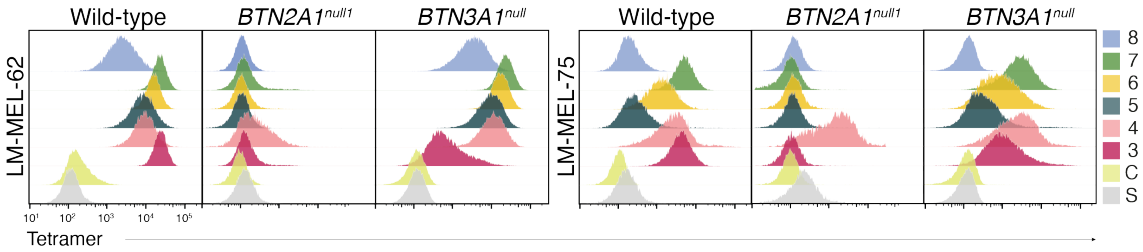

Figure 3.4: *Affinity of Vγ9Vδ2 TCR-tetramer clonotypes in wild-type or respective* BTN-*knockout melanoma cell lines LM-MEL-62 and -75 is dependent on BTN2A1. Streptavidin-PE (S) and conjugated to mouse CD1dα-GalCer as a tetramer control (C) or Vγ9Vδ2 TCR clones 3–8 tests.*

3.4 Validation of *BTN2A1*-Candidate Gene

While the genetic screen on the melanoma LM-MEL-62 cell line resulted in *BTN2A1* as a top-hit, the screen from the K562 did not detect any ligand for the clone TCR 6, and the focus centred to validating the *BTN2A1* target on two independent melanoma established cell lines. Melanoma LM-MEL-62 and -75 *BTN2A1*-CRISPR/Cas9 knock-outs (Sec. A.4) were obtained from our joined collaboration with the ONJCC and in this work, a series of procedures noted in following subsections were used to consolidate the role of the BTN2A1 protein in regulating activation of $\gamma\delta$ T cells.

3.4.1 The Vγ9Vδ2-TCR Affinity Depends on BTN2A1

Melanoma lines present decent levels of BTN2A1 and BTN3A at their surface plasma membranes (Sec. A.4). Furthermore, this seems to predict a substantial affinity for tetramerised Vγ9Vδ2 TCR clones 3 to 7 (Fig. 3.2). Notably, the binding of TCR-tetramer fluorescent probes was abolished when the expression of *BTN2A1* was impeded in CRISP/Cas9-knockouts (Fig. 3.4). Note the peculiar $\gamma\delta$-TCR clone 4 positive signal in LM-MEL-75 cell line could be explained by the existence of a second plausible ligand exclusively of this type. Intriguingly, the absence of *BTN3A1* did not affect either of the melanoma cell lines.

Remarkably, the affinity of our $\gamma\delta$-TCR clone 6 was reestablished in the melanoma *BTN2A1*-knockout cell line when this protein was reintroduced during a transient expression. Per contra, the insertion of *BTN3A1* or *BTN3A2* was redundant in reestablishing the actual signal for the $\gamma\delta$ TCR fluorescent probe, even though, the amount of these proteins at the surface membrane were above to that found in corresponding wild-type cells (Fig. 3.5 a-b). Combination of two separate DNA constructs for the expression of *BTN2A1* and *BTN3A1* proteins in the same cells again restored the de-

tection of a $\gamma\delta$-TCR tetramer probe. Hence, these results reaffirm explicitly the need of expressed BTN2A1 protein on the cell membrane in antigen-presenting cells that stimulate the Vγ9Vδ2 TCR present on $\gamma\delta$ T cells.

Moreover, flow cytometry allowed to measure these protein-to-protein interactions by FRET given the nature of the fluorophore conjugates used (PE donor; AF647 acceptor). The FRET channel captured the realise of subsidiary signal from the AF647 resulting from absorbed energy of the PE emission spectra if these were encountered within a distance less than 10 nm. This extra information came as an additional clue for deducing plausible cooperation between these two BTN molecules considering the enhanced *BTN2A1* expression was persistently providing an elevated FRET signal that correlated to enforced simultaneous expression of *BTN2A1* and *BTN3A1* (Fig. 3.5 b).

3.4.2 Antagonist Antibodies Obstruct $\gamma\delta$TCR Ligand-recognition

A panel of specific monoclonal antibodies specific for tagging the BTN2A1 extracellular domain were used to perturb a supposed weak-chemical bound between the Vγ9Vδ2-TCR and BTN2A1 ligand. Four cell lines (LM-MEL-62, -75, K562, and HEK-293T) with previously reactivity to the Vγ9Vδ2 TCR clone 6 were selected for this assessment (Fig. 3.2), plus a commercial antibody against human BTN2A2 protein (clone 6C7D2) and two in-house produced functional agonist 20.1 or antagonist 103.2 antibodies against BTN3A members were included in the assay to consider additional protein contributions to this interaction further. Most antibodies against the BTN2A1 protein obstructed the Vγ9Vδ2 TCR clone 6 in tumour cell lines excluding clones RF13-235 and RF13-267. Some of these antibodies were highly specific of BTN2A1, whereas others cross-reacted to BTN2A2 (Sec. A.3.2). On the other hand, none of the two antibodies specific for BTN3A molecules (20.1 and 103.2) reported in the literature (Harly et al., 2012) to have functional activity upon Vγ9Vδ2 T cells and bound to surface protein members BTN3A1/2/3 were conditioning the $\gamma\delta$-TCR and BTN2A1 interaction. The affinity of Vγ9Vδ2 TCR for BTN2A1 was shared equivalently between melanoma lines LM-MEL-62, -75, and HEK-293T, but not to K562 cells. Instead, this K562 myelogenous leukaemia cell line presented a modest increased TCR-6 fluorescent detection signal compared to others under a pre-treatment with commercial antibody against the BTN2A2 protein.

Using our in-house BTN2A1 extracellular domain tetramer a reciprocal effect from testing $\gamma\delta$ TCR fluorescent probes stated above was performed by (Sec. A.1). A series of in-house generated antibodies anti-pan-$\gamma\delta$TCR and commercial anti-CD3ϵ

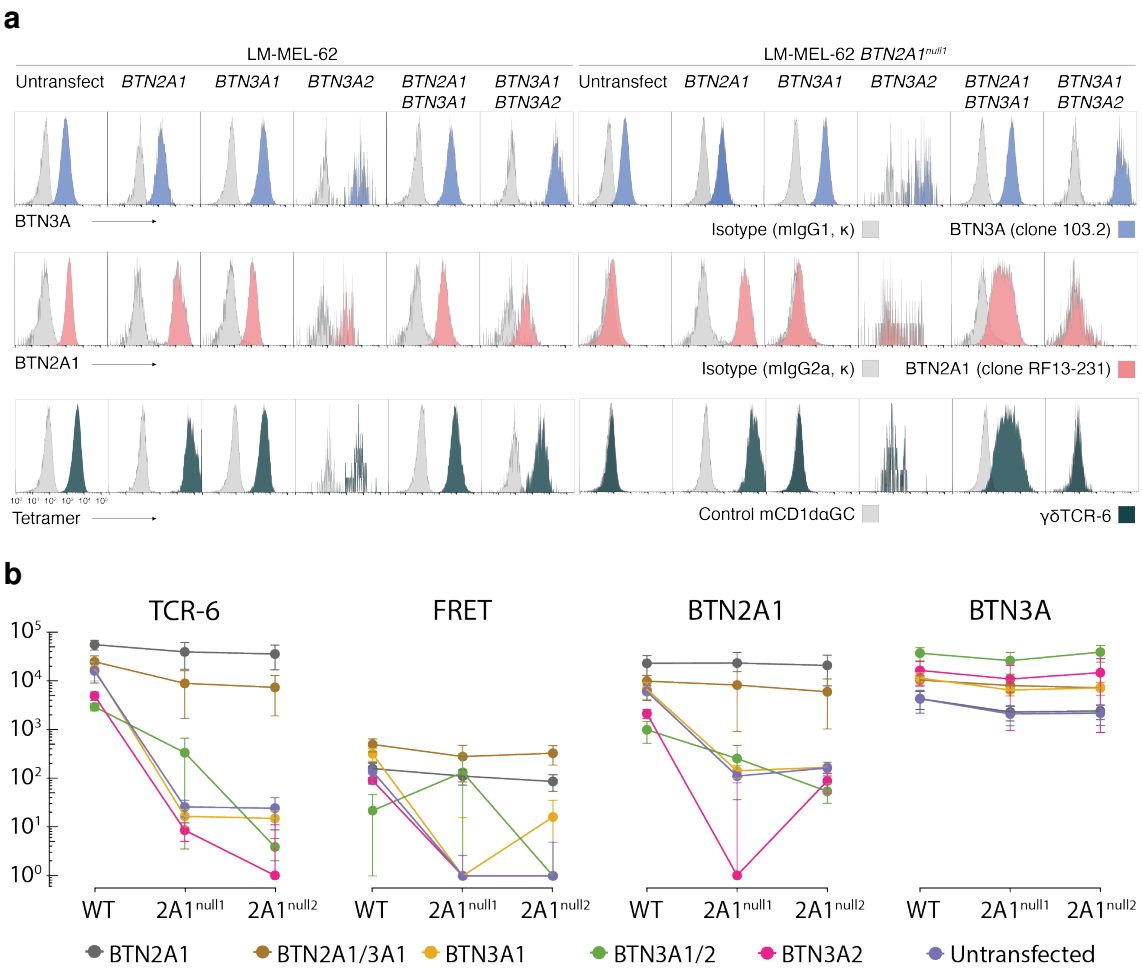

Figure 3.5: *Restoring expression of* BTN2A1 *in two LM-MEL-62 knockouts (*BTN2A1^{null1} *or* BTN2A1^{null2}*) reestablished the affinity for a Vγ9Vδ2 TCR-tetramer clone 6, but reintroducing* BTN3A1 *or* BTN3A2 *have no effect unless combined with* BTN2A1*. (a) Histograms representing raw data representative for successfully transfected cells of one experiment excluding* BTN2A1^{null2} *and the FRET channel; (b) summary subtracting the median fluorescence intensity of each control to test and averaged between four independent experiments. Antibody clone 103.2 (PE) detects BTN3A1, RF13-231 (AF647) BTN2A1, both combined FRET on the 670/30-Y channel, and TCR-6 tetramer (PE) fluorescent probe. Error bars indicate the standard error.*

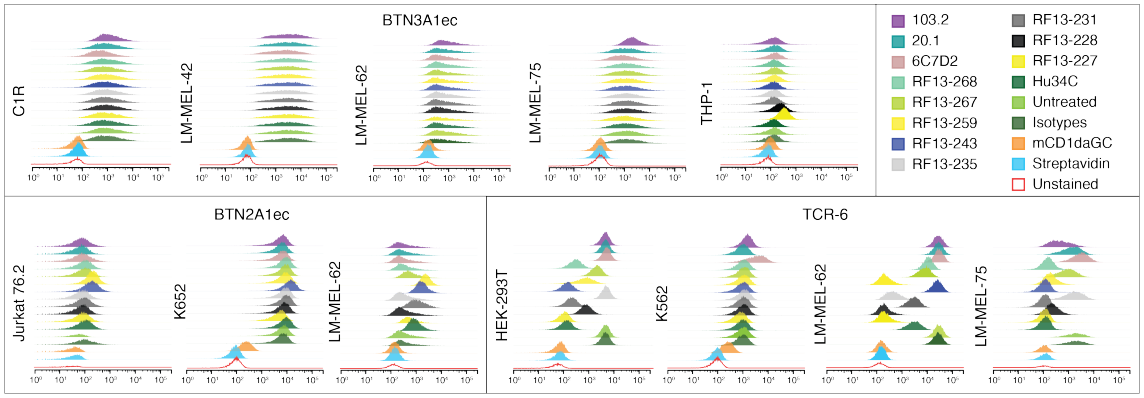

Figure 3.6: *Antibodies against BTN2A1 (clones Hu34C, RF13-227, -228, -231, -235, -243, -259, -267, and -268), BTN2A2 (clone 6C7D2), or BTN3A members (clones 20.1 and 103.2) can alter the affinity of which TCR-6, BTN2A1 or BTN3A1 ectodomain tetramerised fluorescent probes bind to established tumour cell lines (LM-MEL-62, -75, K562, and HEK-293T). Data representative of two independent experiments.*

or specific for the TCRGV9 and TCRDV2 domains were used to target the Vγ9Vδ2 TCR of donor-expanded Vδ2 T cells previously to treatment with BTN2A1 ectodomain fluorescent probes (Fig. 3.7). In this setup, most clones which bond to a different range of epitopes of Vγ9Vδ2 TCR were favouring the interaction between BTN2A1 ectodomain fluorescent probe and expanded $\gamma\delta$ T cells of the Vγ9Vδ2 linage. Among these were antibodies against the CD3ϵ region (clones SK7, OKT3, and UHCT1), pan-$\gamma\delta$TCR (super natant (SN)-13, -60, and clone 3B1), and specific for the Vδ2 domain (clone B6). In contrast, an anti-pan-$\gamma\delta$TCR antibody (clone 5A2) severely prevent binding of the BTN2A1 probe to the expanded Vδ2 T cells and a commercial antibody against the Vγ9 domain had a slightly similar effect. These conjugated anti-pan-$\gamma\delta$TCR (clone 11F2), TCRGV9 (clone B3), and TCRDV2 (clone B6) were visually assessed for a plausible association along with the BTN2A1 ectodomain fluorescent signal in flow cytometry dot plots (Fig. 3.7 b). In line with the empirical results, the antibody against the Vγ9 minimally reduced the fluorescence intensity detected from the BTN2A1 ectodomain probe, and correlation was barely noticeable. Instead, the anti-pan-$\gamma\delta$TCR antibody (clone 11F2) diminished the BTN2A1 signal with a correlation to the BTN2A1 signal still being considered. However, this association was much more accentuated with the antibody against the Vδ2 domain (clone B6), which not only the fluorescence of both markers increased simultaneously, but also the BTN2A1 tetramerised probe experienced an increased affinity for those donor-purified expanded V$\delta2^+$ T cells tested.

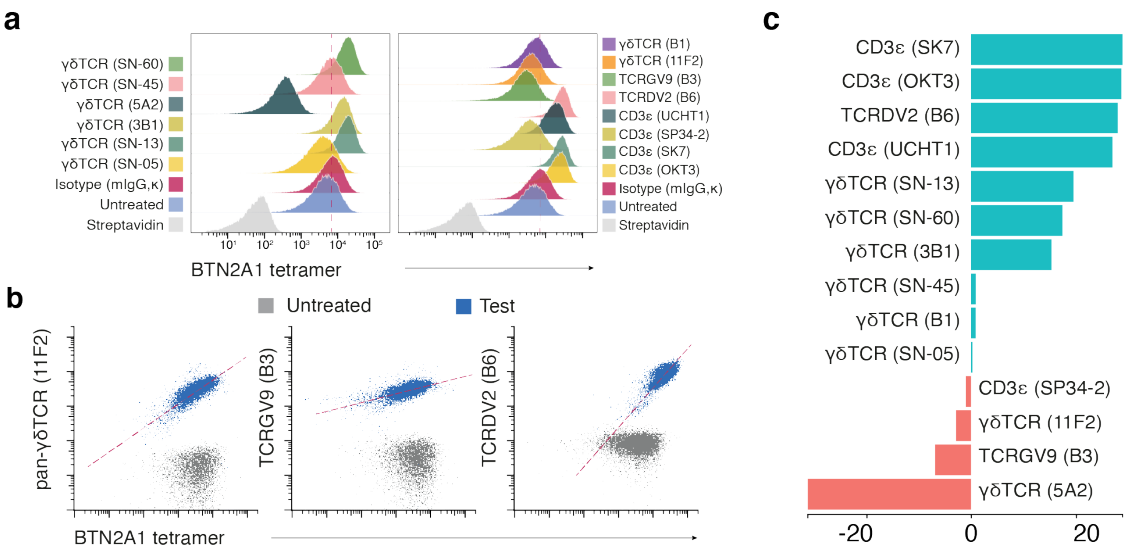

Figure 3.7: *Specific antibodies modify the affinity of a tetramerised BTN2A1 extracellular domain fluorescent probe (BTN2A1ec) for the Vγ9Vδ2 TCR of donor-derived expanded V$\delta2^+$ T cells. (a) Left histograms show in-house produced nanobody immunoglobulin variable domains adhered to a mouse IgG portion directly affect the binding of BTN2A1ec to a $\gamma\delta$TCR; right histograms represent the same using a selection of commercial clones against the CD3ϵ, TCRGV9 or TCRDV2 epitopes. (b) Correlation dot plot of donor-expanded Vδ2+ T cells stained with BTN2A1ec and respective treatment with antibodies targeting pan-$\gamma\delta$TCR, TCRGV9, or TCRDV2 domains. Dash lines denote of the slope. (c) Normalised data in (a) to the isotype control treatment with colours indicating the antagonist (red) or agonist (cyan) effect in regards to the $\gamma\delta$TCR affinity for BTN2A1ec. Data averaged from four independent donors.*

3.4.3 The Vγ9 Domain Binds to BTN2A1

A tetramerised ectodomain BTN2A1 proteins were generated in-house (Sec. 2.2.1) and used to test a direct stand-alone reactivity to the $\gamma\delta$ TCR in flow cytometry. This BTN2A1 probe bound to a defined continuously population of PBMC obtained from random donors, and its detection was segregated to different immune cell types. This disclosure delimited its reactivity exclusively to the $\gamma\delta$ T cell subset (Fig. 3.8 a). Further identification within the primary $\gamma\delta$ T cell antibody markers of the Vδ1, Vδ2, and Vγ9 domains demonstrated the BTN2A1-tetramer reactivity was exclusive of the $\gamma\delta$ T cells expressing the Vγ9 domain (Fig. 3.8 b). None of the eight random donors tested showed reactivity to the probe in any TCR without the Vγ9 domain. Additionally, the possibility to determine a close distance between the BTN2A1 probe and TCR through a FRET assay using the BTN2A1-PE fluorophore as a donor and anti-CD3ϵ-allophycocyanin (APC) conjugated antibody as an acceptor was attractive and promising. Consequently, a FRET signal was observed solely when a co-stain with both donor and acceptor fluorophore conjugates were present in the sample, thus establishing the distance between the two interacting proteins within 10 nm. Moreover, the independent fluorophore signalling recorded form the samples highly correlated as observed from the depicted dot plot graphic representation (Fig. 3.8 c).

Next, the biomolecular interaction between the BTN2A1 ectodomain and the Vγ9 domain was measured based on an induced angle-θ light shift produced by protein interaction on a surface plasmon resonance instrument. The extracellular domain was recognised by $\gamma\delta$ T cell receptors bearing the Vγ9 domains, and recombined receptors with the Vδ2 or Vδ1 made no observable changes in regards to their dissociation constant (Vγ9Vδ2 $K_d = 42.4 \pm 4$ µM; Vγ9Vδ1 $K_d = 50.4 \pm 5$ µM). This biochemical approach consolidates the previous flow cytometry validation experiments in which the BTN2A1 surface protein is a ligand for the Vγ9Vδ2 TCR, and its affinity is determined exclusively by the Vγ9 domain.

3.5 BTN2A1 Is Essential to Phosphoantigen-induced $\gamma\delta$ T-cell Responses

The previous section consolidates the existence of a physical BTN2A1-$\gamma\delta$TCR interaction. Herein, its corresponding functional response in the context of presenting cells and related phosphorylated antigens is examined.

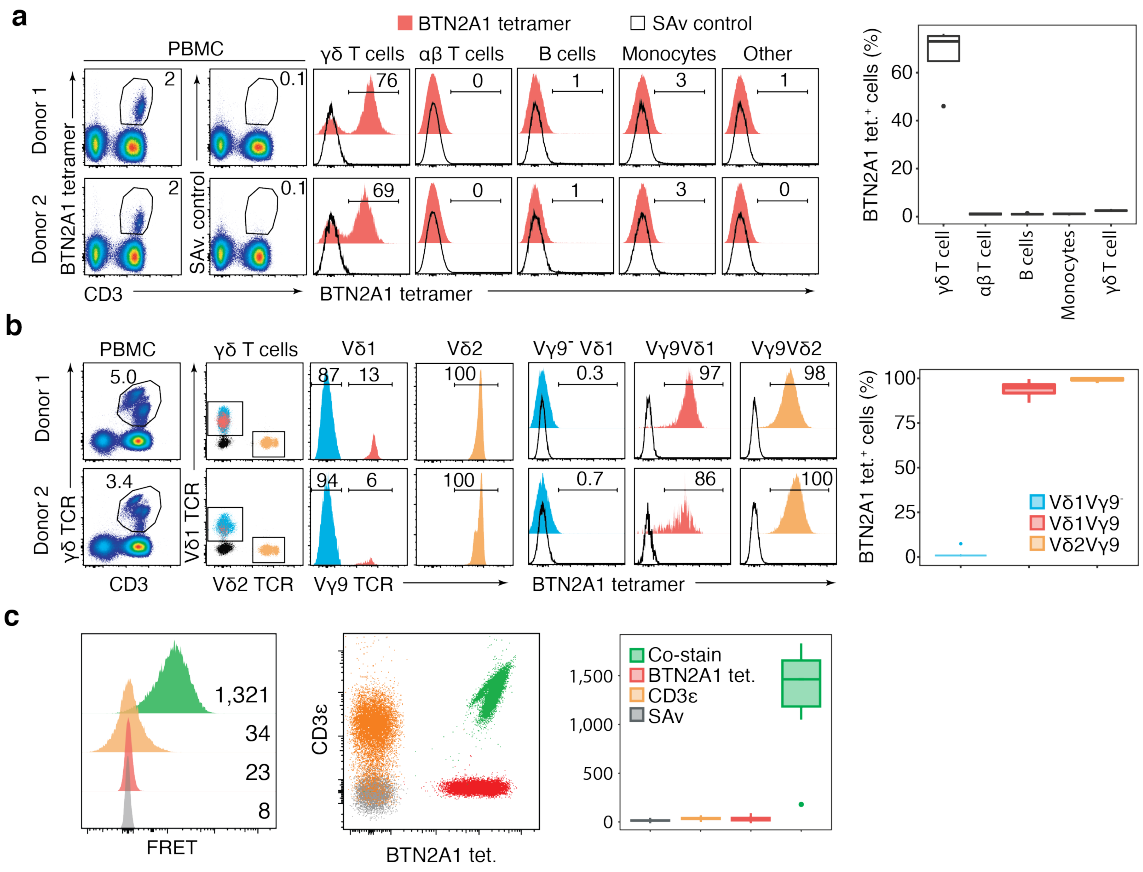

Figure 3.8: *Tetramerised BTN2A1 fluorescent probe binds uniquely to the Vγ9 domain as (a) shows its positive signal defines a population on a dot plot representation from two independent donors, and following gating strategy across different immune cell types identifies the positive signal is restricted to $\gamma\delta$ T lymphocytes. Tukey's boxplot summarises data from eight donors; (b) replicates (a) with expression markers for the three major $\gamma\delta$ TCR chains showing all reactivity is exclusive of the Vγ9Vδ2 T cell subset for potential bias to the Vγ9 domain; (c) seven donors individually stained for BTN2A1 tetramer, anti-CD3ϵ, or streptavidin control (SAv), and co-stain for FRET detection, histogram and dot plot exemplifies data from one donor. Biexponential axis unless indicated.*

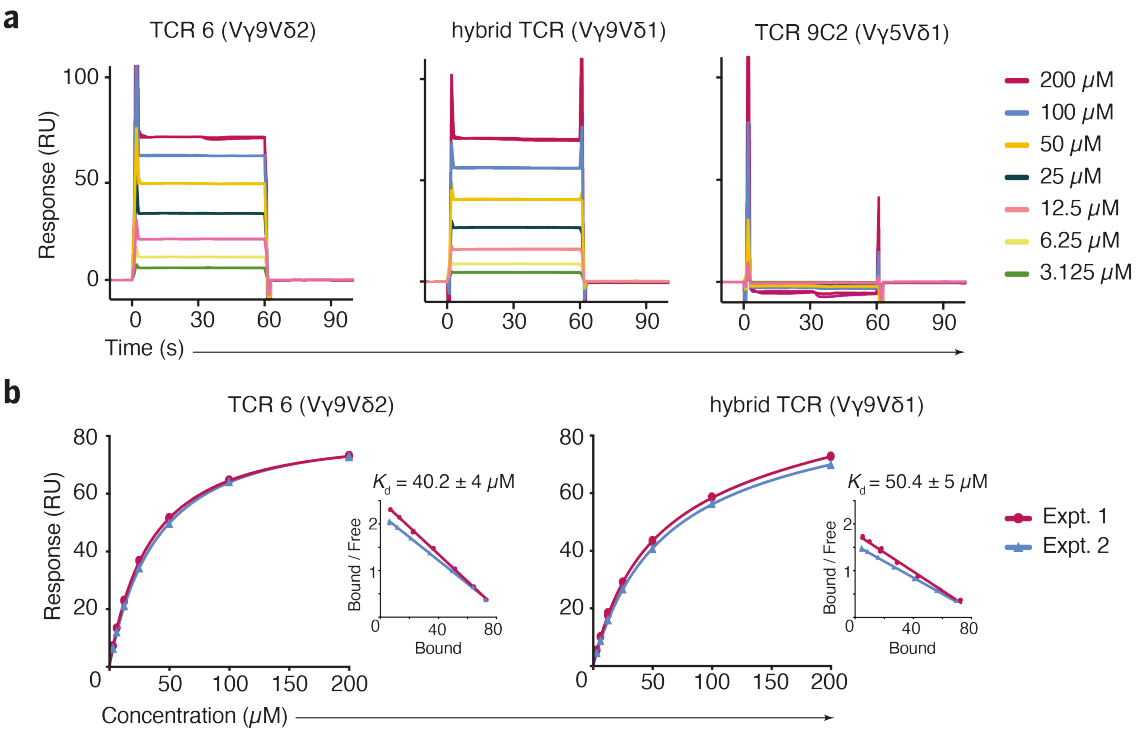

Figure 3.9: *Biomolecular interaction analysis from a surface plasmon resonance consolidates a direct binding between extracellular domain BTN2A1 and the Vγ9 domain of a $\gamma\delta$ TCR. (a) sensorgrams respective of each TCR analysed; (b) saturation binding curve of the Vγ9Vδ2 and Vγ9Vδ1 TCR overlaying two experiments (c) Scatchard analysis determines the dissociation constants.*

Table 3.2: *Statistic results show the estimated marginal mean differences of the percentage of cells upregulating the IL-2 receptor α chain (IL-2 receptor subunit α (CD25)) between treatments with monoclonal antibodies on a linear mixed-model, considering each experiment and condition as fixed variables and donor as a random effect. Degrees-of-freedom (df) method Kenward-Roger and Tukey for the p-value adjustment comparing a family of seven estimate balanced marginal means (estimate). Upper triangle Turkey adjusted p-values < 0.05 (red), $\alpha = 0.05\,\%$, diagonal estimated marginal means in bold, and lower triangle estimated contrast comparisons.*

Contrast	Isotype (BM4)	Untreated	BTN3A (103.2)	BTN2A (Hu34C)	BTN2A1 (RF13-259)	BTN2A (RF13-267)	Unstimulated
Isotype (BM4)	**[27.058]**	0.9837	<0.0001	<0.0001	<0.0001	<0.0001	<0.0001
Untreated	-2.2750	**[29.333]**	<0.0001	<0.0001	<0.0001	<0.0001	<0.0001
BTN3A (103.2)	23.4500	25.7250	**[3.608]**	0.9551	0.6956	0.6932	0.9634
BTN2A (Hu34C)	26.2417	28.5167	2.7917	**[0.817]**	0.1994	0.1979	1.0000
BTN2A1 (RF13-259)	18.3508	20.6258	-5.0992	-7.8908	**[8.708]**	1.0000	0.2139
BTN2A (RF13-267)	18.3383	20.6133	-5.1117	-7.9033	-0.0125	**[8.720]**	0.2123
Unstimulated	26.1250	28.4000	2.6750	-0.1167	7.7742	7.7867	**[0.933]**

3.5.1 Antibodies Impede Drug-induced Vδ2$^+$ T-cell Responses

Approved amino-bisphosphonate drugs are interesting from an immunotherapeutic approach. They can strengthen phosphoantigen-reactive Vγ9Vδ2 T-cell antitumoural activities against cancer cells of diverse origin. Herein, the function of several monoclonal antibodies raised against extracellular domains of BTN2A1/2 or BTN3A proteins was studied on fresh-isolated PBMC challenged with zoledronate drug. Under normal conditions, the Vγ9Vδ2 T-cell population revealed no phenotypic signs of cell activation, nor the non-Vδ2 T cell subset manifested any change (Fig. 3.10 a). It was only when antigen-presenting cells were stimulated with zoledronate drug that the Vγ9Vδ2 subset began to internalise their Vγ9Vδ2 TCR and increase expression of the cytokine IL-2 surface receptor, both features related to lymphocyte activation markers. However, the Vδ2 T cell response under the presence of BTN-specific antibodies impeded immune responses to zoledronate-stimulated cells. The hypothesis of a real difference between antibody treatments and isotype controls was supported in a statistic analysis of which condition was taken as a constant parameter and donors stand for the random variable in a linear mixed-model (Fig. 3.10 b). Resulting p-values are represented in table 3.2.

A zoledronate-induced $\gamma\delta$ T cell immune response resulted in secretion of several cytokines detected in a flow cytometry broad dynamic range analysis of fluorescent antibody-coated beads specific for capturing uniquely granulocyte-macrophage colony-stimulating factor (GM-CSF), IFN-γ, TNF-α, IL-4, interleukin 9 (IL-9), IL-10, IL-13, and IL-17A. These results determined the absence of IL-4, IL-9, IL-10, IL-13, and IL-17A in the cell supernatant of respective PBMC cultures (Fig. 3.10 c). Nonetheless,

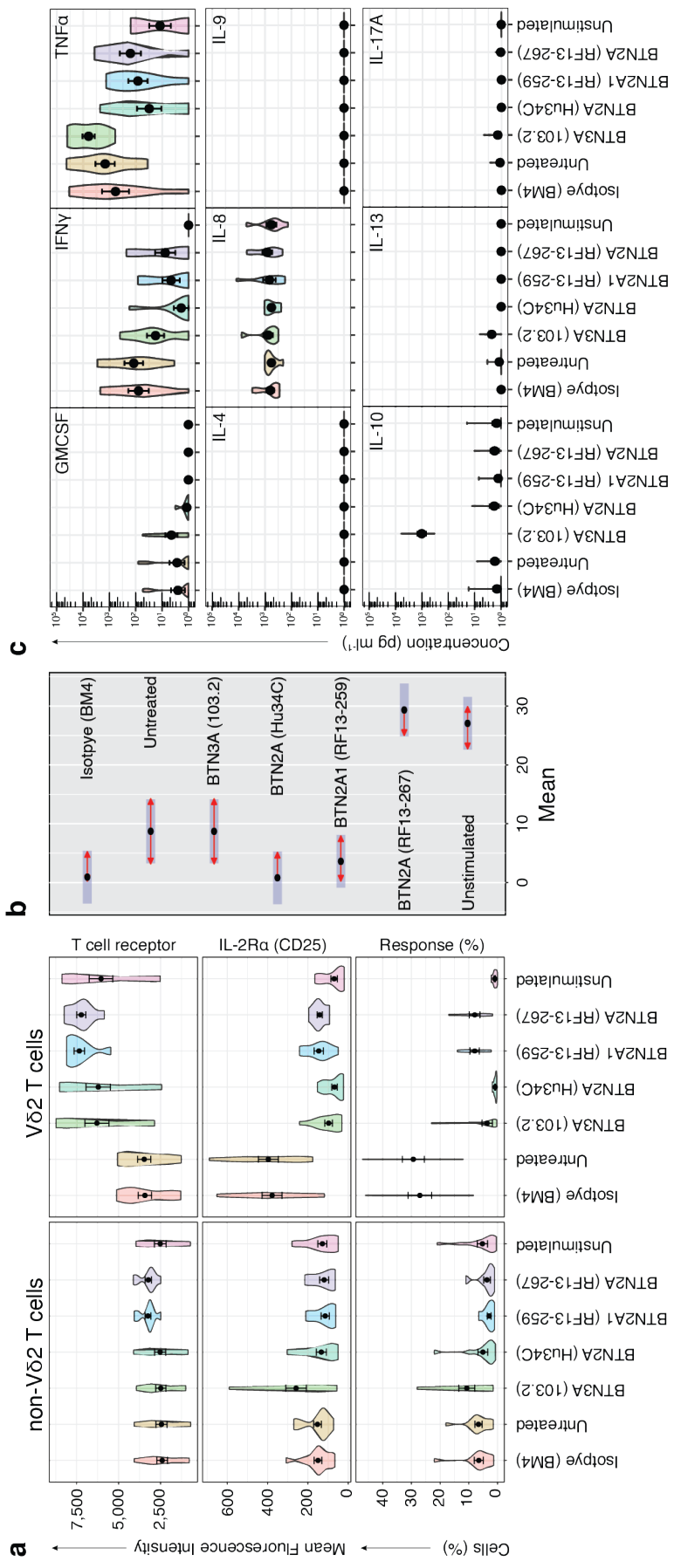

Figure 3.10: *Different monoclonal antibody treatments abrogate drug-induced Vδ2 T cell responses. (a) Violin plots from the two major γδ T cell subset response after an overnight drug-induced stimulation using 4 µM zoledronate on twelve independent fresh-isolated PBMC donor samples carried across three flow cytometry experiments. Reported data from CD3ε, CD25, and percentage of cells expressing CD25 activation marker. Dots are means, and bars indicate standard errors. (b) Graphic representation for estimated marginal means between antibody treatments respective of the percentage of activated cells (CD25⁺); blue bars are confidence intervals and red arrows comparisons among means. (c) Cytometric bead array for detection of indicated secreted cytokines in cell supernatants respective of the Vδ2⁺ T cell population from eight donors gathered from two separate experiments.*

they show a constant and invariable cell secretion of interleukin 8 (IL-8) for all tests, including controls but distinct notorious production of IL-10 under the treatment with anti-BTN3A (clone 103.2) antibody. The anti-BTN3A antibody was not able to reduce the production of TNF-α, whereas those targeting the BTN2A1/2 caused a noticeable reduction regarding its presence in the supernatant similar to the unstimulated reference control. Similar results were obtained form detecting GM-CSF and IFN-γ cytokines. Therefore, the anti-BTN3A antibody treatment response was equivalent to anti-BTN2A clones in respect to analysing surface activation markers, whereas in graphic visualisation of data differed in the secretion of GM-CSF, IFN-γ, TNF-α, and IL-10. Of note, a few days later from the analyses the batch from clone 103.2 became contaminated with bacteria, potentially altering the cytokine results exclusive of this sample.

3.5.2 Drug-induced $\gamma\delta$ T-cell Responses Relay on BTN2A1

Amino-bisphosphonate zoledronate drugs are used to induce accumulation of endogenous phosphoantigens in different in-vitro established tumour cell cultures. Here, changes in the phenotypic response from added donor-purified expanded Vδ2$^+$ T cells were evaluated in flow cytometry by detection of the activation marker CD25. Respective lymphocyte activation was accentuated in response to three cell lines LM-MEL-62, -75, and HEK-293T all of which coincide in expressing elevated levels of surface BTN2A1 protein as previously detected in figure B.2, Sec. 3.2 (Fig. 3.11 a). Drug stimulated leukaemia B-cell lines C1R and K562 were not able to boost a phosphoantigen-driven Vδ2 T cell response. Challenging the K562 myelogenous leukaemia with zoledronate restricted activation to approximately one-fifth of the responding lymphocytes increasing CD25 as a response to these antigen-presenting cells. The responding donor-derived lymphocytes remained irresponsive as in the unstimulated control when cocultured with the lymphoblasts C1R cells. Opposed to the respective parental line, two genetically modified melanoma LM-MEL-62 cells (null 1–2) receding expression of functional BTN2A1 surface protein drastically diminished the immune response form expanded Vδ2 T cells (Fig. 3.11 a). Subsequent statistical approach predicted notorious differences between means of the different groups with a subtracted percentage of default activation controls supporting the notion in which abrogated BTN2A1 functional expression in modified melanoma LM-MEL-62 cells made a change in the percentage of Vδ2 T cell upregulating the activation marker (Fig. 3.11 b and Table. 3.3). Moreover, the analysis confirmed the severe observed differences form LM-MEL-62, -75, and HEK-293T to stand-alone zoledronate-challenged Vδ2 T cell

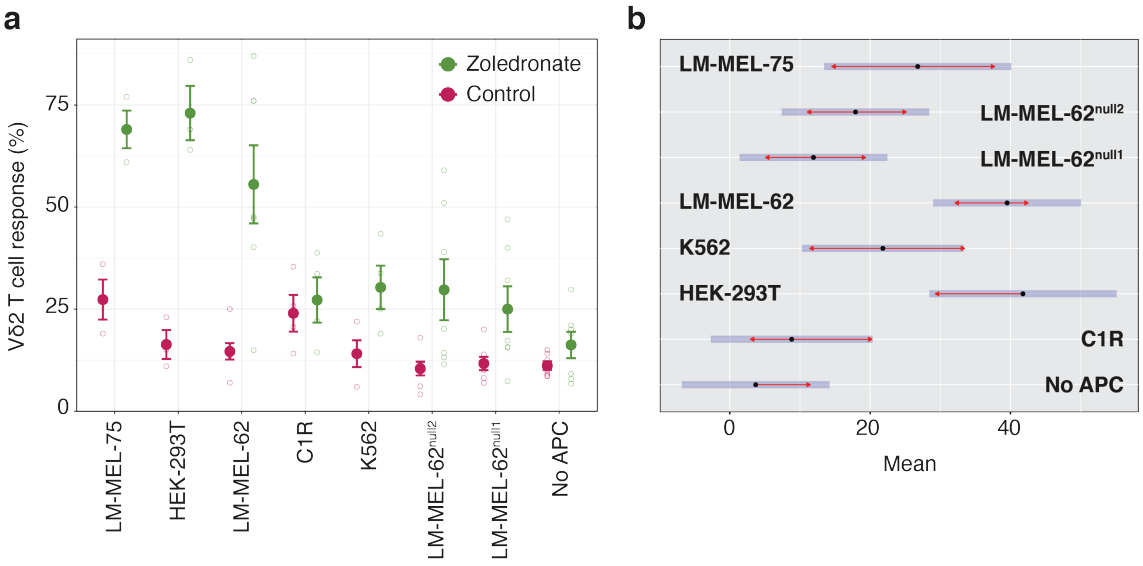

Figure 3.11: *Percentage of donor-derived expanded V$\delta 2^+$ T cells upregulating CD25 in response to drug stimulated (4* µM *zoledronate) tumour cell lines including two LM-MEL-62 melanoma of which are CRISPR/Cas9 knockout for* BTN2A1*. Graphic representation of (a) means representing the percentage of activated cells for stimulated and unstimulated control with standard error bars. Data of three to six donors across four flow cytometry experiments, some of which had quadrupled technical repeats averaged previous to display; (b) estimated marginal means respective of the percentage of activated cells (CD25$^+$); blue bars are confidence intervals and red arrows comparisons among means.*

tests, and showed a marginal influence by the K562 cell line assuming an alpha error lower than 0.05 %.

3.5.3 Antibodies Modify the Immune Response to HMBPP

The immune response to drug-induced $\gamma\delta$ T cells can be neutralised by the use of selective monoclonal antibody treatments (Sec. 3.5.1). Moreover, a broader range of monoclonal antibodies against BTN2A was determined to modulate a self-reacting Vγ9Vδ2 T cell response, even in some occasions was shown a functional activity in preventing stimuli from the most potent microbial phosphoantigen (HMBPP) known to date (Fig. 3.12). Induced stimulation of donor-purified expanded Vγ9Vδ2 T cells with HMBPP was comparable to abrupt TCR-provoked signalling by agonist anti-CD3ϵ (clone OKT3) and - CD28 (clone CD28.2) treatment combined, only leaving behind circa 20 % of unresponding clonotypes under normal conditions (Fig. 3.13 a). When HMBPP-stimulated lymphocytes were pre-treated with a high titre (10 µg µL^{-1}) of an antibody-containing solution before and during the stimulus, some these antibody treatments counteracted the immune response, including several of which abolished it entirely (Fig. 3.12). Conversely, a few clones demonstrated the potential for inducing

Table 3.3: *Statistic table for Vδ2 T cell response accounting for the percentage of cells that upregulate CD25 after overnight exposure to zoledronate stimulated (4 µM) tumour cell lines including two LM-MEL-62 CRISPR/Cas9 BTN2A1-knockouts (null 1–2). Upper triangle Turkey adjusted p-values < 0.05 (red), $\alpha = 0.05$ %, diagonal estimated marginal means in bold, and lower triangle estimated contrast comparisons.*

Contrast	No APC	C1R	HEK-293T	K562	LM-MEL-62	LM-MEL-62^{null1}	LM-MEL-62^{null2}	LM-MEL-75
No APC	**[3.69]**	0.9851	<0.0001	0.0697	<0.0001	0.5967	0.0609	0.0140
C1R	-5.13	**[8.81]**	<0.0030	0.3811	<0.0003	0.9993	0.7625	0.2722
HEK-293T	-38.09	-32.96	**[41.78]**	0.1690	0.9999	<0.0008	0.0102	0.3817
K562	-18.12	-13.00	19.97	**[21.81]**	0.0812	0.6829	0.9971	0.9972
LM-MEL-62	-35.83	-30.70	2.26	-17.71	**[39.52]**	<0.0001	<0.0011	0.4341
LM-MEL-62^{null1}	-8.23	-3.11	29.86	9.89	27.60	**[11.92]**	0.8734	0.2544
LM-MEL-62^{null2}	-14.23	-9.10	23.86	3.89	21.60	-6.00	**[17.92]**	0.8175
LM-MEL-75	-23.09	-17.96	15.00	-4.97	12.74	-14.86	-8.86	**[26.78]**

agonist activity on resting Vγ9Vδ2 T cells. The effector function of selective clones was examined in cells from eight random donors, and clones RF13-244, -253, and -259 observed to exert an agonist activity in resting Vδ2 T cells, with RF13-259 stimulating around 40 % of TCR clones on average (Fig. 3.13 b). Clones RF13-227, -236, -248, -266, and Hu34C had a thorough neutralising effect equal to that of commercial agonist anti-BTN3A antibody clone 103.2. The two clones RF13-259 and -267 elicit lesser effectiveness compared to their counterparts and reduced effectiveness if juxtaposed to their greater effectiveness in obstructing zoledronate-induced responses during in vitro overnight coulters with PBMCs (Sec. 3.5.1, Fig. 3.10).

Table 3.4: *Antibody functional activity assessed statistically determined by Turkey adjusted p-values from estimated marginal means in a linear mixed-model accounting for condition as fixed and donor random as variable. Values are determined comparing each antibody clone against their respective isotype control (IgG1κ or IgG2a/BM4), under normal conditions to assess an agonist functional affect or under an overnight 0.5 ng ml^{-1} HMBPP stimulus to evaluate an antagonist functional activity; a same evaluation was followed studying their respective cytokine INF-γ and TNFα secretion.*

Activity	103.2	Hu34C	RF13-227	RF13-236	RF13-244	RF13-248	RF13-253	RF13-259	RF13-266	RF13-267
Agonist	1.0000	1.0000	1.0000	1.0000	0.8932	1.0000	0.1258	<0.0001	1.0000	1.0000
Antagonist	<0.0001	<0.0001	<0.0001	<0.0001	0.9998	<0.0001	1.0000	0.6597	<0.0001	<0.0001
Unstimulated IFN-γ	1.0000	1.0000	1.0000	1.0000	1.0000	0.9206	0.0036	0.0190	1.0000	1.0000
TNFα	1.0000	1.0000	1.0000	1.0000	1.0000	0.9380	0.0559	0.1253	1.0000	1.0000
HMBPP IFN-γ	0.0417	0.0169	0.0204	0.0185	1.0000	0.7675	1.0000	0.9438	0.0163	0.5571
TNFα	0.0230	0.1363	0.1353	0.1394	1.0000	0.9917	1.0000	0.9829	0.1414	0.8153

Cytokine bead array detection-based methods detected the presence of two main cytokines IFN-γ and TNF-α being released into the culture medium following stimulation with microbial phosphoantigen HMBPP (Fig. 3.13 c). Detection of IFN-γ was notable and comparable to detected levels in the positive stimulating anti-CD3ε/CD28

control. Detection of TNF-α was similar, but the lymphocytes produced less quantity of this cytokine. The secretion of both IFN-γ and TNF-α cytokines was equally prevented under treatment with antibodies against BTN3A clone 103.2 or cross-reactive BTN2A1/2 clones Hu34C, RF13-227, -236, or -266. Also, in normal conditions, these donor-expanded Vδ2-T cells were directly activated if treated with clones RF13-244, -253, or -259, with the latter having the greatest agonist effector function among all. Importantly, treatments with clones either RF13-244 or -259, the production of both IFN-γ and TNF-α cytokines were undoubtedly maintained to the same level and below the untreated HMBPP-stimulated condition irrespectively of whether the stimulus came exclusively from the antibody or phosphoantigen stimuli. This phenomenon resembles the agonist activity of the anti-BTN3A antibody clone 20.1 interference with a phosphoantigen-induced response documented in Starick et al. (2017). The statistical evaluation supported these findings as reported in Table. 3.4.

Other cytokines like interleukin 6 (IL-6), IL-10, IL-17A, and traces of IL-9 were uniformly detected in normal conditions or stimulating the cells with microbial phosphoantigen HMBPP, and inducing stimulus with anti-CD3ϵ/CD28 treatment would increase their production. However, the addition of different antibody treatments incurred no effect on their production or secretion into the surrounding medium in the exception of IL-10 and IL-17A cytokines. In detail, the secretion of these two cytokines following HMBPP-stimulus provoked detection of minor traces in untreated and isotype control samples. Intriguingly, these low cytokine secretions were abrogated completely in treatments with 103.2, Hu34C, RF13-227, -236, and -266 previously described to obstruct activation markers in human Vγ9Vδ2 T cells. In contrast, clones RF13-244, -253, -259, and -267 had no observable effect. Human Vδ2 T cells were not secreting cytokines IL-4, IL-8, nor IL-13 even under the stimulus with anti-CD3ϵ/CD28 antibodies.

3.6 Discussion

The initial flow-cytometry screen with $\gamma\delta$TCR fluorescent probes highlighted the presence of a putative ligand on tumour cell lines including melanoma, leukaemia, and monocytes (Fig. 3.2). This made the basis to undertake a genomic knockout screen which resulted in *BTN2A1* and *SSPL3* having the highest likelihood to be targets of the $\gamma\delta$TCR ligands. Gene-wise narrowed this result identifying *BTN2A1* as the most relevant hit. Evidence in the literature contributed to disregard the *SSPL3* form bing a possible ligand for its intervention in unrelated genetic screens that targeted transmembrane proteins due to its role in producing glycosphingolipid molecules neces-

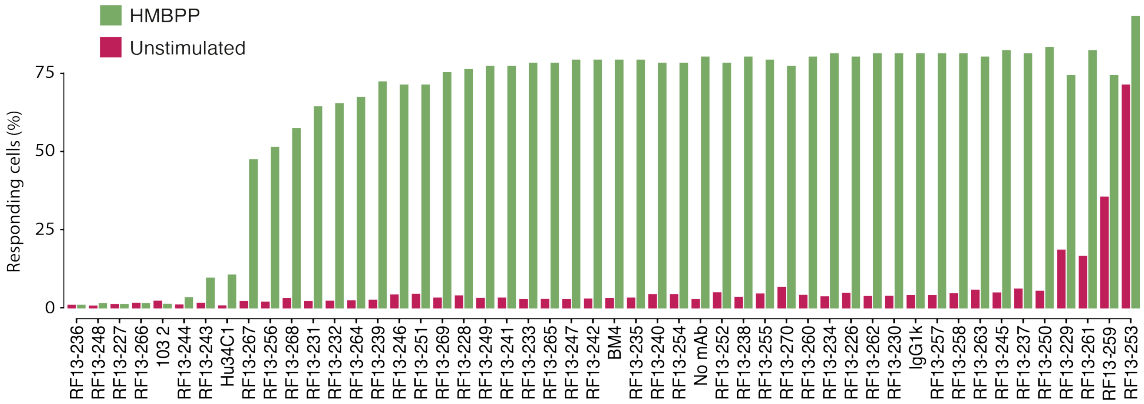

Figure 3.12: *Panel of purified monoclonal antibodies produced by CSL against BTN2A1, though some cross-react to BTN2A2, and corresponding isotype control IgG2a/BM4 and a generated in-house agonist anti-BTN3A (clone 103.2; isotype IgG1κ) modulate in vitro immune response from donor-expanded Vδ2-T cells or inhibit HMBPP-induced stimulus. Considered the percentage of cells upregulating IL2-R detected. Average of two experiments.*

Figure 3.13: *Several purified monoclonal antibodies produced by CSL against BTN2A1 (some having cross-reactivity to BTN2A2) with corresponding isotype control IgG2a/BM4 and a generated in-house agonist anti-BTN3A (clone 103.2; isotype IgG1κ) activate an in vitro immune response from donor-expanded Vδ2-T cells or inhibit a 0.5* ng ml^{-1} *HMBPP-induced stimulus. (a) histograms of a selected batch of functional monoclonal antibodies representative of independent eight donors; (b) predicted mean and standard error in regards to antibody functional antagonist or agonist activity in altering the percentage of activated cells that upregulate IL2-R, in HMBPP or normal conditions, respectively. Data obtained subtracting the value from an absence of antibody and normalised to the CD3ϵ/CD28 stimulus* $\frac{X_i - X_{min}}{X_{max} - X_{min}} 100$*; (c) respective cytokine bead array assay.*

sary for constituting the plasma membrane (Jongsma et al., 2020). Nonetheless, ligands with a lesser affinity for the $\gamma\delta$TCR-teteramer clone-6 could have been missed in the parallel screen targeting K562 cells, or else these cells needed further enrichment before proceeding to the harvest and subsequent analysis. By all means, *BTN2A1* was a suitable candidate that fit within the paradigm of which a required second gene product from the chromosome 6 was needed for $\gamma\delta$ T cells recognise phosphoantigens (Riaño et al., 2014; Vavassori et al., 2013) and is part of the BTN family members which can act as regulators of $\gamma\delta$ T cells (Tab. 1.8).

Validation of the *BTN2A1* follow-up experiments confirmed its involvement and contact to the Vγ9Vδ2 TCR in phosphoantigen-reactive $\gamma\delta$ T cells. Detection of $\gamma\delta$TCR fluorescent probes depended on the presence of BTN2A1 surface protein as knockout models completely lost affinity not only for the $\gamma\delta$TCR clone 6 but also for all other phosphoantigen-reactive clones tested in two melanoma cell lines (Fig. 3.4). Surprisingly, the lost of tetramer stain solely occurred in *BTN2A1* knockout lines and not in *BTN3A* knockout cells, emphasising the role of BTN2A1 being not less essential than the previous BTN3A1 described as a putative $\gamma\delta$TCR ligand (Gu et al., 2018; Vavassori et al., 2013). These tests also put into sight that the clone 4 could have some kind of affinity for a molecule unrelated to BTN2A1, albeit this one still accounted for a decent proportion of the staining when using this $\gamma\delta$TCR clone. Reversing the knockout LM-MEL lines by transient expression of either *BTN* member further consolidated that the *BTN2A1* is responsible for direct contact to the Vγ9Vδ2 TCR, and not even the intervention of *BTN3A2* described by Vantourout et al. (2018) was sufficient for binding to the $\gamma\delta$ TCR clone 6 (Fig. 3.5). Additionally, it arouse the possibility in which these two BTNs would interact to each other as a resulting FRET was detected from donor anti-BTN3A PE fluorophore antibody to the anti-BTN2A1 AF647 acceptor fluorophore when these were combined in a single test.

The attempt to disturb the staining of tetramerised BTN extracellular domain fluorescent probes using specific monoclonal antibodies had a substantial effect with only two clones RF13-227 and -228 slightly increasing the BTN3A1 ectodomain stain in the THP-1 and RF13-103.2 on the melanoma LM-MEL-75 and C1R. Nonetheless, several pre-stains with anti-BTN2A1 clones changed the detection signal from the extracellular domain BTN2A1 probe in Jurkat 76.2 or LM-MEL-62 lines but made no alterations in K562 cells. Although these indications were insufficient due to the relative small detection shifts, they reflected the use of specific monoclonal antibodies could have a potential functional role altering the typical surface configuration of these BTN proteins. Such evidence was in line with pre-treatment blocking tests performed before the stain of the Vγ9Vδ2 TCR clone 6 over HEK-293T or LM-MEL-62 and LM-

MEL-75 cell lines. In contrast, K562 cells retained an unaltered pattern like stated above with the extracellular BTN2A1 domain staining test (Fig. 3.6). In accordance, HEK-293T and these two melanoma lines (LM-MEL-62 and LM-MEL-75) were likely to share similar mechanisms in which contacted to the Vγ9Vδ2 T cells, opposed to K562 cells, which could potentially use a distinct mechanism to contact to this subset of phosphoantigen-reactive $\gamma\delta$ T cells through an alternative ligand-receptor interplay. In line with altering the chemical interaction between the Vγ9Vδ2 TCR-tetramer probe and BTN2A1 protein, many more antibodies, including mouse IgG-nanobody compounds specifically for the variable regions of the $\gamma\delta$ TCR, appeared to have a direct effect on this interplay. Among these existed a divergence promoting an agonist or antagonist function over the potential to increment the affinity in the BTN2A1-$\gamma\delta$TCR clone 6 interaction (Fig. 3.7).

Finally, biochemical analysis SPR spectroscopy reaffirmed the chemical bond between the BTN2A1-$\gamma\delta$TCR clone 6 interaction detected by flow cytometry analyses (Fig. 3.8), and shown it was equivalent to a weak binding strength of $\alpha\beta$ TCR recognition of peptides presented by MHC molecules (Cole et al., 2007; Stone et al., 2009) and comparable to a closer related Vγ5Vδ1 bond to unloaded CD1d presenting molecule ($K_D = 35$ µM) (Uldrich et al., 2013). Although interactions with affinities even lower than 100 µM could be interpreted as eliciting weaker immune responses, they appear to remain highly-specific and maintain a natural immunogenic activity to antigens (Gee et al., 2018). Most importantly, the detected chemical interaction took place exclusively with the Vγ9 domain whereas the δ-chain was independent of a Vγ9 recombined to a Vδ1 or Vδ2 gene-segments ($K_D = 50$ µM and $K_D = 42$ µM, respectively). These findings ensured the essential role for BTN2A1 was directly interact to the $\gamma\delta$ T cells via a phosphoantigen-reactive TCR and left room for those residues located at the CDR segments at the top surface area of the Vγ9Vδ2 TCR, mostly comprised at the δ-chain (Fig. 1.6), for having a secondary role in the signal transduction upon phosphoantigens are sensed by the BTN3A1 transmembrane molecule (Sandstrom et al., 2014; Wang and Morita, 2015).

Until now, BTN3A1 is the only molecule described to be involved in phosphoantigen-reactive immune responses and reported that additional coding proteins in the human chromosome 6 could be determining a response to this particular type of antigens (Riaño et al., 2014). Our study has determined BTN2A1 to contact the Vγ9 domain of the Vγ9Vδ2 T cells and subsequent results using functional specific monoclonal antibodies reflect its direct implication to responses to phosphoantigens when antigen-presenting cells are stimulated with zoledronate drug (Fig. 3.10 and Table 3.2). Moreover, these monoclonal antibodies targeting the BTN2A1 protein had a similar effect

to reported agonist antibody clone 103.2 against the BTN3A members (Harly et al., 2012). Together, all these antagonists reduced the averaged secreted amount of cytokines GM-CSF and IFN-γ produced in normal activation responses by $\gamma\delta$ T cells, even though the use of anti-BTN2A1 antagonists only reduced TNF-α. Also, antagonists against BTN2A1 diverged from the 103.2 clone by a subtle diminishing secretory activity of GM-CSF and IFN-γ when compared to antagonist 103.2. Therefore, these functional antibodies against BTN2A1 or BTN3A members had similar physiological effects to the immune responses by $\gamma\delta$ T cells, with the distinct difference in which those against the BTN2A1 protein also prevented the lymphocyte cells to secrete TNF-α.

Besides, the $\gamma\delta$ T cell zoledronate-induced responses to HEK-293T cells or LM-MEL-62 and LM-MEL-75 were shown stronger than leukaemia K562 or C1R cells in an assay comparing these different antigen-presenting cells (Fig. 3.11). In particular, the leukaemia K562 cell line was equivalent to melanoma LM-MEL-62$^{\text{null}}$ BTN2A1-knockout models providing some signs that some other molecular ligand with much fewer repercussions on the immune responses was plausibly playing a small, subtle role on the receptor of Vγ9Vδ2 T cells.

Several purified monoclonal antibodies against BTN2A1 were also preventing $\gamma\delta$ T-cell responses to microbial phosphorylated antigen HMBPP (Fig. 3.13 and Table 3.4). Clones RF13-259 and to a lesser extent RF13-253 caused stimulation of Vγ9Vδ2 T cell-independent from phosphoantigens like the clone 20.1 against the BTN3A members (Harly et al., 2012). Their functional effect was also noted in the secretion of cytokine profile Th1-like response. On the contrary, RF13-227, -236, -248, -267 -267, and Hu34C had an inhibitory response and prevented TCR-dependent signalling and respective cytokine response akin to clone 103.2.

Chapter 4

BTN2A1 and BTN3A1 Associate to Form a Functional Antigen-presenting Complex

4.1 Introduction

Previous works suggest BTN3A1 functions as an antigen sensor molecule elementary to activate immune responses to several reported phosphoantigens (Morita et al., 1995; Sandstrom et al., 2014). Evidence describes its intracellular B30.2 domain contains a charged inner pocket that attracts negatively charged phosphate groups of microbial HMBPP or eukaryotic IPP metabolites derived from the isoprene metabolic pathway (Wang and Morita, 2015). In the first results chapter we introduced BTN2A1 protein directly interacts to the Vγ9 domain of $\gamma\delta$ T cells, and this is essential for inducing recognition of phosphoantigens. However, it is unclear how this protein interacts or co-operate to the BTN3A1 sensor molecule and whether it is capable to directly interact to phosphoantigens or other tripartite membrane proteins (Wang et al., 2019).

According to reports that study proteins of the BTN family, these transmembrane molecules tend to dimerise and function in pairs to regulate the fate of not only human $\gamma\delta$ T cells but also mouse species (Di Marco Barros et al., 2016; Melandri et al., 2018; Willcox et al., 2019). Also, members of the BTNL family contact and form weak chemical bonds by residues allocated on their extracellular immunoglobulin domains. Examples of these are human BTNL3/8 or murine Btnl1/6 (Di Marco Barros et al., 2016), with BTN2A1 and BTN3A likely to have similar fate. Thus, this work examined the potential of BTN2A1 to function as co-stimulatory molecule for other V$\gamma9^{+}$ T cells, particularly, those that recognise lipids presented by molecules of the CD1 family (Uldrich et al., 2013). To further identify the entire function of BTN2A1 protein, it also investigates the role of the BTN2A1 B30.2 extracellular domain and its affinity for binding to phosphoantigens compared to the sensor-like intracellular domain of its counterpart BTN3A1. Hence, this chapter describes the physical and functional relationship between BTN2A1 and members of the BTN3A family, as well as the intrinsic

mechanism that allows activation of the Vγ9Vδ2 T-cell subset.

4.2 Dual BTN2A1/3A1 Expression Induces Phosphoantigen Responses

Rodent cells lack BTN protein members of the human chromosome 6 MHC-extended cluster and the ability to mediate phosphoantigen derived $\gamma\delta$ T-cell immune responses (Riaño et al., 2014). This makes them ideal candidates to study which combination of BTNs is required to assemble the presentation mechanism necessary to trigger phosphoantigen-induced $\gamma\delta$ T-cell responses. Enforced transfection of a selection of human *BTN* genes in Chinese hamster ovary K1 (CHO-K1) or NIH/3T3 enabled these cells to express several human BTN protein members, of which cell-surface expression of targeted cell lines reached sufficient levels for functional studies — ranging between 5–30 % on average (Fig. 4.1 a). Several combinations of BTN-transfected rodent cells mixed in cultures with responding donor-expanded V$\delta2^+$ T cells under the presence of zoledronate were assessed for evidencing which combination of BTNs induced $\gamma\delta$ T-cell effector responses. Expressing BTN proteins individually resulted non-stimulatory responses equivalent to co-expressing BTNL3/8 control group (Di Marco Barros et al., 2016). In contrast, co-expression of BTN2A1 together with BTN3A1 and either addition of BTN3A2 or BTN3A3 in antigen-presenting rodent cells prompt immune responses by $\gamma\delta$ T cells resulting in an upregulation of activation marker CD25. No $\gamma\delta$ T-cell responses were observed when BTN2A1 was paired solely with members other than BTN3A1. Additionally, the intracellular domain of BTN2A1 appeared to have a decisive role influencing in the underlying mechanism of action because swapping its intracellular B30.2 domain for that of a paired immunoglobulin-like type 2 receptor β (PILRβ) caused no change in the phenotypic readout of responding cells (Fig. 4.1 b-c). Absence of $\gamma\delta$ T cell immune responses were noted with the combination of one rodent antigen-presenting cell line expressing either BTN member with another that expressed an analog BTN. This test explained the response in *trans*, meaning each BTN2A1 or BTN3A1 member expressed in an independent accessory cell, was considered ineffective, even though, these were present within the same condition together with responding lymphocytes. Only the expression in *cis*, signifying both members were simultaneously present on the surface of an antigen-presenting cell, resulted in activation of these lymphocytes. Responses from $\gamma\delta$ T-cells were comparable between hamster or murine accessory cells used, despite mere differences likely to occur due to the variability in transfection efficiency (Fig. 4.1 a). A model to predict the existence of variability between the means in each condition supported the

observed results: zoledronate-stimulated rodent cells with co-expression of BTN2A1 with BTN3A1, with either BTN3A2 or BTN3A3, caused a significant percentage of $\gamma\delta$ T cells to upregulate CD25 (Fig. 4.1 d).

The secretion of diverse cytokines into the medium after drug stimulation was detected and measured for quantification and comparison with previous results (Fig. 4.2). The most prevalent secreted cytokine was IFN-γ, and this was released without the need of stimulatory drug treatment within the amount of IFN-γ ranging between 10 to 1,000 $\mathrm{pg\,ml^{-1}}$ in response to rodent cells expressing BTN2A1 and BTN3A1 in cis. The IFN-γ secretion was also recorded in other combinations where BTN2A1 was present, even though when its intracellular domain was mutated. A notorious difference in secretion of IFN-γ and GM-CSF between unstimulated, and drug-treated samples were detected in cis combinations between BTN2A1 and BTN3A1 or BTN3A1 and BTN3A3 —this later inconsistent with the absence from activation marker CD25 in the previous activation assay (Fig. 4.1). The same combinations of BTN members released IL-4, IL-8, and IL-13, even though, these were detected at very low levels. Both IL-4 and IL-13 are often associated with central regulation of IgE synthesis and allergic responses, which contrast to cytotoxic and Th1-inducible immune response by IFN-γ and GM-CSF. The combinatory group containing mutated BTN2A1-PILRβ molecules elicit spontaneous production of IFN-γ, IL-13, and little IL-8 at equal levels to the same combination involving wild-type BTN2A1. In either case, these observations increased under the zoledronate drug-treated conditions. Interestingly, TNF-α was only produced in amounts below 10 $\mathrm{pg\,ml^{-1}}$ and exclusively in response to cis combined expression of BTN2A1 and BTN3A1 or BTN3A1 and BTN3A3. No traces of IL-9, IL-10, or IL-17A were recorded.

4.3 BTN2A1/3A1 Ectodomains Trigger $\gamma\delta$ T-Cell Responses

A unique conformation arrangement between BTN2A1 and BTN3A1 is necessary for the functional phosphoantigen-presenting mechanism that determines the outcome responses in $\gamma\delta$ T cells. These respective ectodomain portions were immobilised on standard hydrophobic plates to resolve the synergic combination that triggers an antigen-specific response, and subsequent upregulation of lymphocyte activation markers was detected after overnight culture with donor-purified expanded V$\delta2^+$ T cells. These results showed coated assay plates with single isolated ectodomain proteins were redundant to $\gamma\delta$ T cells unless both BTN2A1 and BTN3A1 immunoglobulin domains were combined and attached on the surface of round-bottom culture plates. Activation of responding $\gamma\delta$ T cells occurred exclusively in the presence of

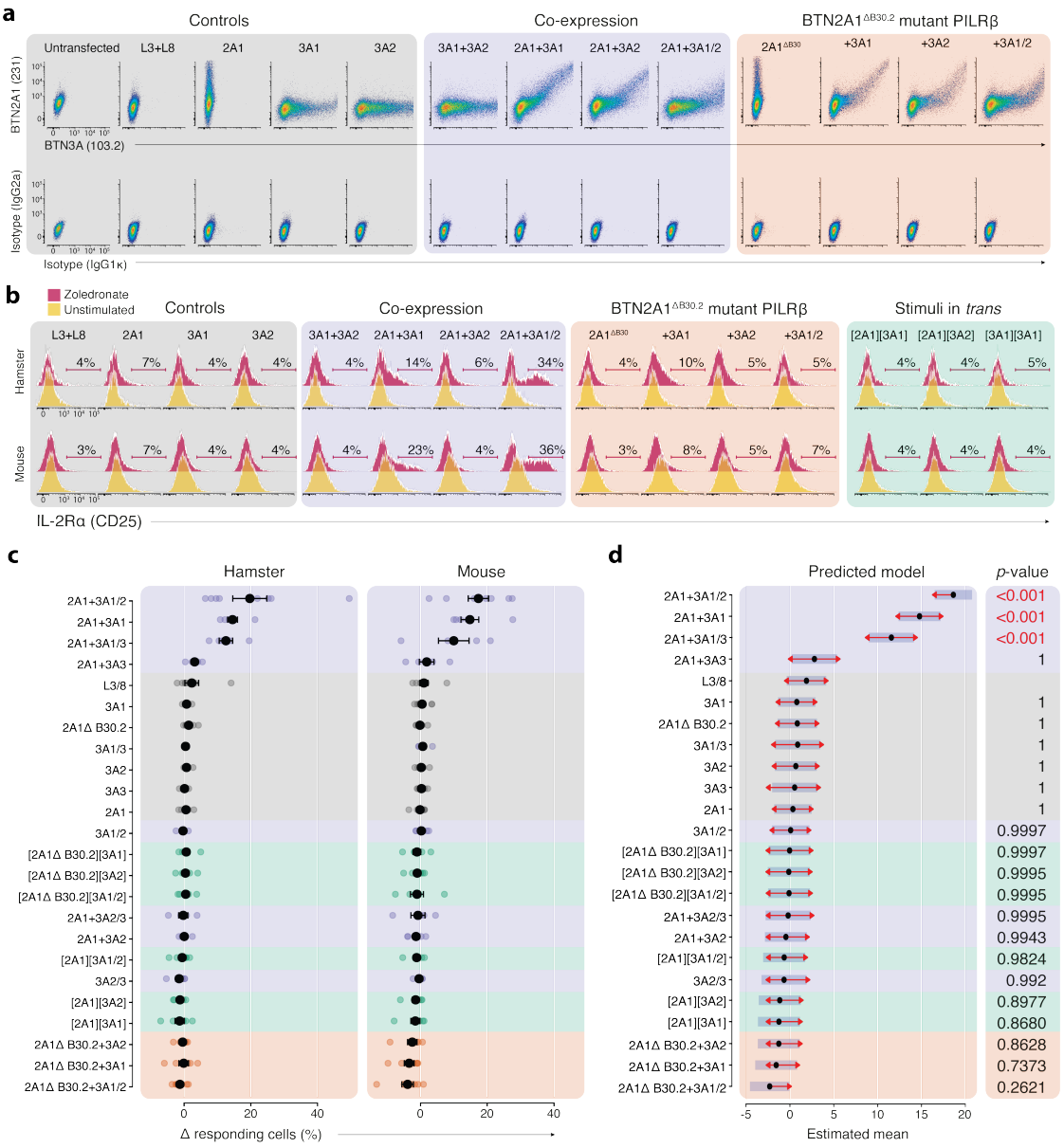

Figure 4.1: *Donor-expanded Vδ2-T cells respond to BTN2A1 and BTN3A1 molecules co-expressed in the same antigen-presenting cell. (a) detection of surface full-length BTN members and a BTN2A1 whose B30.2 intracellular domain was substituted by an irrelevant PILRβ intracellular portion in murine transfected cells; comparison to isotype controls; (b) purified Vδ2-T cells response to rodent enforced-expression of human combination members of the BTN family after an overnight coculture challenged with 4* µM *zoledronate; (c) summary of eight donors over four experiments after referencing to untransfected and unstimulated controls for CHO-K1 or NIH/3T3 cells. Standard-error bars; (d) predicted linear mixed-model to study relationships between different conditions considering antigen-presenting cell and donor as random variables, with respective p-value regarding estimated least-square means.*

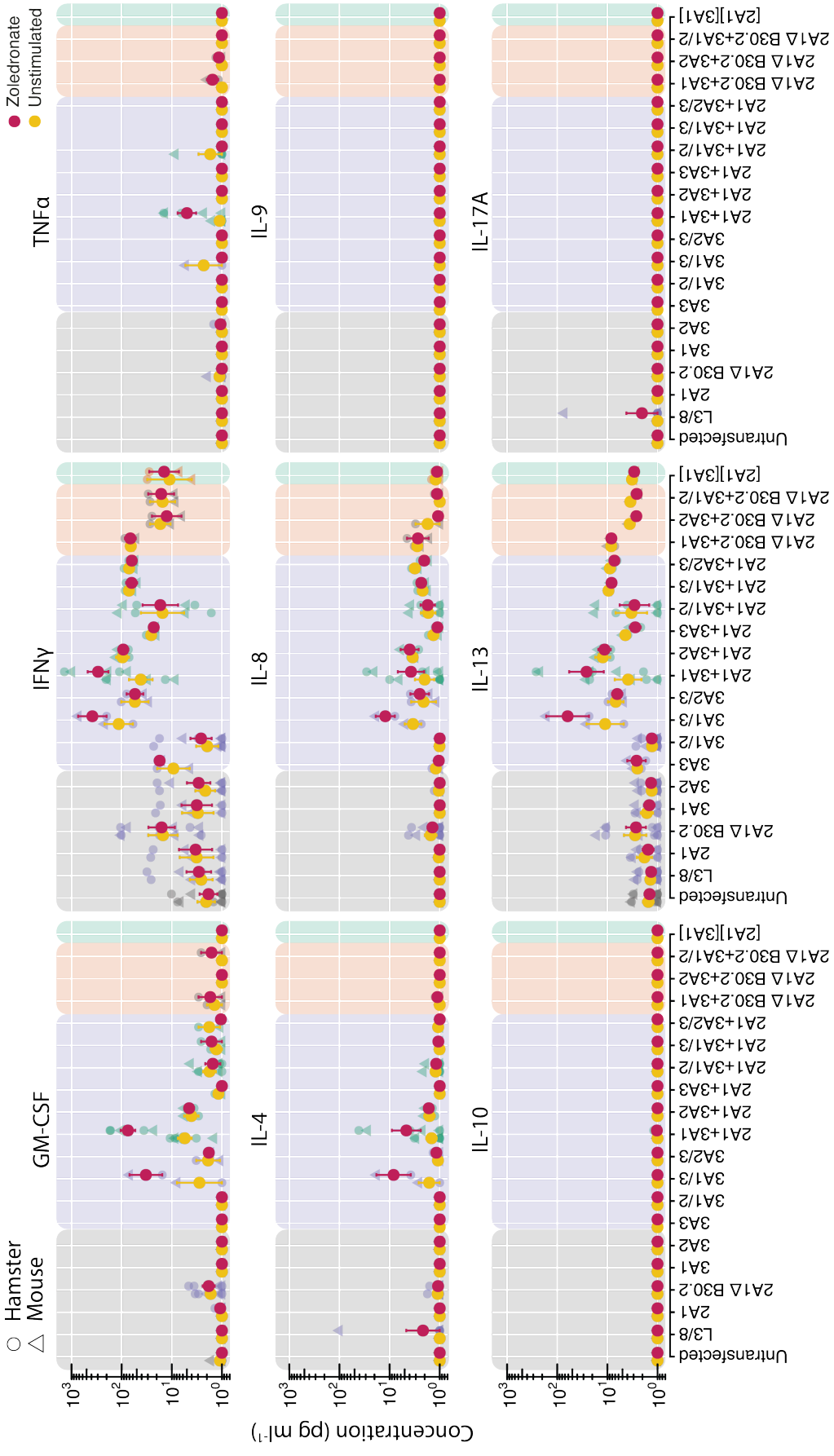

Figure 4.2: *Donor-expanded Vδ2-T cell cytokine secretion in response to rodent BTN-transfected cells after an overnight 4 µM zoledronate challenge. The y-axis indicates the concentration respective of each cytokine predicted from a quantification cytokine-bead assay. Avearage of three donors assessed in independent experiments; standard-error bars.*

Table 4.1: *Assessing the difference in the percentage of responding Vγ9Vδ2 T cells that upregulate CD25 in response to plate-bound BTN2A1 and BTN3A1 ectodomains combined, assessed across two independent experiments where three corresponding donor-purified and expanded V$\delta2^+$ or whole polyclonal $\gamma\delta$ T cell samples were compared. Respective subtractions from uncoated control tests to immobilised BTN2/3A1 conditions, and the calculated value further subtracted from the readout of total $\gamma\delta$ T cell to the V$\delta2^+$ T cell assay (Δ %).*

Donor	*Assessment*	*Vδ2 T cells (%)*	*Total $\gamma\delta$ T cells (%)*	Vγ9Vδ2 (Δ %)
MJ1	BTN2/3A1	84.6	85.9	3.8
MJ1	Uncoated	20.4	25.5	
MJ2	BTN2/3A1	83.7	85.3	-1.0
MJ2	Uncoated	17.1	17.7	
MJ4	BTN2/3A1	81.9	80.7	2.23
MJ4	Uncoated	9.77	10.8	

a dual combination of immobilised BTN2A1 and BTN3A1 proteins and independent of phosphoantigens (Fig. 4.3 a). Although irrelevant, the sole presence of BTN2A1 was enough to sensibilities a few clonotypes. Next, the induced TCR-signal strength was normalised to the maximum achievable T-cell response inducing both CD3ϵ of an antigen-specific receptor and co-stimulating CD28 glycoprotein signals that confer a potent, reliable signal. These results, considering an average from twelve independent donors, predicted dual-coalition between BTN2A1 and BTN3A1 ectodomains induced activation in half of the clonotypes present in the sample wells (Fig. 4.4 a). Additionally, the specific Vγ9Vδ2 T-cell response to ectodomain protein members or functional anti-BTN3A1 agonist clone 20.1 or antagonist 103.2 was studied in a system including a whole population of $\gamma\delta$ T cells. These results found that the activity of functional antibody clones was cancelled using this experimental setup, even thought, the percentage of Vγ9Vδ2 T cells responding to immobilised BTN2A1 and BTN3A1 was equitable to an equivalent experiment using same-donor purified and expanded V$\delta2^+$ T cells (Table. 4.1).

Incrementing by two-fold the concentration of immobilised protein on a standard hydrophilic plate augmented independent reactivity to individual BTN2A1 or BTN3A1 in one donor (Fig. 4.4.d). Nevertheless, contemplating the results across three additional random donors, the observation did not repeat. On average, the lymphocyte immune response to increased concentrations of immobilised BTN2A1 and BTN3A1 combined barely made an observable difference (Fig. 4.4.c). Besides, three different conditions were tested to assess the function of added co-stimulatory CD28 receptor, a substitution of standard $\gamma\delta$ T-cell media into AIM-V serum-free solution, and the use of a flat-bottom plate opposed to the round-bottom assay plates. Consequent addition

of an agonist antibody against the co-stimulatory CD28 glycoprotein had no apparent role in the activation phenotype of responding $\gamma\delta$ T cells. The basic experimental setup of combined immobilised BTN2A1 and BTN3A1 molecules in a flat-bottom plate diminished the lymphocyte responses, suggesting more significant separation of cells reduces the stimulatory potential. Contrary, the use of AIM-V serum-free medium supplemented with IL-2 drastically induced lymphocyte responses across all treatments, including uncoated or immobilised isotype control test (Fig. 4.4 .e and B.3 .a). Wells coated with agonist antibody clone 103.2 resulted in a lesser lymphocyte capacity to upregulate the lymphocyte activation marker but did not abrogate the whole activation response as achieved in conditions using a standard $\gamma\delta$ T cell medium. Under these facts, it is worth to consider the AIM-V medium could have stressed sensible cells and alter both responsiveness and sensibility independently from BTN molecules (Fig. 4.4.f and 4.4.c).

Alternate paired combinations between BTN2A1 and BTN3A1 ectodomain protein domains in immobilised plate-bound, soluble, or tetramer forms were insufficient to activate $\gamma\delta$ T cells unless both BTN2A1 and BTN3A1 ectodomains were attached onto the bottom of the assay well (Fig. 4.4.f). In an isolated case, the immobilised BTN3A1 tetramer achieved transmitting a signal to Vγ9Vδ2 T cells, although combining it with any of the BTN2A1 forms discouraged the immune cell response (Fig. 4.4.d). Functionality of monoclonal antibodies against BTN3A molecules was studied in conjugation to BTN3A1 or BTN2A1 and BTN3A1 combined, the later to identify a possible heterodimer disruption. Additionally, we assessed conditions comparing one- or two-to-one stoichiometry in consideration to the antibody's natural constitution to bind two ligands and under an overnight complex exposure at 37 ℃ forcing possible induced conformational changes within the complexes. Under these conditions, the BTN2A1 and BTN3A1 plate-bound complexes caused the most considerable stimulus to Vγ9Vδ2 T cells, but except combining the treatments with an antagonist antibody clone 103.2 (Fig. 4.4 .b, d-e). Any other alternative exerts no effect stimulating these immune cells.

Lastly, the immune response elicited by immobilising ectodomains from BTN2A1 and BTN3A1 proteins on an assay plate was measured under the cell treatment with two drugs that disrupt the internal intracellular activation cascades realised by stimulated T-cell antigen-specific receptors at two independent signal-stages. The drug AX-024 targets and obstructs the SH3.1 domain in the adapter cytoplasmic protein Nck that interacts with the CD3ϵ subunit in the TCR complex, thereby inhibiting Nck-mediated TCR signalling at an upper specific level. Dasatinib is a small ATP-competitive molecule-inhibitor of SRC-family protein- tyrosine kinases some of which

are essential for completing TCR activating signal cascades. Surprisingly, the action of the AX-024 drug had no real effect on the activation of $\gamma\delta$ T cells, whereas Dasatinib completely abrogated the response (Fig. 4.4.g and 4.4.f and B.3 .a). Differences in assessing low and high doses of the AX-024 drug were not observed in the BTN2A1 and BTN3A1 combined test nor respective agonist antibody or T-cell mitogen phorbol myristate acetate (PMA). Its influence preventing these T-cell signalling could not be interpreted observing these results. Instead, the Dasatinib drug had a specific function in cancelling derived T-cell responses but not under the mitogenic stimulated lymphocytes. Therefore, it was assumed the BTN2/3A1 activation signalling would be cancelled regardless of TCR-dependent signalling or not.

4.4 Membrane Association between BTN2A1/3A1 Proteins

The enforced expression of BTN2A1 and BTN3A1 on the cell membrane of rodent cells or respective immobilised ectodomain portions on an assay well-engaged $\gamma\delta$ T-cell reactivity by the Vγ9Vδ2 TCR (Sec. 4). Moreover, FRET between fluorophores attached to specific monoclonal antibodies for BTN members can deduce whether these targets sit within a distance inferior to 10 nm. To improve detection efficiency of the FRET signal detected previously, fluorophore-conjugated antibodies were pre-tested to find a more suitable combination that caused an assessable FRET resolution should a the two BTN members interact to each other (Sec. A.5). Results determined a favourable signal between donor PE-labeled antibody targeting either BTN3A member to acceptor AF647-conjugated antibody bond to BTN2A1. This combination deduced proximity between the two surface proteins in human melanoma LM-MEL-62 and LM-MEL-75, B-cell RAMOS and RPMI-8226, and monocytic THP-1 cell lines (Fig. 4.5).

These data suggest the extracellular domain of BTN2A1 protein associates with either BTN3A1, 3A2, or 3A3 members on the cell surface membrane. This hypothesis was further assessed by transfection of rodent cells with constructs containing gene-encoding protein members of the human BTN3A family members together with full-length BTN2A1 or an altered BTN2A1, whose B30.2 domain was substituted for a PILRβ alien portion. Following detection with the FRET-paired fluorophore-conjugated antibody clones (RF13-259 and 103.2) deduced these proteins lay within a close distance, therefore their association was required to enable flow cytometry detection of FRET between the two fluorophores (Fig. A.10 .b and 4.6 .b). The altered BTN2A1 containing the intracellular PILRβ portion expressed at lower levels compared to its full-length respective wild-type protein (Fig. A.10 .a and 4.6 .a) potentially

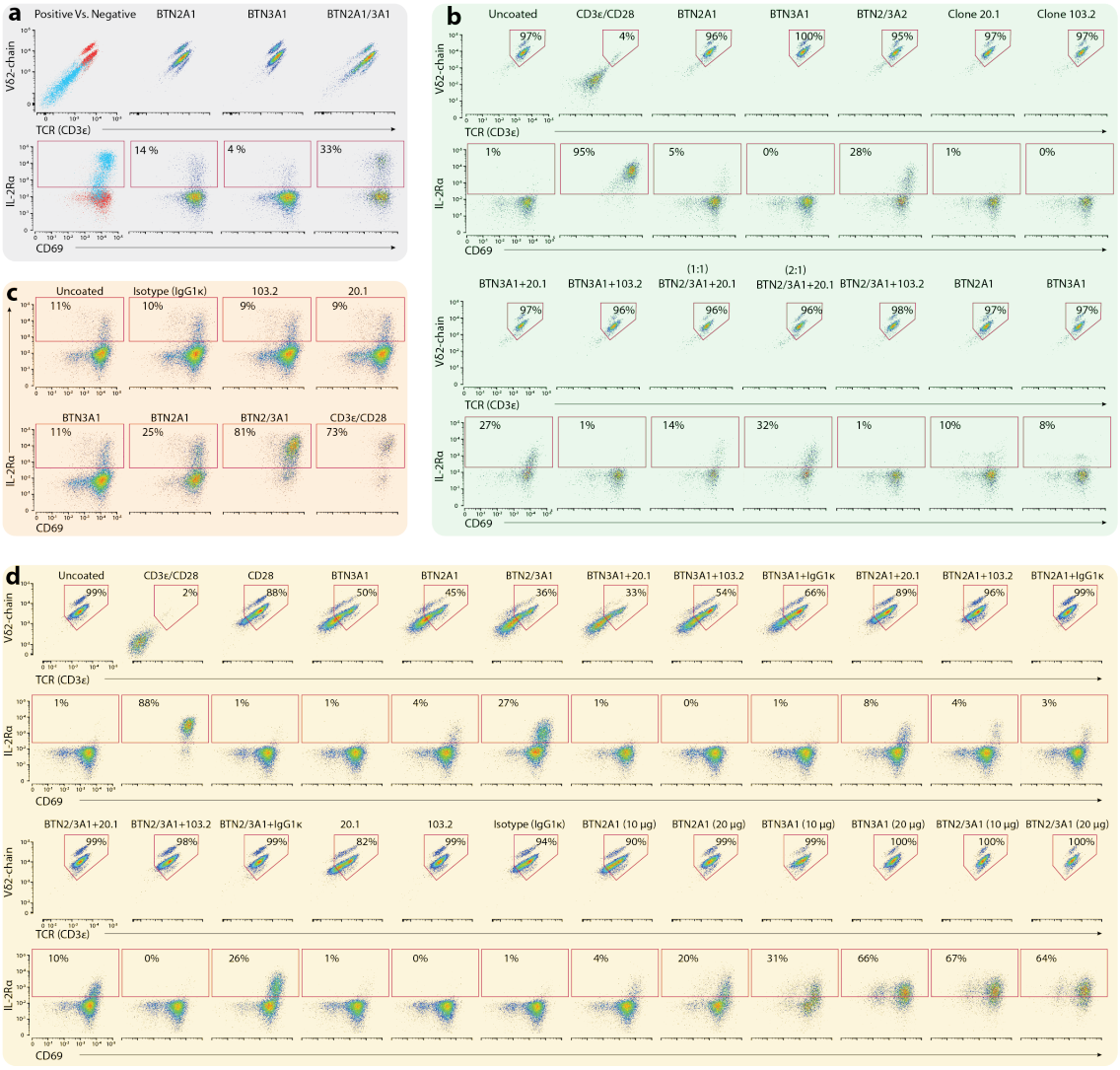

Figure 4.3: *Donor-purified expanded Vδ2$^+$ T-cell signalling response to immobilised BTN2A1 and BTN3A1 combined. (a) represents a dot-plot for one donor; (b) including the assessment with the addition of functional monoclonal antibodies against BTN3A members; (c) responses examining the effect within the entire population of γδ T cells; (d) increasing the concentration of plate-bound BTN ectodomain protein and combination with functional antibodies. Data represents one of at least four random-donor isolated Vδ2$^+$ T cell readouts, done in two or more experiments.*

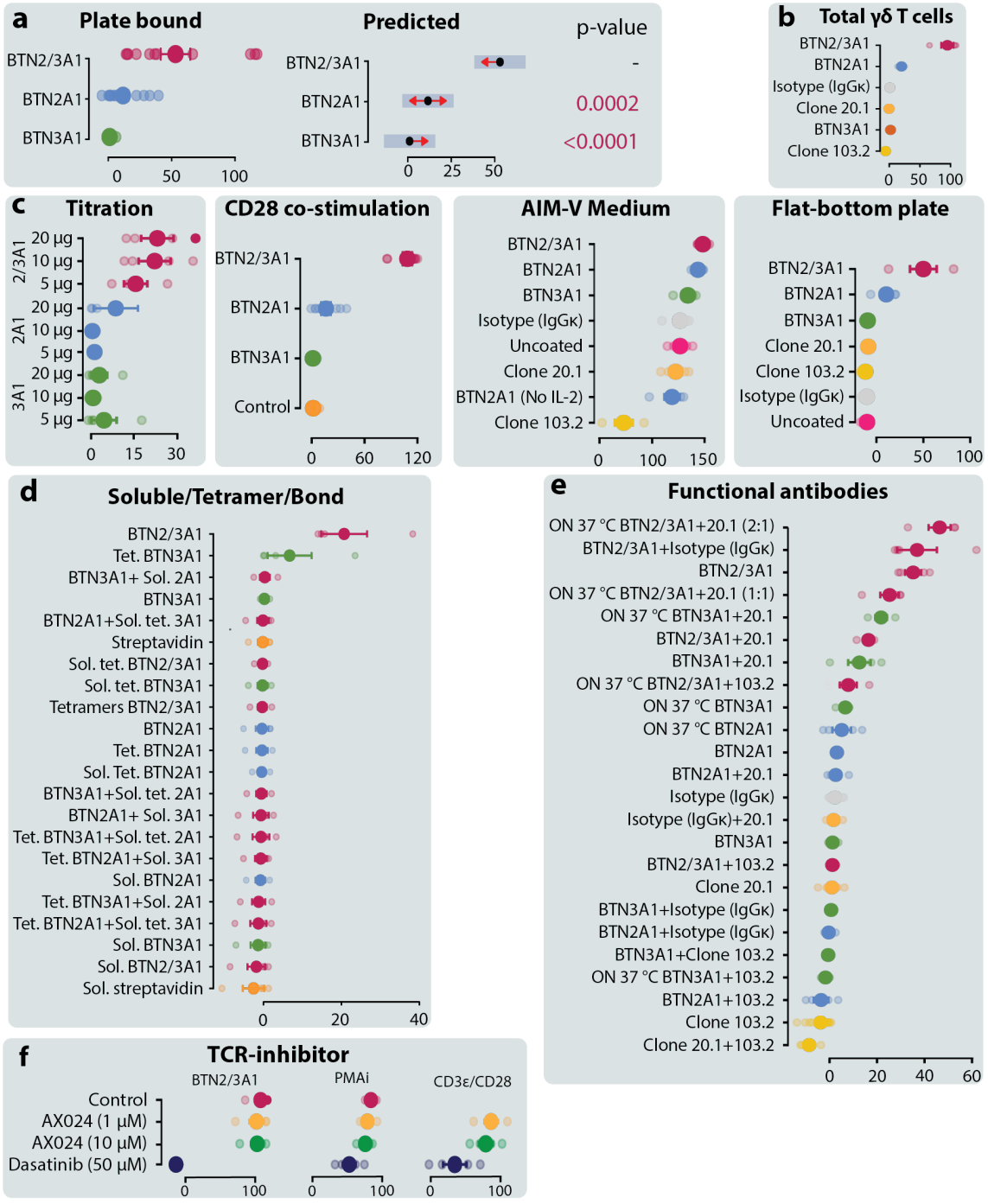

Figure 4.4: *Immobilised plate-bound BTN2A1/3A1 uniquely stimulates Vδ2 T-cells. Normalised Vδ2$^+$ T-cell responses to immobilised protein ($\frac{X_i - X_0}{X_{max} - X_0}$), where max is anti-CD3ε/CD28 stimulation. (a) Averaged twelve random donors with a predicted model of estimated means compared to the BTN2/3A1 test. (b) Total polyclonal γδ T-cell responses. (c) Stimulation Vδ2$^+$ T cells in a titration assay under the presence of anti-CD28 agonist antibody in the media, AIM-V serum-free medium, and the use of a flat-bottom plate. (d) Combination of soluble or tetramer immobilised protein and in solution; (e) functional antibodies and their different conditions as noted in the graph y-axis; (f) effect of TCR-inhibitory signalling cascade drugs AX-024 and Dasatinib. All x-axis represent the normalised percentage of responding Vδ2$^+$ T cells that upregulate the CD25 activation marker in comparison to cells in uncoated control wells. Unless stated, $n = 4$.*

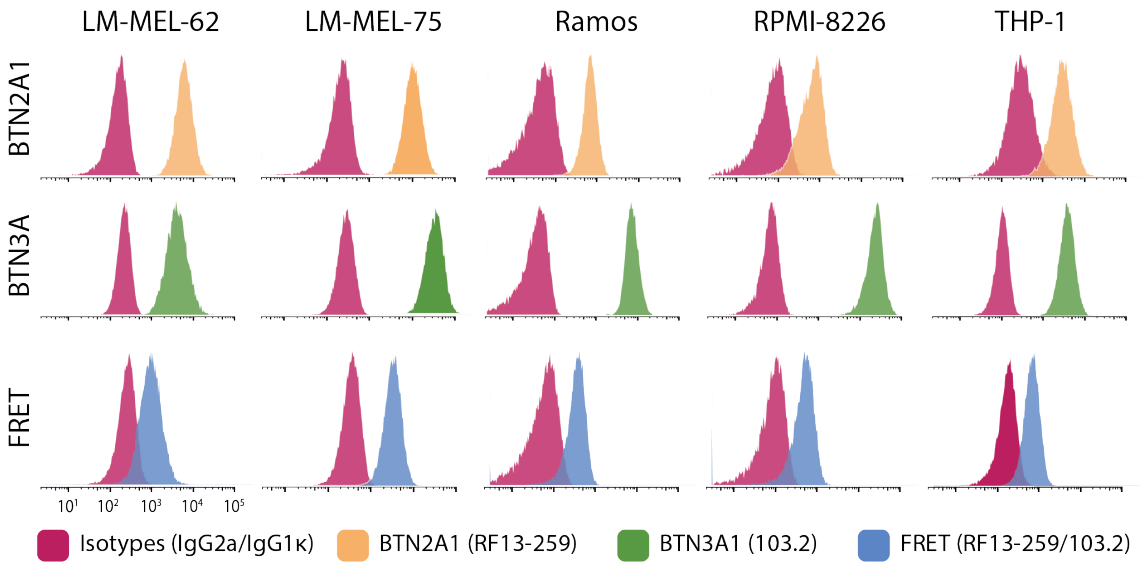

Figure 4.5: *Association of BTN2A1 and BTN3A on the surface of human tumour cell lines detected by FRET between fluorophore-conjugated antibodies specific for targeting BTN2A1 and BTN3A protein members. Human melanoma LM-MEL-62 and -75, B-cell RAMOS and RPMI-8226, and monocytic THP-1 cell lines were assessed for expression of BTN3A members (Clone 103.2 conjugated to PE) or BTN2A1 (clone RF13-259 conjugated to AF647) independently and in combination.*

responsible for an occasional FRET diminished signal. However, considering data from three independent experiments, the plasmid transcription remained constant according to the expression of reporter GFP fluorescent protein and corresponding detection of FRET maintained across each of the three experiments. Thus, a model predicts the BTN2A1 associates to any member of the BTN3A family in rodent transfected cells expressing both BTN2A1 and BTN3A proteins on their cell surface membrane and estimates the intracellular B30.2 domain portion of BTN2A1 has a redundant role for this association (Fig. A.10 .b). Consequently, exchanging the BTN2A1 B30.2 intracellular domain for a PILRβ segment could either disrupt proper transmembrane protein incorporation into the cell's plasma membrane or either hinter the association with its respective BTN3A partnerships in an intracellular milieu. Similar results were observed in the detection of a TCR-fluorescent probe exclusively binging to BTN2A1-transfected cells (Fig. 4.7 .a). The effect of phosphoantigen in transfectant rodent cell lines was therefore examined by the addition of HMBPP or zoledronate drug into the cell culture. The addition of these phosphoantigens in the murine cell cultures became redundant in terms of detecting any alteration in the FRET readout signal (Fig. 4.7 .b). The capacity cell transfectants to bind to the Vγ9Vδ2 TCR in single BTN2A1 murine transfectants or conjunction with any of the BTN3A three members was maintained. Only the swap of the B30.2 for the PILRβ domains in the BTN2A1 limited the affinity

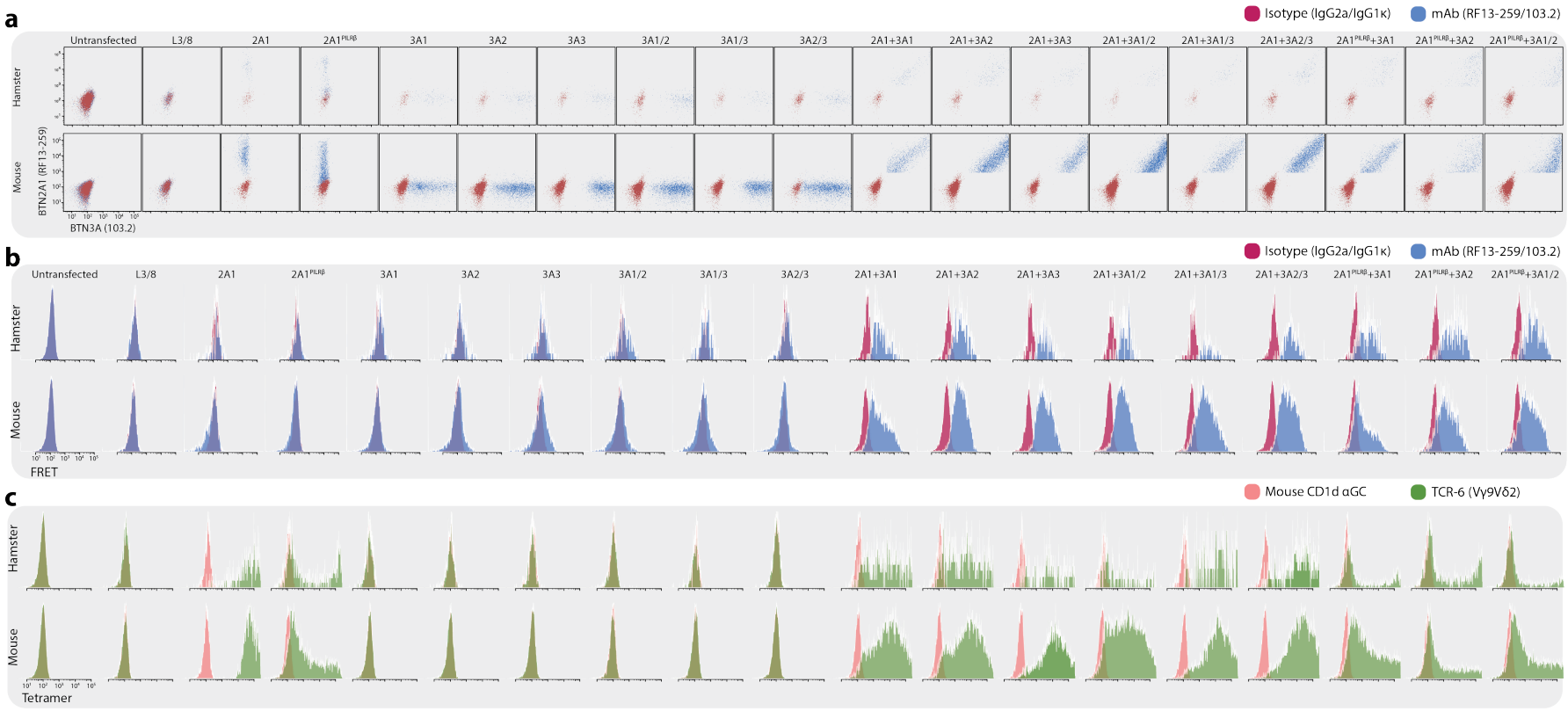

Figure 4.6: *Association of BTN2A1 and BTN3A on the surface of NIH/3T3 or CHO-K1 cell lines detected by FRET and Vγ9Vδ2 TCR affinity for human BTN2A1 transfected cells. (a) Fluorophore-antibody conjugates (Clone 103.2 and RF13-259 carring a PE or an Alexa Fluor™ 647 fluorphores, respectively) caused the electron energy transfer from donor PE to receptor AF647 fluorophores when BTN2A1 was co-expressed with any member of the BTN3A family. Single antibody tests were added for comparison and ensure single fluorophore signal is absence in the FRET readout channel. (c) a Vγ9Vδ2 TCR clone 6 binds all cells transfected with human BTN2A1.*

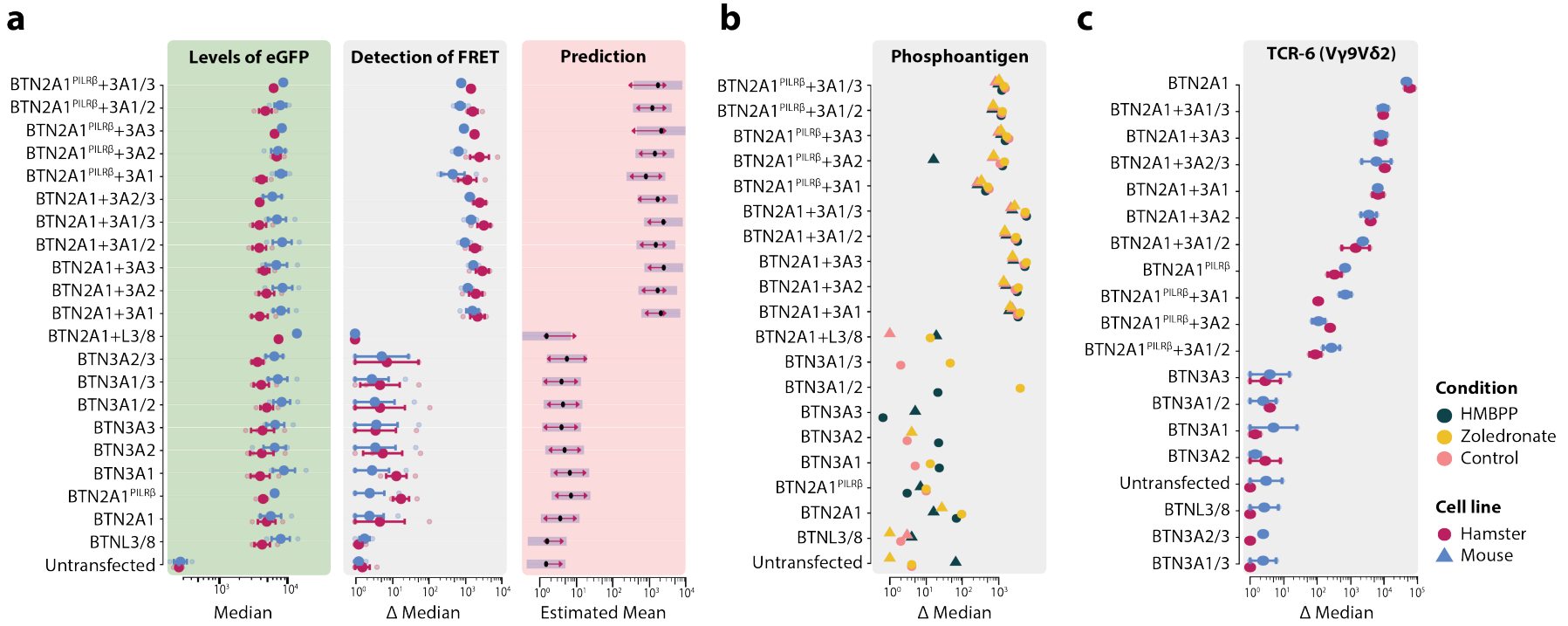

Figure 4.7: *Transfecting human BTN2A1 and BTN3A proteins in NIH/3T3 and CHO-K1 cell lines enables detection of (a) FRET with antibody conjugates (Clone 103.2-PE and RF13-259-AF647) form three independent experiments, considered living cells maintained constant protein expression considering a plasmid reporter enhanced green fluorescent protein (GFP) detection levels. FRET was detected in the 670/14-yellow channel. A predicted model computed for statistical significance where blue bars are confidence intervals for estimated means and red arrows indicate their respective comparisons. If an arrow from one mean overlaps an arrow from another group, there is no significance, based on Tukey-adjusted p-values considering an $\alpha = 0.05$. (b) FRET levels across three different conditions: HMBPP (0.5 ng ml^{-1}), zoledronate (4 µM), and unstimulated control from a single experiment. (c) The difference between the median fluorescence intensity of a Vγ9Vδ2 TCR clone 6 tetramer fluorescent probe and a mouse CD1d-α-GalCer control from two independent experiments.*

of the Vγ9Vδ2-TCR for this protein (Fig. 4.7 .c).

4.4.1 BTN2A1 and BTN3A1 Co-localise in Microscope Imaging

The association between BTN2A1 and BTN3A members was observed in fluorescent microscopy imaging. Antibodies targeting BTN2A1, BTN3A, or control human leukocyte antigen (HLA)-ABC on the surface of LM-MEL-75 melanoma cell line deduced a significant co-localisation between the detection signals at the three-dimensional space in the image field, aka *voxels*. This signal was detected exclusively in the dual presence of BTN2A1 and BTN3A members, while none of these BTN molecules overlaid with HLA-ABC proteins (Fig. 4.8). Those microscopy images were overlapped to conclude which detected a positive signal for both BTN2A1 and BTN3A1 proteins. Nearly half of the voxel counts containing a signal for both BTN2A1 or BTN3A antibody specific markers matched (Fig. 4.8 b-c). Additionally, the FRET between antibody fluorophores targeting specifically BTN2A1 and BTN3A was observed in a co-stain using a high antibody titre (Fig. 4.9 a). Separate single stained controls showed a negative signal at the FRET channel. A three-dimensional space image of co-stained LM-MEL-75 melanoma cells visually confirmed the overlaying between BTN2A1 and BTN3A members, and reassured no fluorescent signal was observed in respective control knockout melanoma lines.

4.4.2 BTN2A1/3A Associate Independently from Phosphoantigen

The intracellular B30.2 domain of BTN3A1 senses phosphorylated antigens and is a functionally necessary element for the activation of Vγ9Vδ2 T cells (Sandstrom et al., 2014). However, its interaction with members of the BTN2A family has not been reported. A constitutively fluorescent protein mTurquoise2 (aka CFP) or mVenus (aka YFP) sequences were appended at the carboxyl-terminal region in altering combinations between *BTNL3* and *BTNL3* for controls and *BTN2A1*, *BTN2A2*, or *BTN3A1* full-length protein constructs to study their respective intracellular interactions when docked at the cellular membrane. A FRET signal shift was detected from the mTurquoise2 channel (450/40-violet) into the FRET readout signal (530/50-violet) when two B30.2 intracellular components of the BTN molecules were in contact. This signal was observable from a known BTNL3/8 interaction (Di Marco Barros et al., 2016) that served as a positive control for the reliability of the final protein product produced and feasibility of the readout FRET signal. When any these single control proteins were transfected in a combination of BTN2A or BTN3A1 members instead, a negative signal resulted. Either combination of CFP or YFP in BTN2A1 or BTN3A1 produced a

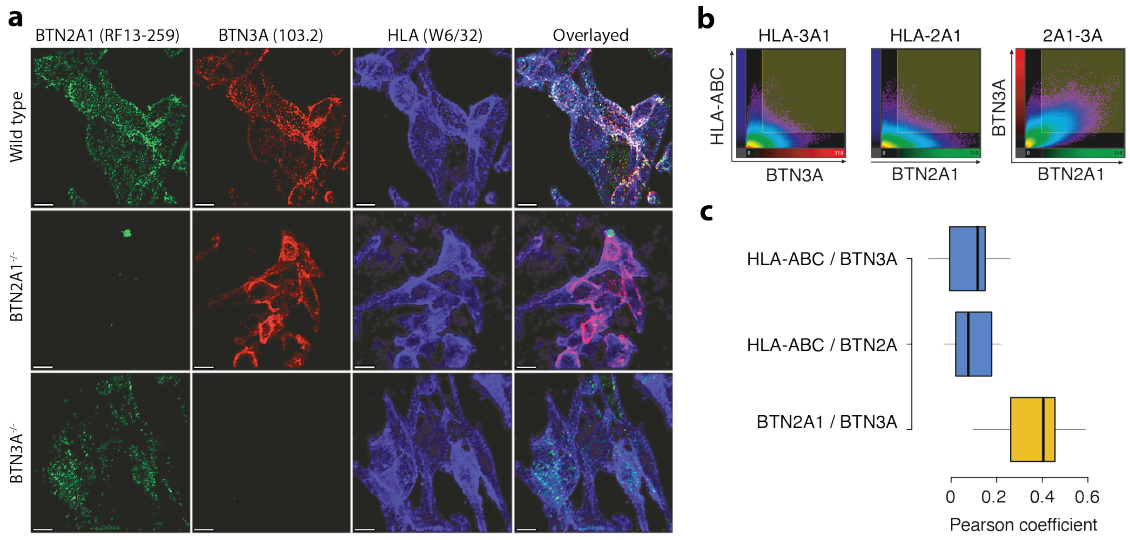

Figure 4.8: *Fluorescence microscopy images show voxel co-localisation between BTN2A1 and BTN3A1 but not to HLA-ABC on the surface of the plasma membrane of LM-MEL-75 melanoma cell line. (a) Images across three channels were detecting an anti-BTN2A1 (RF13-259), anti-BTN3A (103.2), and anti-HLA-ABC (W6/32) control, plus an overlay of all three channels comparing a wild type LM-MEL-75 melanoma cell to respective* BTN2A1 *and* BTN3A *knockout lines. Scale bars are 15* µm*. (b) Voxel correlation between double-channel fluorescence detection across three combinations of a triple-stain sample. (c) Boxplot of computed Pearson coefficient values from two independent experiments where six sample areas were randomly selected for pixel evaluation. The mean from the BTN2A1/BTN3A group statistically differentiates from the other two with a Tukey-adjusted* p*-value* $=< 0.0001$ *considering an* $\alpha = 0.05$ *in a linear mixed-model (fixed experiment and co-stain group; random effect is well-subjected area).*

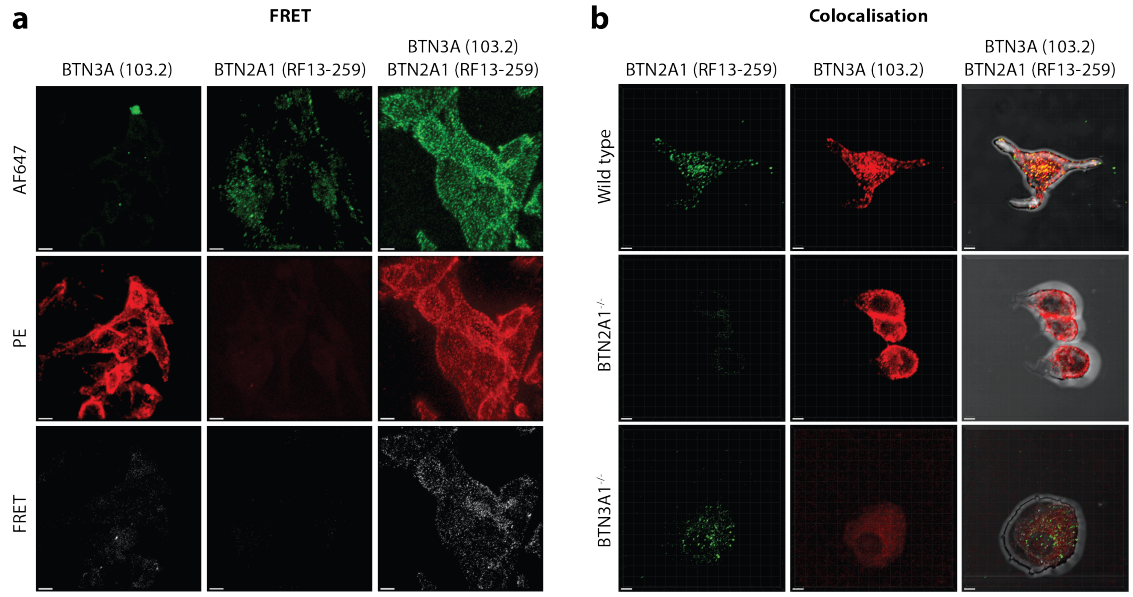

Figure 4.9: *Microscopy images show co-localisation between BTN2A1 and BTN3A members on the surface plasma membrane of LM-MEL-75 melanoma cell line. (a) Monoclonal antibody clone 103.2 in PE (red) targeting all BTN3A members and clone RF13-259 in AF647 (green) specifically binding to BTN2A1 cause FRET signal (white). (b) Overlaying positive pixels for PE and AF647 channels (yellow) determines co-localisation between the two target proteins, which is absent in* BTN2A1 *and* BTN3A *knockouts. Scale bars are (a) 10* µm *and (b) 5* µm.

positive signal for FRET, but this signal was absent when the BTN2A2 substituted the BTN2A1 protein (Fig. 4.10). Moreover, the combination of homodimer proteins showed significant positive interactions for BTN2A1, BTN2A2, and the already known BTN3A1 homodimer formation (Gu et al., 2017).

The influence phosphorylated antigens have in the interaction complexes was examined to understand its function and its role between targeted protein-protein interactions at the molecular level. We treated cells with a high concentration of microbial HMBPP or zoledronate drug. In either case, no difference in comparison to respective unstimulated conditions was observed.

4.4.3 Antibodies Impair Association of the BTN2A1/3A Complex

The incorporation of phosphorylated compounds into cells co-expressing intracellular-fluorescent construct pairs was redundant in altering the resulting FRET signalling but did the treatment with monoclonal antibodies with affinity to BTN2A proteins or BTN2A1, specifically (Fig. A.6 and A.11). This data explains a physical interaction occurred between BTN2A1 and BTN3A1 within a protein complex at the surface of cells which directly impacts on the strategic positioning in their intracellular domains.

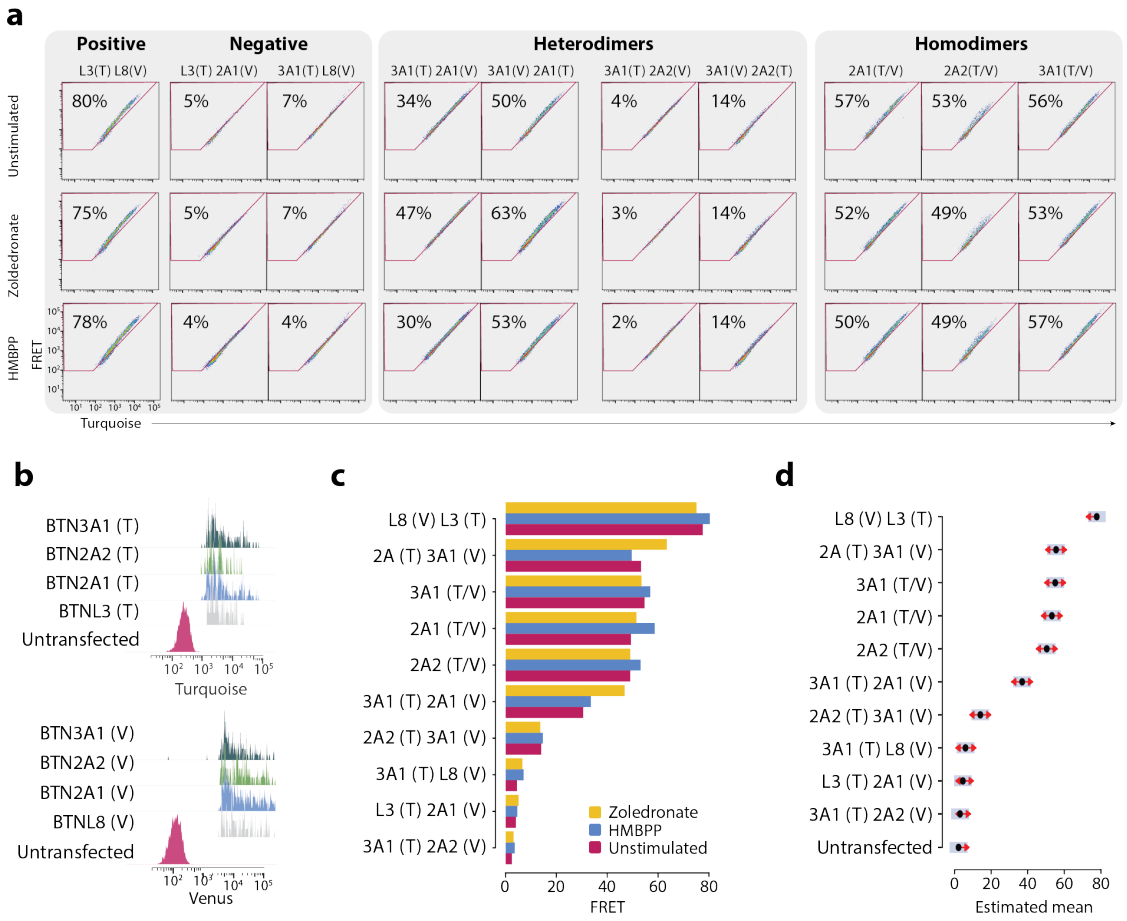

Figure 4.10: *Intracellular domains of BTN2A1 and BTN3A1 associate irrespectively from the presence of phosphorylated microbial HMBPP (100* ng ml^{-1}*) antigen or endogenous phosphorylated metabolites derived from applied zoledronate drug (40* µM*). (a) A dot-plot graphic representation for BTN fluorescent genetic constructs expressed in various heterodimeric combinations on NIH/3T3 cells next to respective positive and negative controls. A FRET positive signal is detected by a fluorescent shift from the turquoise channel (450/40-violet) into the FRET readout signal (530/50-violet). (b) Single transfectant controls expressing the protein of interest. (c) Barplot compares the percentages of cells that emit a fluorescent signal for FRET. (d) Linear mixed-model, including cell transfection as fix effect and stimulation as a random effect, predicts HMBPP or zoledronate has an equal effect to unstimulated transfected cells. Computed for statistical significance for different transfected combinations compared to untransfected cells, where blue bars are confidence intervals for estimated means and red arrows indicate their respective comparisons. If an arrow from one mean overlaps an arrow from another group, there is no significance, based on Tukey-adjusted p-values considering an $\alpha = 0.05$. Showing one experiment for each phosphoantigen.*

Therefore, interactions between B30.2 portions of BTN members were reasonable and likely relevant regarding mechanical operations needed to activate the immune cells. Nearly all antibodies tested altered the expected FRET signal between the two fluorophores at the intracellular domains of these BTN members. Whereas most abrogated the detected signal, a few induced an increased readout (RF13-29, -37, -44, -59, -61) one of which these antibodies, the RF13-259 had a previously detected agonist functionality (Sec. 3.5.3). Their respective effect was compared to an isotype control treatment which set the FRET-max expected detection level in two independent fluorophore combinations between BTN2A1 and BTN3A1. The assessment of their respective functional activity was expressed as a percentage for each reagent tested (Fig. 4.11). Noteworthy, the same antibodies which impaired the microbial HMBPP-phosphoantigen induced response in donor-purified expanded Vδ2^{+} T cells (RF13-227, -236, -248, -266, and Hu34C), were also abolishing the FRET between the intracellular domains of these BTN transmembrane proteins (Sec. 3.5.3). However, some of the antibody's functional effect differs between the two fluorophore combinations assessed. For instance, the Hu34C clone had a complete abolishment of the FRET signalling in the BTN3A1-CFP and BTN2A1-YFP combination, whereas when these fluorophores were swapped, the outcome signal was unaffected by the treatment. In other similar treatments, like for the RF13-268 and -269 antibody clones, the same effect was obtained.

4.5 The Intracellular BTN2A1 Domain Has a Functional Role

The intracellular portion of BTN2A1 was noted as essential to associate with BTN3A1, and together, they confer phosphoantigen-derived responses by $\gamma\delta$ T cells (Sec. 4.4). Nonetheless, the BTN2A1 B30.2 domain interaction to phosphoantigens was not detected by ITC (Sec. 5.3). To elucidate its function, wild-type *BTN2A1* expression constructs were mutated to produce truncated protein products at levels right below of its transmembrane domain, juxtamembrane α-helix, B30.2 domain, and the substitution of the latter B30.2 domain for that of BTN1A1 or a PILRβ intracellular domain. These mutants were then expressed along *BTN3A1* expression constructs on accessory cells to determine whether or not any of these combinations modulated the binding affinity to the Vγ9Vδ2 TCR or altered the response to phosphoantigen antigens.

The expression of DNA constructs and correct folded-protein at the surface of the plasma membrane was validated by the reporter-GFP protein and detection of respective BTN2A1 or BTN3A1 members at the surface membrane. It is noticeable the single gene expression of a *BTN* does not express well at surface membrane un-

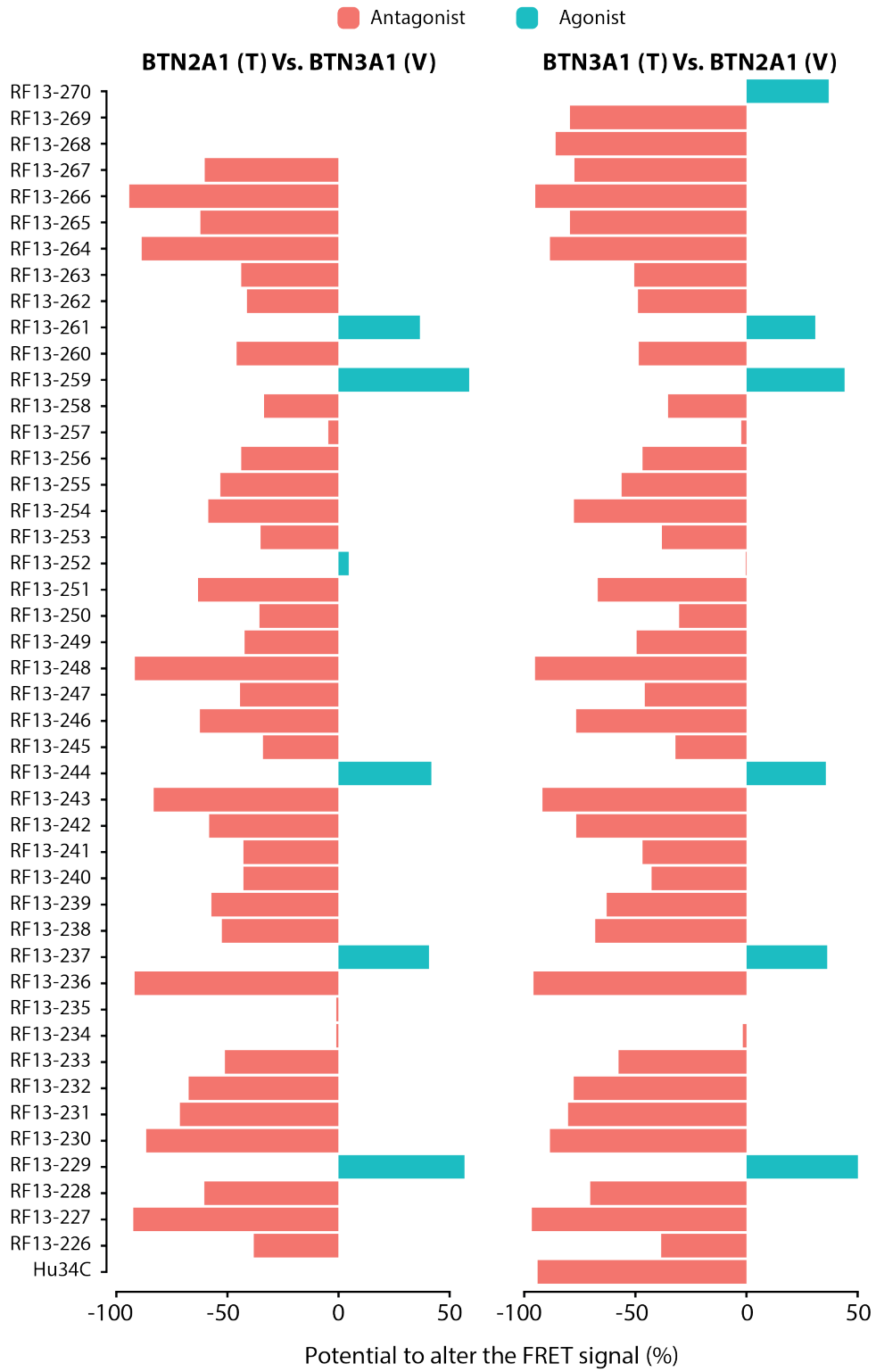

Figure 4.11: *Potential activity of various monoclonal antibodies against BTN2 to dissociate BTN intracellular domains between fluorophore-tagged BTN2A1 and BTN3A1 members that under untreated co-expression conditions emit a FRET signal detected by flow cytometry. Respective activities are expressed as a percentage to the reference isotype control (IgG2a/BM4) signal of neutral effect.*

less another *BTN* of the same species was present, similar to what Vantourout et al. (2018) described. Moreover, the BTN2A1 which lacks the portion below the B30.2 domain or it was entirely substituted by a PILRβ intracellular domain, expressed worse than any other BTN2A1 mutant (Fig. 4.12 a). In the same experiment, these proteins were assessed for whether their respective antibody-conjugate markers altered the detectable FRET signalling between the wild-type pair (Fig. 4.12 b). The results showed similar detection signal strength for the *BTN2A1*$^{\text{BTN1A1 B30.2}}$, *BTN2A1*$^{\Delta\text{TM}}$, and *BTN2A1*$^{\Delta\text{JM}}$ mutants. Opposed to this, mutants *BTN2A1*$^{\Delta\text{B30.2}}$ and *BTN2A1*$^{\text{PILR}\beta}$ abolished a typically observed FRET signal, indicating these two mutants disrupt the association between the BTN2A1 and BTN3A1 proteins. Similarly, the same batch of transfected cells containing the *BTN2A1* mutant expression constructs was stained with tetramerised Vγ9Vδ2 TCR clone 6, to determine alterations in their binding affinity. Indeed, the Vγ9Vδ2 TCR showed a great affinity for all cells expressing the construct with a single *BTN2A1* exogenous protein, and lesser binding capacity for those *BTN2A1*$^{\text{BTN1A1 B30.2}}$, *BTN2A1*$^{\Delta\text{TM}}$, and *BTN2A1*$^{\Delta\text{JM}}$ mutants (Fig. 4.13). Again, the expression of *BTN2A1*$^{\Delta\text{B30.2}}$ and *BTN2A1*$^{\text{PILR}\beta}$ constructs alone was not affine to bind the Vγ9Vδ2-TCR tetramerised fluorescent probe. Of note, co-expression with either *BTN3A1* or *BTNL3* control equally increased the affinity for this Vγ9Vδ2-TCR clone 6, indicating the recognition of the BTN2A1 is exclusive of this protein, and the association to other BTN counterparts facilitates its availability for being sensed by $\gamma\delta$ T cells. Therefore, the topographic localisation of the BTN complex is crucial for inducing $\gamma\delta$ T-cell responses. An overview assessment considering the differential number of cells expressed as a percentage of total efficiently transfected cells is summarised in Fig. 4.14.

Next, transfected murine cells expressing the different forms of BTN2A1-truncated protein were plated in an assay test together with donor-purified and expanded Vγ2^{+} T cells to detect the phenotypic changes on this responding lymphocytes. These experiment results correlated with previous observations in which *BTN2A1*$^{\text{BTN1A1 B30.2}}$, *BTN2A1*$^{\Delta\text{TM}}$, and *BTN2A1*$^{\Delta\text{JM}}$ products similarly alined in their functionality, in that occasion internalising the Vγ9Vδ2 TCR and up-regulating the expression of CD25 surface expression marker on their membranes. A sticking fact, however, was their capacity to stimulate $\gamma\delta$ T cells irrespectively of phosphoantigens, whereas co-expression of the wild-type BTN2A1 and BTN3A1 required a zoledronate pulse for triggering $\gamma\delta$ T cell responses (Fig. 4.15 and A.16). Equally important, the substitution of the BTN2A1 B30.2 intracellular domain for that of BTN1A1 directly constituted a potent continuous stimulus to Vγ9Vδ2 T cells. Again, expression of either *BTN2A1*$^{\Delta\text{B30.2}}$ or *BTN2A1*$^{\text{PILR}\beta}$ constructs were redundant and ineffective to induce an immune re-

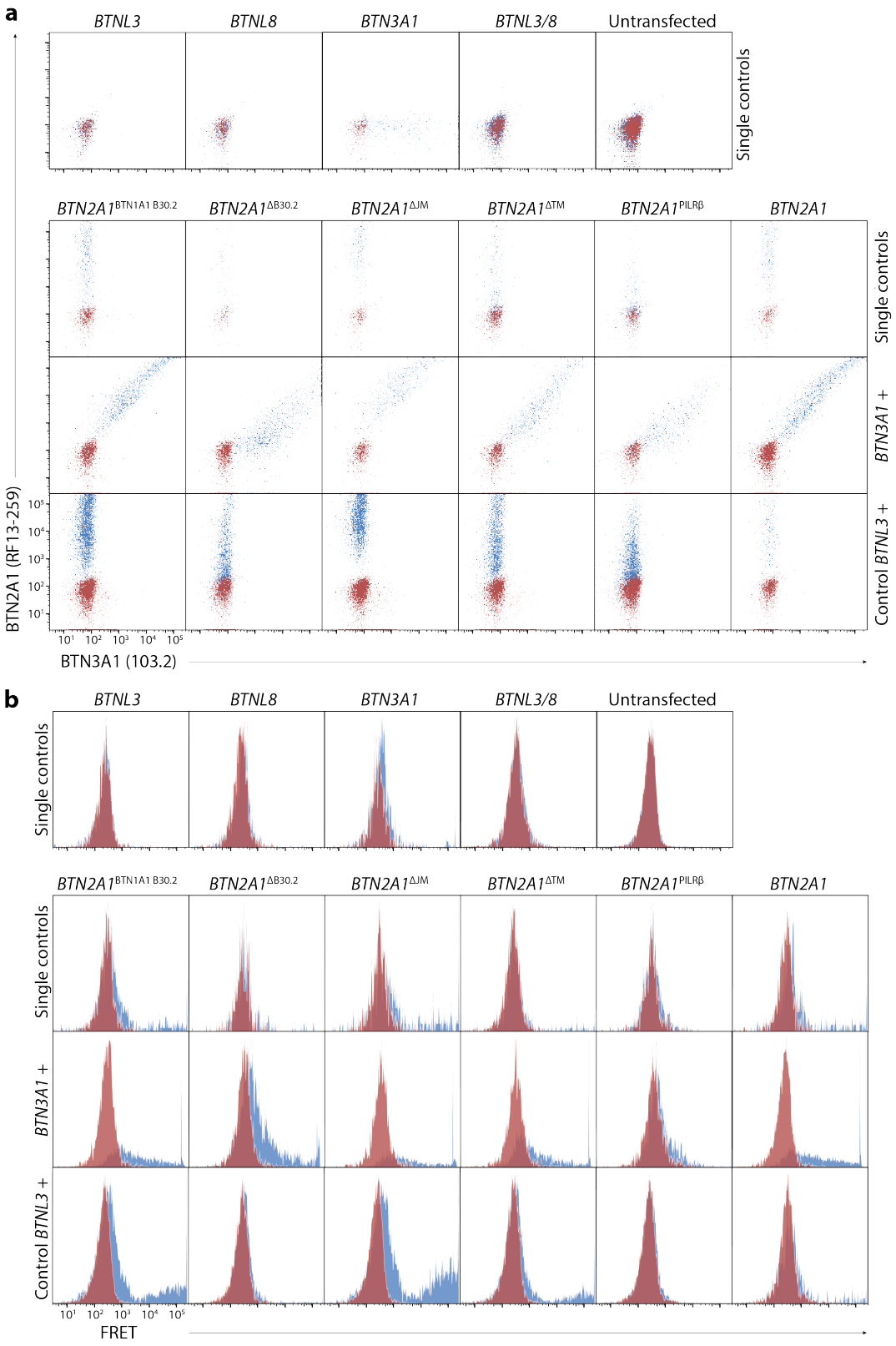

Figure 4.12: *The BTN2A1 B30.2 intracellular domain is needed to join BTN3A1 and form a surface protein complex. (a) Detection of either BTN2A1 (RF13-259) or BTN3A1 (103.2) with antibody mixture that causes a FRET signal depicted in (b) when respective fluorophores locate closely (10* nm*).*

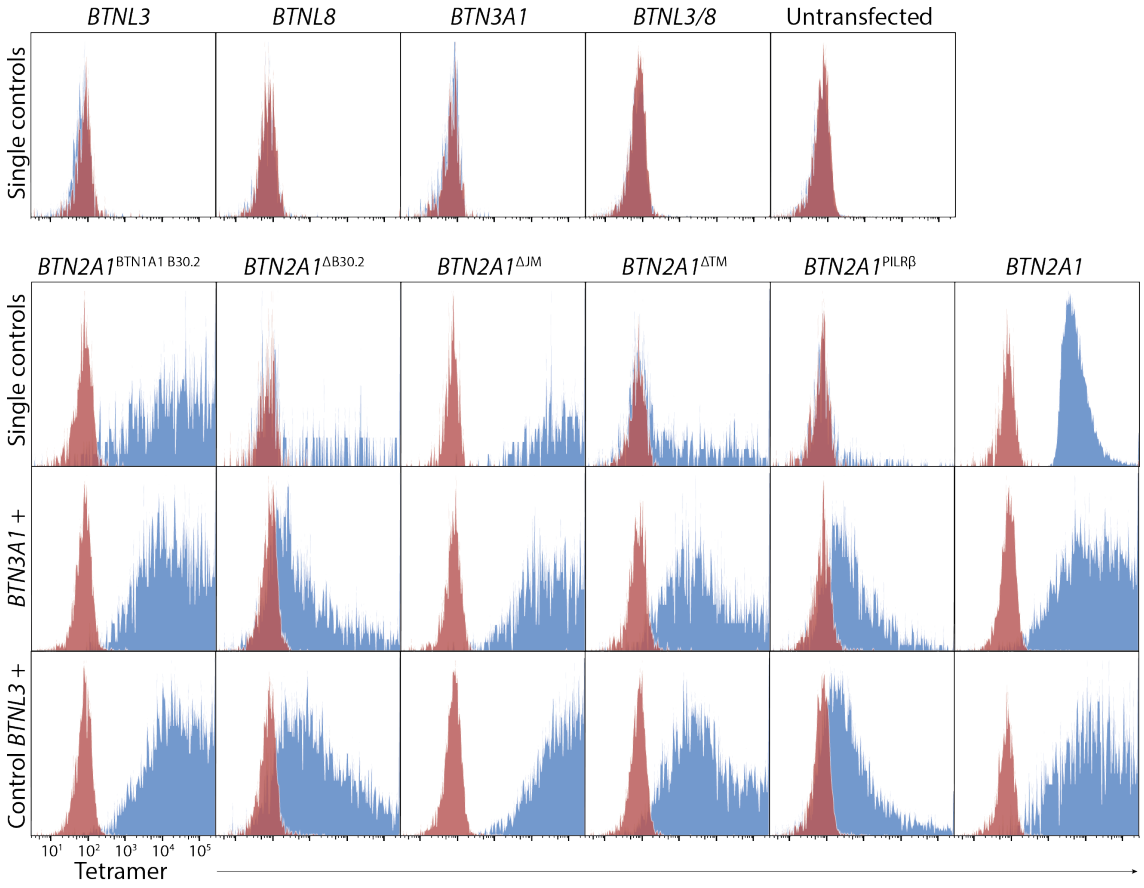

Figure 4.13: *Deletion of BTN2A1 intracellular B30.2 or its substitution for PILRβ disrupts normal affinity for a Vγ9Vδ2 TCR clone 6. Normalised to mode histograms for transfected mouse fibroblast NIH-3T3 cells with indicated constructs when treated with tetramerised Vγ9Vδ2-TCR clone 6 (blue) or mouse CD1d-α-GalCer control.*

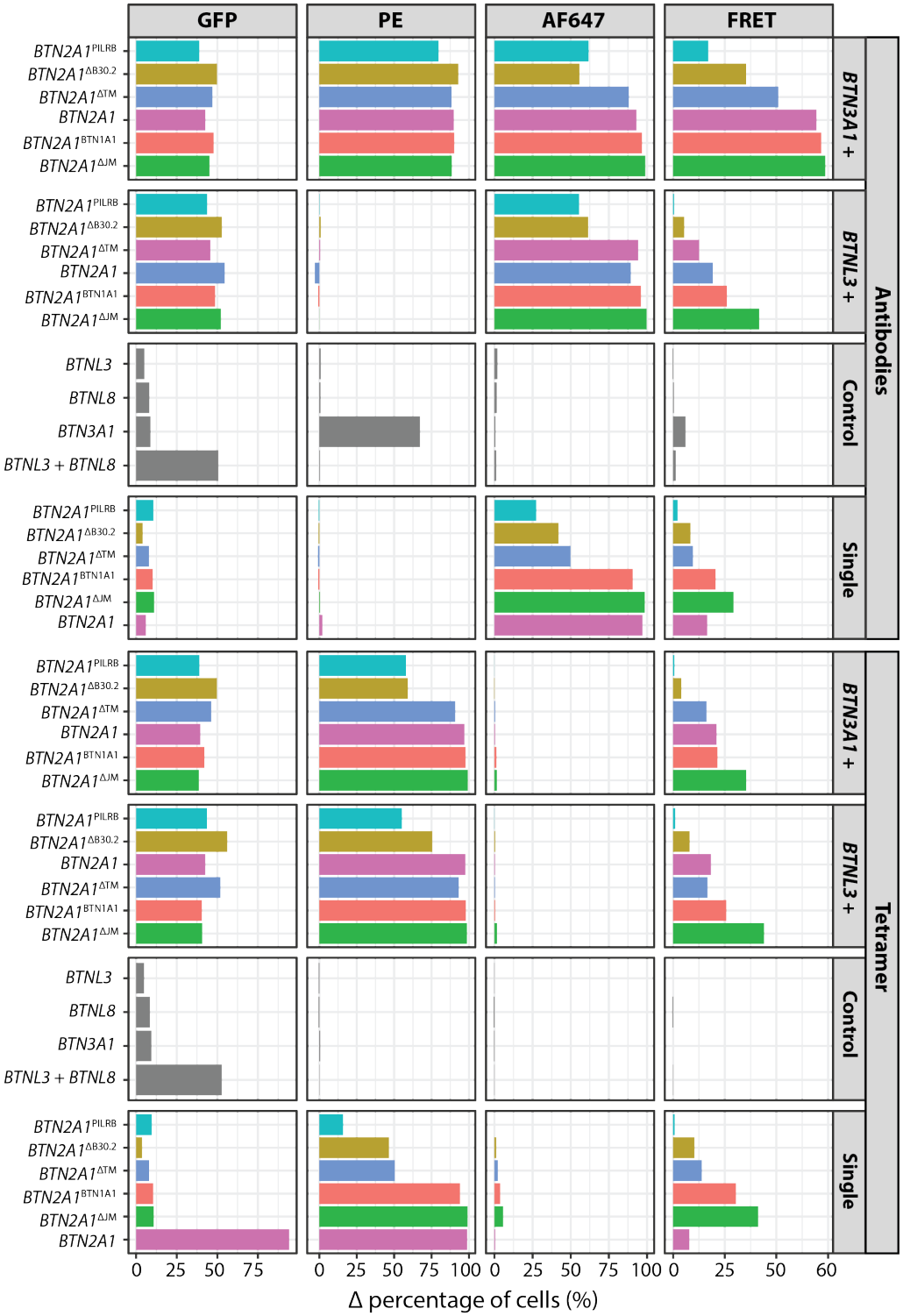

Figure 4.14: *Expression of truncated BTN2A1 at the transmembrane (TM), juxtamembrane (JM), B30.2 domain (B30.2) or its substitution for an irrelevant PILRβ or a B30.2 domain (PILRβ) of BTN1A1 (1A1) in conjunction with BTN3A1 or control BTNL3 protein revels discrepancies when altering the intracellular portion of BTN2A1 protein at the association with BTN3A1 and the affinity for the Vγ9Vδ2 TCR. Transfection reporter green-fluorescent protein (GFP); either anti-BTN3A clone 103.2 or $\gamma\delta$TCR tetramerised clone 6 (PE); anti-BTN2A1 clone RF13-259 (AF647); FRET signal (FRET).*

sponse. Note, the intrinsic BTN2A1 capability to provide Vγ9Vδ2-TCR signalling caused the internalisation of the $\gamma\delta$ TCR when this was co-expressed along BTN3A1 or even the BTNL3 control. At the same time, it was only when cooperating with BTN3A1 that $\gamma\delta$ T cells engaged in an activation phenotype detected by upregulation of CD25. Thus, the model in which these BTN2A1 truncated mutants cooperate with BTN3A1 was predicted taking into account the zoledronate stimulus and denoted the increased, stimulating capacity of the mutant which incorporates the intracellular domain of BTN1A1 over the wild-type protein (Fig. 4.16). The BTN3A1 pairs with either *BTN2A1*$^{\text{BTN1A1 B30.2}}$, *BTN2A1*$^{\Delta\text{TM}}$, or *BTN2A1*$^{\Delta\text{JM}}$ induced similar activation profiles compared to the wild-type BTN2A1, whereas the *BTN2A1*$^{\text{PILR}\beta}$ mutant was inefficient to produce an immune response.

4.6 The BTN2A1 Enhances CD1-restricted $\gamma\delta$ T-Cell Responses

In previous sections of this work, the BTN2A1 protein was determined essential to induce phosphoantigen-driven responses together with BTN3A1. While BTN2A1 acts solely at the Vγ9 of the $\gamma\delta$ TCR, the opposed Vδ2 domain holds a putative BTN3A1 ligand, also necessary for eliciting an immune response to phosphorylated antigens. To questioning whether BTN2A1 additionally boost $\gamma\delta$ T cells responses together with other antigen-presenting molecules, another $\gamma\delta$ T cell subset with recombined variable segment 9 but an alternative variable segment than 2 were tested for their readability responses in cooperation to lipid-presenting molecules of the CD1 linage. Two selected candidate clones were Vγ9Vδ1 CD1c-reactive (clone 1C9) and Vγ9Vδ1 CD1d-reactive expressed on lymphocyte-reporter cell lines which ensures a TCR-dependent signal response (Fig. B.4 and B.4). When these reporter cells were cocultured with mouse fibroblast cells expressing their respective CD1c or CD1d molecular ligands, an increase of activation marker CD69 was noted compared to untransfected cells or corresponding controls (Fig. 4.17). Similar resulting phenotypic changes were detected when BTN2A1 was present on the surface membrane of NIH/3T3 antigen-presenting cells. Furthermore, a balanced enforced expression between BTN2A1 and either CD1c or CD1d lipid-presenting molecules, boosted the lymphocyte-reporter cells' response, resulting in the two ligands working in synergy to accentuate a TCR-dependent immune response.

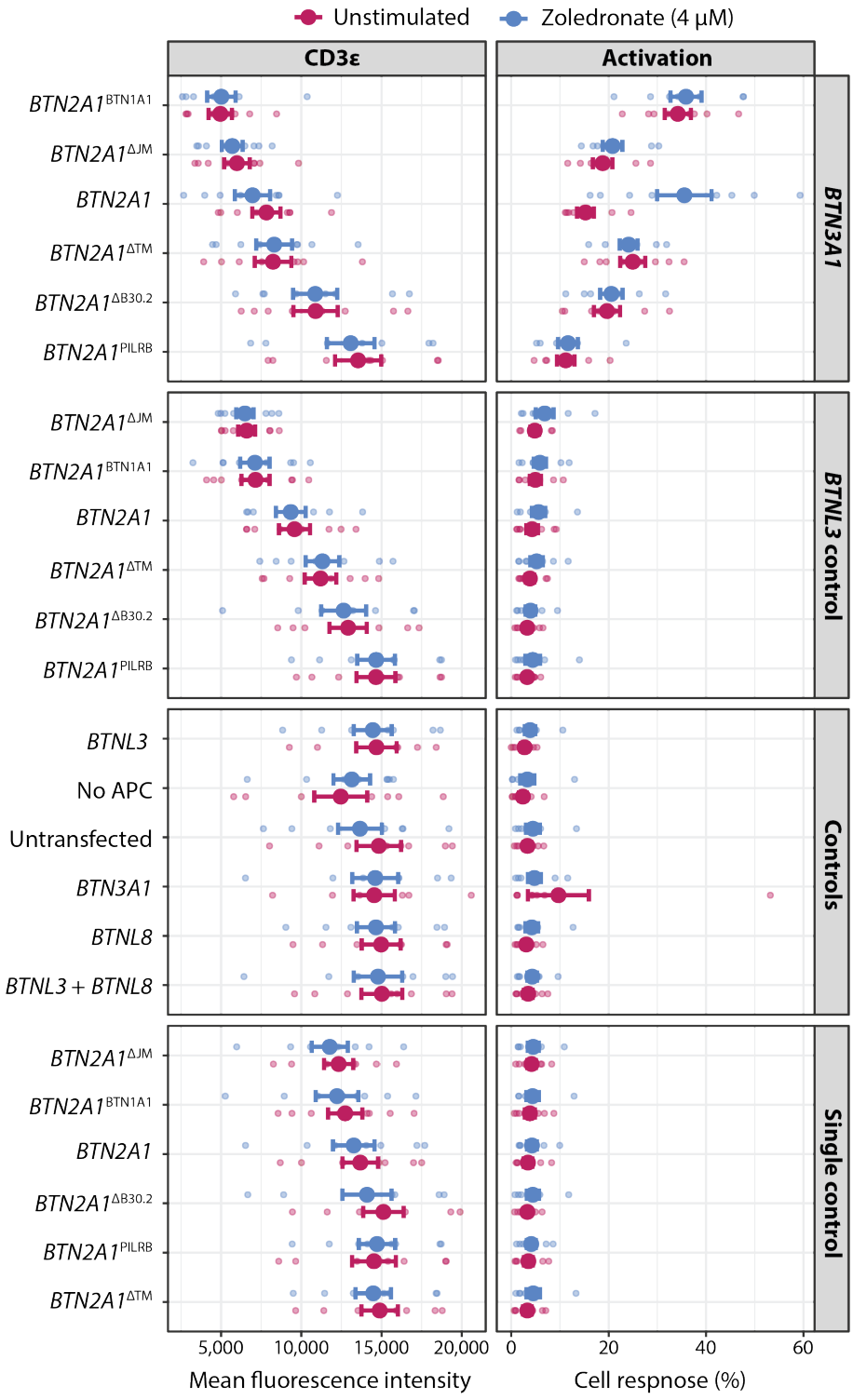

Figure 4.15: *Immune response to truncated BTN2A1 and BTN3A1 by $\gamma\delta$ T cells. Various BTN2A1 mutant protein products expressed on the surface of mouse fibroblast (NIH-3T3) cells together with BTN3A1 or BTNL3 control activate (CD25$^+$ cells) purified-expanded Vδ2$^+$ T cells and internalise their TCR (CD3ϵ) following an overnight stimulus with zoledronate. Data from testing the $\gamma\delta$ T cell response with eight random donors. Bars depict standard errors.*

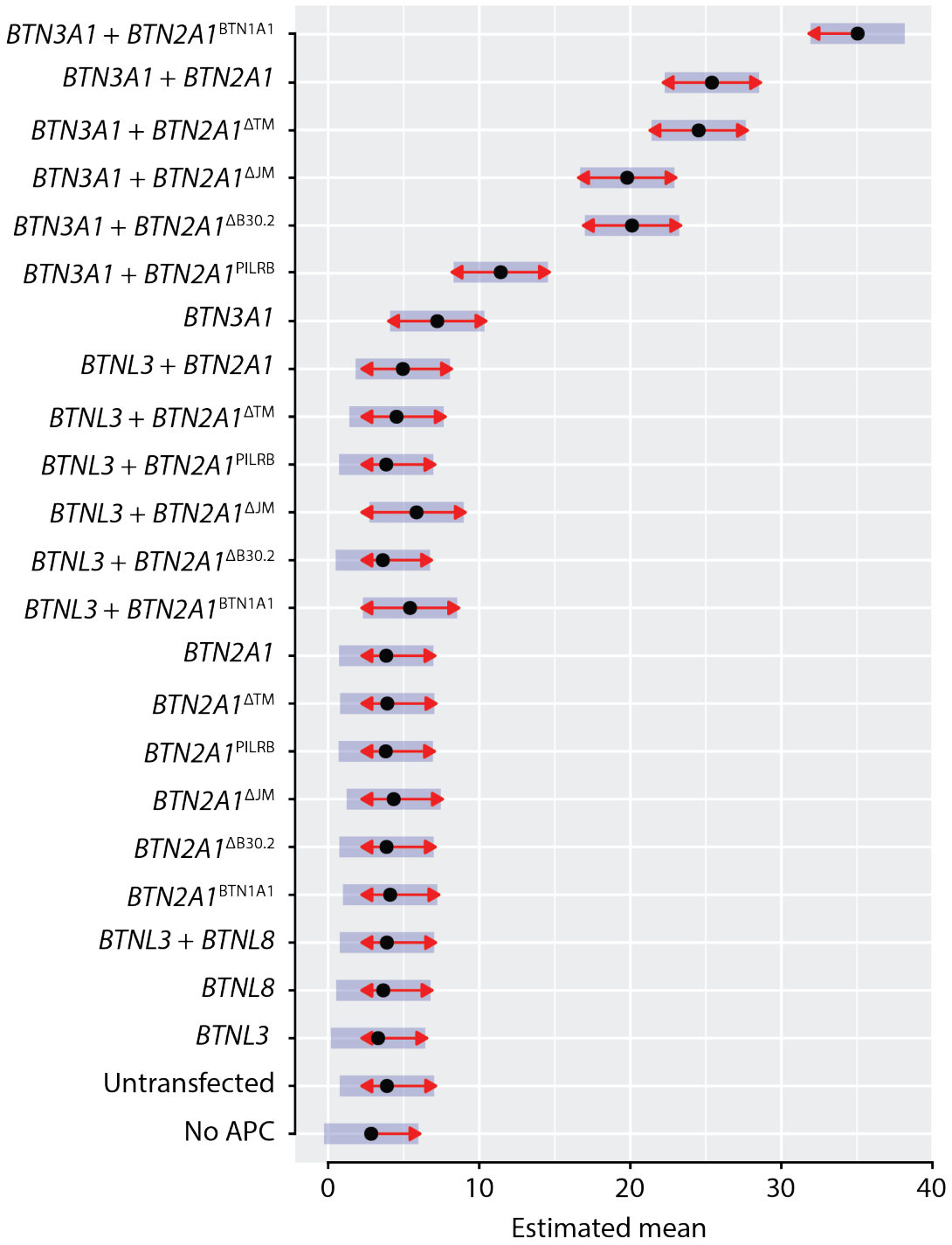

Figure 4.16: *Predicted immune $\gamma\delta$ T-cell responses to truncated BTN2A1 and BTN3A1 in a linear mixed-model considering the stimulus and condition fix effects and eight random donors to estimate the least-squared means for the percentage of activated cells (CD25$^+$) in each condition. Blue bars are confidence intervals for means and red arrows indicate their respective comparisons. If an arrow from one mean overlaps an arrow from another group, there is no significance, based on Tukey-adjusted p-values considering an $\alpha = 0.05$.*

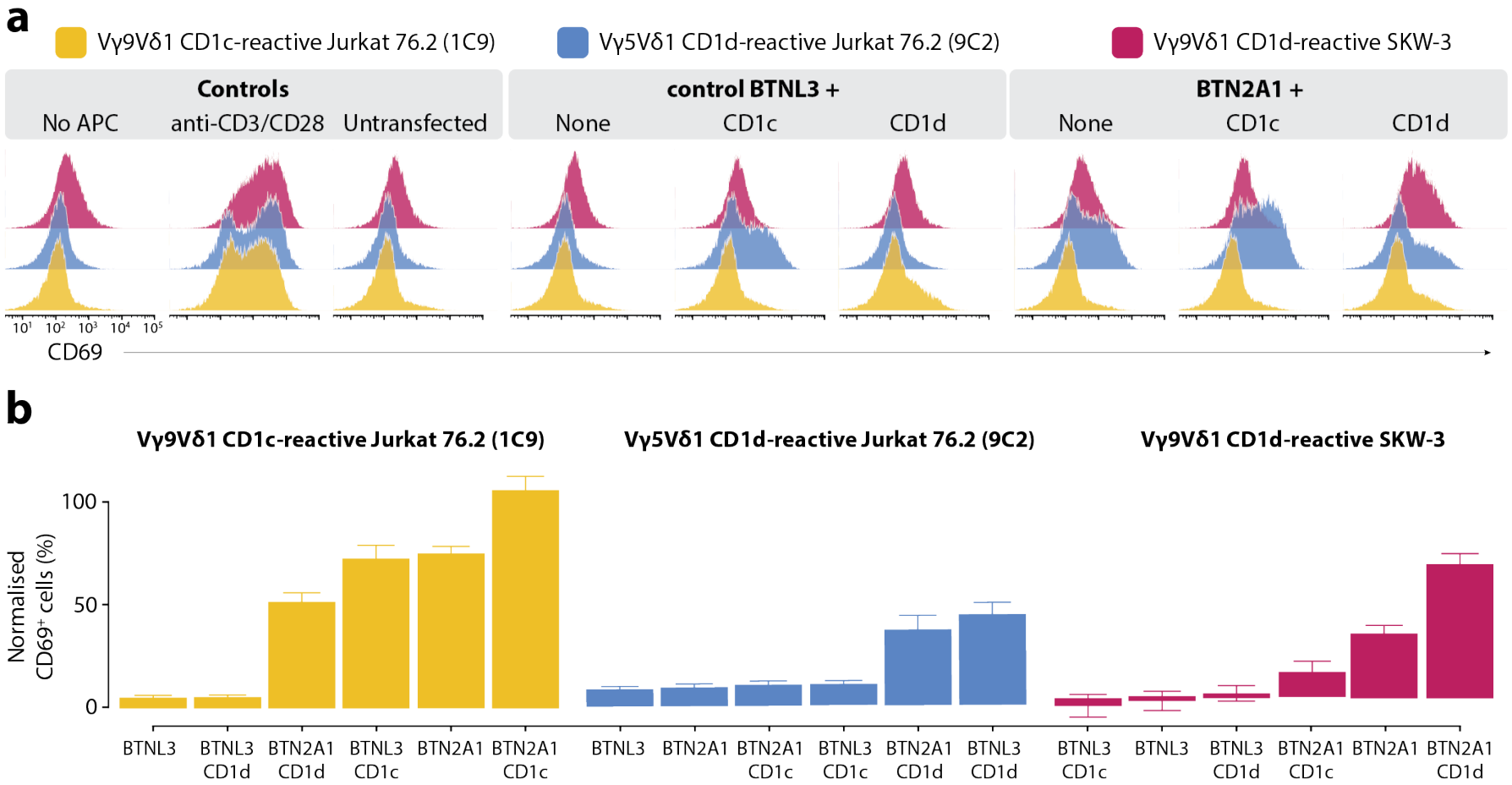

Figure 4.17: *The BTN2A1-Vγ9 interaction enhances γδ T-cell responses to CD1c/d molecules as the activation marker CD69 increases in mouse fibroblast (NIH-3T3) cells co-expressing BTN2A1 in CD1c/d transfectants. (a) Histograms showing the fluorescence intensity for a CD69 marker normalised to the mode. (b) Normalised number of CD69$^+$ cells based on untransfected reference sample ($\frac{X_i - X_{\text{No APC}}}{X_{\text{anti-CD3/CD28}} - X_{\text{No APC}}}$). Data representative from two experiments each with a technical replicate.*

4.7 Discussion

Earlier reports described implications of the BTN3A1 protein member being involved in reactivity by $\gamma\delta$ T cells to phosphoantigens (Harly et al., 2012; Sandstrom et al., 2014). These, together with a series of studies, provided the basis to speculate about attainable cooperation between BTN2A1 and BTN3A1 forging the molecular components required to present phosphoantigens to $\gamma\delta$ T cells. Various experiments were implemented to test that hypothesis and tackle this theory from different perspectives.

Rodent accessory cell lines are ideal candidates to test different combinations of human BTN molecules because of their close similarity with the human biological system and evolutionary divergence which has prevented rodents to naturally encode for genes composing the BTN–Vγ9Vδ2 T-cell axis (Clark et al., 1995; Karunakaran et al., 2014; Kazen and Adams, 2011). Hence, transient expression of combinatory single BTN genes from the human cluster into rodent cells were tested to study their influence in activating $\gamma\delta$ T cells. Our tests shown no combinatory provided signs of activation to donor-derived $\gamma\delta$ T-cells unless both *BTN2A1* and *BTN3A1* were present in cis at the cell surface of these drug-stimulated antigen-presenting cells (Fig. 4.1). Just as documented by Vantourout et al. (2018), the addition of *BTN3A2* onto the complex enhances the driving force that activates phosphoantigen-reactive $\gamma\delta$ T cells, but the sole presence of BTN3A1/2 heterodimeric complex was unable to upregulate common cell-activation markers such as the CD25. However, we observed over-expressing a BTN3A3/2 heterodimeric complex without the presence of BTN2A1 induced secretion of IFN-γ regardless of zoledronate stimulatory treatment and without showing signs of activation cell-surface markers (Fig. 4.2). That result could suggest the BTN3A3 molecule intervenes in the mechanism providing noise on the actual signal, plausibly due to structural differences between this protein and BTN3A1 (Sandstrom et al., 2014).

From another prospect, portions of BTN ectodomains produced in a mammalian system were immobilised on a coated assay plate to identify possible mechanistic forms required to signal the Vγ9Vδ2 TCR of $\gamma\delta$ T cells. These trials backed up the requirements mentioned above, which describes both BTN2A1 and BTN3A1 extracellular domains would be required at the same time and space, working in cis at the surface of the antigen-presenting cells to cause an immune response. These experiments substantiated proper immobilisation of the BTN2A1/3A1 ectodomain complex is independent of phosphoantigens to induce $\gamma\delta$ T cell responses. Thus, providing evidence that phosphoantigens are not acting on the extracellular space of these antigen-presenting molecules, but they modify the topographic ectodomain structure

of that complex instead (Fig. 4.4 a). Besides, the addition of agonist antibody against CD28 co-stimulatory receptor increased the total number of activated responding clones and potentiates the overall immune response identified by the upregulation of CD25 expressed on the cell-surface. This suggested additional co-stimulatory factors might further increase TCR-dependent signals and enhance the response from clonotypes with weak affinity for their ligand. Other signal-enhancing lymphocyte receptors such as NKG2D could have determining roles in communicating the prevailing pathophysiological milieu and adjusting the cytokine profile generated by $\gamma\delta$ T-cell responses (Das et al., 2001a; Rincon-Orozco et al., 2005).

Furthermore, the use of Dasatinib T-cell broad-spectrum inhibitory drug entirely inhibited the phosphoantigen immune response. However, the consequence of administrating a more precise AX-024 drug, which targets the non-catalytic region of tyrosine kinase adapter protein Nck to the CD3ϵ subunit of the TCR, questions whether the TCR-BTN axis has an alternative TCR-signalling pathway or co-stimulating protein factors are needed to generate a final activation signal (Fig. 4.4 f). In this regard, the induction of a phosphoantigen-immune response could share more similarities with those initiated by recognition of superantigens, that relay on alternative biochemical pathways to trigger the activation phenotypic switch (Bueno et al., 2006).

Attempts to detect changes in the stimulatory effect consequence of altering diverse combinations of soluble and tetramerised forms of BTN2A1 and BTN3A1 ectodomain were performed. These resulted all unable to activate the $\gamma\delta$ T cell repertoire. Nonetheless, these series of experiments provided more emphasis in that a BTN2A1 and BTN3A1 ectodomains defined a unique structural conformation were their IgV motives are crucial for the induction of $\gamma\delta$ T-cell responses (Fig. 4.4 d). Applying the 20.1 agonist antibody to BTN2A1-BTN3A1 ectodomain complexes previous to challenging Vδ2$^+$ T cells showed the functional antibody mostly took over the $\gamma\delta$ T-cell response instead of these responding to the active complex structure itself (Fig. 4.4 e). The limited number of activated clones under the effect of this agonist clone is about half of the total Vγ9Vδ2 T-cell population, similar to previous findings (Starick et al., 2017).

First speculations of the BTN2A1-BTN3A1 association during phenotyping tumour cell lines arose from a modest increase in the detection of FRET (Fig. 3.1). Following interchanging fluorophore and different monoclonal specific antibody combinations improved FRET detection signals by an optimised antibody conjugated pairs. Eventually, this technique illustrated the association between BTN2A1 and BTN3A protein members could be detected in both flow cytometry and fluorescent confocal microscopy across different tumour cell lines with elevated surface expression of

these BTN proteins (Fig. 4.5, 4.8, and 4.9). Moreover, this BTN2A1 and BTN3A1 membrane association was attainable not only in established cell lines but also in rodent transfected cells presenting the same human BTN members (Fig. 4.6). Such enforced expression of human proteins in rodent cells remarked the association profile between BTN2A1 and BTN3A molecules was not the only practicable combinatory. Additional fluorescence-labelling BTN-transmembrane proteins intracellularly via genetic engineering supported these conclusions and extended the propensity to form heterodimeric complexes between BTN3A members and BTN2A2, as well as the formation of homodimers in BTN2A1, BTN2A2, or BTN3A1 proteins (Fig. 4.10). Therefore, these insights expand the association capabilities of the human BTN-gene cluster and broaden the framework in which this BTN immunoregulatory cluster of mammalian molecules combine to perform functional roles in the immune system (Di Marco Barros et al., 2016; Melandri et al., 2018; Vantourout et al., 2018).

The substitution of B30.2 domain by an irrelevant PILRβ equivalent in BTN2A1, dramatically decreased the signal of the $\gamma\delta$ TCR-tetramer fluorescent probe in comparison to a wild-type complex or even the stand-alone expression of the BTN2A1 protein. These observations suggested that even though this intracellular domain might not be determinant to form a heterodimeric complex, the BTN2A1 B30.2 intracellular portion could be indeed necessary for maintaining the correct complex morphology necessary to drive a phosphoantigen derived immune response. Hence, the association must retain a cohesive structural position to acquire an affinity for the $\gamma\delta$ TCR in Vγ9Vδ2 T cells. Attempts to modify the complex structure by the addition of phosphoantigens into BTN-transfected rodent cells, cannot alter the detection of FRET by antibody targeting their respective ectodomains nor indirect intracellular fluorophore-tagged protein pairs. These observations apply for both type of endogenous sources like either phosphoantigens induced by zoledronate stimulus or vigorous microbial doses of HMBPP metabolite, the later being the most potent phosphoantigen known to stimulate $\gamma\delta$ T cells (Fig. 1.5, 4.7, and 4.10). However, the association of B30.2 intracellular domains in the BTN complex could be disturbed as a result of treating the cells with specific monoclonal antibodies against the BTN2A1 protein, with most of them achieving a disruption of the FRET detection signal and only a few favouring this potential (Fig. 4.11). Therefore, it is interesting to observe those clones which completely prevented the FRET emission signal correspond to those that abrogate responses to phosphoantigens by $\gamma\delta$ T cells (Fig. 3.13 and Table 3.4). Likewise, the RF13-259 clone favours the physical association between BTN2A1 and BTN3A1 and coincides with its agonist functional agonist activity stimulating about half of the Vγ9Vδ2 T-cell repertoire. However, this was not the case for those other antibody clones of which

have comparable results improving the FRET emission spectra. Therefore suggesting even though some enhanced the complex formation inducing TCR-dependent signals, they required more sophisticated switches.

We questioned whether the intracellular B30.2 domain of BTN2A1 was equally functional and necessary as the phosphoantigen-sensor motif in the BTN3A1 molecule. Consequently, the two B30.2 domains were compared in their affinity to bind two distinct classes of phosphoantigens: the microbial HMBPP and eukaryotic IPP standard representative compounds. The chemical bound between these phosphoantigens and the intracellular B30.2 domain of the BTN3A1 protein was equivalent to previous experimental outcomes (Sandstrom et al., 2014; Yang et al., 2019), and later reported to its non-primate alpaca homolog (Fichtner et al., 2020). Contrary, we were unable to determine a chemical binding interface between the B30.2 motif of BTN2A1 and either phosphoantigen (Fig. 5.7). Under this conclusion, the role of the intracellular B30.2 domain of BTN2A1 seemed not to involve antigen sensing, but denoting its implication in both forming the BTN2A1-BTN3A1 structural complex and strengthening the bond to the Vγ9-domain in the $\gamma\delta$ TCR denoted it must have a crucial, yet hidden functionality (Fig. 4.7).

To further examine which implications the BTN2A1 B30.2 motif represented, expression of mutant BTN2A1 protein models were expressed on the surface of non-human murine cells that lack an integer *BTN*-genomic cluster and compared to an enforced expression of a wild-type BTN2A1 protein and co-expressed BTN3A1 or BTNL3 control protein. Murine cells with truncated BTN2A1 protein right below the transmembrane or juxtamembrane domain had no relevance in altering its association to BTN3A1 protein nor did those mutant cells of which the BTN2A1 intracellular domain was swapped for that of the BTN1A1 (Fig. 4.15). Per contra, a truncated protein below the B30.2 motif or its entire substitution for a PILRβ analogue decreased the FRET detection signal between these BTN2A1 mutants and BTN3A1, implying these alterations hinter the correct association structural complex between BTN2A1 and BTN3A1. Likewise, the same mutations resulted in lowering the complex affinity for the Vγ9Vδ2 TCR, consequently idealising a correlation between disrupting the BTN2A1-BTN3A1 complex module and its binding to a $\gamma\delta$ TCR. According to these observations, the readout phenotypic response from freshly donor-derived V$\delta2^+$ T cells corresponded to expected activation profiles (Fig. 4.16). Though, surprisingly, swapping the intracellular domain for that of its BTN1A1 counterpart favoured $\gamma\delta$ T-cell immune responses. Together, these results signified an essential role for the BTN2A1 B30.2 intracellular domain including its last amino acid sequential ending structure, which despite not being relevant to sense phosphoantigens, this part is indeed func-

tional and necessary to evoke responses by $\gamma\delta$ T cells. Due to the multifunctionality of these SPRY/B30.2 domains and extraordinary affinity for a myriad of molecular ligands (Jeong et al., 2009; Rhodes et al., 2005), it adds complexity to understand the actual significance and function regarding its role in presenting phosphoantigens to $\gamma\delta$ T cells. Some reviews examined its role and noted its exceptional plasticity at the core β sandwich and remark other classical protein-protein interactions with linear motives sharing a substantial core similarity, thus proposed diverse functions including functioning as an adaptor module to assemble macromolecular complexes (Perfetto et al., 2013). Hence, it is plausibly being involved in cross-linking BTN members at the plasma membrane to favour the membrane complex stabilisation providing structural readability to fit onto the recognition binding site of the Vγ9Vδ2 TCR of $\gamma\delta$ T cells.

The contact between the BTN2A1-Vγ9 interplay extends further from the recognition of phosphoantigens. Our data has shown not only the BTN2A1 protein stands for the immune recognition of phosphoantigens, but it can also strengthen the V$\gamma9^{+}$ $\gamma\delta$ T-cell reactivity to lipid-presenting molecules of the CD1 family. The BTN2A1 molecule is likely to create a synergic effect by cooperating with other antigen-presenting molecular transmembrane proteins. In this work we have shown this synergy by co-expressing BTN2A1 together with two CD1 family members independently, in murine antigen-presenting cells, caused an enhanced activation of CD1-reactive Jurkat-reporter cell lines (Fig. 4.17). Accordingly, our data suggested the BTN2A1 contacted the Vγ9-domain and reinforced the recombined Vγ9Vδ1 TCR-signalling stimulatory pathways in $\gamma\delta$ T cells exposed to cis expression of BTN2A1 and CD1c or CD1d glycoproteins on the surface of antigen-presenting cells. This observations manifested the role of BTN2A1 could capture a much broader spectrum than just presentation of phosphoantigens to the most prominent peripheral blood $\gamma\delta$ T-cell Vγ9Vδ2 subset, and contribute in co-stimulatory functions across $\gamma\delta$ T-cell groups that express diverse recombined δ-chains paired with a Vγ9 gene segment.

Chapter 5

How Vγ9Vδ2 T Cells Recognise a Dual-ligand and their Antitumoral Future Perspectives

5.1 Introduction

The vast majority of peripheral blood $\gamma\delta$ T cells in adulthood have a phosphoantigen-reactive Vγ9Vδ2 TCR that protects against pathogenic bacteria and dysregulated cells. Lymphocyte Vγ9Vδ2 T-cells also have a major role in bridging innate and adaptive immunity to direct the fate of some specific immune responses. Upon antigen detection and subsequent activation, these Vγ9Vδ2 T cells usually mature into distinct selected phenotypes. Some of them gain rapid cytotoxic capabilities and secrete cytokines that shape the environmental milieu. Others will express migratory surface markers and initiate homing to lymph nodes, where they prime other immune cellular components to orchestrate a broader generalised immune response (Brandes et al., 2009; Vermijlen et al., 2007). Usually, these cells present two distinctive most common phenotypes adapted at the point they egress the thymus following successful developmental stages. These phenotypic profiles are often documented by their production and secretion of IFN-γ or IL-17A, described as rapid cytotoxic Th1-like activity or pro-inflammatory response, respectively (Dimova et al., 2015).

The $\gamma\delta$TCR is composed of a recombined distinct Vγ and Vδ gene segments with intrinsic characteristics (Allison et al., 2001). The amino acid nature and polar charge content pull their constant regions apart with a pronounced angle between the chains that induces an overall acute torsion. Also, their CDR3δ loop allows multimerisation of several D gene segments forming a much-prolonged loop compared to their $\alpha\beta$ T-cell counterparts. Moreover, there is an increasing evidence $\gamma\delta$ T cells use germline encoding regions, including the HV4 segment to contact to ligand binding molecules (Melandri et al., 2018; Willcox et al., 2019).

This chapter examines the hallmark features that allows the Vγ9Vδ2 TCR to contact the BTN2A1 protein and describes the reactive sites that are important for recog-

nition of phosphoantigens. Furthermore, the relevance of Vγ9Vδ2 T-cell subset in tumour settings, including human-tissue biopsies, is investigated using 3D-organoid cultures. This method facilitates the research of this human $\gamma\delta$ T-cell subset in the tumour microenvironment circumventing the use of animal models. This part is of interest for future work on the Vγ9Vδ2 T-cells and BTN2A1 axis in the field of tumour immunology. Additionally, the clonotype study of phosphoantigen-reactive T cells under different conditions is examined. Sequencing a broad range of phosphoantigen-reactive $\gamma\delta$ T cells could unveil critical Vγ9Vδ2-TCR clones and sequence information that are important for stimulation with phosphoantigens of eukaryotic (Vantourout et al., 2009) or microbial sources (Puan et al., 2007), reactivity to agonist antibodies (Starick et al., 2017), or phosphoantigen-induced stimulus using amino-bisphosphoante drugs (Okuno et al., 2020). This last experiment is presented as an insight to future work expectatives in acquiring single-cell barcoded clonotype and transcriptome data from $\gamma\delta$ T-cell in differently stimulated conditions.

5.2 The Vγ9Vδ2 TCR Recognises a Dual-ligand

The $\gamma\delta$ TCR has an intrinsic binding capacity to recognise dual-ligand molecules by using partly germ-line encoding regions (Melandri et al., 2018). Herein, some nucleotides of the prototype G115 clone were mutated in an alanine screen to infer which amino acids were important to bind to the BTN2/3A1 complex. These mutant $\gamma\delta$TCRs were then expressed in Jurkat-reporter lines to study their effective response to a melanoma cell line challenged with zoledronate.

5.2.1 Vγ9 Germline-regions Have a BTN2A1 Footprint

The G115 has been used in most $\gamma\delta$TCR structural studies to determine the amino acids responsible for conferring phosphoantigen reactivity to $\gamma\delta$ T cells (Sec. 1.4). Alanine residue substitutions were induced by site-directed mutagenesis (Sec. A.6) and resulting vector products transiently transfected into HEK-293T cells for validation of the transfection efficiency (Fig. A.12). Besides, Jurkat-reporter cells were genetically altered and selected for continuous expression of the wild-type G115 TCR or respective mutants. This wild-type G115 was confirmed to bind to in-house BTN2A1 tetramers (Sec. 2.2.1), whereas the control clone, 9C2, expressing a Vγ5Vδ1 TCR, showed no detected reactivity.

Alanine-scanning mutations for arginine (R20A), glutamic acid (E70A), and histidine (H85A) of the γ-chain abrogated binding of BTN2A1-tetramer probes completely (Fig. 5.1 a,c). These amino acids form an electrically charged hotspot that could be

crucial for binding BTN2A1 as observed in the three dimensional space (Fig. 5.2). In the $\gamma\delta$TCR structure model these three amino acids are located at the outer faces of the B, D, and E strands within the Vγ9 side chain of an antiparallel secondary β-sheet folded structure. They lie within a distance of 2.8 Å between E70–H85 and 5.1 Å between H85–R20 and are part of a $\gamma\delta$ TCR germline-encoding region (Fig. 5.3). To a lesser extent, the alanine substitution in glutamic acid (γE22A) impairs binding to the BTN2A1 tetramers, but none of the δ-chain residues arginine (δR51A), lysine (δK108), or leucine (δL97A) substitutions prevented staining with BTN2A1 tetramers (Fig. 5.1 a,c).

5.2.2 Responses to Phosphoantigens Requires a Second Ligand

A Jurkat-reporter leukemic T-cell lymphoblast non-β chain (JRT3-T3.5) cell line expressed the prototype G115 with defined alanine substitutions to construct a pool of TCR alanine-mutants (Sec. A.6.1). This mutants allowed the evaluation of each respective residue in a TCR-dependent manner after these reporter cells were challenged with zoledronate stimulated accessory cells. Jurkat-reporter cells bearing mutated TCR residues at the arginine (δR51) , histidine (δH85), or glutamic acid residues (δE22, δE70) denoted responsible for contacting the BTN2A1 extracellular domain also prevented the immune responsiveness to melanoma antigen-presenting cells when stimulated with zoledronate (Fig. 5.1 b,c). The glutamic acid at position 70, however, was redundant to zoledronate challenge. Arginine residue (δR51A) situated at the δ-chain, in the CDR2δ loop, which did not restrict binding to BTN2A1 tetramer stain, prevented the immune response to zoledronate stimulated melanoma cells. Contrary, the γ-chain lysine to alanine (γK108A) substitution at the CDR3γ that show no effect in the BTN2A1 tetramer stain, halved the number of reporter cells responding to zoledronate stimulus. These two residues (δR51, γK108) seem to constitute a phosphoantigen-reactive site besides the mandatory BTN2A1 footprint. Although these residues belong to distinct chains, only 11 Å separates one from the other, suggesting they could interact on the same subject.

Identical results were observed in a separate experiment were antigen-presenting K562 cell line was challenged with zoledronate stimulus (Fig. 5.4 a). In this experiment, however, a microbial phosphoantigen HMBPP induced subtle responses in responding cells. This could be related to lower levels of BTN3A members on the K562 cell surface, previously detected in (Fig. B.2, Sec. 3.2). Nonetheless, once data is normalised to the maximum expected reactivity to the wild-type TCR-G115, the Jurkat-reporter cell response to zoledronate or HMBPP stimulated K562 cells in a

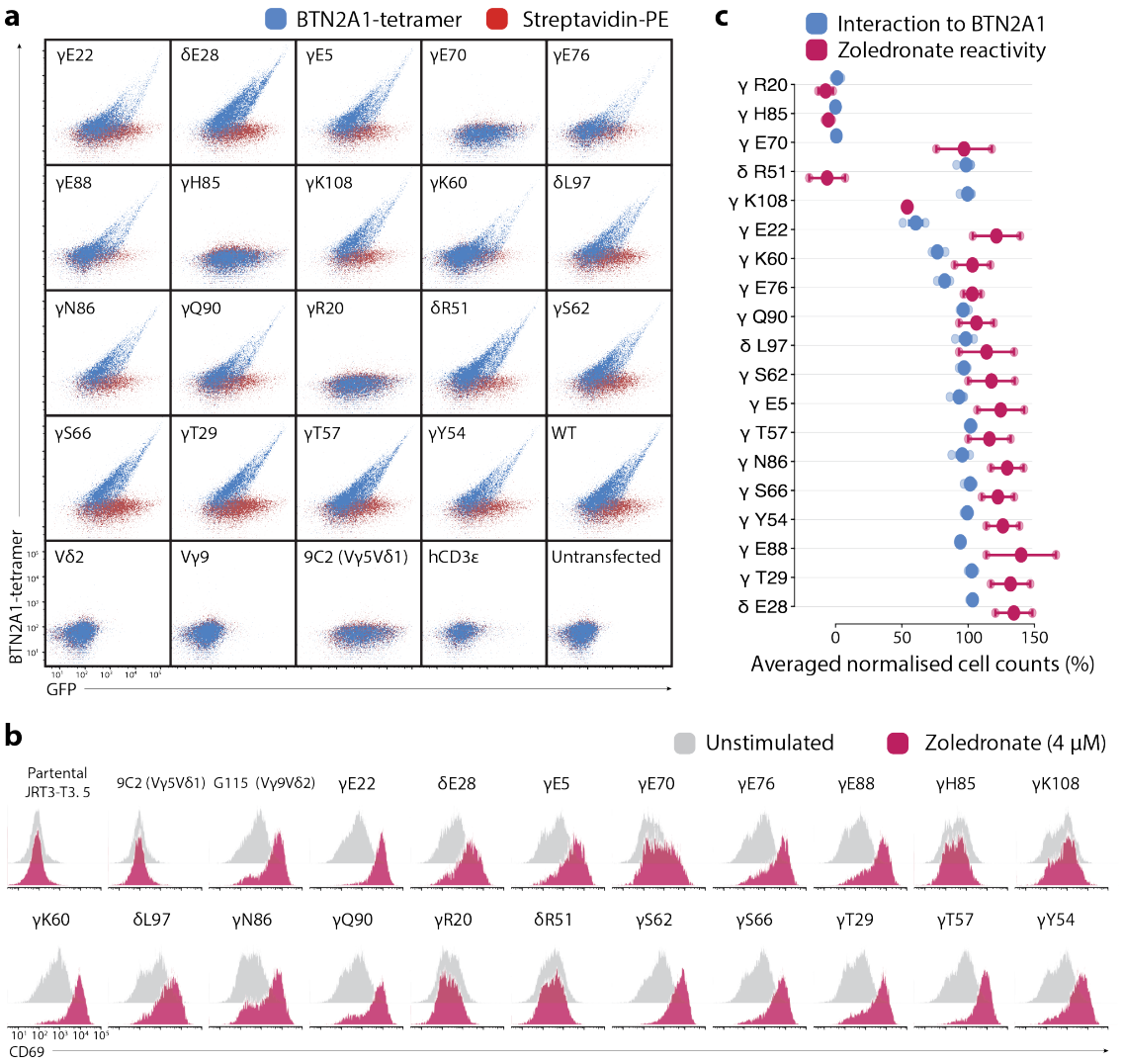

Figure 5.1: *Mutagenic alanine scanning in G115 identifies residues in the Vγ9 domain that abrogate BTN2A1 tetramer stain and another at the Vδ2 domain residues that impair reactivity to LM-MEL75 cells stimulated with 4* μM *zoledronate. (a) Transfected HEK-293T with G115 alanine mutants stained with 5* μg ml^{-1} *BTN2A1 tetramer (blue) overlapped to streptavidin-PE control (red) and versus GFP to assess expression efficiency. Showing one of three experiments. (b) Histograms depict the G115 mutant G115 transfected on JRT3-T3.5 reporter cell line to evaluate responsiveness (CD69) after an overnight coculture with unstimulated (grey) or stimulated with zoledronate (magenta) LM-MEL-75 cells. Showing one of two experiments. (c) Normalised data ($\frac{X_i - X_{9C2}}{X_{G115} - X_{9C2}}$) and averaged between respective experiments, comparing the TCR-binding capacity to BTN2A1 tetramer (blue, $n = 3$) with the G115 response to zoledronate stimulus in* b *(magenta, $n = 2$). Standard error bars.*

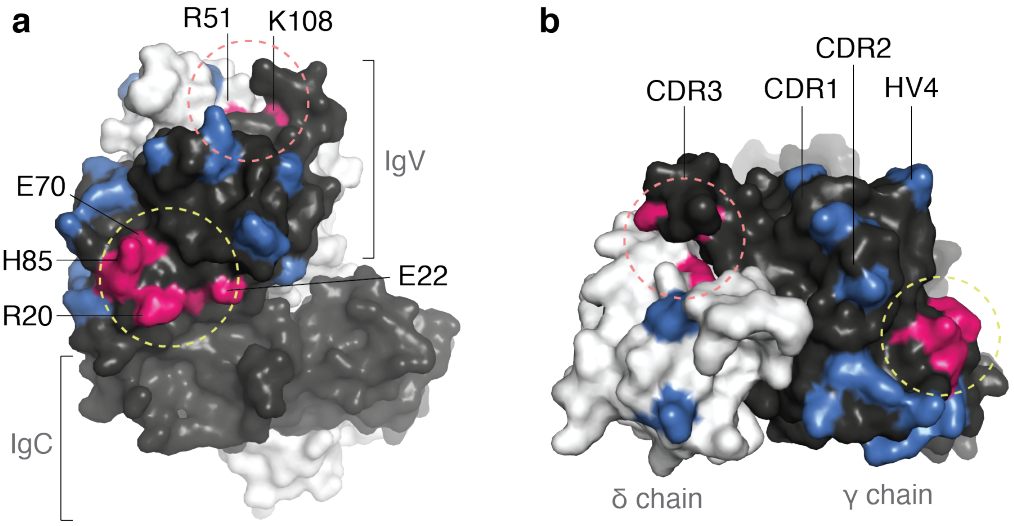

Figure 5.2: *The BTN2A1 footprint reactive sites (yellow circle) of the Vγ9 domain and opposed residues implicated in phosphoantigen response (pink circle) in a G115 molecular model. Residues essential for $\gamma\delta$ T-cell responses are labelled and highlighted in hot-pink, whereas redundant alanine-substituted residues are shown in blue; δ chain in withe and γ chain in black. PyMOL entry 1HXM.*

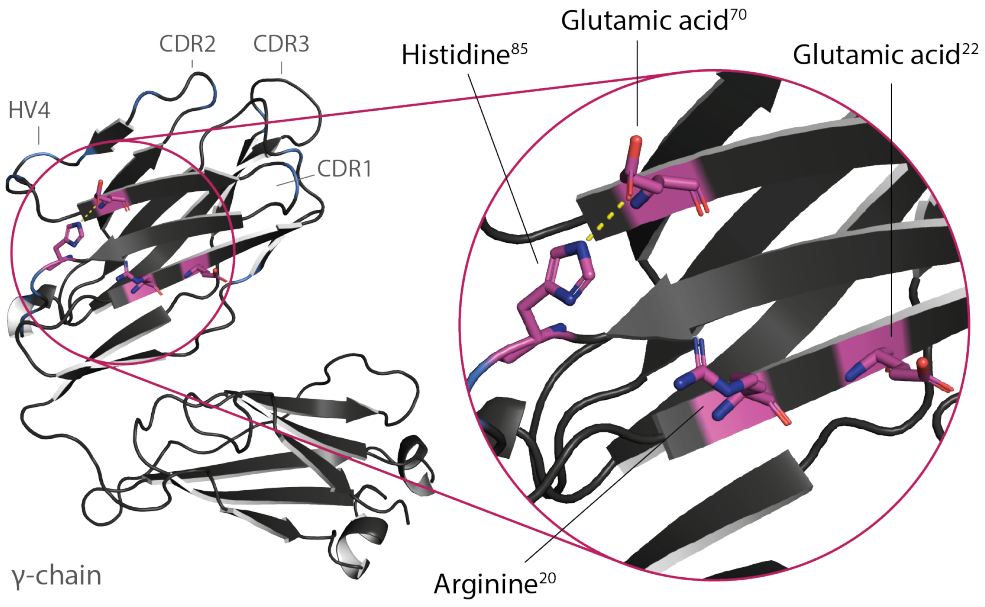

Figure 5.3: *Cartoon molecular representation of BTN2A1 footprint at the γ-chain Vγ9Vδ2 TCR-G115 highlighting the supposed residues implicated in the direct weak-chemical bond interaction with BTN2A1 extracellular variable domain. PyMOL entry 1HXM.*

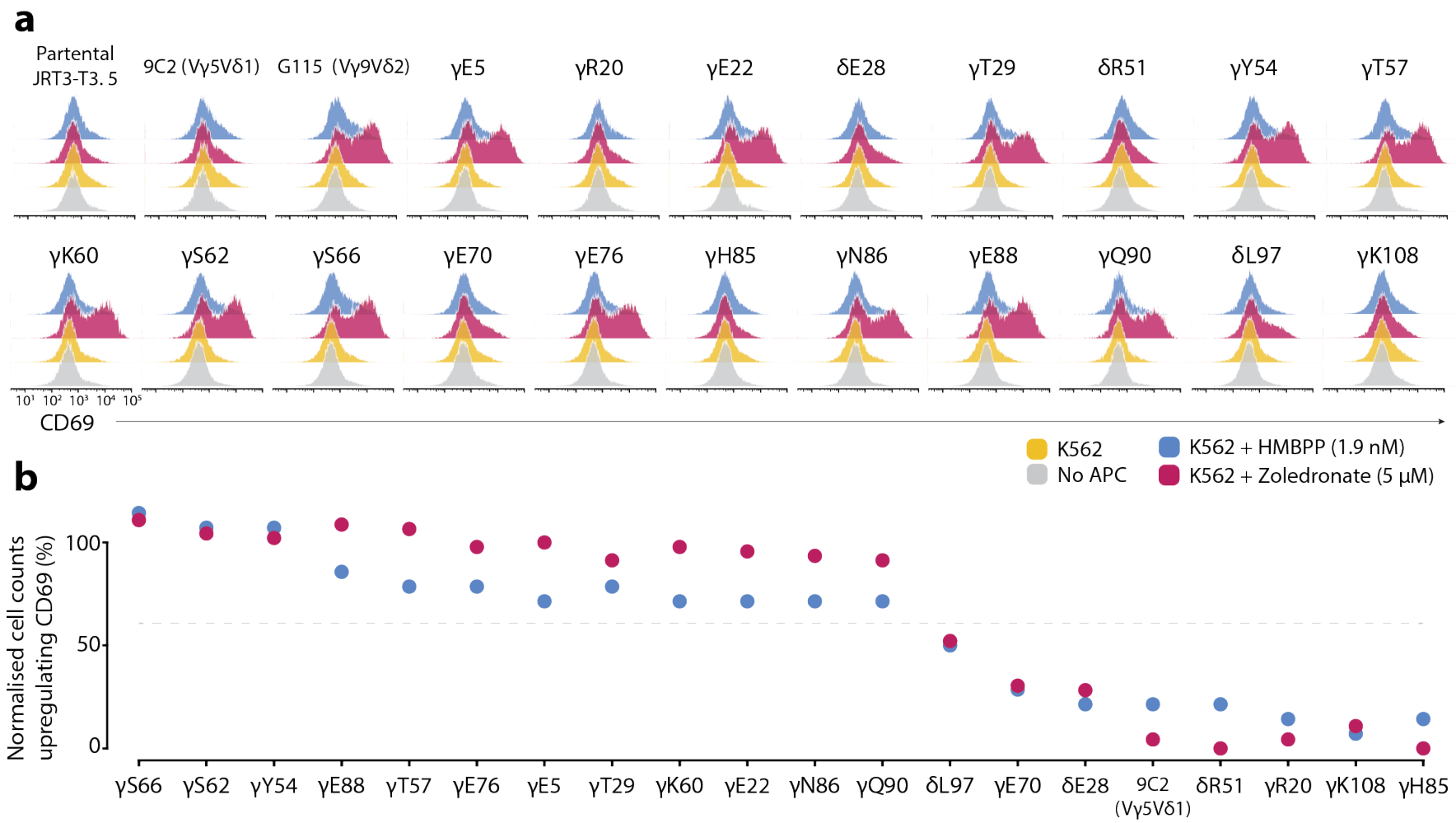

Figure 5.4: *Alanine G115 mutants transfected on JRT3-T3.5 cells impair reactivity to K562 cells. (a) Histograms depict activation marker CD69 on JRT3-T3.5 cells after an overnight coculture with K562 cells stimulated with zoledronate or HMBPP. (b) Normalised data* ($\frac{X_i - X_{Parental}}{X_{G115} - X_{Parental}}$) *for zoledronate or HMBPP stimulated cells.*

similar pattern observed for the LM-MEL-75 cell line (Fig. 5.1 b,c and 5.4 b).

5.2.3 Agonist 20.1 Activity Depends on BTN2A1

Treatment of antigen-presenting cells with the agonist 20.1 antibody against BTN3A members activates Vγ9Vδ2 T cells via their TCR-signal transduction, and irrespective of phosphoantigens (Harly et al., 2012). Given the possibility that BTN3A molecules form a complex together with BTN2A1 protein, this direct agonist activity was tested on the *BTN2A1*-knockout melanoma cell line. These results showed the lack of BTN2A1 at the surface membrane impaired the 20.1 induced response. Therefore, the agonist activity of 20.1 depends not only in BTN3A members but also requires the presence of the BTN2A1 protein at the surface plasma membrane (Fig. 5.5).

Jurkat-reporter cells transfected with either wild-type G115 or alanine mutants that prevented phosphoantigen-induced responses were cocultured with melanoma antigen-presenting cells treated with agonist 20.1 or respective isotype control. Reporter cells expressing the wild-type G115 responded in a TCR-dependent manner to melanoma cells treated with this agonist antibody, whereas they evoked no response to isotype or *BTN2A1*-knockout control cells. Using this alanine scanning method, arginine (R20A) and histidine (H85A) residues, constitutes of the γ-chain BTN2A1 electrically charged fingerprint, totally abrogated the agonist activity of the 20.1 antibody. The complementary glutamic acid (E70A) had similar effectiveness, even though a few responding cells upregulated the CD69 activation marker in response to this stimulation. Interestingly, δ-chain arginine (δR51A) and γ-chain lysine (γK108A) alanine substitutions also obstructed the function of the agonist 20.1 antibody. Note, these two residues are located distal to the γ-chain BTN2A1 footprint described above. The arginine abrogated the antibody activity entirely, and the lysine achieved a drastic decrease in the activation of Jurkat-reporter cells, suggesting these residues influence on the interaction between the agonist antibody's function and related targeted proteins of the BTN3A family. Supporting this, data presented above show these two amino acids had no apparent relation to interact with BTN2A1 extracellular domain, but they were responsible for conveying responses under an abrupt accumulation of phosphoantigens in antigen-presenting cells. Now, also constitutes an essential part that mediates 20.1 antibody's agonist activity. Together, these results depict a dual-ligand function for the Vγ9Vδ2 TCR-G115 prototype and indicate the Vγ9 domain of the $\gamma\delta$ TCR host the BTN2A1 contact, whereas in the crown area at the $\gamma\delta$TCR head and towards the Vδ2 domain is a second location responsible for sensing, plausibly, progressive changes arising from phosphoantigen activity on

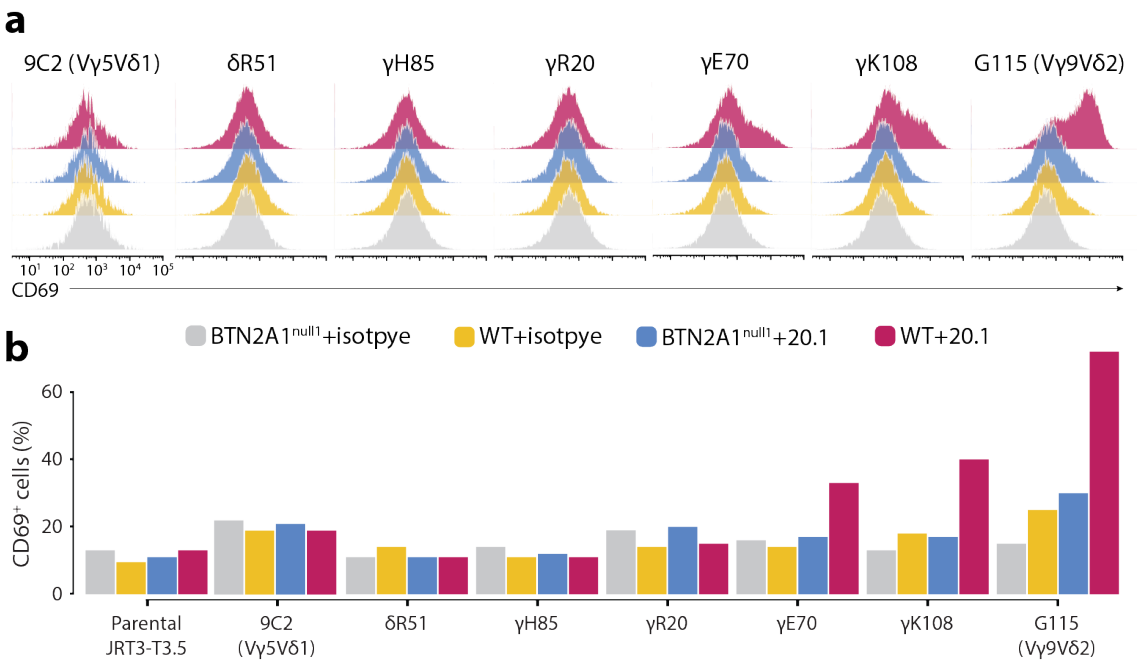

Figure 5.5: *Antibody clone 20.1 agonist activity depends on BTN2A1. (a) Fluorescence intensity for the activation marker CD69 in a Jurkat-reporter cell line transfected with TCR clone 9C2 (Vγ5Vδ2) or G115 (Vγ9Vδ2) and its respective alanine selected mutations after an overnight coculture with treated melanoma LM-MEL-75 or its* BTN2A1^{null1} *knockout cell line with 20.1 antibody or isotype control IgG1κ. (b) Percentage of Jurkat-reporter cells expressing CD69 above levels from a defined gate based on the parental Jurkat cell line.*

BTN3A family members.

5.3 Varying Strengths of $\gamma\delta$ T-cell Responses

Phosphoantigen-reactive $\gamma\delta$ T cells responded differently depending on the nature of phosphoantigen used and antigen-presenting cell line. Whereas some cell lines were more susceptible to $\gamma\delta$ T cells, others, like the K562 cells, required a more potent stimulus to induce a response (Fig. 5.8). This fact is similar to previous studies in which K562 cells require doses above the 100 µM (Idrees et al., 2013; Nguyen et al., 2017). Inducing $\gamma\delta$ T-cell activation against K562 cells required doses above the 50 µM (Fig. 5.8), similar to Idrees et al. (2013). $\gamma\delta$ T-cell responses to another cell line, C1R, were barely noticeable regardless the stimulus induced (Fig. 5.8). Cell lines that induce clear activation of $\gamma\delta$ T cells were of the melanoma type, especially the LM-MEL-75 line. Notably, both melanoma LM-MEL-62 and LM-MEL-75 cell lines expressed similar levels of BTN2A1 and BTN3A proteins (Sec. 3.2).

Assessing the immune response to microbial HMBPP is a challenge due to the ability of $\gamma\delta$ T cell to self-present this soluble antigen. Presumably, $\gamma\delta$ T cells may

internalise this phosphoantigen before it binds to BTN3A1 and cause activation in association with the expression of BTN2A1 on the cell membrane (Sec. 3.5.3 and Sec. A.7). Comparison of the $\gamma\delta$ T cell response to either HMBPP, IPP, or zoledronate stimulus by themselves, or included in cocultures with tumour antigen-presenting cells, showed the presence of antigen-presenting cells enhanced the immune response. Titrating these phosphoantigen species in polyclonal $\gamma\delta$ T cells showed responses were not only observed for the Vγ9Vδ2 T cell subset, which suggest non-Vγ9Vδ2 cell response could result from by-standing activation and secreted cytokines by Vγ9Vδ2 T cells. The Jurkat-reporter cell line with constitutive expression of a Vγ9Vδ2-TCR or control Vγ5Vδ1-TCR indicated responses to phosphoantigens were limited to the Vγ9Vδ2 TCR, and that these lymphocyte-reporter cells required an increased dose of either phosphoantigen to induce CD69 expression when these receptors were expressed on Jurkat cells other than donor-derived lymphocytes.

Strikingly, K562 leukaemia cell and both melanoma cell types LM-MEL-62 and LM-MEL-75 presented endogenous phosphoantigens that derived from zoledronate stimulus to the Jurkat-reporter cell line at lower doses than those required with microbial HMBPP (Fig. 5.8). However, when the test was performed in coculture with donor-purified total $\gamma\delta$ T cells, the HMBPP response prevailed over the zoledronate stimulus at equal doses —these conditions were comparable as phosphoantigen dilutions were matched. These findings may indicate the HMBPP was easily presented by $\gamma\delta$ T cells themselves and potentially melanoma tumour cell lines incorporated more efficiently zoledronate than lymphocytes.

An in-depth assessment of a Jurkat-reporter line expressing the Vγ9Vδ2 G115 receptor to two phosphoantigen-stimulated wild-type melanoma cell lines or their respective *BTN2A1*-knockout subclones showed responses were dependent on surface co-expression of BTN2A1 and BTN3A1 proteins, while the Jurkat-reporter Vγ5Vδ1 9C2 control did not (Fig. 5.6). Absence of either BTN molecule prevented Jurkat G115 clones to respond. The doses of phosphoantigen tested were selected based on a previous titration assay (Fig. 5.8).

The intracellular domain of BTN molecules possesses a polar contact that interacts to phosphorylated antigens (Sandstrom et al., 2014). However, this chemical bond may vary according to the composition of each substance. Using an ITC assay, the capacity of HMBPP to interact with the BTN3A1 B30.2 intracellular domain with an affinity of 1.64 µM was demonstrated, which is close to that reported by Sandstrom et al. (2014). In contrast, soluble eukaryotic IPP metabolite had a weaker binding affinity of 813 µM to the BTN3A1 B30.2 intracellular motif, also noted by Sandstrom et al. (2014). Neither of these two phosphoantigen compounds was found to contact

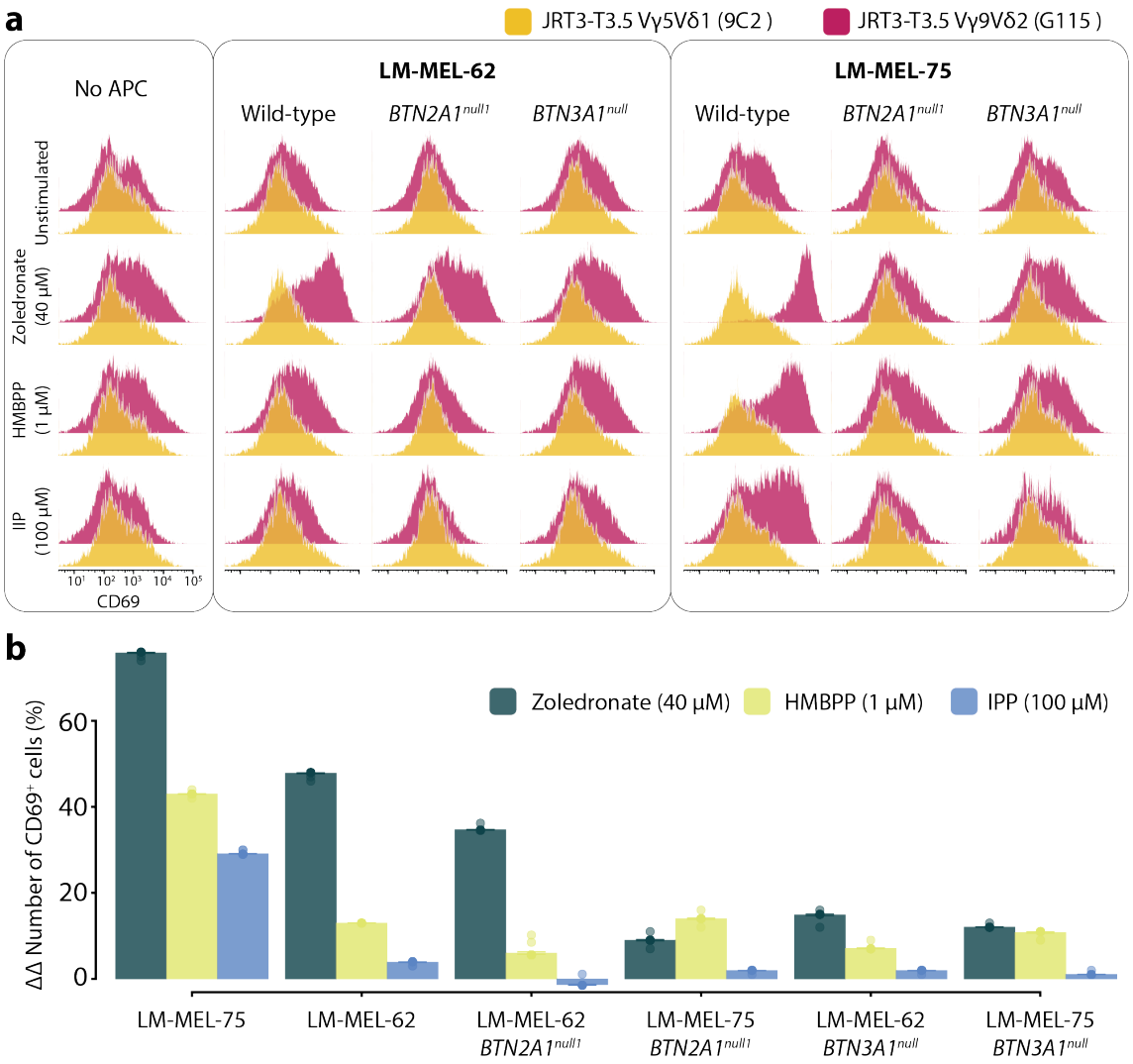

Figure 5.6: *Jurkat-reporter JRT3-T3.5 cells transfected with either Vγ9Vδ2 (clone G115) or Vγ5Vδ1-TCR (clone 9C2) were assessed for their response to LM-MEL-62 or LM-MEL-75 and respective* BTN*-knockout lines, each stimulated with zoledronate, HMBPP, or IPP, compounds. The γδ TCR-dependent signal was determined from their (a) levels of CD69 T-cell activation marker or (b) the increment in the number of cells that upregulate CD69 from the unstimulated and 9C2 transfectant controls. Data collected from four experiments.*

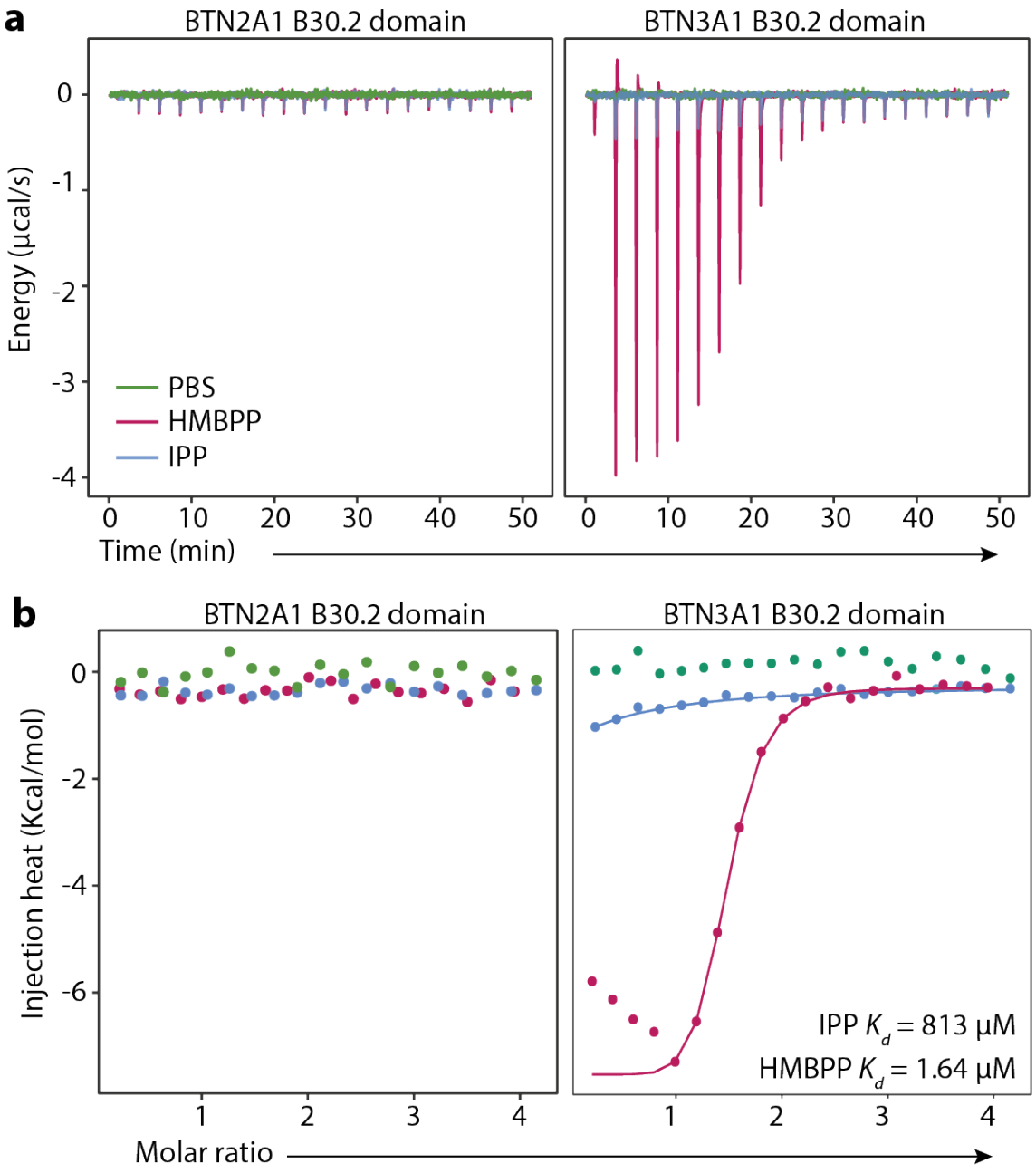

Figure 5.7: *ITC determines HMBPP and IPP interact to the B30.2 intracellular domain of BTN3A1 but not to that of BTN2A1. (a) Raw data trace after serial injections of soluble HMBPP (1.9* mM*, magenta), IPP (2* mM*, blue), and PBS buffer control (green) to soluble B30.2 intracellular domain of respective BTN molecules (100* µM*). (b) Heat realised from binding isotherms and respective K_D calculated after computing a Chi-squared fitting model with $>$200 iterations. Showing one of two experiments.*

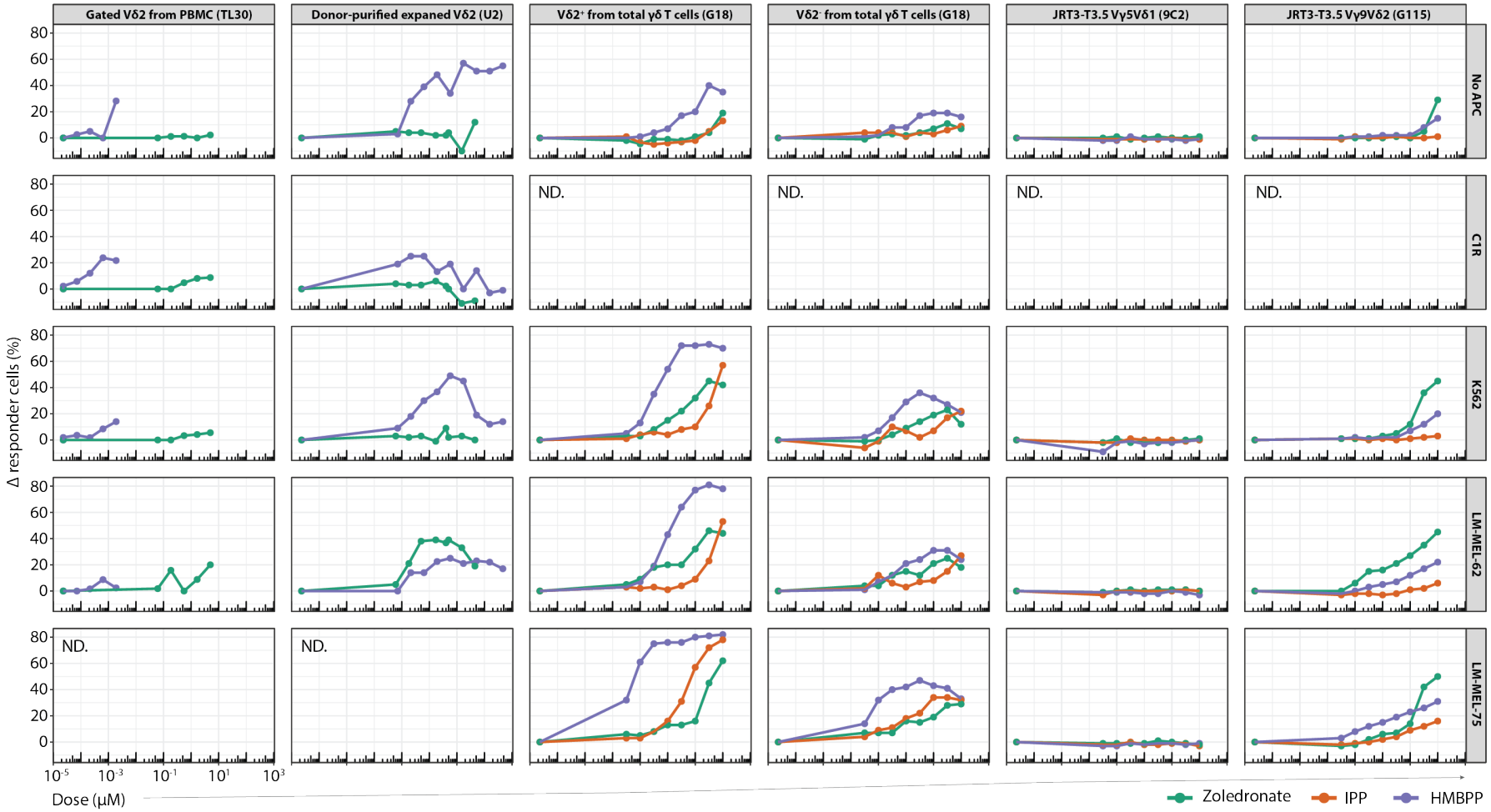

Figure 5.8: *Titration response to microbial HMBPP or eukaryotic IPP phosphoantigens or zoledronate stimulus in whole PBMC, donor-purified expanded Vδ2$^+$ T cells, Vδ2$^+$ or Vδ2$^-$ T cells gated from purified total $\gamma\delta$ T cells, and lymphocyte-reporter JRT3-T3.5 cell line expressing either a Vγ9Vδ2 or Vγ5Vδ1-TCR. The response show the difference in the total number of cells upregulating the activation marker CD25 for $\gamma\delta$ T cells or CD69 for Jurkat-reporter cells between stimulated and normal conditions. One experiment each test.*

with the B30.2 intracellular domain of BTN2A1 (Fig. 5.7).

5.4 Antitumour Vγ9Vδ2 T-cell Responses

The $\gamma\delta$ T-cell subset expressing the Vγ9Vδ2-TCR reacts to phosphoantigen stimulated cells by recognising a prevalent BTN2A1-BTN3A1 complex at the surface membrane of antigen-presenting cells. These immune cell type typically responds in a TCR-dependent manner of which after activation internalises its antigen-specific receptors, up-regulates activation markers such as CD69 or CD25, and preferentially secrete IFN-γ and TNF-α. Here, the capacity of this subset of $\gamma\delta$ T cells to elicit cytotoxicity towards two different tumour cell lines under the presence of zoledronate drug was evaluated. These results demonstrate an explicit cytolytic activity towards the melanoma cell line LM-MEL-75 but, discouraged effectiveness when they cope with the K562 cell line (Fig. 5.9). None of the different drug-dose tests up to 100 µM affected the response from the lymphocytes to the target K562 cells. Contrary, the melanoma LM-MEL-75 cell type was rapidly lysed from the second day at doses as little as 1 µM zoledronate stimulus in a one-to-one cell ratio. Increasing the number of lymphocytes per targeted cancer cell had a minimum effect after one day, and no distinguished response was observed on the second day. Moreover, the absence of either BTN2A1 or BTN3A1 on melanoma tumour cells completely prevented the cytolytic response from Vγ9Vδ2-TCR expressing cells and maintained a continuous growth similar to the K562 cell line.

5.5 The $\gamma\delta$ T cells in the Tumour Microenvironment

In the cancer context, progression of rapidly growing tumour cells is linked to a reduced number of infiltrating $\gamma\delta$ T cells within the tumour site, while the abundance of infiltrated $\gamma\delta$ T cells associates to a favourable prognostic (Gentles et al., 2015). Likewise, there are studies showing that the number of Vγ9Vδ2 T cells correlate with lower mortality and relapse rates (Toia et al., 2016). Still, different tumour cell lines may show variablity in their susceptibility to amino-bisphosphonate drug treatments with leukaemia and mammary carcinoma cell lines having low receptiveness among others. However, several renal carcinoma cell lines such as renal cell adenocarcinoma (ACHN) or hypertriploid renal cell carcinoma (786-O) require low concentrations of zoledronate to potentiate antitumoural effector functions by $\gamma\delta$ T cells (Idrees et al., 2013). Thus, phosphoantigen-reactive $\gamma\delta$ T cell responses are consistent with previous studies in which proved the role of donor-expanded phosphoantigen-reactive $\gamma\delta$ T

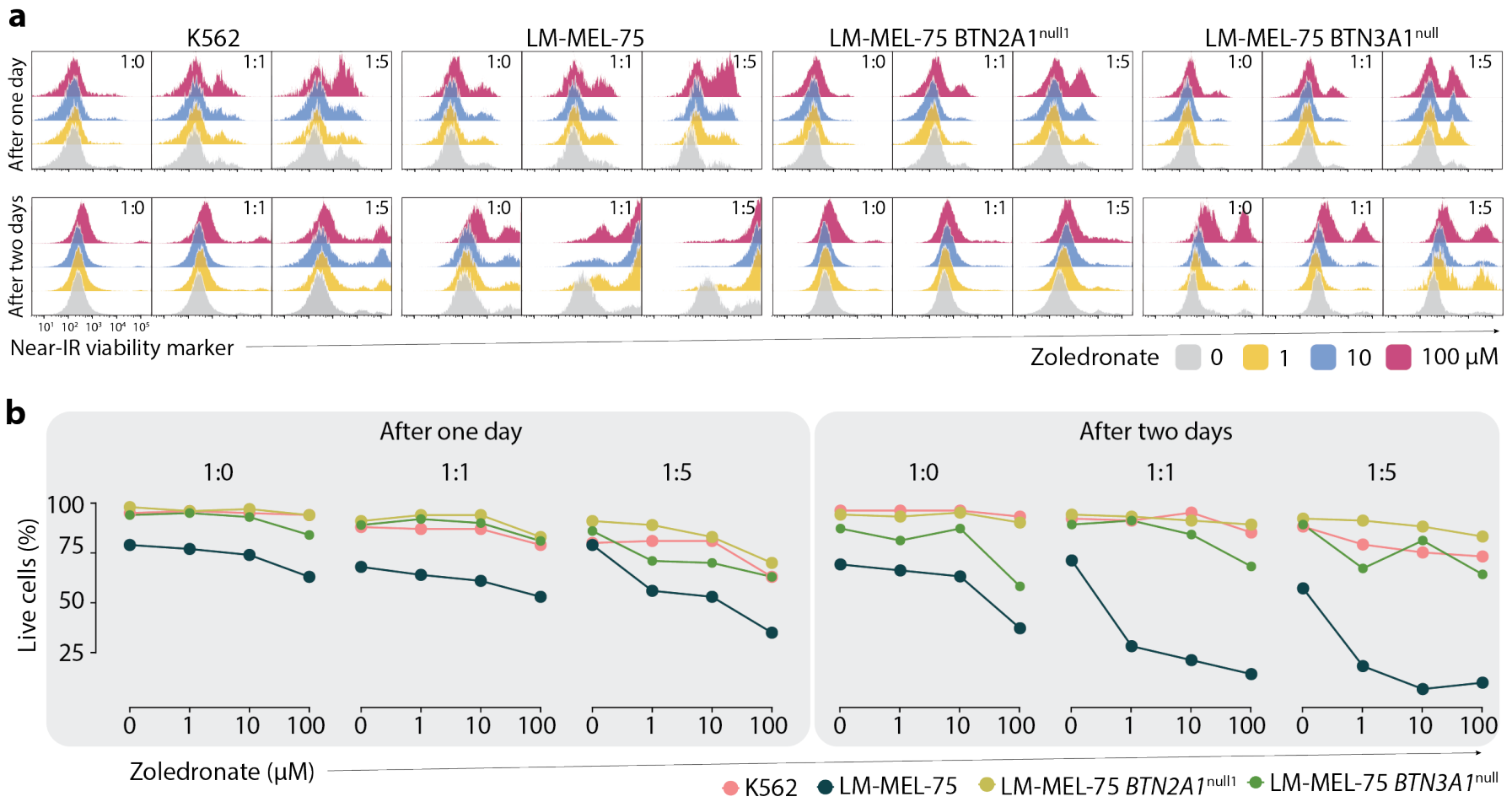

Figure 5.9: *Cytolytic activity of Vγ9Vδ2 T cells to melanoma LM-MEL-75 tumour cell line. (a) Histograms depict the fluorescence intensity of near-infrared viability dye on tumour cell lines pre-labelled with cell-trace violet and gated for this dye. (b) Summary representing the percentage of living tumour cells following one or two days post-coculture of these tumour cells together with purified total γδ T-cells from a random donor and added respective doses of zoledronate. The ratio shows the number of cells cultured in the same test well regarding the target tumour cells versus lymphocyte responders (target:responder).*

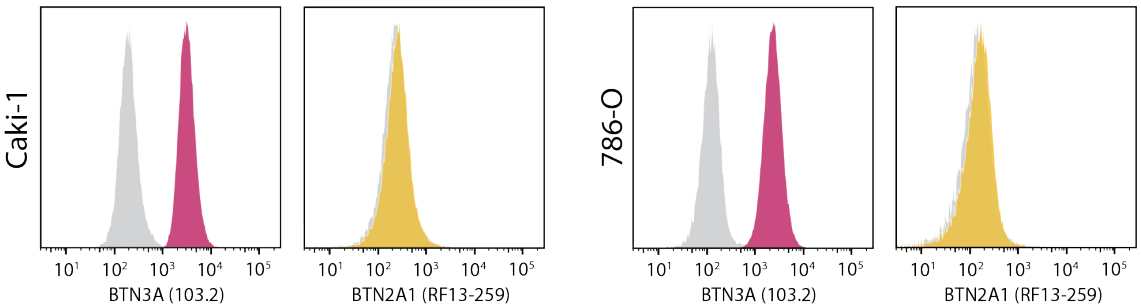

Figure 5.10: *Expression of BTN3A (clone 103.2) or BTN2A1 (clone RF13-259) family members in adenocarcinoma (786-O) and clear cell renal carcinoma (Caki-1) cell lines. One experiment.*

cells in lysing renal cell carcinoma resistant to conventional treatments, while healthy tissue renal cells are untouched (Viey et al., 2005).

This part of the study was performed in collaboration with the University of Bonn, department of Experimental Immunology together with the Institute of Clinical Chemistry and Clinical Pharmacology group lead by Michael Hölzel and the Pathology group of the Universität Klinikum Bonn lead by Marieta Toma to adapt a general patient-derived organoid model for ALI cultures proposed by Neal et al. (2018). This novel culture technique consolidates a renal tumour 3D-organoid tissue growth on in-vitro culture plates. The experimental setup allows to investigate the prevalence of phosphoantigen-reactive $\gamma\delta$ T cells infiltrated, and the proportion of the Vγ9Vδ2 T-cell subgroup, within the microtumoural environment of human kidney carcinogenic tissue.

5.5.1 Detection of BTN2A1 and BTN3A in Renal Carcinoma Cells

The kidney cancer cells seemed to be direct targets by Vγ9Vδ2 T cells, seeing their favourable clinical trial prognostic in renal tumour tissue (Toia et al., 2016) and that a low-dose zoledronate drug is enough to promote $\gamma\delta$ T cell responses to renal-origin cell lines (Idrees et al., 2013). Hence, we initially tested two of the most common renal established cell lines adenocarcinoma 786-O and clear cell renal carcinoma clear renal cell carcinoma (Caki-1) cell lines for the expression of BTN3A and BTN2A1 members. Both cell lines showed surface expression for members of the BTN3A family, but not BTN2A1 (Fig. 5.10). Interestingly, the expression pattern and amount of protein present at the surface of adenocarcinoma and clear cell renal carcinoma cell lines was equivalent. The two cell lines expressed either or all BTN3A members as per detection with clone 103.2 antibody while surface BTN2A1 was not present or detected with antibody clone RF13-259.

5.5.2 Consolidation of Air-liquid Interface Organoid Cultures

The cellular component in the tumour microenvironments is heterogeneous and incorporates many immune cell types that can infiltrate. Simulating a human $\gamma\delta$ T-cell phosphoantigen-reactive system in a non-primate mouse model becomes very difficult due to the evolutionary dissimilarities between these species, of which the axis between the Vγ9Vδ2 TCR and the BTN cluster that evolved in primates is absent in rodent species (Adams et al., 2015). Consequently, the establishment of ALI PDO cultures retain the heterogeneity and an accurate immune spectrum of the microtumoral environment in human tissue (Neal et al., 2018). These organoids facilitate in-vitro studies of phosphoantigen-reactive $\gamma\delta$ T cells within the cancer context and under laboratory conditions. PDOs grow from primary cancer cells in a method that preserves the complex histological tumour microenvironment architecture with tumour parenchyma and stroma, including embedded functional infiltrating T-cell lymphocytes. In addition, this organoid culture system substitutes dealing with non-human animal models and preserve the heterogenic cellular signature of the tumour and tumour-specific immune cells alike in a simple in-vitro ALI-organoid culture. For all the reasons mentioned above, this work reproduced a step-wise procedure for the establishment of ALI-PDO cell cultures from fresh human-surgical tumour-biopsy kidney samples in the laboratory based on previous reported protocols (Neal et al., 2018).

Fresh patient samples were received form the pathology department and immediately dissociated for culture in a collagen matrix (Fig. 5.11). These samples varied in sizes and the number of tumour organoids grew in a 3D-conformation embedded in the collagen matrix. Single-cell suspensions did not proliferate, although they remained in the culture matrix forming a single layer of resting cells. Clusters of organoids proliferated in the same proportion and every fortnight required harvesting and passaging onto a new collagen matrix to prevent cell asphyxiation. On average six to twelve six-well plates could be cultured from a single patient (Fig. 5.12).

5.5.3 Infiltrated $\gamma\delta$ T-cells in the Tumour Microenvironment

Human-surgical biopsy samples from clear cell renal carcinoma tissues acquired from the University Klinikum of Bonn (Germany) represented a random selection from samples within the German population. Preparation of ALI-organoid plates was made by mixing inserts to a collagen gel matrix in trans-well plates with concentrated sterile culture medium containing supplements and transcription factors that sustained the growth of the different cellular types composing the tumour-microenvironment. This collagen matrix contributed to maintain a 3D-structure in which cancerous cells

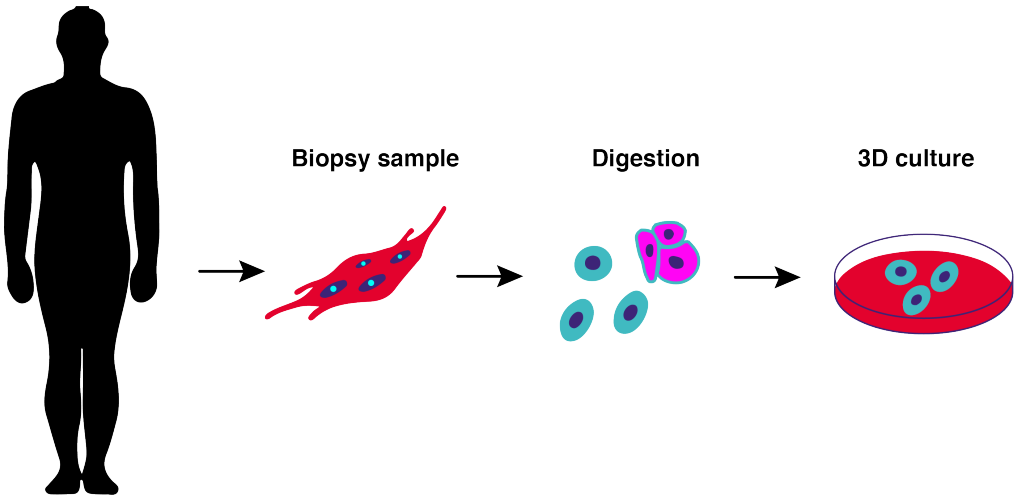

Figure 5.11: *Schematic representation for preparation of PDO-ALI cultures.*

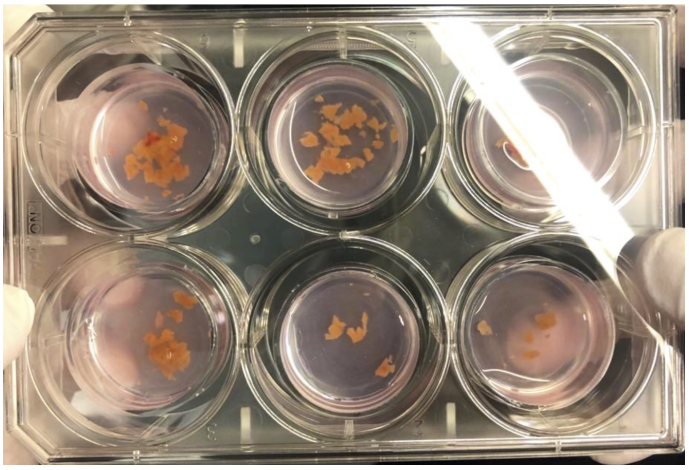

Figure 5.12: *Visual look of carcinogenic 3D-organoid samples in six-well culture plates.*

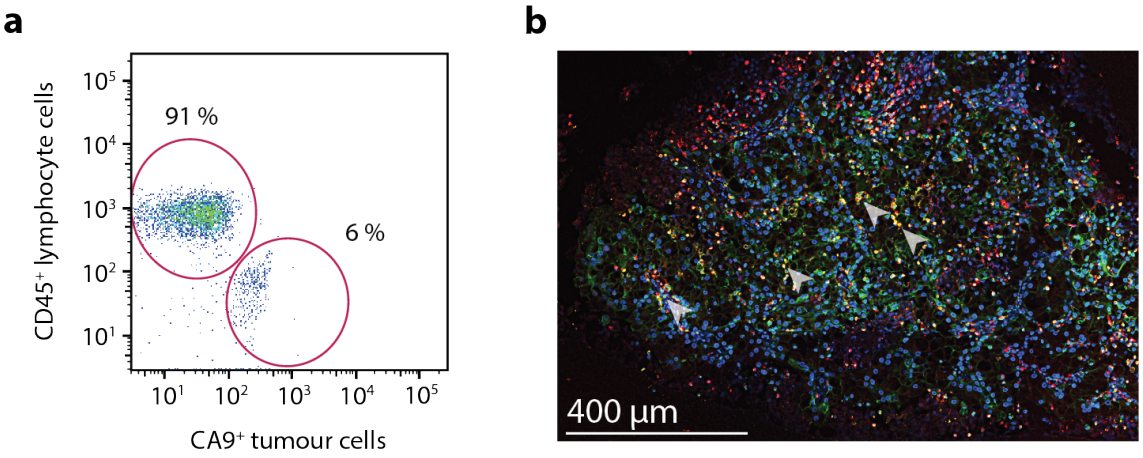

Figure 5.13: *Expression of CD45 cell marker intended for detection of lymphocyte immune cells in (a) flow cytometry (one of three experiments) and (b) microscopy imaging a sample of clear-cell renal carcinogenic cells (one experiment). For flow cytometry cells were dissociated from ALI-PDO samples and filtered through a 40* µm *strain. Microscope samples were formalin-fixed paraffin-embedded, sliced, and adhered onto a glycine-coated glass slides. Colour code for the right microscopy image is cytotoxic $CD8^+$ T-cell (red), degranulation $CD107a^+$ cells (pink), and $CD45^+$ lymphocytes (yellow). Arrows indicate sites with $CD45^+$ lymphocytes.*

grew in form of organoid, developing structures that are comparable to in vivo renal tissue (Neal et al., 2018). After these organoids were recovered and dissociated, isolated cells were phenotyped in flow cytometry analysis to determine whether they contained infiltrated $\gamma\delta$ T cells. These cells were labelled with fluorescent antibodies and most recovered cells were identified with expression of a lymphocyte transmembrane protein marker CD45, an essential regulator of T-cell or B-cell functions involved in the regulation of signal transduction (Fig. 5.13). After organoid processing and dissociation, tumour cells were not detected in flow cytometry analysis. Nonetheless, they were obvious in sliced formalin-fixed paraffin-embedded samples stained with a general panel of antibodies to characterise phenotypically the tumour heterogeneity. Cancerous cells were targeted with an antibody against the carbonic anhydrase IX (CA9) transmembrane protein, which is a marker for a wide variety of tumour types, especially in clear cell renal cell carcinoma (Stillebroer et al., 2010). Hence, this suggests dissociated organoid samples for flow cytometry segregates the population of $CD45^+$ lymphocytes from degrading tumour cells, while formalin-fixed paraffin-embedded samples on glycin-coated slides maintains the heterogenic population these tumour cells, as well as the immune scenario (Fig. 5.13).

Tumour infiltrated $CD45^+$ lymphocytes, were also labeled with specific commercial antibodies against $V\delta1^+$ or $V\delta2^+$ TCR-chains to separate and deduce the percentages of these two classes of $\gamma\delta$ T cells within the tumour. The proportion of these $\gamma\delta$

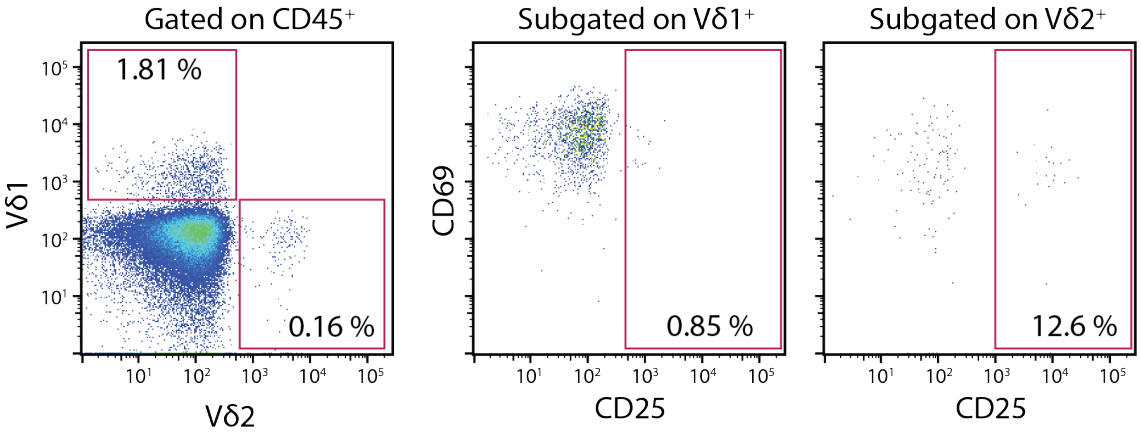

Figure 5.14: *Tumour infiltrating $\gamma\delta$ T-cells in processed renal carcinoma organoids account for 2 % of total CD45$^+$ lymphocytes. Subsequent segregation of these infiltrated $\gamma\delta$ T cells into Vδ1$^+$ or Vδ2$^+$ T cells show both expressed elevated levels of CD69 activation marker, and a small fraction of the later were presenting upregulated levels of CD25 activation marker. One experiment.*

T-cell populations in the tumour was low in comparison to the total lymphocytes. The Vδ1$^+$ T-cell subset represented about 1.8 % whereas the Vδ2$^+$ T-cells were below 1 % of the total CD45$^+$ lymphocytes (Fig. 5.14). Additionally, both linages expressed elevated levels of CD69, which is implicated in T-cell activation and sometimes known to retain lymphocytes in lymphoid organs (Shiow et al., 2006). Moreover, around one-tenth of Vδ2$^+$ T cells were expressing high levels of activation marker CD25.

5.6 Clonotype Sequencing Paired with Single-cell Transcriptome

The era of single-cell sequencing is advancing towards rapid, efficient and straightforward technologies that analyse thousands of individual cells with ease. Cell separation technologies are diverging to novel methods among those recently develop are drop-based and nano-well array separation protocols (Gierahn et al., 2017; Macosko et al., 2015). In this study, we proposed a planing protocol to determine the clonotypic profile of $\gamma\delta$ T cells in the German population that reacts to phosphorylated antigens, and link this data to their respective transcriptome. The merge of both datasets should lead not only to determine the principal characteristics of the $\gamma\delta$TCR topography and conserved reactivity sites, but it would also reveal a broad $\gamma\delta$ T-cell profile after activation via respective stimuli. That transcriptome information can become crucial data to understand the real value and diversification of the $\gamma\delta$ T-cell population to not only determine the cytotoxic activity profile but the expression of chemokines and cytokine secretion signals they produce and utilise to elaborate for triggering a broader immune

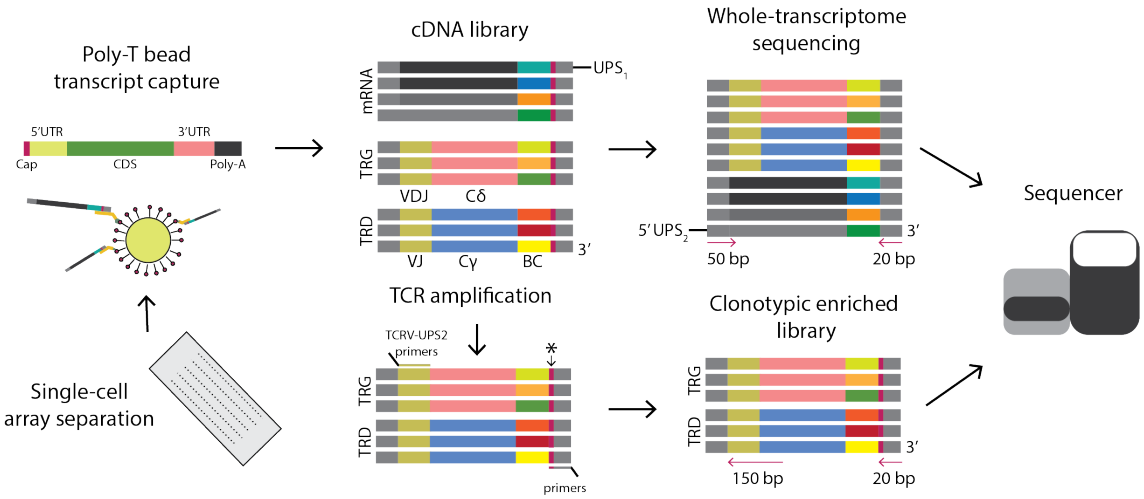

Figure 5.15: *Schematic clonotype paired transcriptome sequencing procedure diverged from Tu et al. (2019) by the use of two base pairs at the first universal primer site (UPS)1 that allow direct and selected enrichment of TRVD/G transcripts without the need to pull them down with constant oligo biotin-streptavidin beads.*

response.

Here we isolate the $\gamma\delta$ T-cell population from PBMC and prepare readily high-throughput cDNA libraries for massive parallel single-cell RNA sequencing akin to Gierahn et al. (2017). The use of *Seq-well* subnanoliter array slide methodology allows separation of individual single-cell barcoded transcriptomes prepared for subsequent sequence modification steps. During subsequent amplification of the cDNA library, we opt to include a pair of determining nucleotides between the single-cell barcode and template switch oligo (TSO)-primer sequence that tags TCR-transcripts of the amplified whole-transcriptome library. This step-wise amplification is what differentiates our method from others (Gierahn et al., 2017; Tu et al., 2019). From this point, one fraction of the 3'-barcoded whole-transcriptome amplified cDNA product is sequenced to decipher and quantify individual-cell transcriptomes; whereas the other fraction enriched by the TCRD/G transcripts would be used to sequence the clonotype profile of single cells independently.

5.7 Discussion

The alanine scanning method served to locate a BTN2A1 footprint in the topographic representative module of the G115 Vγ9Vδ2 TCR prototype. Interestingly, this reactive footprint was situated away from previously mutated residues which targeted the top surface area of the receptor structural domain (Table 1.7 and Fig. 1.6). That is the BTN2A1-footprint, and the two independent residues at the joined-domain region

abrogate phosphoantigen responses by two essential reactive binding sites located poles apart on the $\gamma\delta$ TCR. Together with the BTN2A1-BTN3A1 complex that mimics the BTNL3-BTNL8 or mouse Btnl1-Btnl6 heteromeric complexes, all responsible for regulating and controlling the $\gamma\delta$ T-cell fate, seems likely that each of these $\gamma\delta$ TCR binding sites provides contact to a respective BTN member.

Interestingly, the BTN2A1 footprint represents an entirely conserved region that is even distinct and more conserved than the HV4 encoding segment described by Melandri et al. (2018). Hence, the BTN2A1 contact to the V9γ-domain represents a universal receptor-ligand interaction which is conceivable for any given clone of that domain, as recombining it to alternative Vδ-domains probed this interaction was maintained at equal affinity in two different recombined Vγ9 receptors (Fig. 3.9). With two glutamic acid residues and two histidine and arginine residues, this reactive footprint might form a polar forceps that grips to corresponding counterpart residues at the variable immunoglobulin domain of the BTN2A1 extracellular domain portion (Fig. 5.3). Equally relevant, the residues providing BTN2A1-reactivity, as well as BTN2A1-knockout cell lines, have proved to be essential for the agonist functionality of the monoclonal antibody clone 20.1 that targets all three BTN3A members (Fig. 5.5). Altogether, these results provide strong evidence to hypothesise this antigen-recognition system works via a dual-ligand binding mode where BTN2A1 anchors the receptor and BTN3A1 acts as a sensor activation-switch that directly initiates phosphoantigen-reactive Vγ9Vδ2 T-cell responses.

Small antigenic metabolites that activate $\gamma\delta$ T cells exist in different shapes and forms (Fig. 1.2). These are distinguished by their varying intrinsic ability to become immunogenic which mostly correspond to designated biological groups catalogued by their sources such as microbial or eukaryotic origin, plant alkylamines, and biopharmaceutical commercialised compounds, or even synthetic prodrugs (Fig. 1.5). Generally, microbial compounds are the most potent antigenic phosphoantigens with distinguished nanomolar activity with standing popularity for the HMBPP in research use. Contrary, phosphoantigens from a eukaryotic source are much less potent and require doses at the micromolar range. On the other hand, amino-bisphosphonate drugs (Table. 1.1), which indirectly causes accumulation of eukaryotic phosphoantigens from the mevalonate biosynthetic metabolic pathway (Fig. 1.3), may require lesser doses as consequently promotes an increasing titre of diverse eukaryotic antigen forms. Plant alkylamines metabolites are non-phosphate containing groups, but like amino-bisphosphonates obstruct the eukaryotic isoprenoid metabolism and indirectly promote an increase of eukaryotic phosphoantigens inside the antigen-presenting cell (Bukowski et al., 1999).

The robust biological activity of microbial representative HMBPP show prominent immunogenic responses from donor-purified Vδ2$^+$ T cells despite requiring more prominent doses to promote activation of Jurkat-reporter Vγ9Vδ2 TCR-transfected cell lines (Fig. 5.8). This fact was also observed form eukaryotic IPP soluble compound even though this was much less potent activator of the immune cells. However, when both types of responding cells were challenged with zoledronate drug, the EC_{50} dose was maintained between purified fresh isolated Vδ2$^+$ T cells and the Jurkat-reporter cell line. This observation might arise the possibility that additional co-stimulatory molecules influence signalling transduction factors. Nevertheless, this variation could also be described as donor-purified Vδ2$^+$ T cells hold a much burden range of diverse clonotypes reactive to phosphorylated antigens than this unique Vγ9Vδ2 TCR clone 6 receptor expressed on the Jurkat-reporter cell line. Single selected doses which stimulated to similar extend the Jurkat-reporter cell line tested in two melanoma BTN2A1 or BTN3A knockout lines reflected the essentiality of either member in response to phosphoantigen regarding its source (Fig. 5.6). Thus generalising the phosphoantigen-presenting mechanism as a universal tool for the immune system, and specific of the Vγ9Vδ2 $\gamma\delta$ T-cell subset, to recognise pathogenic infections or tissue disruptions alike.

The current third generation of amino-bisphosphonate drug treatments (Table. 1.1) are convenient methods to explore in the field of phosphoantigen-reactive $\gamma\delta$ T cells for their wide-availability and approved clinical trials. Hence, the effect of zoledronate drug was tested in two established tumour cell types for evaluation of its in-vitro potential for either constraining tumour growth or eliminating targeted cells. The effect of this drug in removing targeted antigen-presenting cells was barely noticeable after one day, despite the fact, several studies and our data determine the activation phenotypic profile is detectable after a short term, even within hours (Sec. 3.5) (Dhar and Chiplunkar, 2010; Idrees et al., 2013). However, the effects were determined after observing virtually no tumour cells survived two days after the zoledronate challenge (Fig. 5.9). This $\gamma\delta$ T-cell cytolytic capability appeared to be indistinct from the number of lymphocytes present in cocultures with relatively low ratios such as one-to-one or five-to-one effector to target cells. However, when a much higher proportion of effector lymphocytes to tumour target cells is used can result in lymphocytes responding with a more rapid cytotoxic activity after only four hours (Dhar and Chiplunkar, 2010). Interestingly, our results also showed imperceptible differences between the doses of zoledronate drug used, which drastically varied from 1, 10, or 100 µM challenges. Accordingly, these observations symbolise a few $\gamma\delta$ T cells might be enough to initiate a whole potent immunologic response within a matter of two days, time of which se-

creted cytokines are present in the environmental milieu and contribute to the overall response. Nonetheless, it is worth mentioning that divergences from the immune response to different targeted cell types could result from varying levels of surface BTN transmembrane members (Fig. 3.1), a tripartite protein hampers the structural activation complex module (Gu et al., 2018), or even divergent membrane permeability of such cells in uptaking the zoledronate drug (Kalyan et al., 2014).

After observing the successful potential cytolytic effects of purified-expanded Vδ2$^+$ $\gamma\delta$ T cells challenged with zoledronate-stimulated tumour cell lines in in-vitro experimental conditions, we proposed to study the reactivity of these $\gamma\delta$ T cells in a more realistic human approach tumour microenvironment. The in-vitro culture of this tissue in an ALI environment maintains most of the heterogeneity of cancer cells and the immune spectrum found in in-vivo tissues (Neal et al., 2018). More organoid 3D-culture systems are in the pipeline and some already showing exciting results in the range of analysis they ofter. These advanced tissue cultures are also burgeoning from the steam-cell level, which with the addition of the adequate supplements, hormones, and transcription factors are providing excellent results with structural integer organ parts developing closely to those in the human body (Czerniecki et al., 2018). Additionally, the facility of having ease access to human conserved cancer tissue right in the laboratory is staggering.

The establishment of this type of collagen matrix-based 3D-organoid cultures is more robust and represents the cellular diversity within human cancer diseases. In our cultures, we could determine the presence of infiltrating Vδ2$^+$ T cells was minimal, although this subset was indeed present in the tissue (Fig. 5.14). Other studies have reported histological dye markers of the Vδ2$^+$ T cell with a higher representation subset of these cells in the renal tumour tissue (Viey et al., 2005). However, our results suggest a much lower proportion of infiltrated $\gamma\delta$ T cells in the 3D-organoid tissue cultures, which ranges around 1 % of total infiltrated CD45$^+$ lymphocyte cells. Our results are, therefore, similar to those later reported by Inman et al. (2008) over an evaluation of 248 renal carcinoma patient-derived tissues. Still, Viey et al. (2005) showed how purified-expanded Vδ2$^+$ T cells may control autologous primary kidney tumour growth by inducing cytolytic responses that are directed and specific toward cancerous renal cells and not to healthy tissue in eleven out of fifteen donors Viey et al. (2005). Moreover, these authors remarked this $\gamma\delta$ T-cell response was directed through TCR- and NKG2D-dependent signals, which potentiate the role of Vγ9Vδ2 T-cells as opposed to other reports (Inman et al., 2008).

Besides discrepancies on the role in which $\gamma\delta$ T cells play in renal cancer, implementing 3D-organoid cell cultures methods can circumvent the use of animal models

in the laboratory. The $\gamma\delta$ T-cell and BTN family regulatory molecules in rodent species are inexistent. Therefore, the implementation of both human Vγ9Vδ2 T cells and the chromosome 6 BTN genetic cluster should be introduced in immunodeficient mice to construct a genetically engineered system in any rodent animal model. Working in lab-based established organoid systems avoids working with immunocompromised mice, which might disrupt the normal functioning of the entire immune system in that organism. (Viey et al., 2005)

As a future continuation of this work, the understanding of clonotype diversity and corresponding transcriptome at a single-cell analysis should be continued. The acquisition of that information can greatly contribute to phenotypically decode all the $\gamma\delta$ T-cell spectrum and functional plasticity in response to phosphorylated antigens. Moreover, the novelty of single-cell barcoded multi-nano pore array-based separation methods together with clonotype paired to transcriptome analyses of the $\gamma\delta$ T-cell subset may become a milestone for the novelty of $\gamma\delta$ T cell sequencing using that recently developed methodology (Gierahn et al., 2017; Macosko et al., 2015; Tu et al., 2019). This thesis, proposes an additional change in the initial protocol established by (Tu et al., 2019), where the TCR-transcript enrichment by the use of biotin-streptavidin beads could be substituted by a differentiating amplification step instead. That takes advantage of two irrelevant basepairs at the 3'-UPS1 during the template switch oligo otherwise unused. The addition of alternative dual bases in this position would be used to differentially amplify the TCR-transcriptome from the general transcript cDNA single-cell barcoded library. It will be interesting to experimentally probe whether or not these two basepairs are sufficient to segregate the TCR-transcriptome from the main transcript cDNA library.

Chapter 6

Overall Discussion

Human $\gamma\delta$ T cells have a role in coordinating immune development and confer innate protection against infectious pathogens and disease (Chien et al., 2014). They constitute part of innate immunity despite expressing an atypical recombined heterodimeric TCR composed by the γ and δ variable gene loci. The Vγ9Vδ2 T-cell subset represents the most prevalent $\gamma\delta$ T-cell phenotype in human blood and particularly recognises phosphoantigens that are present in many photogenic bacteria and cancer cells. Phosphoantigens can alert the immune system when accumulating inside eukaryotic cells which suffer from stress or abnormal growth such as cancer. Nonetheless, microbes and some pathogenic pathogens produce and realise highly potent small phosphorylated compounds that even a tiny proportion in solution causes rapid activation of this innate-like T-cell subset. Besides, recently improved third-generation of amino-bisphosphonate drugs represent an indirect method to accentuate the concentration of phosphoantigens inside eukaryotic cells due to impeding a functional activity of the FPPS enzyme of the isoprenoid metabolism. Patients treated with this type of drugs improve $\gamma\delta$ T-cell responsiveness to immunogenic pathogens and potentiate antitumour activity in cancer patients (Girardi et al., 2001; Gober et al., 2003; Guenther et al., 2010; Idrees et al., 2013).

The mode of phosphoantigen recognition is comparable to four other major antigen-recognition groups, with peptides, lipids, and vitamin-B derivates. Small non-peptidic metabolite phosphoantigens are recognised via non-classic MHC antigen-presentation mechanisms and involves members of the BTN family (Gu et al., 2018; Harly et al., 2012). Upon activation, phosphoantigen-reactive $\gamma\delta$ T cells respond rapidly with direct-targeted cytotoxic immune activity, although they may show proprieties of both innate and adaptive systems (Wang et al., 2001). For instance, these also elaborate active *cross-talks* and show aptness to boot orchestrated immune responses after an encounter with microbial or tumour non-peptidic antigens (Brandes et al., 2009) and contribute to clonal expansion after bacterial infections (Shen et al., 2002).

The activation mechanism of Vγ9Vδ2 T cells by phosphoantigens have been mostly unknown nearly since a quarter-century ago and its understanding is of vital interest for the development of immunotherapeutic therapies (Brenner et al., 1986; Sebestyen et al., 2020; Tanaka et al., 1995; Willcox and Willcox, 2019). First insights on phosphoantigen presentation showed a linked to BTN3A1, a gene of the BTN family that is independent of classic MHC molecules (Harly et al., 2012). Contrasting options surged on whether the phosphoantigen was coupling to the extracellular domain of BTN3A1 or else it was detected intracellularly by its B30.2 functional group (Sandstrom et al., 2014; Vavassori et al., 2013), with following reports supporting the later hypothesis (Wang and Morita, 2015). Nevertheless, none of these studies reported clear evidence of the Vγ9Vδ2 TCR binding to BTN3A1, and related insights revealed that additional proteins located at the human chromosome 6 were required to induce a complete activation of $\gamma\delta$ T cells (Riaño et al., 2014).

The family of BTN molecules evolved to collectively regulate $\gamma\delta$ T cell functions in the jaw vertebrate immune system and contribute to home $\gamma\delta$ T cells into tissue compartments, where they constitute immune integrity and tissue immunosurveillance (Abeler-Dörner et al., 2012; Arnett and Viney, 2014; Di Marco Barros et al., 2016). For instance, the murine Skint-1 and Skint-2 are explicitly expressed by thymic epithelial cells and selects for the DETC $\gamma\delta$ T-cell subset, which protects from cutaneous carcinogens. Other mouse Btnl molecules also shape $\gamma\delta$ T-cell tissue compartments like the Btnl1 and Btnl6 in intestinal lining enterocytes. These two members heterodimerise and attract the presence of V$\gamma7^+$ T-cells in the murine intestine which represent an important protective element of the intestine immune system. In the same fashion, human BTNL3 and BTNL8 cooperate similarly in human enterocytes and control the fate of V$\gamma4^+$ T cells in the gut immune system. Therefore, murine or human molecules of the BTN family jointly induce selective $\gamma\delta$ T cell TCR-dependent responses.

This work has identified the human BTN2A1 as a ligand for the Vγ9Vδ2 T cells receptor, which precisely contacts o to the Vγ9 domain and it is essential for the presentation of phosphoantigens. Likewise this study proposes an active interaction between BTN2A1 and BTN3A necessary to from the phosphoantigen presenting complex. Cooperation between members of the BTN family has been described previously as above-mentioned. The tendency for BTN members to dimerise probably comes from their symmetric resemblance and weak chemical forces that join their extracellular domains together (Melandri et al., 2018; Palakodeti et al., 2012). In the phosphoantigen presentation framework, either BTN3A2 or BTN3A3 appear to heterodimerise with BTN3A1, which allows this protein member to migrate towards the surface plasma

membrane in the form of an active antigen-presenting complex (Vantourout et al., 2018). The dimerisation of BTN members was also described between human BTNL3 and BTNL8 proteins, which together form a complex that moves towards the surface of colon epithelial cells. Similarly cooperate murine Btnl1 and Btnl6 in the intestine to regulate the fate of $\gamma\delta$ T-cells (Di Marco Barros et al., 2016). To further extend the knowledge of the Vγ9Vδ2 T-cell subset in disease models in-vitro organoid cultures from kidney tumour samples were generated, which enables to determine the prevalence tumour-infiltrated Vγ9Vδ2 T and study their role in future cancer therapies. To reveal the full potential and plasticity among phosphoantigen-reactive $\gamma\delta$ T-cell subtypes, a plan to sequence the clonotypic diversity in a single-based approach has been proposed to allow linking clonotype data with respective transcriptome profiles.

6.1 BTN2A1 Is a Ligand for the Vγ9 Domain of $\gamma\delta$ T Cells

Our study performed a negative-selection genetic screen based on tetrameric phosphoantigen-reactive $\gamma\delta$TCR tetramerised fluorescent probes that were previously confirmed to detect a ligand on several human tumour cell lines (Fig. 3.2). The analysis in a melanoma cell line indicated that *BTN2A1* and *SSPL3* single-guides were the most prominent after the selection phenotype, and a subsequent gene-wise analysis narrowed this result to the *BTN2A1* being the most relevant genetic target. The *SSPL3* appeared as a protein necessary for constituting and maintaining stability to the plasma membrane and not being related to the presentation of phosphoantigens (Jongsma et al., 2020). However, in a parallel screen using leukaemia K562 cells as targets for the same Vγ9Vδ2 TCR-tetramer prove, no relevant targets were detected. Thus, other plausible ligands with a much lesser affinity for the Vγ9Vδ2 TCR-tetramer clone 6 may exist. According to previous studies, the BTN2A1 protein found in the melanoma genetic screen matches all expectations and requirements to be a direct ligand for the Vγ9Vδ2 TCR. This is located in the chromosome 6 loci, a condition previously reported for this additional requirement apart from BTN3A1 to activate phosphoantigen-stimulated $\gamma\delta$ T cells (Riaño et al., 2014). Still, Vavassori et al. (2013) arose controversy by showing downplaying the expression profile of this BTN2A1 with the use of interference RNA was enough to discard BTN2A1 as a potential target for the Vγ9Vδ2 T-cell reactivity to phosphoantigens. This study, however, manifested the presence of this protein could not have been abrogated for completely, probably leaving a small amount of protein in the background, enough to cause activation of Vγ9Vδ2 T cells. More recently, other theories suggest that BTN3A1 acts as a sensory phosphoantigen molecule and other proteins are required to enhance the presenta-

tion to $\gamma\delta$ T cells (Gu et al., 2018). In this new framework, the BTN2A1 seem to take an essential role in contacting to the Vγ9Vδ2 TCR directly, and together with BTN3A1 induce phosphoantigen responses by $\gamma\delta$ T cells. Unlike BTN2A1, BTN3A1 was not reported in the top-ranked gene list after the analysis, indicating that BTN3A1 might not be responsible at all for the binding to the Vγ9Vδ2 TCR.

Solely in the melanoma LM-MEL-62 but not in the leukaemia K562 genetic screen the BTN2A1 as the most relevant gene conferring Vγ9Vδ2 TCR affinity. All subsequent validation experiments confirmed the *BTN2A1* candidate-gene was indeed a direct contact to the Vγ9Vδ2 TCR of phosphoantigen-reactive $\gamma\delta$ T cells. Nonetheless, there is the possibility the Vγ9Vδ2 TCR have multiple ligands of distinct affinities, as the already reported F_1-ATPase motif (Scotet et al., 2005). This work demonstrates that $\gamma\delta$TCR tetramers depended on the presence of BTN2A1 protein. The two melanoma cell line knockout models abrogated reactivity to six Vγ9Vδ2 TCR clones tested. (Fig. 3.4). As the lost of tetramer stain was only observable in those lines that lost surface expression of *BTN2A1* but not *BTN3A* members, the role BTN2A1 seemed more critical than BTN3A1, which the literature described as a putative ligand for the subset of Vγ9Vδ2 T cells (Gu et al., 2018; Vavassori et al., 2013). Interestingly, reversing the knockout genetic alteration by reintroducing the expression of BTN2A1 shows the staining of the Vγ9Vδ2 TCR-tetramer probe can be recovered, unlike the addition of either BTN3A1 or BTN3A2 members which did not have the same effect and melanoma BTN2A1-knockout cells remained incapable of binding the Vγ9Vδ2 TCR-probe (Fig. 3.5).

More experimental evidence supported the BTN2A1-Vγ9Vδ2 TCR interplay. Extracellular domain BTN fluorescent tetramers were prevented from interacting to cells expressing the Vγ9Vδ2 TCR by the use of specific antagonist antibodies, while others show an agonist effect. Many antibodies which targeted either BTN2A1, BTN3A1, or the $\gamma\delta$ TCR, exhibit competence to modify their interaction moderately (Fig. 3.6 and 3.7). Previous to this work, only one antagonist and another agonist were reported with the capacity to significantly, alter the activation of phosphoantigen-reactive $\gamma\delta$ T-cells (Harly et al., 2012).

The biochemical analysis provides evidence for an existing weak chemical bond between the BTN2A1 and the $\gamma\delta$TCR clone 6. Our reported affinity was comparable to the average $\alpha\beta$ TCR recognition of peptides presented by MHC molecules (Cole et al., 2007; Stone et al., 2009), and very similar to Vγ5Vδ1 interaction with CD1d lipid-presenting molecule ($K_D = 35$ µM) (Uldrich et al., 2013). Remarkably, this chemical interaction was exclusively between the Vγ9 domain and BTN2A1 uniquely; thus, the BTN3A1 was not implied. Neither of the δ-chains encoded by the Vδ1 or Vδ2 gene

segments controlled or altered the interaction between BTN2A1 and Vγ9 domain. These findings determined BTN2A1 was interacting to Vγ9$^+$ T cells exclusively.

6.2 The BTN2A1-BTN3A1 Functional Complex

Considering the datasets of this work, the BTN2A1 cooperates with BTN3A members, and together consolidate a functional heterodimer dual-complex which is necessary to convey phosphoantigen responses to $\gamma\delta$ T cells. Like other members of the BTN family, these two proteins dimerise and regulate the functionality of a distinct $\gamma\delta$ T-cell subset. Nonetheless, additional BTN3A members could take part in constructing a more robust structural complex. However, these may not be essential, nor required for inducing activation signals to $\gamma\delta$ T cells, but rather confer sturdy stability to facilitate $\gamma\delta$ T cell recognition of the phosphoantigen-presentation complex. In this line, Vantourout et al. (2018) reported that BTN3A1 heterodimerise with BTN3A2 or BTN3A3 proteins favouring its migration from the endoplasmic reticulum or cytoplasm to the cellular surface. Whether the BTN3A1 retains BTN3A2 or BTN3A3 proteins after reaching the surface membrane is a problem yet to be resolved. The BTN2A1 seems to migrate to the plasma membrane directly and bind to the Vγ9Vδ2 TCR, as in transfection experiments with single expression of *BTN2A1* in rodent cell lines was sufficient to detect the highest detection signal when stained with Vγ9Vδ2 TCR tetramers.

In some flow cytometry studies assessing the association between intracellular domains between different BTN pairs, was observed that either BTN2A and BTN3A members could form homodimers or heterodimers between BTN2A1 and any of the BTN3A members. Now, a recent report suggests that disulfide cysteine joins between two proteins form homodimers by their constant immunoglobulin domain extracellular units, akin to BTN3A members (Karunakaran et al., 2020). Membrane-related cytoskeletal linker periplakin and RhoB proteins may also contribute to regulating the stability of BTN members at the plasma membrane. The periplakin may establish a bond to the B30.2 membrane-proximal di-leucine motif of BTN3A1. However, this excludes homolog proteins BTN3A2 and BTN3A3 due to the absence of this proximal putative reactive site (Rhodes et al., 2015). Besides, the guanosine triphosphate (GTP)ase activity of RhoB could contribute in reorganising the phosphoantigen-signalling complex on the cell surface membrane (Sebestyen et al., 2016).

This BTN2A1-BTN3A1 complex structure must be dynamic and even though there is no detection nor dissociation changes mediating FRET flow cytometry assays during the addition of phosphoantigens, this study notices the heterodimeric form is disrupted after the addition of many different monoclonal specific antibodies against

BTN2A1. Therefore, this complex holds a basic two structures which some reports already suggested. These are the V-shaped and head-to-tail conformations from BTN3A molecules (Gu et al., 2017), which still might be able to take place in a BTN2A1-BTN3A1 complex. More recently, another study supported this hypothesis in which BTN3A1 stands in a resting V-shaped conformation whereas it switches into a head-to-tail structure after binding to a microbial phosphoantigen HMBPP (Yang et al., 2019). In light of the data from this thesis, these putative conformations might be correct, while the BTN2A1 protein might hold close relationship with BTN3A1 in either conformation. Otherwise, BTN2A1 could conjugate with BTN3A1 and constitute a heterodimeric molecular conformation, plausibly including BTN3A2 or BTN3A3 tripartite proteins as these also interact with BTN3A1 (Vantourout et al., 2018).

6.3 Phosphoantigen-reactive $\gamma\delta$ T-cells Recognise a Dual-ligand

The BTN2A1 interacts to a germline-encoding region at the side Vγ9 domain of $\gamma\delta$ T cells, involving the outer faces of B, D, and E strands. There are at least four amino acids that form a polar BTN2A1 footprint with arginine, histidine, and glutamic acid radical groups. Unlike MHC-like classic TCR-ligand interactions, the recognition mode of BTN2A1 does not seem to involve either CDR segments of γ or δ chains, even though these may be implicated in recognising another ligand. Instead, the BTN2A1 interacts to a conserved region that is located below those domains of which most TCR use to recognise antigens, and so the binding of BTN2A1 could be more comparable to some superantigen-TCR interactions (Fields et al., 1996; Rust and Koning, 1993). Therefore this characteristic interaction model might free the Vδ2 domain and CDR fragments plausibly responsible for the involvement of a second ligand contact and signal triggering function.

Mutational analysis performed in this work described two more relevant amino acids were essential to induce $\gamma\delta$ T-cell signalling cascades after recognition of phosphoantigens, although these appeared as irrelevant to confer a BTN2A1 binding contact (Fig. 1.9). A similar strategy seems to be used by other BTN members that regulate $\gamma\delta$ T cells in the intestine and potentially, a general recognition mode by the family of BTN immune-regulatory molecules (Melandri et al., 2018). Our studies also show that altering residues situated at the top of the G115 prototype Vγ9Vδ2 TCR, situated at the CDR of Vδ2 domain, prevented phosphoantigen-driven responses by $\gamma\delta$ T cells, despite it is confirmed these were not determined in the direct interaction between the TCR and BTN2A1 ligand. Hence, some members of the BTN3A family which associate with BTN2A1 may have a role in contacting these residues and even-

tually transmit the sensor activity that is dominated by the B30.2 intracellular domain of BTN3A1 protein.

Besides, there are many possible functionalities for the BTN3A1 and BTN2A1 B30.2 intracellular domains. For instance, these two intracellular motives could interact with each other by the presence of phosphoantigens (Wang et al., 2019), although this was not detectable in the flow cytometry analysis with B30.2-fluorescent constructs performed in this work. Also, the B30.2 domains in BTN molecules may represent an important part that allows these proteins to stagger together with neighbouring members at the plasma membrane. In turn, that could favour multimerisation like it does the function agonist activity by the antibody clone 20.1 (Palakodeti et al., 2012). What is critical to understand next is how phosphoantigens change the complex structure and the role of BTN B30.2 domains in terms of aggregation and structural arrangements necessary to activate Vγ9Vδ2 T cells (Wang et al., 2019; Yang et al., 2019).

In sum, the close relationship between BTN2A1 and BTN3A1 is indisputable following FRET and co-transfection assays from this study (Rigau et al., 2020) and subsequent protein co-precipitation analysis by another independent group (Karunakaran et al., 2020). Importantly, these data have substantial evidence to suggest that the agonist functional activity of clone 20.1, plausibly cross-linking BTN3A members, was dependent on BTN2A1. Thus, reassuring the BTN2A1-3A1/2 complex works in alliance (Rigau et al., 2020). Besides, reporter Jurkat cells enforcing a $\gamma\delta$ TCR gene expression that include a range of individual γ-mutant chain residues at the BTN2A1 binding site were unable to confer phosphoantigen reactivity even under stimulus with agonist antibody, further confirming the dual-ligand hypothesis.

6.4 The Biological Implication of the Vγ9Vδ2 T-cells in Kidney Organoids

The clear cell renal carcinoma originates in the proximal convoluted tubule and is among the tenth worldwide most prevalent cancer forms with life-threatening consequences (Rini et al., 2009). This type of cancer is associated to *VHL*, *PBRM1*, *SETD2* and *BAP1* mutated genes, often used as a prognostic markers (Gulati et al., 2014; Huang et al., 2019). However, for detecting renal carcinoma cells with antibodies, the CA9 transmembrane antigen is among the most known makers today, especially for microscopy imaging (Stillebroer et al., 2010). Contrary, the protein expression of surface BTN molecules in the kidney tissue has not been thoroughly studied, despite several subsequent reports suggest the C$\rightarrow$T polymorphism (rs6929846)

in BTN2A1 might relate to suffering from chronic kidney disease (Oguri et al., 2013; Yoshida et al., 2011a). The relation between this polymorphism and $\gamma\delta$ T cells has not been reported yet, albeit in-vitro experiments show renal adenocarcinoma and clear cell tumours are highly susceptible to treatments with the zoledronate drug causing activation of phosphoantigen-reactive $\gamma\delta$ T cells (Idrees et al., 2013). Indeed, some research describe $\gamma\delta$ T cells defends the body from renal carcinoma cells and noted that the activation phenotypic profile of these lymphocytes increases and an oligoclonal population expands, indicating they would recognise certain antigens on these cancerous cells (Kobayashi et al., 2001). Likewise, Viey et al. (2005) points these donor-expanded phosphoantigen-reactive $\gamma\delta$ T cells can remove renal cell carcinoma without damaging healthy tissue, even though the tumour cells showed previous resistance to conventional treatments. Moreover, they report this lymphocyte activity is TCR-dependent with enhanced co-stimulatory effects by the NKG2D co-receptor. Lastly, these group also noticed an increment phosphoantigen-reactive $\gamma\delta$ T cells infiltrated in tumours (Viey et al., 2005).

With the above mentioned, herein is established in-vitro organoid renal-cell ALI-cultures derived from freshly isolated biopsy kidney cancerous tissue to study the prevalence of infiltrated Vγ9Vδ2 T cells in the kidney. This recently developed methodology has the advantage that conserves most of the tumour microenvironment, including the tumour heterogeneity and immune cell spectrum (Neal et al., 2018). Although our preliminary data contrasted to Viey et al. (2005), who obtained a high number of infiltrated phosphoantigen-reactive clones, it showed a bare representation of total $\gamma\delta$ T cells circa 1 %, more in line with results reported by others who revised the prevalence of the $\gamma\delta$ T-cell population over two-hundred patient-derived clear cell renal carcinoma samples (Inman et al., 2008). Under these observations, it seems that only a defined small population of infiltrated $\gamma\delta$ T-cell lymphocytes resides in the clear cell renal carcinoma tumour microenvironment of PDO-ALI organoid sample. Even though these Vγ9Vδ2 T cells may not have a crucial determining immunosurveillance role preventing the tumour growth, they could still retain the potential to become active cytotoxic cells if samples were challenged with an amino-bisphosphonate drug stimulus.

6.5 The Scenario of Vγ9Vδ2 T Cells in the Clinic

In light of the study by Gentles et al. (2015), infiltrated $\gamma\delta$ T cells represent the most favorable prognostic indicator across diverse blood and solid cancers, and independent reports evidence for Vγ9Vδ2 T cells as excellent candidates in the next generation of

cancer immunotherapies (Bennouna et al., 2010; Bouet-Toussaint et al., 2008; Corvaisier et al., 2005; Godder et al., 2007; Toia et al., 2016). Eradicating tumours has now been attainable by enhancing antitumoural activity with amino-bisphosphonate drug treatments (Cordova et al., 2012; Toia et al., 2016). Challenging patient expanded in-vitro Vγ9Vδ2 T cells mixed with autologous renal tumour cell lines also shown specific, selective lysis of primary tumour cells in dependency of TCR and NKG2D receptors (Viey et al., 2005). Likewise, lymphocytes may require TCR and NKG2D dependent ligand recognition to induced antitumour potential in hepatocellular and colorectal carcinomas (Bouet-Toussaint et al., 2008; Corvaisier et al., 2005). Hence, $\gamma\delta$ T cells are have been engineered with chimeric co-stimulatory receptors to mount targeted cytotoxic effects (Fisher et al., 2019). These innate-like T cell therapies elude alloreactivity as proven in a follow-up treatment where subjects with blood cancer received infiltrated $\gamma\delta$ T cells and demonstrate no noticeable incidence of acute GvHD disease (Godder et al., 2007). A combination of recombinant variable chains in engineered Vγ9Vδ2 T cells is also possible to increase receptor affinity for targets and direct the lymphocytes toward malicious components to elicit specific cytolysis and clonal expansion (Gründer et al., 2012). Another approach involves the use of chimeric antigen receptor T (CAR-T) cells derived from single-chain Fv fragments of antibodies; thus, they recognise conformational epitopes independently of their TCR evading unspecific targets. Despite these therapies are proven in $\alpha\beta$ T cells, trials using $\gamma\delta$ T cells are promising and more appealing due to related allograph minor risks (Gründer et al., 2012). For instance, polyclonal engineered bispecific CD19/CD28-specific CAR-T Vγ9Vδ2 cells expanded with amino-bisphosphonate drug demonstrates increased efficacy in targeting leukaemia K562 cell line and proves alloreactivity symptoms-free in mice leukaemia xenografts (Deniger et al., 2013).

Many reasons support the rationale for harnessing Vγ9Vδ2 T cells in immunotherapy. These $\gamma\delta$ T cells are the most prominent in peripheral blood, whose extraction is simple. They infiltrate in tumours and interact with cancer cells, as well as demonstrate potent cytotoxic activity against a broad spectrum of infection or cancer diseases. Also, they facilitate allograph transplants thanks to unrestricted-reactivity to MHC class molecules, evoke rapid cytotoxicity, secrete adequate cytokines, and can prime Th cells for triggering acquired immunity. Additionally, synthetic phosphoantigen-based compounds are currently under development such as phase I bromohydrin pyrophosphate (phosphostim/BrHPP/IPH1101, Innate Pharma, France) (Bennouna et al., 2010; Burjanadzé et al., 2007), prodrugs alternatives (Hsiao et al., 2014; Zgani et al., 2004), or already approved like broadly used zoledronate used for treating osteolysis (Novartis, Switzerland). Besides, supplementary co-stimulatory molecules and

antibody treatments applied may limit clonal anergy (Sharma and Allison, 2015). In terms of cancer therapy, the addition of cytokines or even alternative immune checkpoint anticancer drugs (PD1, PD-L1, and CTLA-4) can turn the balance for a better survival outcome. Most importantly, current developments in new therapeutic monoclonal antibodies against members of the BTN family such as clone 20.1 targeting BTN3A family members (Harly et al., 2012) or bispecific antibodies against the $\gamma\delta$ TCR (de Bruin et al., 2017) may show adequate progress to clinical trials, and some therapeutic successes will eventually emerge with novel anti-BTN2A1 antibody drugs (Rigau et al., 2020). Thereby, novel regimens combining phosphoantigen drugs and engineered $\gamma\delta$ TCRs are under investigation. These advances might represent the next generation of immunotherapeutic approaches in the near future.

6.6 Concluding Remarks

The data in this thesis represents a leap forward in defining the role for the BTN2A1 protein being an essential component of the phosphoantigen-presenting complex that alerts the immune system not only from infectious diseases or tissue-dysregulated cells but including also many blood and solid tumour cancers (Gentles et al., 2015; James et al., 2007; Rigau et al., 2020). Conclusions are that BTN2A1 is an essential ligand, albeit not unique, for the Vγ9 of the phosphoantigen-reactive Vγ9Vδ2 TCR, which is a prevalent subset among human peripheral blood $\gamma\delta$ T cells. That has a profound implication in the innate-like immune responses to phosphoantigens product of bacterial infections (Morita et al., 1999; Shen et al., 2002; Wang et al., 2001) and cancers (Godfrey et al., 2018; Sebestyen et al., 2020). Moreover, the role of BTN2A1 is implied on the functional antagonist and agonist activity of monoclonal specific antibodies that bear great potential in the biopharmaceutical industry (Sec. 3.5), as well as connoting its direct relation to the commercial agonist clone 20.1 antibody against the BTN3A members (Sec. 5.2.3).

Until now, little was known about BTN2A1 functions. The BTN2A1 transcript is expressed in most human tissues despite its low expression in leukocytes (Malcherek et al., 2007), and particularly $\gamma\delta$ T cells (Sec. A.7). An independent research group constructed an Ig-fusion BTN2A1 soluble protein and demonstrated it bound to immature monocyte-derived DC. However, the contact diminished after cell maturation and such binding went undetected in Langerhans DC. Additionally, that interaction required the presence of Ca^{2+} and was strictly dependent on high-mannose oligosaccharide glycosylation (Malcherek et al., 2007). Nevertheless, these data suggested a glycosylated BTN2A1 protein lowers the affinity for its putative ligand on monocyte-

derived DC compared to a deglycosylated protein that binds more prominently to the same cells (Fig. A.15 a-b). Moreover, empirical data has shown the glycosylation profile seems not to impede the contact between BTN2A1 and the Vγ9Vδ2 TCR of either donor-purified V$\delta2^+$ T cells or to the Vγ9Vδ2 clone G115 when expressed on a Jurkat-reporter cell line (Fig. A.15). Hence, according to observations, the glycosylation profile has redundant implications in recognition of the BTN2A1 protein by the Vγ9Vδ2 TCR and its ligand monocyte-derived DC remains a question which needs further analyses.

Additionally, this work determines cooperation between BTN2A1 and BTN3A1, of which the BTN3A1 member acts as a phosphoantigen sensor molecule in a complex-like structure. For the presentation of phosphoantigens, the presence of this complex is necessary, and like Vantourout et al. (2018), it is noted BTN3A2 assists in the migration of BTN3A1 from the cytoplasm compartment to the cell surface membrane. Thus, enhancing phosphoantigen presentation to the $\gamma\delta$ T cells in a tripartite molecular complex system (Sec. 4). In some of these results, the potential of some agonist and antagonist functional antibodies that enable regulatory functions of phosphoantigen-reactive Vγ9Vδ2 T-cells is observed. Similar to the commercially available agonist 20.1 clone (Harly et al., 2012), here is reported RF13-259 clone with selected specificity against the BTN2A1 may have a similar cross-linking effect over its target (Palakodeti et al., 2012), and activate designed clonotypes as reported previously for the 20.1 clone (Starick et al., 2017).

The alanine scanning method has revealed four essential residues located at the germline encoding regions construct the BTN2A1-reactive footprint of the G115 Vγ9Vδ2 $\gamma\delta$ T-cell prototype, involving the outer faces of B, D, and E strands (Sec. 5.2). This could be extrapolated to other V$\gamma9^+$ clonotypes because co-expressing BTN2A1 together with molecules of the CD1 family can promote V$\gamma9^+$ CD1-reactive $\gamma\delta$ T cell activation. Likewise, two more residues were identified to be related in $\gamma\delta$ TCR-signal transduction by phosphoantigen-reactive $\gamma\delta$ T cells. These were located facing one another at the γ- and δ-chains, near other reported residues situated at the CDR segments of either chain (Gründer et al., 2012; Wang et al., 2010; Xi et al., 2010; Yamashita et al., 2003). Assuming that the BTN2A1 cooperates with BTN3A1 and plausibly with other members of the BTN3A family, it is likely that the Vδ2 domain of Vγ9Vδ2 T cells interact with either BTN3A member upon phosphoantigens binds to the B30.2 intracellular domain of BTN3A1, inducing a putative conformation change that is sensed by the CDR and Vδ2-domain reactive sites of the Vγ9Vδ2 TCR. Thus, phosphoantigens are recognised by $\gamma\delta$ T cells through a dual-ligand binding molecular complex composed by at least BTN2A1 and BTN3A1 proteins.

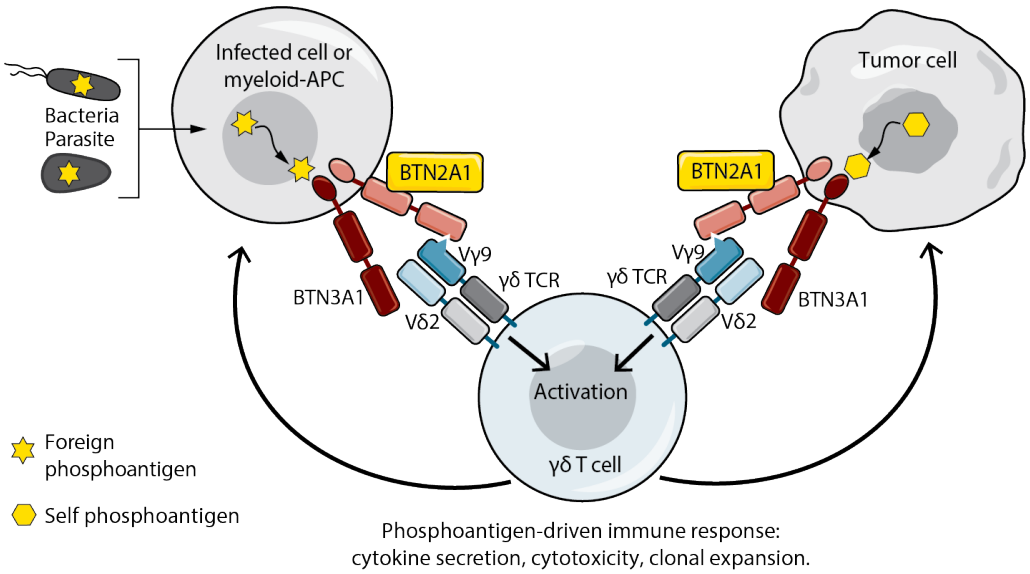

Figure 6.1: *Presentation of phosphoantigens to $\gamma\delta$ T cells is modelled by a putative BTN2A1-BTN3A1 complex structural domain, where BTN2A1 has an essential role in contacting to a germline encoding region of the Vγ9-domain and BTN3A1 acts as a phosphoantigen-sensor molecule (Rigau et al., 2020).*

In sum, this mechanism might sense internal phosphoantigens via the BTN3A1 intracellular B30.2 motif, which after binding phosphoantigens, regarding their source, undertakes a structural conformational change sufficient to trigger activation signals through the $\gamma\delta$ TCR of responding lymphocytes. Notably, the Vγ9-domain directly establishes contact via a conserved motif with presenting-molecule BTN2A1, whereas, plausibly the BTN3A1 partner molecule shifts after an interaction to phosphoantigens inducing a twist necessary to execute rapid innate-like $\gamma\delta$ T-cell immune responses (Fig. 6.1). Interestingly, the BTN3A1 structural shift renders to a conserved amino acid composition at the *CFG* face of its extracellular immunoglobulin variable domain located at the C' or G β-strands, as (R73E or K136M) amino acid changes deters activation of $\gamma\delta$ T cells by phosphoantigens, like in those reactive regions of BTNL3 that contact the Vγ4^{+} TCR (Willcox et al., 2019). Consequently, different models composed of BTN family members converge by their reactive and polar sites, which could enable ease formation of multiplexing functional structures and potentiate the effect over immune responses akin to enforced cross-linking by the use of specific antibodies (Palakodeti et al., 2012; Simone et al., 2010; Yamashiro et al., 2010).

From these observations, several hypotheses are drawn one of which describes the aforementioned phosphoantigen-presenting model might work from an antigen-presenting cellular complex. Solvent molecules of the BTN family heterodimerise and homodimerise each another in a defined manner (Di Marco Barros et al., 2016; Gu et al., 2017; Melandri et al., 2018), that is also manifested in association experimental

analysis (Sec. 4.4). Although solely the presence of BTN2A1 and BTN3A1 is essential and necessary to activate phosphoantigen reactive $\gamma\delta$ T cells (Sec. 4), GTP-binding protein RhoB or cytoskeletal periplakin may assist as secondary enhancer molecules that probably stabilise the membrane complex and fulfil small requirements (Laplagne et al., 2020; Rhodes et al., 2015; Sebestyen et al., 2016). However, the existence of previously mentioned multiplexes or intervention of tripartite proteins in the functional complex remains a reasonable hypothesis (Palakodeti et al., 2012; Uldrich et al., 2020). The high homology between the three BTN3A members consolidates stable dimers between themselves, which is reported and observable on the surface of artificial lipid-like membrane nanodiscs (Gu et al., 2017; Vantourout et al., 2018). Like human BTNL3/BTNL8 or mouse Btnl1/Btnl6 heterodimers (Di Marco Barros et al., 2016), these data indicates association BTN2A1 and BTN3A1 exists (Rigau et al., 2020). Later, others reaffirm these findings in pull-down assays and determine the alliance between BTN2A1-BTN3A1 complex is feasible due to weak chemical bonds by their extracellular immunoglobulin variable domains (Karunakaran et al., 2020). Likewise, the BTN2A1 incorporates a membrane-proximal interchain disulphide bond that allows the formation of soluble V-shape homodimers, albeit its homodimerisation seems redundant for the activation of phosphoantigen-reactive Vγ9Vδ2 T cells as a single copy of BTN2A1 and BTN3A1 is sufficient to prime $\gamma\delta$ T cell responses. Hence, several heterodimeric compositions for the phosphoantigen membrane presenting complex are possible (Fig. 6.2).

In conclusion, these data reports a distinct model in which the BTN2A1-BTN3A1 complex senses-phosphoantigens and indirectly presents them to $\gamma\delta$ T cells of the Vγ9Vδ2 subset. Consequently, one molecular inter-player contacts a conserved germline encoding region at the $\gamma\delta$ TCR, whereas the other senses antigen inducing a crucial conformational molecular twist that engages TCR signalling and resulting immune response. This singular indirect antigen-presentation mechanism is differs from the classical MHC-recognition system; and importantly, it shares homology with other members of the BTN family involved in the regulation of $\gamma\delta$ T cells, regardless species origin (Di Marco Barros et al., 2016; Melandri et al., 2018; Willcox et al., 2019). Moreover, establishing human-organoid cell cultures facilitates the study of the Vγ9Vδ2 T-cell subset under laboratory conditions to further examine their role in the tumour microenvironment milieu under the presence of amino-bisphosphonate drugs. Thus, understanding of these mechanistic processes within human biopsy samples may potentiate the development of $\gamma\delta$ T cell-based immunotherapies extrapolated to many diseases, including pathogenic infections, tissue homeostasis, and cancer.

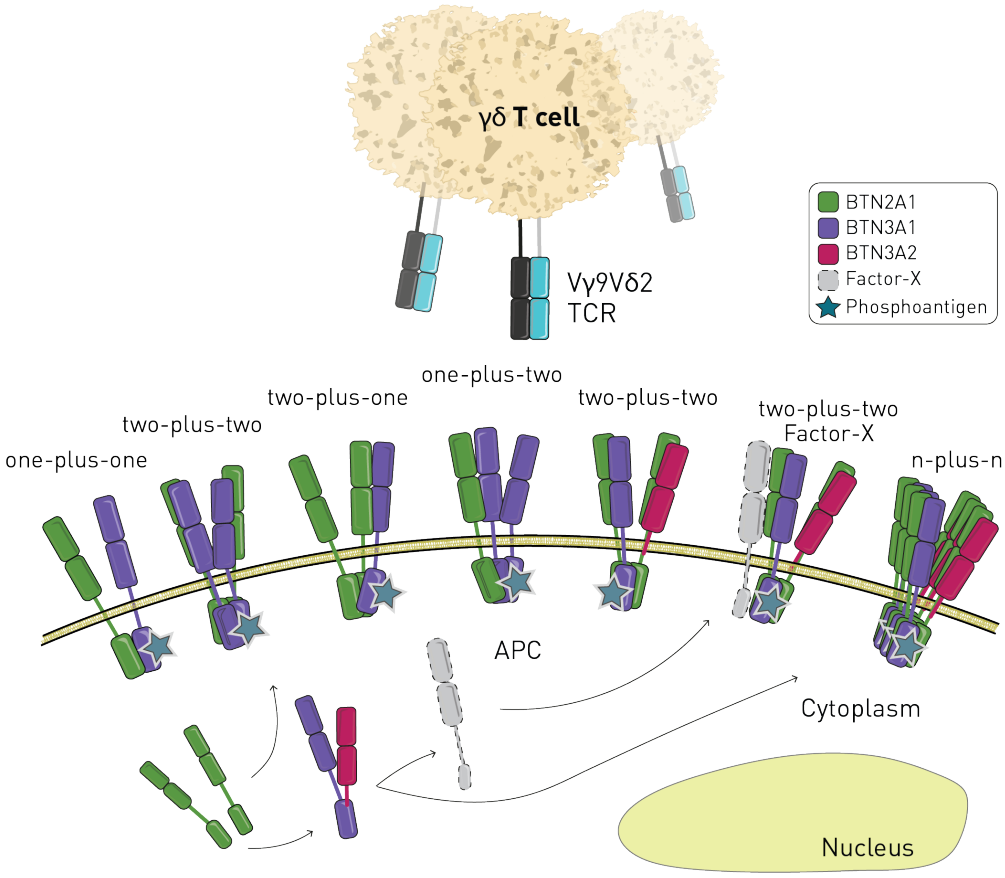

Figure 6.2: *Different theoretical antigen-presentation multi-complex models that upon arrangement and correct structural conformation, indirectly present small phosphoantigens that are present inside professional antigen-presenting, infected, or dysregulated cells.*

6.7 Future Work

How $\gamma\delta$ T cells recognise phosphoantigens was a burning question since reports described they have essential roles in rendering immune responses to pathogenic infections and tissue disorders like cancer. The work in this thesis represents a step forward in finding BTN2A1 cooperates with BTN3A1 and together induce rapid $\gamma\delta$ T-cell innate-like responses. The absence of Vγ9Vδ2 T-cell type and respective BTN cluster in the rodent genome makes it difficult and hampers the use of mouse animal models to study this system. Therefore, the role of these Vγ9Vδ2 T cells in tumour organoids embedded in a complex culture media which preserves the tumour-cell heterogeneity and immune spectrum of in-situ tissue samples was examined. The prevalence of the Vγ9Vδ2 T-cell subset in this organoids is flawed like some studies have found previously (Inman et al., 2008). However, there is controversy as several reports have shown that this Vγ9Vδ2 T-cell type could have a potential role in the tumour immunosurveillance of some cancer tissues, especially the kidney (Kobayashi et al., 2001; Viey et al., 2005). Stimulating this small population of infiltrated Vγ9Vδ2 T cells by treating the organoid cultures with zoledronate and observe whether these cells expand or induce a broader immune response after treatment could become interesting experiments. Under this condition, cancer cells may indirectly increment phosphoantigen levels and potentiate the phosphoantigen-presentation mechanisms to the few infiltrated Vγ9Vδ2 T cells. A time-line follow-up count and determination of any increase in the infiltrated population of $\gamma\delta$ T cells could deduce whether this subset activates and undergoes clonotype expansion. Similarly, the evaluation in the organoid size over time and cancer cell survival may provide indirect methods to estimate the immune efficiency potential induced by phosphoantigen-induced $\gamma\delta$ T cells compared to untreated samples.

Besides, the understanding of clonotypic variations that define high-specific phosphoantigen-reactive $\gamma\delta$ T-cells clones and their associated gene expression profiles which decide whether these lymphocytes turn in cytotoxic or adaptive helper-like cell types is of interest for using Vγ9Vδ2 T cells in the clinic. Today, the gene expression profiles of phosphoantigen-reactive T cells are puny and outdated compared to the state-of-the-art sequencing technology currently available. A study reported a list of the most murine transcript genes by serial analysis of gene expression in intraepithelial $\gamma\delta$ T cells (Shires et al., 2001) Titration of phosphoantigens, some Jurkat-reporter line expressing the specific clonotype G115 were less reactive to HMBPP than polyclonal purified-expanded V$\delta2^+$ T cells, wheres their reaction to zoledronate was comparable in the relative number of responding cells (Fig. 5.8). Also,

another study reported the gene expression profile of a bulk sequencing of human phosphoantigen-reactive $\gamma\delta$ T cells. This study denoted the transcriptomes after six hours post-stimulus with microbial phosphoantigen differed from the same analysis done a week after, whose transcriptome was comparable to that of a fortnight analysis of zoledronate-stimulated cells (Pont et al., 2012). These data indicate the gene transcripts varies after time post-phosphoantigen exposure but missed comparing same timepoints with different phosphoantigen stimulus.

On the other side, Starick et al. (2017) defines that there is a differential sensibility to activate Vγ9Vδ2 T-cell clones after an agonist antibody activity, and probably some differ from sensing microbial phosphoantigen HMBPP. Davey et al. (2018) reported the latest clonotypic analysis characterising distinct compartments of Vδ2^{+} T cells, and explicitly showing the diversity within the CDR3 segments, which emphasised the diversity in the Vγ9Vδ2 T-cell subset relayed on the CDR3δ fragments. The $\gamma\delta$ T-cell reactivity to phosphoantigens extends further from the CDR segments. Clonotyping phosphoantigen-reactive $\gamma\delta$TCRs could provide the broad picture of which residues are more necessary to confer reactivity, and linking clonotype data to respective single-cell sequenced transcriptomes could infer whether there are some clonotype features that show tendency to result in particular defined immune responses. This type of experiments have been performed in canonical $\alpha\beta$ T cells but none in $\gamma\delta$ T cells. Thus, we could provide the basis for sequencing single-cell $\gamma\delta$ T cells similarly to the most recent protocols described today (Gierahn et al., 2017; Macosko et al., 2015; Tu et al., 2019).

Bibliography

Lucie Abeler-Dörner, Mahima Swamy, Gareth Williams, Adrian C Hayday, and Anna Bas. Butyrophilins: an emerging family of immune regulators. *Trends Immunol*, 33(1):34–41, Jan 2012. doi: 10.1016/j.it.2011.09.007.

Erin J Adams and Adrienne M Luoma. The adaptable major histocompatibility complex (mhc) fold: structure and function of nonclassical and mhc class i-like molecules. *Annu Rev Immunol*, 31:529–61, Jan 2013. doi: 10.1146/annurev-immunol-032712-095912.

Erin J Adams, Pavel Strop, Sunny Shin, Yueh-Hsiu Chien, and K Christopher Garcia. An autonomous CDR3δ is sufficient for recognition of the nonclassical MHC class I molecules T10 and T22 by $\gamma\delta$ T cells. *Nat Immunol*, 9(7):777–84, Jul 2008. doi: 10.1038/ni.1620.

Erin J Adams, Siyi Gu, and Adrienne M Luoma. Human gamma delta t cells: Evolution and ligand recognition. *Cell Immunol*, 296(1):31–40, Jul 2015. doi: 10.1016/j.cellimm.2015.04.008.

Hassnae Afrache, Pierre Pontarotti, Laurent Abi-Rached, and Daniel Olive. Evolutionary and polymorphism analyses reveal the central role of BTN3A2 in the concerted evolution of the BTN3 gene family. *Immunogenetics*, 69(6):379–390, 06 2017. doi: 10.1007/s00251-017-0980-z.

Johanna Aigner, Sergi Villatoro, Raquel Rabionet, Jaume Roquer, Jordi Jiménez-Conde, Eulàlia Martí, and Xavier Estivill. A common 56-kilobase deletion in a primate-specific segmental duplication creates a novel butyrophilin-like protein. *BMC Genet*, 14:61, Jul 2013. doi: 10.1186/1471-2156-14-61.

Timothy J Allison and David N Garboczi. Structure of gammadelta T cell receptors and their recognition of non-peptide antigens. *Mol Immunol*, 38(14):1051–61, May 2002. doi: 10.1016/s0161-5890(02)00034-2.

Timothy J. Allison, Christine C. Winter, Jean-Jacques Fournié, Marc Bonneville, and David N. Garboczi. Structure of a human $\gamma\delta$T-cell antigen receptor. *Nature*, 411(6839):820–824, Jun 2001. doi: 10.1038/35081115.

Heather A. Arnett and Joanne L. Viney. Immune modulation by butyrophilins. *Nature Reviews Immunology*, 14(8):559–569, Jul 2014. ISSN 1474-1741. doi: 10.1038/nri3715.

Heather A Arnett, Sabine S Escobar, Eva Gonzalez-Suarez, Alison L Budelsky, Lori A Steffen, Norman Boiani, Ming Zhang, Gerald Siu, Avery W Brewer, and Joanne L Viney. BTNL2, a butyrophilin/B7-like molecule, is a negative costimulatory molecule modulated in intestinal inflammation. *J Immunol*, 178(3):1523–33, Feb 2007. doi: 10.4049/jimmunol.178.3.1523.

Heather A Arnett, Sabine S Escobar, and Joanne L Viney. Regulation of costimulation in the era of butyrophilins. *Cytokine*, 46(3):370–5, Jun 2009. doi: 10.1016/j.cyto.2009.03.009.

J Banchereau and R M Steinman. Dendritic cells and the control of immunity. *Nature*, 392(6673):245–52, Mar 1998. doi: 10.1038/32588.

Anna Bas, Mahima Swamy, Lucie Abeler-Dörner, Gareth Williams, Dick J Pang, Susannah D Barbee, and Adrian C Hayday. Butyrophilin-like 1 encodes an enterocyte protein that selectively regulates functional interactions with T lymphocytes. *Proc Natl Acad Sci U S A*, 108(11):4376–81, Mar 2011. doi: 10.1073/pnas.1010647108.

Douglas Bates, Martin Mächler, Ben Bolker, and Steve Walker. Fitting linear mixed-effects models using lme4. *Journal of Statistical Software*, 67(1):1–48, 2015. doi: 10.18637/jss.v067.i01.

S Bauer, V Groh, J Wu, A Steinle, J H Phillips, L L Lanier, and T Spies. Activation of NK cells and T cells by NKG2D, a receptor for stress-inducible MICA. *Science*, 285(5428):727–9, Jul 1999. doi: 10.1126/science.285.5428.727.

Andreas Behren, Matthew Anaka, Pu-Han Lo, Laura J Vella, Ian D Davis, Jenny Catimel, Tracy Cardwell, Craig Gedye, Christopher Hudson, Rodica Stan, and Jonathan Cebon. The ludwig institute for cancer research melbourne melanoma cell line panel. *Pigment Cell Melanoma Res*, 26(4):597–600, Jul 2013. doi: 10.1111/pcmr.12097.

C Belles, A Kuhl, R Nosheny, and S R Carding. Plasma membrane expression of heat shock protein 60 in vivo in response to infection. *Infect Immun*, 67(8):4191–200, Aug 1999.

C Belmant, E Espinosa, F Halary, Y Tang, M A Peyrat, H Sicard, A Kozikowski, R Buelow, R Poupot, M Bonneville, and J J Fournié. A chemical basis for selective recognition of nonpeptide antigens by human δ T cells. *FASEB J*, 14(12):1669–70, Sep 2000. doi: 10.1096/fj.99-0909fje.

A Bendelac, N Killeen, D Littman, and R Schwartz. A subset of $CD4^+$ thymocytes selected by MHC class I molecules. *Science*, 263(5154):1774–1778, Mar 1994. ISSN 0036-8075. doi: 10.1126/science.7907820.

Jaafar Bennouna, Vincent Levy, Hélène Sicard, Hélène Senellart, Marie Audrain, Sandrine Hiret, Frédéric Rolland, Heriberto Bruzzoni-Giovanelli, Marie Rimbert, Céline Galéa, Jérome Tiollier, and Fabien Calvo. Phase i study of bromohydrin pyrophosphate (BrHPP, IPH 1101), a Vγ9Vδ2 T lymphocyte agonist in patients with solid tumors. *Cancer Immunol Immunother*, 59(10):1521–30, Oct 2010. doi: 10.1007/s00262-010-0879-0.

Patricia M Benveniste, Sobhan Roy, Munehide Nakatsugawa, Edward L Y Chen, Linh Nguyen, Douglas G Millar, Pamela S Ohashi, Naoto Hirano, Erin J Adams, and Juan Carlos Zúñiga-Pflücker. Generation and molecular recognition of melanoma-associated antigen-specific human $\gamma\delta$ T cells. *Sci Immunol*, 3(30), Dec 2018. doi: 10.1126/sciimmunol.aav4036.

Ismahène Benzaïd, Hannu Mönkkönen, Verena Stresing, Edith Bonnelye, Jonathan Green, Jukka Mönkkönen, Jean-Louis Touraine, and Philippe Clézardin. High phosphoantigen levels in bisphosphonate-treated human breast tumors promote vγ9vδ2 T-cell chemotaxis and cytotoxicity in vivo. *Cancer Res*, 71(13):4562–72, Jul 2011. doi: 10.1158/0008-5472.CAN-10-3862.

Helen M. Berman, John Westbrook, Zukang Feng, Gary Gilliland, T. N. Bhat, Helge Weissig, Ilya N. Shindyalov, and Philip E. Bourne. The Protein Data Bank. *Nucleic Acids Research*, 28(1):235–242, 01 2000. ISSN 0305-1048. doi: 10.1093/nar/28.1.235.

Benjamin Bian, Daniele Fanale, Nelson Dusetti, Julie Roque, Sonia Pastor, Anne-Sophie Chretien, Lorena Incorvaia, Antonio Russo, Daniel Olive, and Juan Iovanna. Prognostic significance of circulating PD-1, PD-L1, pan-BTN3As, BTN3A1 and BTLA in patients with pancreatic adenocarcinoma. *Oncoimmunology*, 8(4):e1561120, 2019. doi: 10.1080/2162402X.2018.1561120.

Angélique Boëdec, Hélène Sicard, Jean Dessolin, Gaëtan Herbette, Sophie Ingoure, Cédric Raymond, Christian Belmant, and Jean-Louis Kraus. Synthesis and biological activity of phosphonate analogues and geometric isomers of the highly potent phosphoantigen (E)-1-hydroxy-2-methylbut-2-enyl 4-diphosphate. *J Med Chem*, 51(6):1747–54, Mar 2008. doi: 10.1021/jm701101g.

M Bonneville, K Ito, E G Krecko, S Itohara, D Kappes, I Ishida, O Kanagawa, C A Janeway, D B Murphy, and S Tonegawa. Recognition of a self major histocompatibility complex TL region product by gamma delta T-cell receptors. *Proc Natl Acad Sci U S A*, 86(15):5928–32, Aug 1989. doi: 10.1073/pnas.86.15.5928.

Marc Bonneville, Rebecca L O'Brien, and Willi K Born. $\gamma\delta$ T cell effector functions: a blend of innate programming and acquired plasticity. *Nat Rev Immunol*, 10(7):467–78, Jul 2010. doi: 10.1038/nri2781.

W H Boom, K A Chervenak, M A Mincek, and J J Ellner. Role of the mononuclear phagocyte as an antigen-presenting cell for human $\gamma\delta$ T cells activated by live ycobacterium tuberculosis. *Infect Immun*, 60(9):3480–8, Sep 1992.

Natalie A Borg, Kwok S Wun, Lars Kjer-Nielsen, Matthew C J Wilce, Daniel G Pellicci, Ruide Koh, Gurdyal S Besra, Mandvi Bharadwaj, Dale I Godfrey, James McCluskey, and Jamie Rossjohn. Cd1d-lipid-antigen recognition by the semi-invariant nkt t-cell receptor. *Nature*, 448(7149):44–9, Jul 2007. doi: 10.1038/nature05907.

W K Born, M Vollmer, C Reardon, E Matsuura, D R Voelker, P C Giclas, and R L O'Brien. Hybridomas expressing gammadelta t-cell receptors respond to cardiolipin and beta2-glycoprotein 1 (apolipoprotein h). *Scand J Immunol*, 58(3):374–81, Sep 2003. doi: 10.1046/j.1365-3083.2003.01315.x.

Francoise Bouet-Toussaint, Florian Cabillic, Olivier Toutirais, Matthieu Le Gallo, Cécile Thomas de la Pintière, Pascale Daniel, Noëlle Genetet, Bernard Meunier, Eric Dupont-Bierre, Karim Boudjema, and Véronique Catros. Vγ9Vδ2 T cell-mediated recognition of human solid tumors. potential for immunotherapy of hepatocellular and colorectal carcinomas. *Cancer Immunol Immunother*, 57(4): 531–9, Apr 2008. doi: 10.1007/s00262-007-0391-3.

Lynn M Boyden, Julia M Lewis, Susannah D Barbee, Anna Bas, Michael Girardi, Adrian C Hayday, Robert E Tigelaar, and Richard P Lifton. Skint1, the prototype of a newly identified immunoglobulin superfamily gene cluster, positively selects epidermal $\gamma\delta$ T cells. *Nat Genet*, 40(5):656–62, May 2008. doi: 10.1038/ng.108.

Marlène Brandes, Katharina Willimann, and Bernhard Moser. Professional antigen-presentation function by human $\gamma\delta$ T cells. *Science*, 309(5732):264–8, Jul 2005. doi: 10.1126/science.1110267.

Marlène Brandes, Katharina Willimann, Gilles Bioley, Nicole Lévy, Matthias Eberl, Ming Luo, Robert Tampé, Frédéric Lévy, Pedro Romero, and Bernhard Moser. Cross-presenting human $\gamma\delta$ T cells induce robust CD8+ $\alpha\beta$ T cell responses. *Proc Natl Acad Sci U S A*, 106(7):2307–12, Feb 2009. doi: 10.1073/pnas.0810059106.

M B Brenner, J McLean, D P Dialynas, J L Strominger, J A Smith, F L Owen, J G Seidman, S Ip, F Rosen, and M S Krangel. Identification of a putative second T-cell receptor. *Nature*, 322(6075): 145–9, Jul 1986. doi: 10.1038/322145a0.

Jessica Bruder, Katherina Siewert, Birgit Obermeier, Joachim Malotka, Peter Scheinert, Josef Kellermann, Takuya Ueda, Reinhard Hohlfeld, and Klaus Dornmair. Target specificity of an autoreactive pathogenic human $\gamma\delta$-T cell receptor in myositis. *J Biol Chem*, 287(25):20986–95, Jun 2012. doi: 10.1074/jbc.M112.356709.

Clara Bueno, Caitlin D Lemke, Gabriel Criado, Miren L Baroja, Stephen S G Ferguson, A K M Nur-Ur Rahman, Constantine D Tsoukas, John K McCormick, and Joaquin Madrenas. Bacterial superantigens bypass Lck-dependent T cell receptor signaling by activating a Gα11-dependent, PLC-β-mediated pathway. *Immunity*, 25(1):67–78, Jul 2006. doi: 10.1016/j.immuni.2006.04.012.

J F Bukowski, C T Morita, H Band, and M B Brenner. Crucial role of TCR gamma chain junctional region in prenyl pyrophosphate antigen recognition by gamma delta T cells. *Journal of immunology (Baltimore, Md. : 1950)*, 161(1):286–93, Apr 1998. ISSN 0022-1767.

Jack F Bukowski, Craig T Morita, and Michael B Brenner. Human $\gamma\delta$ T cells recognize alkylamines derived from microbes, edible plants, and tea: Implications for innate immunity. *Immunity*, 11(1): 57–65, Jul 1999. ISSN 1074-7613. doi: 10.1016/S1074-7613(00)80081-3.

Maka Burjanadzé, Maud Condomines, Thierry Reme, Philippe Quittet, Pascal Latry, Cécile Lugagne, François Romagne, Yanis Morel, Jean François Rossi, Bernard Klein, and Zhao Yang Lu. In vitro expansion of $\gamma\delta$ T cells with anti-myeloma cell activity by Phosphostim and IL-2 in patients with multiple myeloma. *Br J Haematol*, 139(2):206–16, Oct 2007. doi: 10.1111/j.1365-2141.2007.06754.x.

Manish J Butte, Mary E Keir, Theresa B Phamduy, Arlene H Sharpe, and Gordon J Freeman. Programmed death-1 ligand 1 interacts specifically with the B7-1 costimulatory molecule to inhibit T cell responses. *Immunity*, 27(1):111–22, Jul 2007. doi: 10.1016/j.immuni.2007.05.016.

Nadia Caccamo, Luca Battistini, Marc Bonneville, Fabrizio Poccia, Jean Jacques Fournié, Serena Meraviglia, Giovanna Borsellino, Richard A Kroczek, Carmela La Mendola, Emmanuel Scotet, Francesco Dieli, and Alfredo Salerno. CXCR5 identifies a subset of Vγ9Vδ2 T cells which secrete IL-4 and IL-10 and help B cells for antibody production. *J Immunol*, 177(8):5290–5, Oct 2006. doi: 10.4049/jimmunol.177.8.5290.

Cristiana Cairo, Cheryl L Armstrong, Jean Saville Cummings, Carl O Deetz, Ming Tan, Changwan Lu, Charles E Davis, and C David Pauza. Impact of age, gender, and race on circulating $\gamma\delta$ T cells. *Hum Immunol*, 71(10):968–75, Oct 2010. doi: 10.1016/j.humimm.2010.06.014.

Simon R Carding and Paul J Egan. $\gamma\delta$ T cells: functional plasticity and heterogeneity. *Nat Rev Immunol*, 2(5):336–45, May 2002. doi: 10.1038/nri797.

Jae Jin Chae, Geryl Wood, Katharina Richard, Howard Jaffe, Nona T Colburn, Seth L Masters, Deborah L Gumucio, Nitza G Shoham, and Daniel L Kastner. The familial mediterranean fever protein, pyrin, is cleaved by caspase-1 and activates NF-κB through its N-terminal fragment. *Blood*, 112(5): 1794–803, Sep 2008. doi: 10.1182/blood-2008-01-134932.

Crystal Y Chen, Shuyu Yao, Dan Huang, Huiyong Wei, Helene Sicard, Gucheng Zeng, Hassan Jomaa, Michelle H Larsen, William R Jacobs, Jr, Richard Wang, Norman Letvin, Yun Shen, Liyou Qiu, Ling Shen, and Zheng W Chen. Phosphoantigen/IL2 expansion and differentiation of Vγ2Vδ2 T cells increase resistance to tuberculosis in nonhuman primates. *PLoS Pathog*, 9(8):e1003501, Aug 2013. doi: 10.1371/journal.ppat.1003501.

Qingyun Chen, Kun Wen, Aizhen Lv, Ming Liu, Ke Ni, Zheng Xiang, Yinping Liu, and Wenwei Tu. Human Vγ9Vδ2-T cells synergize CD4$^+$ T follicular helper cells to produce influenza virus-specific antibody. *Front Immunol*, 9:599, 2018. doi: 10.3389/fimmu.2018.00599.

Sidi Chen, Neville E Sanjana, Kaijie Zheng, Ophir Shalem, Kyungheon Lee, Xi Shi, David A Scott, Jun Song, Jen Q Pan, Ralph Weissleder, Hakho Lee, Feng Zhang, and Phillip A Sharp. Genome-wide CRISPR screen in a mouse model of tumor growth and metastasis. *Cell*, 160(6):1246–60, Mar 2015. doi: 10.1016/j.cell.2015.02.038.

Yong Chen, Lingyun Shao, Zahida Ali, Jiye Cai, and Zheng W Chen. NSOM/QD-based nanoscale immunofluorescence imaging of antigen-specific T-cell receptor responses during an in vivo clonal Vγ2Vδ2 T-cell expansion. *Blood*, 111(8):4220–32, Apr 2008. doi: 10.1182/blood-2007-07-101691.

Marie Cherrier, Shinichiro Sawa, and Gérard Eberl. Notch, Id2, and RORγt sequentially orchestrate the fetal development of lymphoid tissue inducer cells. *J Exp Med*, 209(4):729–40, Apr 2012. doi: 10.1084/jem.20111594.

Yueh-hsiu Chien, Christina Meyer, and Marc Bonneville. $\gamma\delta$ T cells: First line of defense and beyond. *Annual Review of Immunology*, 32(1):121 155, Jan 2014. ISSN 0732-0582. doi: 10.1146/annurev-immunol-032713-120216.

Grzegorz Chodaczek, Veena Papanna, M Anna Zal, and Tomasz Zal. Body-barrier surveillance by epidermal $\gamma\delta$ TCRs. *Nat Immunol*, 13(3):272–82, Feb 2012. doi: 10.1038/ni.2240.

S P Clark, B Arden, D Kabelitz, and T W Mak. Comparison of human and mouse T-cell receptor variable gene segment subfamilies. *Immunogenetics*, 42(6):531–40, 1995. doi: 10.1007/BF00172178.

F Cocchi, A L DeVico, A Garzino-Demo, S K Arya, R C Gallo, and P Lusso. Identification of RANTES, MIP-1α, and MIP-1β as the major HIV-suppressive factors produced by CD8$^+$ T cells. *Science*, 270 (5243):1811–5, Dec 1995. doi: 10.1126/science.270.5243.1811.

David K Cole, Nicholas J Pumphrey, Jonathan M Boulter, Malkit Sami, John I Bell, Emma Gostick, David A Price, George F Gao, Andrew K Sewell, and Bent K Jakobsen. Human TCR-binding affinity is governed by MHC class restriction. *J Immunol*, 178(9):5727–34, May 2007. doi: 10.4049/jimmunol.178.9.5727.

P Constant, Y Poquet, M A Peyrat, F Davodeau, M Bonneville, and J J Fournié. The antituberculous mycobacterium bovis BCG vaccine is an attenuated mycobacterial producer of phosphorylated nonpeptidic antigens for human gamma delta T cells. *Infection and Immunity*, 63(12):4628–4633, Jun 1995. ISSN 0019-9567.

Alexandra J Corbett, Sidonia B G Eckle, Richard W Birkinshaw, Ligong Liu, Onisha Patel, Jennifer Mahony, Zhenjun Chen, Rangsima Reantragoon, Bronwyn Meehan, Hanwei Cao, Nicholas A Williamson, Richard A Strugnell, Douwe Van Sinderen, Jeffrey Y W Mak, David P Fairlie, Lars Kjer-Nielsen, Jamie Rossjohn, and James McCluskey. T-cell activation by transitory neo-antigens derived from distinct microbial pathways. *Nature*, 509(7500):361–5, May 2014. doi: 10.1038/nature13160.

Adriana Cordova, Francesca Toia, Carmela La Mendola, Valentina Orlando, Serena Meraviglia, Gaetana Rinaldi, Matilde Todaro, Giuseppe Cicero, Leonardo Zichichi, Paolo Li Donni, Nadia Caccamo, Giorgio Stassi, Francesco Dieli, and Francesco Moschella. Characterization of human $\gamma\delta$ T lymphocytes infiltrating primary malignant melanomas. *PLoS One*, 7(11):e49878, 2012. doi: 10.1371/journal.pone.0049878.

Murielle Corvaisier, Agnès Moreau-Aubry, Elisabeth Diez, Jaafar Bennouna, Jean-Francois Mosnier, Emmanuel Scotet, Marc Bonneville, and Francine Jotereau. Vγ9Vδ2 T cell response to colon carcinoma cells. *J Immunol*, 175(8):5481–8, Oct 2005. doi: 10.4049/jimmunol.175.8.5481.

Giulia Costa, Séverine Loizon, Marianne Guenot, Iulia Mocan, Franck Halary, Geneviève de Saint-Basile, Vincent Pitard, Julie Déchanet-Merville, Jean-François Moreau, Marita Troye-Blomberg, Odile Mercereau-Puijalon, and Charlotte Behr. Control of plasmodium falciparum erythrocytic cycle: $\gamma\delta$ T cells target the red blood cell-invasive merozoites. *Blood*, 118(26):6952–62, Dec 2011. doi: 10.1182/blood-2011-08-376111.

Rachel N Cotton, Adam Shahine, Jamie Rossjohn, and D Branch Moody. Sciencedirect lipids hide or step aside for CD1-autoreactive T cell receptors. *Current Opinion in Immunology*, 52(Cell 80 1995): 93 99, May 2018. ISSN 0952-7915. doi: 10.1016/j.coi.2018.04.013.

M P Crowley, A M Fahrer, N Baumgarth, J Hampl, I Gutgemann, L Teyton, and Y Chien. A population of murine gammadelta t cells that recognize an inducible mhc class ib molecule. *Science*, 287(5451): 314–6, Jan 2000. doi: 10.1126/science.287.5451.314.

Stefan M Czerniecki, Nelly M Cruz, Jennifer L Harder, Rajasree Menon, James Annis, Edgar A Otto, Ramila E Gulieva, Laura V Islas, Yong Kyun Kim, Linh M Tran, Timothy J Martins, Jeffrey W Pippin, Hongxia Fu, Matthias Kretzler, Stuart J Shankland, Jonathan Himmelfarb, Randall T Moon, Neal Paragas, and Benjamin S Freedman. High-throughput screening enhances kidney organoid differentiation from human pluripotent stem cells and enables automated multidimensional phenotyping. *Cell Stem Cell*, 22(6):929–940.e4, Jun 2018. doi: 10.1016/j.stem.2018.04.022.

Yumei Dai, Hui Chen, Chen Mo, Lianxian Cui, and Wei He. Ectopically expressed human tumor biomarker MutS homologue 2 is a novel endogenous ligand that is recognized by human $\gamma\delta$ T cells to induce innate anti-tumor/virus immunity. *J Biol Chem*, 287(20):16812–9, May 2012. doi: 10.1074/jbc.M111.327650.

Patricia A Darrah, Joseph J Zeppa, Pauline Maiello, Joshua A Hackney, Marc H Wadsworth, 2nd, Travis K Hughes, Supriya Pokkali, Phillip A Swanson, 2nd, Nicole L Grant, Mark A Rodgers, Megha Kamath, Chelsea M Causgrove, Dominick J Laddy, Aurelio Bonavia, Danilo Casimiro, Philana Ling Lin, Edwin Klein, Alexander G White, Charles A Scanga, Alex K Shalek, Mario Roederer, JoAnne L Flynn, and Robert A Seder. Prevention of tuberculosis in macaques after intravenous bcg immunization. *Nature*, 577(7788):95–102, 01 2020. doi: 10.1038/s41586-019-1817-8.

H Das, V Groh, C Kuijl, M Sugita, C T Morita, T Spies, and J F Bukowski. MICA engagement by human Vγ2Vδ2 T cells enhances their antigen-dependent effector function. *Immunity*, 15(1):83–93, Jul 2001a. doi: 10.1016/s1074-7613(01)00168-6.

H Das, L Wang, A Kamath, and J F Bukowski. Vγ2vδ2 T-cell receptor-mediated recognition of aminobisphosphonates. *Blood*, 98(5):1616–8, Sep 2001b. doi: 10.1182/blood.v98.5.1616.

Martin S Davey, Carrie R Willcox, Stuart Hunter, Sofya A Kasatskaya, Ester B M Remmerswaal, Mahboob Salim, Fiyaz Mohammed, Frederike J Bemelman, Dmitriy M Chudakov, Ye H Oo, and Benjamin E Willcox. The human Vδ2$^+$ T-cell compartment comprises distinct innate-like Vγ9$^+$ and adaptive Vγ9$^-$ subsets. *Nat Commun*, 9(1):1760, 05 2018. doi: 10.1038/s41467-018-04076-0.

F Davodeau, M A Peyrat, M M Hallet, I Houde, H Vie, and M Bonneville. Peripheral selection of antigen receptor junctional features in a major human $\gamma\delta$ subset. *Eur J Immunol*, 23(4):804–8, Apr 1993. doi: 10.1002/eji.1830230405.

Akshay A D'Cruz, Jeffrey J Babon, Raymond S Norton, Nicos A Nicola, and Sandra E Nicholson. Structure and function of the SPRY/B30.2 domain proteins involved in innate immunity. *Protein Sci*, 22(1):1–10, Jan 2013. doi: 10.1002/pro.2185.

Renée C G de Bruin, John P Veluchamy, Sinéad M Lougheed, Famke L Schneiders, Silvia Lopez-Lastra, Roeland Lameris, Anita G Stam, Zsolt Sebestyen, Jürgen Kuball, Carla F M Molthoff, Erik Hooijberg, Rob C Roovers, James P Di Santo, Paul M P van Bergen En Henegouwen, Henk M W Verheul, Tanja D de Gruijl, and Hans J van der Vliet. A bispecific nanobody approach to leverage the potent and widely applicable tumor cytolytic capacity of Vγ9Vδ2-T cells. *Oncoimmunology*, 7(1): e1375641, May 2017. doi: 10.1080/2162402X.2017.1375641.

Annemieke de Jong, Tan-Yun Cheng, Shouxiong Huang, Stephanie Gras, Richard W Birkinshaw, Anne G Kasmar, Ildiko Van Rhijn, Victor Peña-Cruz, Daniel T Ruan, John D Altman, Jamie Rossjohn, and D Branch Moody. CD1a-autoreactive T cells recognize natural skin oils that function as headless antigens. *Nat Immunol*, 15(2):177–85, Feb 2014. doi: 10.1038/ni.2790.

Drew C Deniger, Kirsten Switzer, Tiejuan Mi, Sourindra Maiti, Lenka Hurton, Harjeet Singh, Helen Huls, Simon Olivares, Dean A Lee, Richard E Champlin, and Laurence J N Cooper. Bispecific T-cells expressing polyclonal repertoire of endogenous $\gamma\delta$ T-cell receptors and introduced CD19-specific chimeric antigen receptor. *Mol Ther*, 21(3):638–47, Mar 2013. doi: 10.1038/mt.2012.267.

Katrien Deroost and Jean Langhorne. Gamma/Delta T cells and their role in protection against malaria. *Front Immunol*, 9:2973, Dec 2018. doi: 10.3389/fimmu.2018.02973.

K Deusch, F Lüling, K Reich, M Classen, H Wagner, and K Pfeffer. A major fraction of human intraepithelial lymphocytes simultaneously expresses the γ/δ T cell receptor, the CD8 accessory molecule and preferentially uses the Vδ1 gene segment. *Eur J Immunol*, 21(4):1053–9, Apr 1991. doi: 10.1002/eji.1830210429.

Swati Dhar and Shubhada V. Chiplunkar. Lysis of aminobisphosphonate-sensitized MCF-7 breast tumor cells by Vγ9Vδ2 T cells. *Cancer Immunity Archive*, 10(1), Nov 2010. ISSN 1424-9634.

Rafael Di Marco Barros, Natalie A Roberts, Robin J Dart, Pierre Vantourout, Anett Jandke, Oliver Nussbaumer, Livija Deban, Sara Cipolat, Rosie Hart, Maria Luisa Iannitto, Adam Laing, Bradley Spencer-Dene, Philip East, Deena Gibbons, Peter M Irving, Pablo Pereira, Ulrich Steinhoff, and Adrian Hayday. Epithelia use butyrophilin-like molecules to shape organ-specific $\gamma\delta$ T cell compartments. *Cell*, 167(1):203–218, Sep 2016. doi: 10.1016/j.cell.2016.08.030.

Mélanie Dieudé, Harald Striegl, Aaron J Tyznik, Jing Wang, Samuel M Behar, Ciriaco A Piccirillo, Jerrold S Levine, Dirk M Zajonc, and Joyce Rauch. Cardiolipin binds to CD1d and stimulates CD1d-restricted $\gamma\delta$ T cells in the normal murine repertoire. *J Immunol*, 186(8):4771–81, Apr 2011. doi: 10.4049/jimmunol.1000921.

Tanya Dimova, Margreet Brouwer, Françoise Gosselin, Joël Tassignon, Oberdan Leo, Catherine Donner, Arnaud Marchant, and David Vermijlen. Effector Vγ9Vδ2 T cells dominate the human fetal $\gamma\delta$ T-cell repertoire. *Proc Natl Acad Sci U S A*, 112(6):E556–65, Feb 2015. doi: 10.1073/pnas.1412058112.

James E. Dunford, Keith Thompson, Fraser P. Coxon, Steven P. Luckman, Frederick M. Hahn, C. Dale Poulter, Frank H. Ebetino, and Michael J. Rogers. Structure-activity relationships for inhibition of farnesyl diphosphate synthase in vitro and inhibition of bone resorption in vivo by nitrogen-containing bisphosphonates. *Journal of Pharmacology and Experimental Therapeutics*, 296(2):235–242, Oct 2001. ISSN 0022-3565.

Matthias Eberl, Martin Hintz, Armin Reichenberg, Ann-Kristin Kollas, Jochen Wiesner, and Hassan Jomaa. Microbial isoprenoid biosynthesis and human $\gamma\delta$ T cell activation. *FEBS Lett*, 544(1-3): 4–10, Jun 2003. doi: 10.1016/s0014-5793(03)00483-6.

Matthias Eberl, Hassan Jomaa, and Adrian C Hayday. Integrated immune responses to infection - cross-talk between human gammadelta T cells and dendritic cells. *Immunology*, 112(3):364–8, Jul 2004. doi: 10.1111/j.1365-2567.2004.01921.x.

Lisa M Ebert, Simone Meuter, and Bernhard Moser. Homing and function of human skin $\gamma\delta$ T cells and NK cells: relevance for tumor surveillance. *J Immunol*, 176(7):4331–6, Apr 2006. doi: 10.4049/jimmunol.176.7.4331.

Sidonia B G Eckle, Richard W Birkinshaw, Lyudmila Kostenko, Alexandra J Corbett, Hamish E G McWilliam, Rangsima Reantragoon, Zhenjun Chen, Nicholas A Gherardin, Travis Beddoe, Ligong Liu, Onisha Patel, Bronwyn Meehan, David P Fairlie, Jose A Villadangos, Dale I Godfrey, Lars Kjer-Nielsen, James McCluskey, and Jamie Rossjohn. A molecular basis underpinning the T cell receptor heterogeneity of mucosal-associated invariant T cells. *J Exp Med*, 211(8):1585–600, Jul 2014. doi: 10.1084/jem.20140484.

W Eisenreich, A Bacher, D Arigoni, and F Rohdich. Biosynthesis of isoprenoids via the non-mevalonate pathway. *Cell Mol Life Sci*, 61(12):1401–26, Jun 2004. doi: 10.1007/s00018-004-3381-z.

S Noushin Emami, Bo G Lindberg, Susanna Hua, Sharon R Hill, Raimondas Mozuraitis, Philipp Lehmann, Göran Birgersson, Anna-Karin Borg-Karlson, Rickard Ignell, and Ingrid Faye. A key malaria metabolite modulates vector blood seeking, feeding, and susceptibility to infection. *Science*, 355(6329):1076–1080, 03 2017. doi: 10.1126/science.aah4563.

Eric Espinosa, Christian Belmant, Hélène Sicard, Rémy Poupot, Marc Bonneville, and Jean-Jacques Fournié. Y2K+1 state-of-the-art on non-peptide phosphoantigens, a novel category of immunostimulatory molecules. *Microbes and Infection*, 3(8):645 – 654, Jul 2001. ISSN 1286-4579.

Xiying Fan and Alexander Y Rudensky. Hallmarks of tissue-resident lymphocytes. *Cell*, 164(6):1198 1211, Mar 2016. ISSN 0092-8674. doi: 10.1016/j.cell.2016.02.048.

Juliane Feurle, Eric Espinosa, Susanne Eckstein, Frédéric Pont, Volker Kunzmann, Jean-Jacques Fournié, Markus Herderich, and Martin Wilhelm. *Escherichia coli* produces phosphoantigens activating human $\gamma\delta$ T cells. *J Biol Chem*, 277(1):148–54, Jan 2002. doi: 10.1074/jbc.M106443200.

Alina S. Fichtner, Mohindar M. Karunakaran, Siyi Gu, Christopher T. Boughter, Marta T. Borowska, Lisa Starick, Anna Nöhren, Thomas W. Göbel, Erin J. Adams, and Thomas Herrmann. Alpaca (Vicugna pacos), the first nonprimate species with a phosphoantigen-reactive vγ9vδ2 T cell subset. *Proceedings of the National Academy of Sciences*, 117(12):6697–6707, Feb 2020. ISSN 0027-8424. doi: 10.1073/pnas.1909474117.

B A Fields, E L Malchiodi, H Li, X Ysern, C V Stauffacher, P M Schlievert, K Karjalainen, and R A Mariuzza. Crystal structure of a T-cell receptor β-chain complexed with a superantigen. *Nature*, 384(6605):188–92, Nov 1996. doi: 10.1038/384188a0.

P Fisch, M Malkovsky, S Kovats, E Sturm, E Braakman, B S Klein, S D Voss, L W Morrissey, R DeMars, and W J Welch. Recognition by human vγ9/vδ2 T cells of a GroEL homolog on Daudi Burkitt's lymphoma cells. *Science*, 250(4985):1269–73, Nov 1990. doi: 10.1126/science.1978758.

Jonathan Fisher, Roshan Sharma, Dilu Wisidagamage Don, Marta Barisa, Marina Olle Hurtado, Pierre Abramowski, Lucy Porter, William Day, Roberto Borea, Sarah Inglott, John Anderson, and Dana Pe'er. Engineering $\gamma\delta$T cells limits tonic signaling associated with chimeric antigen receptors. *Sci Signal*, 12(598), 09 2019. doi: 10.1126/scisignal.aax1872.

Jason D Fontenot and Alexander Y Rudensky. A well adapted regulatory contrivance: regulatory T cell development and the forkhead family transcription factor Foxp3. *Nat Immunol*, 6(4):331–7, Apr 2005. doi: 10.1038/ni1179.

Stephan D Gadola, Nathan R Zaccai, Karl Harlos, Dawn Shepherd, Julio C Castro-Palomino, Gerd Ritter, Richard R Schmidt, E Yvonne Jones, and Vincenzo Cerundolo. Structure of human CD1b with bound ligands at 2.3 A, a maze for alkyl chains. *Nature Immunology*, 3(8):721 726, Jul 2002. ISSN 1529-2908. doi: 10.1038/ni821.

J J García-Vallejo, J M Ilarregui, H Kalay, S Chamorro, N Koning, W W Unger, M Ambrosini, V Montserrat, R J Fernandes, S C M Bruijns, J R T van Weering, N J Paauw, T O'Toole, J van Horssen, P van der Valk, K Nazmi, J G M Bolscher, J Bajramovic, C D Dijkstra, B A 't Hart, and Y van Kooyk. CNS myelin induces regulatory functions of DC-SIGN-expressing, antigen-presenting cells via cognate interaction with MOG. *J Exp Med*, 211(7):1465–83, Jun 2014. doi: 10.1084/jem.20122192.

Marvin H Gee, Leah V Sibener, Michael E Birnbaum, Kevin M Jude, Xinbo Yang, Ricardo A Fernandes, Juan L Mendoza, Caleb R Glassman, and K Christopher Garcia. Stress-testing the relationship between T cell receptor/peptide-MHC affinity and cross-reactivity using peptide velcro. *Proc Natl Acad Sci U S A*, 115(31):E7369–E7378, 07 2018. doi: 10.1073/pnas.1802746115.

De Libero Gennaro. Sentinel function of broadly reactive human $\gamma\delta$ T cells. *Immunology Today*, 18(1): 22 – 26, Jan 1997. ISSN 0167-5699. doi: 10.1016/S0167-5699(97)80010-2.

Andrew J Gentles, Aaron M Newman, Chih Long Liu, Scott V Bratman, Weiguo Feng, Dongkyoon Kim, Viswam S Nair, Yue Xu, Amanda Khuong, Chuong D Hoang, Maximilian Diehn, Robert B West, Sylvia K Plevritis, and Ash A Alizadeh. The prognostic landscape of genes and infiltrating immune cells across human cancers. *Nat Med*, 21(8):938–945, Aug 2015. doi: 10.1038/nm.3909.

D J Gerber, V Azuara, J P Levraud, S Y Huang, M P Lembezat, and P Pereira. Il-4-producing $\gamma\delta$ T cells that express a very restricted TCR repertoire are preferentially localized in liver and spleen. *J Immunol*, 163(6):3076–82, Sep 1999.

Todd M Gierahn, Marc H Wadsworth, 2nd, Travis K Hughes, Bryan D Bryson, Andrew Butler, Rahul Satija, Sarah Fortune, J Christopher Love, and Alex K Shalek. Seq-well: portable, low-cost RNA sequencing of single cells at high throughput. *Nat Methods*, 14(4):395–398, Apr 2017. doi: 10.1038/nmeth.4179.

Pauline Girard, Benedicte Ponsard, Julie Charles, Laurence Chaperot, and Caroline Aspord. Potent bidirectional cross-talk between plasmacytoid dendritic cells and $\gamma\delta$ T cells through BTN3A, type I/II IFNs and immune checkpoints. *Front Immunol*, 11:861, 2020. doi: 10.3389/fimmu.2020.00861.

M Girardi, D E Oppenheim, C R Steele, J M Lewis, E Glusac, R Filler, P Hobby, B Sutton, R E Tigelaar, and A C Hayday. Regulation of cutaneous malignancy by $\gamma\delta$ T cells. *Science*, 294(5542):605–9, Oct 2001. doi: 10.1126/science.1063916.

Hans-Jürgen Gober, Magdalena Kistowska, Lena Angman, Paul Jenö, Lucia Mori, and Gennaro De Libero. Human T cell receptor $\gamma\delta$ cells recognize endogenous mevalonate metabolites in tumor cells. *J Exp Med*, 197(2):163–8, Jan 2003. doi: 10.1084/jem.20021500.

K T Godder, P J Henslee-Downey, J Mehta, B S Park, K-Y Chiang, S Abhyankar, and L S Lamb. Long term disease-free survival in acute leukemia patients recovering with increased $\gamma\delta$ T cells after partially mismatched related donor bone marrow transplantation. *Bone Marrow Transplant*, 39(12): 751–7, Jun 2007. doi: 10.1038/sj.bmt.1705650.

Dale I Godfrey, Adam P Uldrich, James McCluskey, Jamie Rossjohn, and D Branch Moody. The burgeoning family of unconventional T cells. *Nat Immunol*, 16(11):1114–23, Nov 2015. doi: 10.1038/ni.3298.

Dale I Godfrey, Jérôme Le Nours, Daniel M Andrews, Adam P Uldrich, and Jamie Rossjohn. Unconventional T cell targets for cancer immunotherapy. *Immunity*, 48(3):453–473, Mar 2018. doi: 10.1016/j.immuni.2018.03.009.

J L Goldstein and M S Brown. Regulation of the mevalonate pathway. *Nature*, 343(6257):425–30, Feb 1990. doi: 10.1038/343425a0.

William Gossman and Eric Oldfield. Quantitative structure–activity relations for gammadelta T cell activation by phosphoantigens. *J Med Chem*, 45(22):4868–74, Oct 2002. doi: 10.1021/jm020224n.

V Groh, A Steinle, S Bauer, and T Spies. Recognition of stress-induced MHC molecules by intestinal epithelial gammadelta T cells. *Science*, 279(5357):1737–40, Mar 1998. doi: 10.1126/science.279.5357.1737.

Cordula Gründer, Suzanne van Dorp, Samantha Hol, Esther Drent, Trudy Straetemans, Sabine Heijhuurs, Kirsten Scholten, Wouter Scheper, Zsolt Sebestyen, Anton Martens, Roland Strong, and Jürgen Kuball. γ9 and δ2CDR3 domains regulate functional avidity of T cells harboring γ9δ2TCRs. *Blood*, 120(26):5153–62, Dec 2012. doi: 10.1182/blood-2012-05-432427.

Siyi Gu, Joseph R Sachleben, Christopher T Boughter, Wioletta I Nawrocka, Marta T Borowska, Jeffrey T Tarrasch, Georgios Skiniotis, Benoît Roux, and Erin J Adams. Phosphoantigen-induced conformational change of butyrophilin 3A1 (BTN3A1) and its implication on Vγ9Vδ2 T cell activation. *PNAS*, 114(35):E7311–E7320, 08 2017. doi: 10.1073/pnas.1707547114.

Siyi Gu, Marta T Borowska, Christopher T Boughter, and Erin J Adams. Butyrophilin3A proteins and Vγ9Vδ2 T cell activation. *Semin Cell Dev Biol*, 84:65–74, 12 2018. doi: 10.1016/j.semcdb.2018.02.007.

Andreas Guenther, Sharon Gordon, Markus Tiemann, Renate Burger, Frank Bakker, Jonathan R Green, Wolfgang Baum, Anke J Roelofs, Michael J Rogers, and Martin Gramatzki. The bisphosphonate zoledronic acid has antimyeloma activity in vivo by inhibition of protein prenylation. *Int J Cancer*, 126(1):239–46, Jan 2010. doi: 10.1002/ijc.24758.

Sakshi Gulati, Pierre Martinez, Tejal Joshi, Nicolai Juul Birkbak, Claudio R Santos, Andrew J Rowan, Lisa Pickering, Martin Gore, James Larkin, Zoltan Szallasi, Paul A Bates, Charles Swanton, and Marco Gerlinger. Systematic evaluation of the prognostic impact and intratumour heterogeneity of clear cell renal cell carcinoma biomarkers. *Eur Urol*, 66(5):936–48, Nov 2014. doi: 10.1016/j.eururo.2014.06.053.

Y Guo, H K Ziegler, S A Safley, D W Niesel, S Vaidya, and G R Klimpel. Human T-cell recognition of listeria monocytogenes: recognition of listeriolysin O by TcR $\alpha\beta^+$ and TcR $\gamma\delta^+$ T cells. *Infection and Immunity*, 63(6):2288–2294, Dec 1995. ISSN 0019-9567.

G Häcker, S Kromer, K Heeg, J Ivanyi, H Wagner, and K Pfeffer. Opportunist mycobacteria express ligands that stimulate production of human vγ9vδ2 T lymphocytes. *Infection and Immunity*, 60(7): 2753–2757, Apr 1992.

Franck Halary, Vincent Pitard, Dorota Dlubek, Roman Krzysiek, Henri de la Salle, Pierre Merville, Claire Dromer, Dominique Emilie, Jean-François Moreau, and Julie Déchanet-Merville. Shared reactivity of vdelta2(neg) gammadelta t cells against cytomegalovirus-infected cells and tumor intestinal epithelial cells. *J Exp Med*, 201(10):1567–78, May 2005. doi: 10.1084/jem.20041851.

M P Happ, R T Kubo, E Palmer, W K Born, and R L O'Brien. Limited receptor repertoire in a mycobacteria-reactive subset of $\gamma\delta$ T lymphocytes. *Nature*, 342(6250):696–8, Dec 1989. doi: 10.1038/342696a0.

Christelle Harly, Yves Guillaume, Steven Nedellec, Cassie-Marie Peigné, Hannu Mönkkönen, Jukka Mönkkönen, Jianqiang Li, Jürgen Kuball, Erin J Adams, Sonia Netzer, Julie Déchanet-Merville, Alexandra Léger, Thomas Herrmann, Richard Breathnach, Daniel Olive, Marc Bonneville, and Emmanuel Scotet. Key implication of CD277/butyrophilin-3 (BTN3A) in cellular stress sensing by a major human $\gamma\delta$ T-cell subset. *Blood*, 120(11):2269–79, Sep 2012. doi: 10.1182/blood-2012-05-430470.

Melanie J Harriff, Curtis McMurtrey, Cara A Froyd, Haihong Jin, Meghan Cansler, Megan Null, Aneta Worley, Erin W Meermeier, Gwendolyn Swarbrick, Aaron Nilsen, Deborah A Lewinsohn, William Hildebrand, Erin J Adams, and David M Lewinsohn. MR1 displays the microbial metabolome driving selective MR1-restricted T cell receptor usage. *Sci Immunol*, 3(25), 07 2018. doi: 10.1126/sciimmunol.aao2556.

S Hata, K Satyanarayana, P Devlin, H Band, J McLean, J L Strominger, M B Brenner, and M S Krangel. Extensive junctional diversity of rearranged human T cell receptor delta genes. *Science*, 240(4858): 1541–4, Jun 1988. doi: 10.1126/science.3259726.

W L Havran, Y H Chien, and J P Allison. Recognition of self antigens by skin-derived T cells with invariant $\gamma\delta$ antigen receptors. *Science*, 252(5011):1430–2, Jun 1991. doi: 10.1126/science.1828619.

A C Hayday, H Saito, S D Gillies, D M Kranz, G Tanigawa, H N Eisen, and S Tonegawa. Structure, organization, and somatic rearrangement of T cell gamma genes. *Cell*, 40(2):259–69, Feb 1985. doi: 10.1016/0092-8674(85)90140-0.

Adrian Hayday and Robert Tigelaar. Immunoregulation in the tissues by $\gamma\delta$ T cells. *Nat Rev Immunol*, 3(3):233–42, Mar 2003. doi: 10.1038/nri1030.

Adrian C Hayday. Gammadelta t cells and the lymphoid stress-surveillance response. *Immunity*, 31 (2):184–96, Aug 2009. doi: 10.1016/j.immuni.2009.08.006.

Xuan He, Hua Liang, Kunxue Hong, Haishan Li, Hong Peng, Yangyang Zhao, Manxue Jia, Yuhua Ruan, and Yiming Shao. The potential role of CD16$^+$ Vγ2Vδ2 T cell-mediated antibody-dependent cell-mediated cytotoxicity in control of HIV type 1 disease. *AIDS Res Hum Retroviruses*, 29(12): 1562–70, Dec 2013. doi: 10.1089/AID.2013.0111.

J S Heilig and S Tonegawa. Diversity of murine gamma genes and expression in fetal and adult T lymphocytes. *Nature*, 322(6082):836–40, Aug 1986. doi: 10.1038/322836a0.

M Hiramatsu, M Oguri, K Kato, T Yoshida, T Fujimaki, H Horibe, K Yokoi, S Watanabe, K Satoh, Y Aoyagi, M Tanaka, H Yoshida, S Shinkai, Y Nozawa, T Murohara, and Y Yamada. Association of a polymorphism of BTN2A1 with type 2 diabetes mellitus in Japanese individuals. *Diabet Med*, 28 (11):1381–7, Nov 2011. doi: 10.1111/j.1464-5491.2011.03358.x.

Hideki Horibe, Chikara Ueyama, Tetsuo Fujimaki, Mitsutoshi Oguri, Kimihiko Kato, Sahoko Ichihara, and Yoshiji Yamada. Association of a polymorphism of BTN2A1 with dyslipidemia in community-dwelling individuals. *Mol Med Rep*, 9(3):808–12, Mar 2014. doi: 10.3892/mmr.2014.1902.

Chia-Hung Christine Hsiao, Xiaochen Lin, Rocky J Barney, Rebekah R Shippy, Jin Li, Olga Vinogradova, David F Wiemer, and Andrew J Wiemer. Synthesis of a phosphoantigen prodrug that potently activates Vγ9Vδ2 T-lymphocytes. *Chem Biol*, 21(8):945–54, Aug 2014. doi: 10.1016/j.chembiol.2014.06.006.

Yi Huang, Jiayin Wang, Peilin Jia, Xiangchun Li, Guangsheng Pei, Changxi Wang, Xiaodong Fang, Zhongming Zhao, Zhiming Cai, Xin Yi, Song Wu, and Baifeng Zhang. Clonal architectures predict clinical outcome in clear cell renal cell carcinoma. *Nat Commun*, 10(1):1245, 03 2019. doi: 10.1038/s41467-019-09241-7.

Atif S M Idrees, Tomoharu Sugie, Chiyomi Inoue, Kaoru Murata-Hirai, Haruki Okamura, Craig T Morita, Nagahiro Minato, Masakazu Toi, and Yoshimasa Tanaka. Comparison of $\gamma\delta$ T cell responses and farnesyl diphosphate synthase inhibition in tumor cells pretreated with zoledronic acid. *Cancer Sci*, 104(5):536–42, May 2013. doi: 10.1111/cas.12124.

F Imani and M J Soloski. Heat shock proteins can regulate expression of the tla region-encoded class ib molecule qa-1. *Proc Natl Acad Sci U S A*, 88(23):10475–9, Dec 1991. doi: 10.1073/pnas.88.23.10475.

Brant A Inman, Xavier Frigola, Kimberley J Harris, Susan M Kuntz, Christine M Lohse, Bradley C Leibovich, and Eugene D Kwon. Questionable relevance of $\gamma\delta$ T lymphocytes in renal cell carcinoma. *J Immunol*, 180(5):3578–84, Mar 2008. doi: 10.4049/jimmunol.180.5.3578.

K Ito, L Van Kaer, M Bonneville, S Hsu, D B Murphy, and S Tonegawa. Recognition of the product of a novel MHC TL region gene (27b) by a mouse $\gamma\delta$ T cell receptor. *Cell*, 62(3):549–61, Aug 1990. doi: 10.1016/0092-8674(90)90019-b.

S Itohara, A G Farr, J J Lafaille, M Bonneville, Y Takagaki, W Haas, and S Tonegawa. Homing of a $\gamma\delta$ thymocyte subset with homogeneous T-cell receptors to mucosal epithelia. *Nature*, 343(6260):754–7, Feb 1990. doi: 10.1038/343754a0.

Ivaylo I Ivanov, Brent S McKenzie, Liang Zhou, Carlos E Tadokoro, Alice Lepelley, Juan J Lafaille, Daniel J Cua, and Dan R Littman. The orphan nuclear receptor RORγt directs the differentiation program of proinflammatory IL-17$^+$ T helper cells. *Cell*, 126(6):1121–33, Sep 2006. doi: 10.1016/j.cell.2006.07.035.

Alex Jahng, Igor Maricic, Carlos Aguilera, Susanna Cardell, Ramesh C Halder, and Vipin Kumar. Prevention of autoimmunity by targeting a distinct, noninvariant CD1d-reactive T cell population reactive to sulfatide. *J Exp Med*, 199(7):947–57, Apr 2004. doi: 10.1084/jem.20031389.

Leo C James, Anthony H Keeble, Zahra Khan, David A Rhodes, and John Trowsdale. Structural basis for PRYSPRY-mediated tripartite motif (TRIM) protein function. *Proc Natl Acad Sci U S A*, 104(15):6200–5, Apr 2007. doi: 10.1073/pnas.0609174104.

Anett Jandke, Daisy Melandri, Leticia Monin, Dmitry S Ushakov, Adam G Laing, Pierre Vantourout, Philip East, Takeshi Nitta, Tomoya Narita, Hiroshi Takayanagi, Regina Feederle, and Adrian Hayday. Butyrophilin-like proteins display combinatorial diversity in selecting and maintaining signature intraepithelial $\gamma\delta$ t cell compartments. *Nat Commun*, 11(1):3769, 07 2020. doi: 10.1038/s41467-020-17557-y.

Anke Janssen, Jose Villacorta Hidalgo, Dennis X Beringer, Sanne van Dooremalen, Febilla Fernando, Eline van Diest, Antonela R Terrizi, Peter Bronsert, Sylvia Kock, Annette Schmitt-Gräff, Martin Werner, Kerstin Heise, Marie Follo, Trudy Straetemans, Zsolt Sebestyen, Dmitry M Chudakov, Sofya A Kasatskaya, Felix E Frenkel, Sarina Ravens, Eric Spierings, Immo Prinz, Ralf Küppers,

Miroslav Malkovsky, Paul Fisch, and Jürgen Kuball. $\gamma\delta$ T-cell receptors derived from breast cancer-infiltrating T lymphocytes mediate antitumor reactivity. *Cancer Immunol Res*, 8(4):530–543, Apr 2020. doi: 10.1158/2326-6066.CIR-19-0513.

Jaekwang Jeong, Anita U. Rao, Jinling Xu, Sherry L. Ogg, Yetrib Hathout, Catherine Fenselau, and Ian H. Mather. The PRY/SPRY/B30.2 domain of butyrophilin 1A1 (BTN1A1) binds to xanthine oxidoreductase. *Journal of Biological Chemistry*, 284(33):22444–22456, Jun 2009. ISSN 1083-351X. doi: 10.1074/jbc.m109.020446.

R M Johnson, D W Lancki, A I Sperling, R F Dick, P G Spear, F W Fitch, and J A Bluestone. A murine CD4-, CD8- T cell receptor-gamma delta T lymphocyte clone specific for herpes simplex virus glycoprotein i. *The Journal of Immunology*, 148(4):983–988, Feb 1992. ISSN 0022-1767.

Marlieke Jongsma, Matthijs Raaben, Antonius De Waard, Tao Zhang, Birol Cabukusta, Rene Platzer, Vincent Blomen, Anastasia Xagara, Tamara Verkerk, Sophie Bliss, Lennert Janssen, Elmer Stickel, Stephanie Holst, Rosina Plomp, Arend Mulder, Soldano Ferrone, Frans Claas, Mirjam Heemskerk, Marieke Griffioen, and Robbert Spaapen. The SPPL3-defined glycosphingolipid repertoire regulates immune responses by improving HLA class I access. *SSRN Electronic Journal*, 01 2020. doi: 10.2139/ssrn.3584519.

Julia Joung, Silvana Konermann, Jonathan S Gootenberg, Omar O Abudayyeh, Randall J Platt, Mark D Brigham, Neville E Sanjana, and Feng Zhang. Genome-scale CRISPR-Cas9 knockout and transcriptional activation screening. *Nature Protocols*, 12(4):828–863, 04 2017. doi: 10.1038/nprot.2017.016.

Elvin A. Kabat. *Sequences of proteins of immunological interest*. Columbia University, Public Health Service, National Institutes of Health., Bethesda, MD, U.S. Dept. of Health and Human Services, 5 edition, 1991.

D Kabelitz, A Bender, T Prospero, S Wesselborg, O Janssen, and K Pechhold. The primary response of human γ/δ^+ T cells to *mycobacterium tuberculosis* is restricted to V gamma 9-bearing cells. *J Exp Med*, 173(6):1331–8, Jun 1991. doi: 10.1084/jem.173.6.1331.

Dieter Kabelitz, Daniela Wesch, Elke Pitters, and Margot Zöller. Potential of human gammadelta T lymphocytes for immunotherapy of cancer. *Int J Cancer*, 112(5):727–32, Dec 2004. doi: 10.1002/ijc.20445.

Shirin Kalyan, Vijayanand Chandrasekaran, Elgar S Quabius, Thisbe K Lindhorst, and Dieter Kabelitz. Neutrophil uptake of nitrogen-bisphosphonates leads to the suppression of human peripheral blood $\gamma\delta$ T cells. *Cell Mol Life Sci*, 71(12):2335–46, Jun 2014. doi: 10.1007/s00018-013-1495-x.

Ning Kang, Jianhua Zhou, Tie Zhang, Lifang Wang, Fang Lu, Ying Cui, Lianxian Cui, and Wei He. Adoptive immunotherapy of lung cancer with immobilized anti-tcrgammadelta antibody-expanded human gammadelta t-cells in peripheral blood. *Cancer Biol Ther*, 8(16):1540–9, Aug 2009. doi: 10.4161/cbt.8.16.8950.

Mohindar M Karunakaran, Thomas W Göbel, Lisa Starick, Lutz Walter, and Thomas Herrmann. Vγ9 and Vδ2 T cell antigen receptor genes and butyrophilin 3 (BTN3) emerged with placental mammals and are concomitantly preserved in selected species like alpaca (*vicugna pacos*). *Immunogenetics*, 66(4):243–54, Apr 2014. doi: 10.1007/s00251-014-0763-8.

Mohindar M Karunakaran, Carrie R Willcox, Mahboob Salim, Daniel Paletta, Alina S Fichtner, Angela Noll, Lisa Starick, Anna Nöhren, Charlotte R Begley, Katie A Berwick, Raphaël A G Chaleil, Vincent Pitard, Julie Déchanet-Merville, Paul A Bates, Brigitte Kimmel, Timothy J Knowles, Volker Kunzmann, Lutz Walter, Mark Jeeves, Fiyaz Mohammed, Benjamin E Willcox, and Thomas Herrmann. Butyrophilin-2A1 directly binds germline-encoded regions of the Vγ9Vδ2 TCR and is essential for phosphoantigen sensing. *Immunity*, 52(3):487–498.e6, Mar 2020. doi: 10.1016/j.immuni.2020.02.014.

Allison R Kazen and Erin J Adams. Evolution of the V, D, and J gene segments used in the primate $\gamma\delta$ T-cell receptor reveals a dichotomy of conservation and diversity. *Proc Natl Acad Sci U S A*, 108 (29):E332–40, Jul 2011. doi: 10.1073/pnas.1105105108.

Richard B Kennedy, Inna G Ovsyannikova, Iana H Haralambieva, Nathaniel D Lambert, V Shane Pankratz, and Gregory A Poland. Genetic polymorphisms associated with rubella virus-specific cellular immunity following MMR vaccination. *Hum Genet*, 133(11):1407–17, Nov 2014. doi: 10.1007/s00439-014-1471-z.

Camille Khairallah, Timothy H Chu, and Brian S Sheridan. Tissue adaptations of memory and tissue-resident gamma delta T cells. *Front Immunol*, 9:2636, Nov 2018. doi: 10.3389/fimmu.2018.02636.

Ashley M Kilcollins, Jin Li, Chia-Hung Christine Hsiao, and Andrew J Wiemer. HMBPP analog prodrugs bypass energy-dependent uptake to promote efficient BTN3A1-mediated malignant cell lysis by Vγ9Vδ2 T lymphocyte effectors. *J Immunol*, 197(2):419–28, 07 2016. doi: 10.4049/jimmunol.1501833.

Magdalena Kistowska. *Antigen recognition and thymic maturation of human TCR Vgamma9-Vdelta2 cells*. Phd thesis, University of Basel, Faculty of Science, Feb 2009.

Lars Kjer-Nielsen, Onisha Patel, Alexandra J Corbett, Jérôme Le Nours, Bronwyn Meehan, Ligong Liu, Mugdha Bhati, Zhenjun Chen, Lyudmila Kostenko, Rangsima Reantragoon, Nicholas A Williamson, Anthony W Purcell, Nadine L Dudek, Malcolm J McConville, Richard A J O'Hair, George N Khairallah, Dale I Godfrey, David P Fairlie, Jamie Rossjohn, and James McCluskey. MR1 presents microbial vitamin B metabolites to MAIT cells. *Nature*, 491(7426):717–23, Nov 2012. doi: 10.1038/nature11605.

Andrea Knight, Alejandro J Madrigal, Sarah Grace, Janani Sivakumaran, Panagiotis Kottaridis, Stephen Mackinnon, Paul J Travers, and Mark W Lowdell. The role of Vδ2-negative $\gamma\delta$ T cells during cytomegalovirus reactivation in recipients of allogeneic stem cell transplantation. *Blood*, 116 (12):2164–72, Sep 2010. doi: 10.1182/blood-2010-01-255166.

H Kobayashi, Y Tanaka, J Yagi, H Toma, and T Uchiyama. Gamma/delta T cells provide innate immunity against renal cell carcinoma. *Cancer Immunol Immunother*, 50(3):115–24, May 2001. doi: 10.1007/s002620100173.

Yan Kong, Wei Cao, Xueyan Xi, Chi Ma, Lianxian Cui, and Wei He. The NKG2D ligand ULBP4 binds to TCRγ9/δ2 and induces cytotoxicity to tumor cells through both TCR$\gamma\delta$ and NKG2D. *Blood*, 114 (2):310–7, Jul 2009. doi: 10.1182/blood-2008-12-196287.

Satoshi Konno, Daisuke Takahashi, Nobuyuki Hizawa, Takeshi Hattori, Ayumu Takahashi, Akira Isada, Yukiko Maeda, Shau-Ku Huang, and Masaharu Nishimura. Genetic impact of a butyrophilin-like 2 (BTNL2) gene variation on specific IgE responsiveness to *dermatophagoides farinae* (Der f) in japanese. *Allergol Int*, 58(1):29–35, Mar 2009. doi: 10.2332/allergolint.08-OA-0005.

D Kozbor, G Trinchieri, D S Monos, M Isobe, G Russo, J A Haney, C Zmijewski, and C M Croce. Human TCR-gamma+/delta+, cd8+ T lymphocytes recognize tetanus toxoid in an MHC-restricted fashion. *J Exp Med*, 169(5):1847–51, May 1989. doi: 10.1084/jem.169.5.1847.

D Kozbor, M A Cassatella, S Lessin, J Kagan, S Finver, J Faust, G Trinchieri, and C M Croce. Expression and function of gamma delta- and alpha beta-T cell receptor heterodimers on human somatic T cell hybrids. *J Immunol*, 144(10):3677–83, May 1990.

Taras Kreslavsky, Adam K Savage, Robin Hobbs, Fotini Gounari, Roderick Bronson, Pablo Pereira, Pier Paolo Pandolfi, Albert Bendelac, and Harald von Boehmer. TCR-inducible PLZF transcription factor required for innate phenotype of a subset of $\gamma\delta$ T cells with restricted tcr diversity. *Proc Natl Acad Sci U S A*, 106(30):12453–8, Jul 2009. doi: 10.1073/pnas.0903895106.

S N Kumar, L L Seelig, Jr, and J R Head. Migration of radiolabeled, adoptively transferred T-lymphocytes into the mammary gland and milk of lactating rats. *J Reprod Immunol*, 8(2-3):235–48, Nov 1985. doi: 10.1016/0165-0378(85)90043-9.

V Kunzmann, E Bauer, J Feurle, F Weissinger, H P Tony, and M Wilhelm. Stimulation of $\gamma\delta$ T cells by aminobisphosphonates and induction of antiplasma cell activity in multiple myeloma. *Blood*, 96(2): 384–92, Jul 2000.

Telma Lança, Daniel V Correia, Catarina F Moita, Helena Raquel, Ana Neves-Costa, Cristina Ferreira, José S Ramalho, João T Barata, Luís F Moita, Anita Q Gomes, and Bruno Silva-Santos. The MHC class Ib protein ULBP1 is a nonredundant determinant of leukemia/lymphoma susceptibility to $\gamma\delta$ T-cell cytotoxicity. *Blood*, 115(12):2407–11, Mar 2010. doi: 10.1182/blood-2009-08-237123.

Chloé Laplagne, Sarah Meddour, Sarah Figarol, Marie Michelas, Olivier Calvayrac, Gilles Favre, Camille Laurent, Jean-Jacques Fournié, Stéphanie Cabantous, and Mary Poupot. Vγ9Vδ2 T cells activation through phosphoantigens can be impaired by a RHOB rerouting in lung cancer. *Front Immunol*, 11:1396, 2020. doi: 10.3389/fimmu.2020.01396.

Jérôme Le Nours, Nicholas A Gherardin, Sri H Ramarathinam, Wael Awad, Florian Wiede, Benjamin S Gully, Yogesh Khandokar, T Praveena, Jacinta M Wubben, Jarrod J Sandow, Andrew I Webb, Anouk von Borstel, Michael T Rice, Samuel J Redmond, Rebecca Seneviratna, Maria L Sandoval-Romero, Shihan Li, Michael N T Souter, Sidonia B G Eckle, Alexandra J Corbett, Hugh H Reid, Ligong Liu, David P Fairlie, Edward M Giles, Glen P Westall, Richard W Tothill, Martin S Davey, Richard Berry, Tony Tiganis, James McCluskey, Daniel G Pellicci, Anthony W Purcell, Adam P Uldrich, Dale I Godfrey, and Jamie Rossjohn. A class of $\gamma\delta$ T cell receptors recognize the underside of the antigen-presenting molecule MR1. *Science*, 366(6472):1522–1527, 12 2019. doi: 10.1126/science.aav3900.

Cécile Le Page, Alexandre Marineau, Patrick K Bonza, Kurosh Rahimi, Louis Cyr, Ingrid Labouba, Jason Madore, Nathalie Delvoye, Anne-Marie Mes-Masson, Diane M Provencher, and Jean-François Cailhier. Btn3a2 expression in epithelial ovarian cancer is associated with higher tumor infiltrating t cells and a better prognosis. *PLoS One*, 7(6):e38541, Jun 2012. doi: 10.1371/journal.pone.0038541.

Marie-Paule Lefranc, Christelle Pommié, Manuel Ruiz, Véronique Giudicelli, Elodie Foulquier, Lisa Truong, Valérie Thouvenin-Contet, and Gérard Lefranc. IMGT unique numbering for immunoglobulin and T cell receptor variable domains and Ig superfamily V-like domains. *Developmental and Comparative Immunology*, 27(1):55 – 77, Jan 2003. ISSN 0145-305X. doi: 10.1016/S0145-305X(02)00039-3.

Marie-Paule Lefranc, Véronique Giudicelli, Patrice Duroux, Joumana Jabado-Michaloud, Géraldine Folch, Safa Aouinti, Emilie Carillon, Hugo Duvergey, Amélie Houles, Typhaine Paysan-Lafosse, Saida Hadi-Saljoqi, Souphatta Sasorith, Gérard Lefranc, and Sofia Kossida. IMGT®, the international ImMunoGeneTics information system® 25 years on. *Nucleic Acids Research*, 43(D1):D413–422, Jan 2015. doi: 10.1093/nar/gku1056.

Mateusz Legut, David K Cole, and Andrew K Sewell. The promise of $\gamma\delta$ T cells and the $\gamma\delta$ T cell receptor for cancer immunotherapy. *Cell Mol Immunol*, 12(6):656–68, Nov 2015. doi: 10.1038/cmi.2015.28.

Marco Lepore, Lucia Mori, and Gennaro De Libero. The conventional nature of non-MHC-restricted T cells. *Front Immunol*, 9:1365, Jun 2018. doi: 10.3389/fimmu.2018.01365.

B Li, M D Rossman, T Imir, A F Oner-Eyuboglu, C W Lee, R Biancaniello, and S R Carding. Disease-specific changes in gammadelta T cell repertoire and function in patients with pulmonary tuberculosis. *The Journal of Immunology*, 157(9):4222–4229, 1996. ISSN 0022-1767.

Haishan Li, Hong Peng, Pengfei Ma, Yuhua Ruan, Bing Su, Xinping Ding, Chen Xu, C David Pauza, and Yiming Shao. Association between Vγ9Vδ2 T cells and disease progression after infection with closely related strains of HIV in china. *Clin Infect Dis*, 46(9):1466–72, May 2008. doi: 10.1086/587107.

Hong Li, Zheng Xiang, Ting Feng, Jinrong Li, Yinping Liu, Yingying Fan, Qiao Lu, Zhongwei Yin, Meixing Yu, Chongyang Shen, and Wenwei Tu. Human Vγ9Vδ2-T cells efficiently kill influenza virus-infected lung alveolar epithelial cells. *Cell Mol Immunol*, 10(2):159–64, Mar 2013. doi: 10.1038/cmi.2012.70.

Li Li and Chang-You Wu. CD4$^+$ CD25$^+$ Treg cells inhibit human memory $\gamma\delta$ T cells to produce IFN-γ in response to *m. tuberculosis* antigen ESAT-6. *Blood*, 111(12):5629–36, Jun 2008. doi: 10.1182/blood-2008-02-139899.

Peiyao Li, Gang Xu, Guiyuan Li, and Minghua Wu. Function and mechanism of tumor suppressor gene LRRC4/NGL-2. *Mol Cancer*, 13:266, Dec 2014. doi: 10.1186/1476-4598-13-266.

Yihua Lin, Jia Wei, Lili Fan, and Deyun Cheng. BTNL2 gene polymorphism and sarcoidosis susceptibility: a meta-analysis. *PLoS One*, 10(4):e0122639, 2015. doi: 10.1371/journal.pone.0122639.

David Liñares, Paula Mañá, Melinda Goodyear, Anne M Chow, Chelsea Clavarino, Nicholas D Huntington, Louise Barnett, Frank Koentgen, Ryo Tomioka, Claude C A Bernard, Manuel Freire-Garabal, and Hugh H Reid. The magnitude and encephalogenic potential of autoimmune response to mog is enhanced in mog deficient mice. *J Autoimmun*, 21(4):339–51, Dec 2003. doi: 10.1016/j.jaut.2003.09.001.

Di Liu, Qian Lu, Xing Wang, Jun Wang, Ning Lu, Zefei Jiang, Xiaopeng Hao, Jianbin Li, Jing Liu, Pengbo Cao, Guilin Peng, Yuandong Tao, Dianyuan Zhao, Fuchu He, and Li Tang. LSECtin on tumor-associated macrophages enhances breast cancer stemness via interaction with its receptor BTN3A3. *Cell Res*, 29(5):365–378, 05 2019. doi: 10.1038/s41422-019-0155-6.

Adrienne M Luoma, Caitlin D Castro, Toufic Mayassi, Leslie A Bembinster, Li Bai, Damien Picard, Brian Anderson, Louise Scharf, Jennifer E Kung, Leah V Sibener, Paul B Savage, Bana Jabri, Albert Bendelac, and Erin J Adams. Crystal structure of Vδ1 T cell receptor in complex with CD1d-sulfatide shows MHC-like recognition of a self-lipid by human $\gamma\delta$ T cells. *Immunity*, 39(6):1032–42, Dec 2013. doi: 10.1016/j.immuni.2013.11.001.

Kirsten E Lyke, Andrew S Ishizuka, Andrea A Berry, Sumana Chakravarty, Adam DeZure, Mary E Enama, Eric R James, Peter F Billingsley, Anusha Gunasekera, Anita Manoj, Minglin Li, Adam J Ruben, Tao Li, Abraham G Eappen, Richard E Stafford, Natasha Kc, Tooba Murshedkar, Floreliz H Mendoza, Ingelise J Gordon, Kathryn L Zephir, LaSonji A Holman, Sarah H Plummer, Cynthia S Hendel, Laura Novik, Pamela J M Costner, Jamie G Saunders, Nina M Berkowitz, Barbara J Flynn, Martha C Nason, Lindsay S Garver, Matthew B Laurens, Christopher V Plowe, Thomas L Richie, Barney S Graham, Mario Roederer, B Kim Lee Sim, Julie E Ledgerwood, Stephen L Hoffman, and Robert A Seder. Attenuated PfSPZ vaccine induces strain-transcending T cells and durable protection against heterologous controlled human malaria infection. *Proc Natl Acad Sci U S A*, 114 (10):2711–2716, Mar 2017. doi: 10.1073/pnas.1615324114.

Evan Z Macosko, Anindita Basu, Rahul Satija, James Nemesh, Karthik Shekhar, Melissa Goldman, Itay Tirosh, Allison R Bialas, Nolan Kamitaki, Emily M Martersteck, John J Trombetta, David A Weitz, Joshua R Sanes, Alex K Shalek, Aviv Regev, and Steven A McCarroll. Highly parallel genome-wide expression profiling of individual cells using nanoliter droplets. *Cell*, 161(5):1202–1214, May 2015. doi: 10.1016/j.cell.2015.05.002.

Jeffrey Y W Mak, Weijun Xu, Robert C Reid, Alexandra J Corbett, Bronwyn S Meehan, Huimeng Wang, Zhenjun Chen, Jamie Rossjohn, James McCluskey, Ligong Liu, and David P Fairlie. Stabilizing short-lived schiff base derivatives of 5-aminouracils that activate mucosal-associated invariant T cells. *Nat Commun*, 8:14599, 03 2017. doi: 10.1038/ncomms14599.

Georg Malcherek, Luzia Mayr, Pedro Roda-Navarro, David Rhodes, Nigel Miller, and John Trowsdale. The B7 homolog butyrophilin BTN2A1 is a novel ligand for DC-SIGN. *J Immunol*, 179(6):3804–11, Sep 2007. doi: 10.4049/jimmunol.179.6.3804.

K J Maloy, B Odermatt, H Hengartner, and R M Zinkernagel. Interferon γ-producing $\gamma\delta$ T cell-dependent antibody isotype switching in the absence of germinal center formation during virus infection. *Proc Natl Acad Sci U S A*, 95(3):1160–5, Feb 1998. doi: 10.1073/pnas.95.3.1160.

Paula Mañá, Melinda Goodyear, Claude Bernard, Ryo Tomioka, Manuel Freire-Garabal, and David Liñares. Tolerance induction by molecular mimicry: prevention and suppression of experimental autoimmune encephalomyelitis with the milk protein butyrophilin. *Int Immunol*, 16(3):489–99, Mar 2004. doi: 10.1093/intimm/dxh049.

Romain Marlin, Angela Pappalardo, Hannah Kaminski, Carrie R Willcox, Vincent Pitard, Sonia Netzer, Camille Khairallah, Anne-Marie Lomenech, Christelle Harly, Marc Bonneville, Jean-François Moreau, Emmanuel Scotet, Benjamin E Willcox, Benjamin Faustin, and Julie Déchanet-Merville. Sensing of cell stress by human $\gamma\delta$ TCR-dependent recognition of annexin A2. *Proc Natl Acad Sci U S A*, 114(12):3163–3168, Mar 2017. doi: 10.1073/pnas.1621052114.

Marcel Martin. Cutadapt removes adapter sequences from high-throughput sequencing reads. *EMBnet.journal*, 17:10–12, 2011. doi: 10.14806/ej.17.1.200.

L A Matis, A M Fry, R Q Cron, M M Cotterman, R F Dick, and J A Bluestone. Structure and specificity of a class II MHC alloreactive $\gamma\delta$ T cell receptor heterodimer. *Science*, 245(4919):746–9, Aug 1989. doi: 10.1126/science.2528206.

Hamish E G McWilliam, Sidonia B G Eckle, Alex Theodossis, Ligong Liu, Zhenjun Chen, Jacinta M Wubben, David P Fairlie, Richard A Strugnell, Justine D Mintern, James McCluskey, Jamie Rossjohn, and Jose A Villadangos. The intracellular pathway for the presentation of vitamin B-related antigens by the antigen-presenting molecule MR1. *Nat Immunol*, 17(5):531–7, May 2016. doi: 10.1038/ni.3416.

Daisy Melandri, Iva Zlatareva, Raphaël A G Chaleil, Robin J Dart, Andrew Chancellor, Oliver Nussbaumer, Oxana Polyakova, Natalie A Roberts, Daniela Wesch, Dieter Kabelitz, Peter M Irving, Susan John, Salah Mansour, Paul A Bates, Pierre Vantourout, and Adrian C Hayday. The $\gamma\delta$TCR combines innate immunity with adaptive immunity by utilizing spatially distinct regions for agonist selection and antigen responsiveness. *Nat Immunol*, 19(12):1352–1365, 12 2018. doi: 10.1038/s41590-018-0253-5.

Simone Meuter, Matthias Eberl, and Bernhard Moser. Prolonged antigen survival and cytosolic export in cross-presenting human $\gamma\delta$ T cells. *Proc Natl Acad Sci U S A*, 107(19):8730–5, May 2010. doi: 10.1073/pnas.1002769107.

F Miyagawa, Y Tanaka, S Yamashita, and N Minato. Essential requirement of antigen presentation by monocyte lineage cells for the activation of primary human $\gamma\delta$ T cells by aminobisphosphonate antigen. *J Immunol*, 166(9):5508–14, May 2001. doi: 10.4049/jimmunol.166.9.5508.

K Miyamoto, S Miyake, and T Yamamura. A synthetic glycolipid prevents autoimmune encephalomyelitis by inducing TH2 bias of natural killer T cells. *Nature*, 413(6855):531–4, Oct 2001. doi: 10.1038/35097097.

Rania Hassan Mohamed, Yoichi Sutoh, Yasushi Itoh, Noriyuki Otsuka, Yukiko Miyatake, Kazumasa Ogasawara, and Masanori Kasahara. The SKINT1-like gene is inactivated in hominoids but not in all primate species: implications for the origin of dendritic epidermal T cells. *PLoS One*, 10(4): e0123258, Apr 2015. doi: 10.1371/journal.pone.0123258.

Marlo Möller, Ruta Kwiatkowski, Almut Nebel, Paul D van Helden, Eileen G Hoal, and Stefan Schreiber. Allelic variation in BTNL2 and susceptibility to tuberculosis in a South African population. *Microbes Infect*, 9(4):522–8, Apr 2007. doi: 10.1016/j.micinf.2007.01.011.

Lucia Mori, Marco Lepore, and Gennaro De Libero. The immunology of CD1- and MR1-restricted T cells. *Annual Review of Immunology*, 34(1):479 510, Feb 2016. ISSN 0732-0582. doi: 10.1146/annurev-immunol-032414-112008.

C T Morita, E M Beckman, J F Bukowski, Y Tanaka, H Band, B R Bloom, D E Golan, and M B Brenner. Direct presentation of nonpeptide prenyl pyrophosphate antigens to human $\gamma\delta$ T cells. *Immunity*, 3 (4):495–507, Oct 1995. doi: 10.1016/1074-7613(95)90178-7.

C T Morita, H K Lee, D S Leslie, Y Tanaka, J F Bukowski, and E Märker-Hermann. Recognition of nonpeptide prenyl pyrophosphate antigens by human $\gamma\delta$ T cells. *Microbes Infect*, 1(3):175–86, Mar 1999.

C T Morita, R A Mariuzza, and M B Brenner. Antigen recognition by human gamma delta t cells: pattern recognition by the adaptive immune system. *Springer Semin Immunopathol*, 22(3):191–217, Sep 2000. doi: 10.1007/s002810000042.

C T Morita, H K Lee, H Wang, H Li, R A Mariuzza, and Y Tanaka. Structural features of nonpeptide prenyl pyrophosphates that determine their antigenicity for human gamma delta t cells. *J Immunol*, 167(1):36–41, Jul 2001. doi: 10.4049/jimmunol.167.1.36.

Craig T Morita, Chenggang Jin, Ghanashyam Sarikonda, and Hong Wang. Nonpeptide antigens, presentation mechanisms, and immunological memory of human vγ2vδ2 T cells: discriminating friend from foe through the recognition of prenyl pyrophosphate antigens. *Immunol Rev*, 215:59–76, Feb 2007. doi: 10.1111/j.1600-065X.2006.00479.x.

Bernhard Moser and Matthias Eberl. $\gamma\delta$ T-APCs: a novel tool for immunotherapy? *Cell Mol Life Sci*, 68(14):2443–52, Jul 2011. doi: 10.1007/s00018-011-0706-6.

James T Neal, Xingnan Li, Junjie Zhu, Valeria Giangarra, Caitlin L Grzeskowiak, Jihang Ju, Iris H Liu, Shin-Heng Chiou, Ameen A Salahudeen, Amber R Smith, Brian C Deutsch, Lillian Liao, Allison J Zemek, Fan Zhao, Kasper Karlsson, Liora M Schultz, Thomas J Metzner, Lincoln D Nadauld, Yuen-Yi Tseng, Sahar Alkhairy, Coyin Oh, Paula Keskula, Daniel Mendoza-Villanueva, Francisco M De La Vega, Pamela L Kunz, Joseph C Liao, John T Leppert, John B Sunwoo, Chiara Sabatti, Jesse S Boehm, William C Hahn, Grace X Y Zheng, Mark M Davis, and Calvin J Kuo. Organoid modeling of the tumor immune microenvironment. *Cell*, 175(7):1972–1988.e16, 12 2018. doi: 10.1016/j.cell.2018.11.021.

Khiem Nguyen, Jin Li, Robbins Puthenveetil, Xiaochen Lin, Michael M Poe, Chia-Hung Christine Hsiao, Olga Vinogradova, and Andrew J Wiemer. The butyrophilin 3A1 intracellular domain undergoes a conformational change involving the juxtamembrane region. *FASEB J*, 31(11):4697–4706, 11 2017. doi: 10.1096/fj.201601370RR.

Hayato Nishimura, Makoto Hirokawa, Naohito Fujishima, Masumi Fujishima, Ikuo Miura, and Ken-ichi Sawada. Contribution of complementarity-determining region 3 of the T-cell receptor Vδ2 chain to the recognition of aminobisphosphonates by human $\gamma\delta$ T-cells. *Int J Hematol*, 79(4):369–76, 05 2004. doi: 10.1532/ijh97.03157.

Toyoki Nishimura, Ai Yamada, Mariko Kinoshita, Osamu Ohara, and Hiroshi Moritake. BTNL2 germline variants may be involved in the pathogenesis of renal granuloma. *Pediatr Int*, 61(8):834–836, Aug 2019. doi: 10.1111/ped.13923.

Rebecca L O'Brien and Willi K Born. Dermal $\gamma\delta$ T cells –what have we learned? *Cell Immunol*, 296 (1):62–9, Jul 2015. doi: 10.1016/j.cellimm.2015.01.011.

Sherry L Ogg, Anne K Weldon, Lorraine Dobbie, Andrew J H Smith, and Ian H Mather. Expression of butyrophilin (btn1a1) in lactating mammary gland is essential for the regulated secretion of milk-lipid droplets. *Proc Natl Acad Sci U S A*, 101(27):10084–9, Jul 2004. doi: 10.1073/pnas.0402930101.

Mitsutoshi Oguri, Tetsuo Fujimaki, Hideki Horibe, Kimihiko Kato, Sahoko Ichihara, and Yoshiji Yamada. Association of a polymorphism of BTN2A1 with chronic kidney disease in community-dwelling individuals. *Biomed Rep*, 1(6):868–872, Nov 2013. doi: 10.3892/br.2013.176.

Daisuke Okuno, Yuki Sugiura, Noriho Sakamoto, Mohammed S O Tagod, Masashi Iwasaki, Shuto Noda, Akihiro Tamura, Hiroaki Senju, Yasuhiro Umeyama, Hiroyuki Yamaguchi, Makoto Suematsu, Craig T Morita, Yoshimasa Tanaka, and Hiroshi Mukae. Comparison of a novel bisphosphonate prodrug and zoledronic acid in the induction of cytotoxicity in human vγ2vδ2 T cells. *Front Immunol*, 11:1405, 2020. doi: 10.3389/fimmu.2020.01405.

Akifumi Ootani, Xingnan Li, Eugenio Sangiorgi, Quoc T Ho, Hiroo Ueno, Shuji Toda, Hajime Sugihara, Kazuma Fujimoto, Irving L Weissman, Mario R Capecchi, and Calvin J Kuo. Sustained in vitro intestinal epithelial culture within a wnt-dependent stem cell niche. *Nat Med*, 15(6):701–6, Jun 2009. doi: 10.1038/nm.1951.

Aparna Palakodeti, Andrew Sandstrom, Lakshmi Sundaresan, Christelle Harly, Steven Nedellec, Daniel Olive, Emmanuel Scotet, Marc Bonneville, and Erin J Adams. The molecular basis for modulation of human Vγ9Vδ2 T cell responses by CD277/butyrophilin-3 (BTN3A)-specific antibodies. *J Biol Chem*, 287(39):32780–90, Sep 2012. doi: 10.1074/jbc.M112.384354.

C M Parker, V Groh, H Band, S A Porcelli, C Morita, M Fabbi, D Glass, J L Strominger, and M B Brenner. Evidence for extrathymic changes in the T cell receptor gamma/delta repertoire. *J Exp Med*, 171(5):1597–612, May 1990. doi: 10.1084/jem.171.5.1597.

Sushil Kumar Pathak, Sanchita Basu, Kunal Kumar Basu, Anirban Banerjee, Shresh Pathak, Asima Bhattacharyya, Tsuneyasu Kaisho, Manikuntala Kundu, and Joyoti Basu. Direct extracellular interaction between the early secreted antigen ESAT-6 of *mycobacterium tuberculosis* and TLR2 inhibits TLR signaling in macrophages. *Nat Immunol*, 8(6):610–8, Jun 2007. doi: 10.1038/ni1468.

Kyle K Payne, Jessica A Mine, Subir Biswas, Ricardo A Chaurio, Alfredo Perales-Puchalt, Carmen M Anadon, Tara Lee Costich, Carly M Harro, Jennifer Walrath, Qianqian Ming, Evgenii Tcyganov, Andrea L Buras, Kristen E Rigolizzo, Gunjan Mandal, Jason Lajoie, Michael Ophir, Julia Tchou, Douglas Marchion, Vincent C Luca, Piotr Bobrowicz, Brooke McLaughlin, Ugur Eskiocak, Michael Schmidt, Juan R Cubillos-Ruiz, Paulo C Rodriguez, Dmitry I Gabrilovich, and Jose R Conejo-Garcia. BTN3A1 governs antitumor responses by coordinating $\alpha\beta$ and $\gamma\delta$ T cells. *Science*, 369(6506):942–949, 08 2020. doi: 10.1126/science.aay2767.

Abraham Peedicayil, Robert A Vierkant, Lynn C Hartmann, Brooke L Fridley, Zachary S Fredericksen, Kristin L White, Elaine A Elliott, Catherine M Phelan, Ya-Yu Tsai, Andrew Berchuck, Edwin S Iversen, Jr, Fergus J Couch, Prema Peethamabaran, Melissa C Larson, Kimberly R Kalli, Matthew L Kosel, Vijayalakshmi Shridhar, David N Rider, Mark Liebow, Julie M Cunningham, Joellen M Schildkraut, Thomas A Sellers, and Ellen L Goode. Risk of ovarian cancer and inherited variants in relapse-associated genes. *PLoS One*, 5(1):e8884, Jan 2010. doi: 10.1371/journal.pone.0008884.

Cassie-Marie Peigné, Alexandra Léger, Marie-Claude Gesnel, Fabienne Konczak, Daniel Olive, Marc Bonneville, Richard Breathnach, and Emmanuel Scotet. The juxtamembrane domain of butyrophilin BTN3A1 controls phosphoantigen-mediated activation of human Vγ9Vδ2 T cells. *J Immunol*, 198 (11):4228–4234, Jun 2017. doi: 10.4049/jimmunol.1601910.

Daniel G Pellicci, Adam P Uldrich, Jérôme Le Nours, Fiona Ross, Eric Chabrol, Sidonia B G Eckle, Renate de Boer, Ricky T Lim, Kirsty McPherson, Gurdyal Besra, Amy R Howell, Lorenzo Moretta, James McCluskey, Mirjam H M Heemskerk, Stephanie Gras, Jamie Rossjohn, and Dale I Godfrey. The molecular bases of $\delta/\alpha\beta$ T cell-mediated antigen recognition. *J Exp Med*, 211(13):2599–615, Dec 2014. doi: 10.1084/jem.20141764.

Pablo Pereira, Laurent Boucontet, and Ana Cumano. Temporal predisposition to $\alpha\beta$ and $\gamma\delta$ T cell fates in the thymus. *J Immunol*, 188(4):1600–8, Feb 2012. doi: 10.4049/jimmunol.1102531.

Livia Perfetto, Pier Federico Gherardini, Norman E Davey, Francesca Diella, Manuela Helmer-Citterich, and Gianni Cesareni. Exploring the diversity of SPRY/B30.2-mediated interactions. *Trends Biochem Sci*, 38(1):38–46, Jan 2013. doi: 10.1016/j.tibs.2012.10.001.

Gyorgy Petrovics, Aijun Liu, Syed Shaheduzzaman, Bungo Furusato, Bungo Furasato, Chen Sun, Yongmei Chen, Martin Nau, Lakshmi Ravindranath, Yidong Chen, Albert Dobi, Vasantha Srikantan, Isabell A Sesterhenn, David G McLeod, Maryanne Vahey, Judd W Moul, and Shiv Srivastava. Frequent overexpression of ETS-related gene-1 (ERG1) in prostate cancer transcriptome. *Oncogene*, 24(23):3847–52, May 2005. doi: 10.1038/sj.onc.1208518.

K Pfeffer, B Schoel, H Gulle, S H Kaufmann, and H Wagner. Primary responses of human T cells to mycobacteria: a frequent set of γ/δ T cells are stimulated by protease-resistant ligands. *Eur J Immunol*, 20(5):1175–9, May 1990. doi: 10.1002/eji.1830200534.

José Pinheiro and Douglas Bates. *Mixed-Effects Models in S and S-PLUS*. Springer-Verlag New York, 1 edition, 2000. doi: 10.1007/b98882.

José Pinheiro, Douglas Bates, Saikat DebRoy, and Deepayan Sarkar. **nlme**: Linear and nonlinear mixed effects models. Technical report, R Core Team, 2020.

Vincent Pitard, David Roumanes, Xavier Lafarge, Lionel Couzi, Isabelle Garrigue, Marie-Edith Lafon, Pierre Merville, Jean-François Moreau, and Julie Déchanet-Merville. Long-term expansion of effector/memory Vδ2-$\gamma\delta$ T cells is a specific blood signature of CMV infection. *Blood*, 112(4):1317–24, Aug 2008. doi: 10.1182/blood-2008-01-136713.

Fabrizio Poccia, Cristiana Gioia, Federico Martini, Alessandra Sacchi, Paola Piacentini, Massimo Tempestilli, Chiara Agrati, Alessandra Amendola, Amina Abdeddaim, Chrysoula Vlassi, Miroslav Malkovsky, and Gianpiero D'Offizi. Zoledronic acid and interleukin-2 treatment improves immunocompetence in hiv-infected persons by activating vgamma9vdelta2 t cells. *AIDS*, 23(5):555–65, Mar 2009. doi: 10.1097/QAD.0b013e3283244619.

Fréderic Pont, Julien Familiades, Sébastien Déjean, Séverine Fruchon, Delphine Cendron, Mary Poupot, Rémy Poupot, Fatima L'faqihi-Olive, Nais Prade, Bernard Ycart, and Jean-Jacques Fournié. The gene expression profile of phosphoantigen-specific human $\gamma\delta$ T lymphocytes is a blend of $\alpha\beta$ T-cell and NK-cell signatures. *Eur J Immunol*, 42(1):228–40, Jan 2012. doi: 10.1002/eji.201141870.

Y Poquet, P Constant, F Halary, M A Peyrat, M Gilleron, F Davodeau, M Bonneville, and J J Fournié. A novel nucleotide-containing antigen for human blood $\gamma\delta$ T lymphocytes. *Eur J Immunol*, 26(10): 2344–9, Oct 1996. doi: 10.1002/eji.1830261011.

Kia-Joo Puan, Chenggang Jin, Hong Wang, Ghanashyam Sarikonda, Amy M Raker, Hoi K Lee, Megan I Samuelson, Elisabeth Märker-Hermann, Ljiljana Pasa-Tolic, Edward Nieves, José-Luis Giner, Tomohisa Kuzuyama, and Craig T Morita. Preferential recognition of a microbial metabolite by human Vγ2Vδ2 T cells. *Int Immunol*, 19(5):657–73, May 2007. doi: 10.1093/intimm/dxm031.

Gang Qin, Huawei Mao, Jian Zheng, Sin Fun Sia, Yinping Liu, Ping-Lung Chan, Kwok-Tai Lam, J S Malik Peiris, Yu-Lung Lau, and Wenwei Tu. Phosphoantigen-expanded human $\gamma\delta$ T cells display potent cytotoxicity against monocyte-derived macrophages infected with human and avian influenza viruses. *J Infect Dis*, 200(6):858–65, Sep 2009. doi: 10.1086/605413.

R Core Team. *R: A Language and Environment for Statistical Computing*. R Foundation for Statistical Computing, Vienna, Austria, 2019.

Weronika Ratajczak, Paulina Niedźwiedzka-Rystwej, Beata Tokarz-Deptuła, and Wiesław Deptuła. Immunological memory cells. *Cent Eur J Immunol*, 43(2):194–203, 2018. doi: 10.5114/ceji.2018.77390.

D A Rhodes, M Stammers, G Malcherek, S Beck, and J Trowsdale. The cluster of BTN genes in the extended major histocompatibility complex. *Genomics*, 71(3):351–62, Feb 2001. doi: 10.1006/geno.2000.6406.

David A Rhodes, Bernard de Bono, and John Trowsdale. Relationship between SPRY and B30.2 protein domains. evolution of a component of immune defence? *Immunology*, 116(4):411–7, Dec 2005. doi: 10.1111/j.1365-2567.2005.02248.x.

David A Rhodes, Hung-Chang Chen, Amanda J Price, Anthony H Keeble, Martin S Davey, Leo C James, Matthias Eberl, and John Trowsdale. Activation of human $\gamma\delta$ T cells by cytosolic interactions of BTN3A1 with soluble phosphoantigens and the cytoskeletal adaptor periplakin. *J Immunol*, 194 (5):2390–8, Mar 2015. doi: 10.4049/jimmunol.1401064.

David A Rhodes, Walter Reith, and John Trowsdale. Regulation of immunity by butyrophilins. *Annu Rev Immunol*, 34:151–72, 05 2016. doi: 10.1146/annurev-immunol-041015-055435.

Felipe Riaño, Mohindar M Karunakaran, Lisa Starick, Jianqiang Li, Claus J Scholz, Volker Kunzmann, Daniel Olive, Sabine Amslinger, and Thomas Herrmann. Vγ9Vδ2 TCR-activation by phosphorylated antigens requires butyrophilin 3 A1 (BTN3A1) and additional genes on human chromosome 6. *Eur J Immunol*, 44(9):2571–6, Sep 2014. doi: 10.1002/eji.201444712.

Rubén Felipe Riaño. *BTN3A1 in the immune response of Vγ9Vδ2 T cells*. Phd thesis, Julius-Maximilians-Universität Würzburg, 2016.

Marc Rigau, Simone Ostrouska, Thomas S. Fulford, Darryl N. Johnson, Katherine Woods, Zheng Ruan, Hamish E.G. McWilliam, Christopher Hudson, Candani Tutuka, Adam K. Wheatley, Stephen J. Kent, Jose A. Villadangos, Bhupinder Pal, Christian Kurts, Jason Simmonds, Matthias Pelzing, Andrew D. Nash, Andrew Hammet, Anne M. Verhagen, Gino Vairo, Eugene Maraskovsky, Con Panousis, Nicholas A. Gherardin, Jonathan Cebon, Dale I. Godfrey, Andreas Behren, and Adam P. Uldrich. Butyrophilin 2A1 is essential for phosphoantigen reactivity by $\gamma\delta$ T cells. *Science*, 367(6478), Feb 2020. ISSN 0036-8075. doi: 10.1126/science.aay5516.

Bladimiro Rincon-Orozco, Volker Kunzmann, Philine Wrobel, Dieter Kabelitz, Alexander Steinle, and Thomas Herrmann. Activation of Vγ9Vδ2 T cells by NKG2D. *Journal of immunology*, 175(4):2144–51, Aug 2005. doi: 10.4049/jimmunol.175.4.2144.

Brian I Rini, Steven C Campbell, and Bernard Escudier. Renal cell carcinoma. *Lancet*, 373(9669): 1119–32, Mar 2009. doi: 10.1016/S0140-6736(09)60229-4.

Horst Robenek, Oliver Hofnagel, Insa Buers, Stefan Lorkowski, Michael Schnoor, Mirko J Robenek, Hans Heid, David Troyer, and Nicholas J Severs. Butyrophilin controls milk fat globule secretion. *Proc Natl Acad Sci U S A*, 103(27):10385–10390, Jul 2006. doi: 10.1073/pnas.0600795103.

Mark D. Robinson, Davis J. McCarthy, and Gordon K. Smyth. edgeR: a Bioconductor package for differential expression analysis of digital gene expression data. *Bioinformatics*, 26(1):139–140, 11 2009. ISSN 1367-4803. doi: 10.1093/bioinformatics/btp616.

E P Rock, P R Sibbald, M M Davis, and Y H Chien. CDR3 length in antigen-specific immune receptors. *J Exp Med*, 179(1):323–8, Jan 1994. doi: 10.1084/jem.179.1.323.

M Rohmer. The discovery of a mevalonate-independent pathway for isoprenoid biosynthesis in bacteria, algae and higher plants. *Nat Prod Rep*, 16(5):565–74, Oct 1999. doi: 10.1039/a709175c.

Stephen C De Rosa, James P Andrus, Stephen P Perfetto, John J Mantovani, Leonard A Herzenberg, Leonore A Herzenberg, and Mario Roederer. Ontogeny of $\gamma\delta$ T cells in humans. *The Journal of Immunology*, 172(3):1637 1645, Apr 2004. ISSN 0022-1767. doi: 10.4049/jimmunol.172.3.1637.

Ellen V Rothenberg. Programming for t-lymphocyte fates: modularity and mechanisms. *Genes Dev*, 33(17-18):1117–1135, 09 2019. doi: 10.1101/gad.327163.119.

R G Russell, P I Croucher, and M J Rogers. Bisphosphonates: pharmacology, mechanisms of action and clinical uses. *Osteoporos Int*, 9 Suppl 2:S66–80, Apr 1999. doi: 10.1007/pl00004164.

C J Rust and F Koning. Gamma delta T cell reactivity towards bacterial superantigens. *Semin Immunol*, 5(1):41–6, Feb 1993. doi: 10.1006/smim.1993.1006.

C J Rust, F Verreck, H Vietor, and F Koning. Specific recognition of staphylococcal enterotoxin A by human T cells bearing receptors with the Vγ9 region. *Nature*, 346(6284):572–4, Aug 1990. doi: 10.1038/346572a0.

Mahboob Salim, Timothy J Knowles, Alfie T Baker, Martin S Davey, Mark Jeeves, Pooja Sridhar, John Wilkie, Carrie R Willcox, Hachemi Kadri, Taher E Taher, Pierre Vantourout, Adrian Hayday, Youcef Mehellou, Fiyaz Mohammed, and Benjamin E Willcox. BTN3A1 discriminates $\gamma\delta$ T cell phosphoantigens from nonantigenic small molecules via a conformational sensor in its B30.2 domain. *ACS chemical biology*, 12(10):2631–2643, 10 2017. doi: 10.1021/acschembio.7b00694.

Andrew Sandstrom, Erin J. Adams, Emmanuel Scotet, Marc Bonneville, Richard Breathnach, Marie-Claude Gesnel, Fabienne Konczak, James E. Crooks, Alexandra Léger, and Cassie-Marie Peigné. The intracellular B30.2 domain of butyrophilin 3A1 binds phosphoantigens to mediate activation of human Vγ9Vδ2 t cells. *Immunity*, 40:490–500, Apr 2014. ISSN 1074-7613. doi: 10.1016/j.immuni.2014.03.003.

Kerstin Sarter, Elisa Leimgruber, Florian Gobet, Vishal Agrawal, Isabelle Dunand-Sauthier, Emmanuèle Barras, Béatris Mastelic-Gavillet, Arun Kamath, Paola Fontannaz, Leslie Guéry, Fernanda do Valle Duraes, Carla Lippens, Ulla Ravn, Marie-Laure Santiago-Raber, Giovanni Magistrelli, Nicolas Fischer, Claire-Anne Siegrist, Stéphanie Hugues, and Walter Reith. Btn2a2, a T cell immunomodulatory molecule coregulated with MHC class II genes. *The Journal of experimental medicine*, 213(2): 177–187, 02 2016. doi: 10.1084/jem.20150435.

Adam K Savage, Michael G Constantinides, Jin Han, Damien Picard, Emmanuel Martin, Bofeng Li, Olivier Lantz, and Albert Bendelac. The transcription factor PLZF directs the effector program of the NKT cell lineage. *Immunity*, 29(3):391–403, Sep 2008. doi: 10.1016/j.immuni.2008.07.011.

R Sciammas and Jeff Bluestone. HSV-1 glycoprotein I-reactive TCR $\gamma\delta$ cells directly recognize the peptide backbone in a conformationally dependent manner. *Journal of immunology*, 161:5187–92, Dec 1998.

R Sciammas, R M Johnson, A I Sperling, W Brady, P S Linsley, P G Spear, F W Fitch, and J A Bluestone. Unique antigen recognition by a herpesvirus-specific TCR-$\gamma\delta$ cell. *The Journal of Immunology*, 152(11):5392–5397, Jun 1994. ISSN 0022-1767.

Emmanuel Scotet, Laurent O Martinez, Ethan Grant, Ronald Barbaras, Paul Jenö, Martine Guiraud, Bernard Monsarrat, Xavier Saulquin, Sophie Maillet, Jean-Pierre Estève, Frédéric Lopez, Bertrand Perret, Xavier Collet, Marc Bonneville, and Eric Champagne. Tumor recognition following Vγ9Vδ2 T cell receptor interactions with a surface F1-ATPase-related structure and apolipoprotein A-I. *Immunity*, 22(1):71–80, Jan 2005. doi: 10.1016/j.immuni.2004.11.012.

S. R. Searle, F. M. Speed, and G. A. Milliken. Population marginal means in the linear model: An alternative to least squares means. *The American Statistician*, 34(4):216–221, 1980. ISSN 00031305.

Zsolt Sebestyen, Wouter Scheper, Anna Vyborova, Siyi Gu, Zuzana Rychnavska, Marleen Schiffler, Astrid Cleven, Coraline Chéneau, Martje van Noorden, Cassie-Marie Peigné, Daniel Olive, Robert Jan Lebbink, Rimke Oostvogels, Tuna Mutis, Gerrit Jan Schuurhuis, Erin J Adams, Emmanuel Scotet, and Jürgen Kuball. RhoB mediates phosphoantigen recognition by Vγ9Vδ2 T cell receptor. *Cell Rep*, 15(9):1973–85, May 2016. doi: 10.1016/j.celrep.2016.04.081.

Zsolt Sebestyen, Immo Prinz, Julie Déchanet-Merville, Bruno Silva-Santos, and Jurgen Kuball. Translating gammadelta ($\gamma\delta$) T cells and their receptors into cancer cell therapies. *Nat Rev Drug Discov*, 19(3):169–184, 03 2020. doi: 10.1038/s41573-019-0038-z.

Padmanee Sharma and James P Allison. The future of immune checkpoint therapy. *Science*, 348 (6230):56–61, Apr 2015. doi: 10.1126/science.aaa8172.

Yun Shen, Dejiang Zhou, Liyou Qiu, Xioamin Lai, Meredith Simon, Ling Shen, Zhongchen Kou, Qifan Wang, Liming Jiang, Jim Estep, Robert Hunt, Michelle Clagett, Prabhat K Sehgal, Yunyaun Li, Xuejun Zeng, Craig T Morita, Michael B Brenner, Norman L Letvin, and Zheng W Chen. Adaptive immune response of Vγ2Vδ2 T cells during mycobacterial infections. *Science*, 295(5563):2255–8, Mar 2002. doi: 10.1126/science.1068819.

Sunny Shin, Ramy El-Diwany, Steven Schaffert, Erin J Adams, K Christopher Garcia, Pablo Pereira, and Yueh-Hsiu Chien. Antigen recognition determinants of $\gamma\delta$ T cell receptors. *Science*, 308(5719): 252–5, Apr 2005. doi: 10.1126/science.1106480.

Lawrence R Shiow, David B Rosen, Nadezda Brdicková, Ying Xu, Jinping An, Lewis L Lanier, Jason G Cyster, and Mehrdad Matloubian. CD69 acts downstream of interferon-α/β to inhibit S1P1 and lymphocyte egress from lymphoid organs. *Nature*, 440(7083):540–4, Mar 2006. doi: 10.1038/nature04606.

J Shires, E Theodoridis, and A C Hayday. Biological insights into TCR$\gamma\delta^+$ and TCR$\alpha\beta^+$ intraepithelial lymphocytes provided by serial analysis of gene expression (SAGE). *Immunity*, 15(3):419–34, Sep 2001. doi: 10.1016/s1074-7613(01)00192-3.

G K Sim, R Rajaserkar, M Dessing, and A Augustin. Homing and in situ differentiation of resident pulmonary lymphocytes. *Int Immunol*, 6(9):1287–95, Sep 1994. doi: 10.1093/intimm/6.9.1287.

Rita Simone, Bernadette Barbarat, Andrea Rabellino, Giancarlo Icardi, Marcello Bagnasco, Giampaola Pesce, Daniel Olive, and Daniele Saverino. Ligation of the BT3 molecules, members of the B7 family, enhance the proinflammatory responses of human monocytes and monocyte-derived dendritic cells. *Mol Immunol*, 48(1-3):109–18, 2010. doi: 10.1016/j.molimm.2010.09.005.

Isobel A Smith, Brittany R Knezevic, Johannes U Ammann, David A Rhodes, Danielle Aw, Donald B Palmer, Ian H Mather, and John Trowsdale. BTN1A1, the mammary gland butyrophilin, and BTN2A2 are both inhibitors of T cell activation. *J Immunol*, 184(7):3514–25, Apr 2010. doi: 10.4049/jimmunol.0900416.

M J Soloski, M Oudshoorn-Snoek, G Einhorn, and P Demant. Molecular basis of Qa-11 antigen and paradoxical Qa-gene expression in an H-2 recombinant. *J Immunol*, 143(9):3074–3080, Nov 1989. ISSN 0022-1767 (Print); 0022-1767 (Linking).

F M Spada, E P Grant, P J Peters, M Sugita, A Melián, D S Leslie, H K Lee, E van Donselaar, D A Hanson, A M Krensky, O Majdic, S A Porcelli, C T Morita, and M B Brenner. Self-recognition of CD1 by γ/δ T cells: implications for innate immunity. *J Exp Med*, 191(6):937–48, Mar 2000. doi: 10.1084/jem.191.6.937.

Lisa Starick, Felipe Riano, Mohindar M Karunakaran, Volker Kunzmann, Jianqiang Li, Matthias Kreiss, Sabine Amslinger, Emmanuel Scotet, Daniel Olive, Gennaro De Libero, and Thomas Herrmann. Butyrophilin 3A (BTN3A, CD277)-specific antibody 20.1 differentially activates Vγ9Vδ2 TCR clonotypes and interferes with phosphoantigen activation. *Eur J Immunol*, 47(6):982–992, 06 2017. doi: 10.1002/eji.201646818.

A Stefferl, A Schubart, M Storch2, A Amini, I Mather, H Lassmann, and C Linington. Butyrophilin, a milk protein, modulates the encephalitogenic T cell response to myelin oligodendrocyte glycoprotein in experimental autoimmune encephalomyelitis. *J Immunol*, 165(5):2859–65, Sep 2000. doi: 10.4049/jimmunol.165.5.2859.

Alexander B Stillebroer, Peter F A Mulders, Otto C Boerman, Wim J G Oyen, and Egbert Oosterwijk. Carbonic anhydrase IX in renal cell carcinoma: implications for prognosis, diagnosis, and therapy. *Eur Urol*, 58(1):75–83, Jul 2010. doi: 10.1016/j.eururo.2010.03.015.

Jennifer D Stone, Adam S Chervin, and David M Kranz. T-cell receptor binding affinities and kinetics: impact on T-cell activity and specificity. *Immunology*, 126(2):165–76, Feb 2009. doi: 10.1111/j.1365-2567.2008.03015.x.

Jessica Strid, Olga Sobolev, Biljana Zafirova, Bojan Polic, and Adrian Hayday. The intraepithelial T cell response to NKG2D-ligands links lymphoid stress surveillance to atopy. *Science*, 334(6060): 1293–7, Dec 2011. doi: 10.1126/science.1211250.

S J Szabo, S T Kim, G L Costa, X Zhang, C G Fathman, and L H Glimcher. A novel transcription factor, T-bet, directs Th1 lineage commitment. *Cell*, 100(6):655–69, Mar 2000. doi: 10.1016/s0092-8674(00)80702-3.

M Takamizawa, F Fagnoni, A Mehta-Damani, A Rivas, and E G Engleman. Cellular and molecular basis of human gamma delta T cell activation. role of accessory molecules in alloactivation. *J Clin Invest*, 95(1):296–303, Jan 1995. doi: 10.1172/JCI117654.

Y Tanaka, M B Brenner, B R Bloom, and C T Morita. Recognition of nonpeptide antigens by T cells. *J Mol Med*, 74(5):223–31, May 1996. doi: 10.1007/bf00196576.

Yoshimasa Tanaka, Craig T. Morita, Yoko Tanaka, Edward Nieves, Michael B. Brenner, and Barry R. Bloom. Natural and synthetic non-peptide antigens recognized by human $\gamma\delta$ T cells. *Nature*, 375 (6527):155–158, May 1995. doi: 10.1038/375155a0.

Francesca Toia, Simona Buccheri, Ampelio Anfosso, Francesco Moschella, Francesco Dieli, Serena Meraviglia, and Adriana Cordova. Skewed differentiation of circulating Vγ9Vδ2 T lymphocytes in melanoma and impact on clinical outcome. *PLoS One*, 11(2):e0149570, Feb 2016. doi: 10.1371/journal.pone.0149570.

Antoine Toulon, Lionel Breton, Kristen R Taylor, Mayer Tenenhaus, Dhaval Bhavsar, Caroline Lanigan, Ross Rudolph, Julie Jameson, and Wendy L Havran. A role for human skin-resident T cells in wound healing. *J Exp Med*, 206(4):743–50, Apr 2009. doi: 10.1084/jem.20081787.

Ang A Tu, Todd M Gierahn, Brinda Monian, Duncan M Morgan, Naveen K Mehta, Bert Ruiter, Wayne G Shreffler, Alex K Shalek, and J Christopher Love. Tcr sequencing paired with massively parallel 3' RNA-seq reveals clonotypic T cell signatures. *Nat Immunol*, 20(12):1692–1699, 12 2019. doi: 10.1038/s41590-019-0544-5.

W W Tu, Y L Lau, and J S M Peiris. Use of humanised mice to study antiviral activity of human $\gamma\delta$-T cells against influenza A viruses. *Hong Kong Med J*, 20 Suppl 6:4–6, Dec 2014.

Gleb Turchinovich and Adrian C Hayday. Skint-1 identifies a common molecular mechanism for the development of interferon-γ-secreting versus interleukin-17-secreting $\gamma\delta$ T cells. *Immunity*, 35(1): 59–68, Jul 2011. doi: 10.1016/j.immuni.2011.04.018.

Adam P Uldrich, Jérôme Le Nours, Daniel G Pellicci, Nicholas A Gherardin, Kirsty G McPherson, Ricky T Lim, Onisha Patel, Travis Beddoe, Stephanie Gras, Jamie Rossjohn, and Dale I Godfrey. CD1d-lipid antigen recognition by the $\gamma\delta$ TCR. *Nat Immunol*, 14(11):1137–45, Nov 2013. doi: 10.1038/ni.2713.

Adam P Uldrich, Marc Rigau, and Dale I Godfrey. Immune recognition of phosphoantigen-butyrophilin molecular complexes by $\gamma\delta$ T cells. *Immunol Rev*, Oct 2020. doi: 10.1111/imr.12923.

Ruta Valentonyte, Jochen Hampe, Klaus Huse, Philip Rosenstiel, Mario Albrecht, Annette Stenzel, Marion Nagy, Karoline I Gaede, Andre Franke, Robert Haesler, Andreas Koch, Thomas Lengauer, Dirk Seegert, Norbert Reiling, Stefan Ehlers, Eberhard Schwinger, Matthias Platzer, Michael Krawczak, Joachim Müller-Quernheim, Manfred Schürmann, and Stefan Schreiber. Sarcoidosis is associated with a truncating splice site mutation in BTNL2. *Nat Genet*, 37(4):357–64, Apr 2005. doi: 10.1038/ng1519.

Angélique B van 't Wout, J Victor Swain, Michael Schindler, Ushnal Rao, Melissa S Pathmajeyan, James I Mullins, and Frank Kirchhoff. Nef induces multiple genes involved in cholesterol synthesis and uptake in human immunodeficiency virus type 1-infected T cells. *J Virol*, 79(15):10053–8, Aug 2005. doi: 10.1128/JVI.79.15.10053-10058.2005.

Pierre Vantourout and Adrian Hayday. Six-of-the-best: unique contributions of $\gamma\delta$ T cells to immunology. *Nat Rev Immunol*, 13(2):88–100, Feb 2013. doi: 10.1038/nri3384.

Pierre Vantourout, Jayati Mookerjee-Basu, Corinne Rolland, Frédéric Pont, Hélène Martin, Christian Davrinche, Laurent O Martinez, Bertrand Perret, Xavier Collet, Christian Périgaud, Suzanne Peyrottes, and Eric Champagne. Specific requirements for Vγ9Vδ2 T cell stimulation by a natural adenylated phosphoantigen. *J Immunol*, 183(6):3848–57, Sep 2009. doi: 10.4049/jimmunol.0901085.

Pierre Vantourout, Adam Laing, Martin J Woodward, Iva Zlatareva, Luis Apolonia, Andrew W Jones, Ambrosius P Snijders, Michael H Malim, and Adrian C Hayday. Heteromeric interactions regulate butyrophilin (BTN) and BTN-like molecules governing $\gamma\delta$ T cell biology. *Proc Natl Acad Sci U S A*, 115(5):1039–1044, Jan 2018. doi: 10.1073/pnas.1701237115.

Stefano Vavassori, Anil Kumar, Gan Siok Wan, Gundimeda S Ramanjaneyulu, Marco Cavallari, Sary El Daker, Travis Beddoe, Alex Theodossis, Neal K Williams, Emma Gostick, David A Price, Dinish U Soudamini, Kong Kien Voon, Malini Olivo, Jamie Rossjohn, Lucia Mori, and Gennaro De Libero. Butyrophilin 3A1 binds phosphorylated antigens and stimulates human $\gamma\delta$ T cells. *Nat Immunol*, 14 (9):908–16, Sep 2013. doi: 10.1038/ni.2665.

Rodrigo Vazquez-Lombardi, Rodrigo Vazquez-Lombardi, Damien Nevoltris, Damien Nevoltris, Ansha Luthra, Ansha Luthra, Peter Schofield, Peter Schofield, Carsten Zimmermann, Carsten Zimmermann, Daniel Christ, and Daniel Christ. Transient expression of human antibodies in mammalian cells. *Nature Protocols*, 13(1):99 117, 2017. ISSN 1750-2799. doi: 10.1038/nprot.2017.126.

Francisco M Vega and Anne J Ridley. The RhoB small GTPase in physiology and disease. *Small GTPases*, 9(5):384–393, Sep 2018. doi: 10.1080/21541248.2016.1253528.

David Vermijlen, Peter Ellis, Cordelia Langford, Anne Klein, Rosel Engel, Katharina Willimann, Hassan Jomaa, Adrian C Hayday, and Matthias Eberl. Distinct cytokine-driven responses of activated blood $\gamma\delta$ T cells: insights into unconventional T cell pleiotropy. *J Immunol*, 178(7):4304–14, Apr 2007. doi: 10.4049/jimmunol.178.7.4304.

Erik Verschueren, Bushra Husain, Kobe Yuen, Yi Sun, Sairupa Paduchuri, Yasin Senbabaoglu, Isabelle Lehoux, Tia A. Arena, Blair Wilson, Steve Lianoglou, Corey Bakalarski, Yvonne Franke, Pamela Chan, Athena W. Wong, Lino C. Gonzalez, Sanjeev Mariathasan, Shannon J. Turley, Jennie R. Lill, and Nadia Martinez-Martin. The immunoglobulin superfamily receptome defines cancer-relevant networks associated with clinical outcome. *Cell*, 182:1–16, July 2020. doi: 10.1016/j.cell.2020.06.007.

Damir Vidović, Mihovil Roglić, Keith McKune, Sylvie Guerder, Charles MacKay, and Zlatko Dembić. Qa-1 restricted recognition of foreign antigen by a $\gamma\delta$ T-cell hybridoma. *Nature*, 340(6235):646–650, Aug 1989. ISSN 0028-0836. doi: 10.1038/340646a0.

Emilie Viey, Gaëlle Fromont, Bernard Escudier, Yannis Morel, Sylvie Da Rocha, Salem Chouaib, and Anne Caignard. Phosphostim-activated $\gamma\delta$ T cells kill autologous metastatic renal cell carcinoma. *J Immunol*, 174(3):1338–47, Feb 2005. doi: 10.4049/jimmunol.174.3.1338.

M K Viken, A Blomhoff, M Olsson, H E Akselsen, F Pociot, J Nerup, I Kockum, A Cambon-Thomsen, E Thorsby, D E Undlien, and B A Lie. Reproducible association with type 1 diabetes in the extended class i region of the major histocompatibility complex. *Genes Immun*, 10(4):323–33, Jun 2009. doi: 10.1038/gene.2009.13.

Franz F Wagner, Joyce Poole, and Willy A Flegel. Scianna antigens including rd are expressed by ERMAP. *Blood*, 101(2):752–7, Jan 2003. doi: 10.1182/blood-2002-07-2064.

Hong Wang and Craig T Morita. Sensor function for butyrophilin 3A1 in prenyl pyrophosphate stimulation of human Vγ2Vδ2 T cells. *Journal of immunology*, 195(10):4583–4594, 11 2015. doi: 10.4049/jimmunol.1500314.

Hong Wang, Hoi K Lee, Jack F Bukowski, Hongmin Li, Roy A Mariuzza, Zheng W Chen, Ki-Hoan Nam, and Craig T Morita. Conservation of nonpeptide antigen recognition by rhesus monkey Vγ2Vδ2 T cells. *J Immunol*, 170(7):3696–706, Apr 2003. doi: 10.4049/jimmunol.170.7.3696.

Hong Wang, Zhimei Fang, and Craig T Morita. Vγ2Vδ2 T cell receptor recognition of prenyl pyrophosphates is dependent on all CDRs. *J Immunol*, 184(11):6209–22, Jun 2010. doi: 10.4049/jimmunol.1000231.

Hong Wang, Mohanad H Nada, Yoshimasa Tanaka, Shun Sakuraba, and Craig T Morita. Critical roles for coiled-coil dimers of butyrophilin 3A1 in the sensing of prenyl pyrophosphates by human Vγ2Vδ2 T cells. *J Immunol*, 203(3):607–626, 08 2019. doi: 10.4049/jimmunol.1801252.

L Wang, A Kamath, H Das, L Li, and J F Bukowski. Antibacterial effect of human Vγ2Vδ2 T cells in vivo. *J Clin Invest*, 108(9):1349–57, Nov 2001. doi: 10.1172/JCI13584.

L Wen, W Pao, F S Wong, Q Peng, J Craft, B Zheng, G Kelsoe, L Dianda, M J Owen, and A C Hayday. Germinal center formation, immunoglobulin class switching, and autoantibody production driven by "non-α/β" T cells. *J Exp Med*, 183(5):2271–82, May 1996. doi: 10.1084/jem.183.5.2271.

Heinz Wiendl, Joachim Malotka, Brigitte Holzwarth, Hans-Ulrich Weltzien, Hartmut Wekerle, Reinhard Hohlfeld, and Klaus Dornmair. An autoreactive $\gamma\delta$ TCR derived from a polymyositis lesion. *J Immunol*, 169(1):515–21, Jul 2002. doi: 10.4049/jimmunol.169.1.515.

Benjamin E. Willcox and Carrie R. Willcox. $\gamma\delta$ TCR ligands: the quest to solve a 500-million- year-old mystery. *Nat Immunol*, 20:121–128, Feb 2019. doi: 10.1038/s41590-018-0304-y.

Carrie R Willcox, Vincent Pitard, Sonia Netzer, Lionel Couzi, Mahboob Salim, Tobias Silberzahn, Jean-François Moreau, Adrian C Hayday, Benjamin E Willcox, and Julie Déchanet-Merville. Cytomegalovirus and tumor stress surveillance by binding of a human $\gamma\delta$ T cell antigen receptor to endothelial protein C receptor. *Nat Immunol*, 13(9):872–9, Sep 2012. doi: 10.1038/ni.2394.

Carrie R Willcox, Pierre Vantourout, Mahboob Salim, Iva Zlatareva, Daisy Melandri, Leonor Zanardo, Roger George, Svend Kjaer, Mark Jeeves, Fiyaz Mohammed, Adrian C Hayday, and Benjamin E Willcox. Butyrophilin-like 3 directly binds a human Vγ4+ T cell receptor using a modality distinct from clonally-restricted antigen. *Immunity*, 51(5):813–825.e4, Nov 2019. doi: 10.1016/j.immuni.2019.09.006.

C Wingren, M P Crowley, M Degano, Y Chien, and I A Wilson. Crystal structure of a $\gamma\delta$ T cell receptor ligand T22: a truncated MHC-like fold. *Science*, 287(5451):310–4, Jan 2000. doi: 10.1126/science.287.5451.310.

Wing Ki Wong, Jinwoo Leem, and Charlotte M Deane. Comparative analysis of the CDR loops of antigen receptors. *Frontiers in Immunology*, 10:2454, Oct 2019. doi: 10.3389/fimmu.2019.02454.

Di Wu and Gordon K Smyth. Camera: a competitive gene set test accounting for inter-gene correlation. *Nucleic Acids Res*, 40(17):e133, Sep 2012. doi: 10.1093/nar/gks461.

Jennifer Wu, Veronika Groh, and Thomas Spies. T cell antigen receptor engagement and specificity in the recognition of stress-inducible MHC class I-related chains by human epithelial $\gamma\delta$ T cells. *J Immunol*, 169(3):1236–40, Aug 2002. doi: 10.4049/jimmunol.169.3.1236.

Xueyan Xi, Lianxian Cui, and Wei He. The recognition of gammadelta TCR to protein antigen does not depend on the hydrophobic I97 residue of CDR3δ. *Int Immunol*, 22(4):299–306, Apr 2010. doi: 10.1093/intimm/dxq011.

Bin Xu, Juan C Pizarro, Margaret A Holmes, Christine McBeth, Veronika Groh, Thomas Spies, and Roland K Strong. Crystal structure of a gammadelta T-cell receptor specific for the human MHC class I homolog MICA. *PNAS*, 108(6):2414–2419, 02 2011. doi: 10.1073/pnas.1015433108.

Ryoji Yagi, Chao Zhong, Daniel L Northrup, Fang Yu, Nicolas Bouladoux, Sean Spencer, Gangqing Hu, Luke Barron, Suveena Sharma, Toshinori Nakayama, Yasmine Belkaid, Keji Zhao, and Jinfang Zhu. The transcription factor GATA3 is critical for the development of all IL-7Rα-expressing innate lymphoid cells. *Immunity*, 40(3):378–88, Mar 2014. doi: 10.1016/j.immuni.2014.01.012.

Hiromichi Yamashiro, Shinji Yoshizaki, Toshimasa Tadaki, Kohji Egawa, and Naohiro Seo. Stimulation of human butyrophilin 3 molecules results in negative regulation of cellular immunity. *J Leukoc Biol*, 88(4):757–67, Oct 2010. doi: 10.1189/jlb.0309156.

Seiji Yamashita, Yoshimasa Tanaka, Masashi Harazaki, Bunzo Mikami, and Nagahiro Minato. Recognition mechanism of non-peptide antigens by human $\gamma\delta$ T cells. *Int Immunol*, 15(11):1301–7, Nov 2003. doi: 10.1093/intimm/dxg129.

Tomohide Yamazaki, Iñigo Goya, Daniel Graf, Suzanne Craig, Natalia Martin-Orozco, and Chen Dong. A butyrophilin family member critically inhibits T cell activation. *J Immunol*, 185(10):5907–14, Nov 2010. doi: 10.4049/jimmunol.1000835.

Yang Yang, Xikui K Liu, Thang Nguyen, Caroline Bishop, Daniel Graf, and Chen Dong. Characterization of B7S3 as a novel negative regulator of T cells. *J Immunol*, 178(6):3661–7, Mar 2007. doi: 10.4049/jimmunol.178.6.3661.

Yunyun Yang, Liping Li, Linjie Yuan, Xiaoying Zhou, Jianxin Duan, Hongying Xiao, Ningning Cai, Shuai Han, Xianqiang Ma, Weidong Liu, Chun-Chi Chen, Lingle Wang, Xin Li, Jiahuan Chen, Ning Kang, Jing Chen, Zhixun Shen, Satish R. Malwal, Wanli Liu, Yan Shi, Eric Oldfield, Rey-Ting Guo, and Yonghui Zhang. A structural change in butyrophilin upon phosphoantigen binding underlies phosphoantigen-mediated vγ9vγ2 T cell activation. *Immunity*, 50(4):1043 – 1053.e5, Apr 2019. ISSN 1074-7613. doi: 10.1016/j.immuni.2019.02.016.

T Z Ye, C T Gordon, Y H Lai, Y Fujiwara, L L Peters, A C Perkins, and D H Chui. Ermap, a gene coding for a novel erythroid specific adhesion/receptor membrane protein. *Gene*, 242(1-2):337–45, Jan 2000. doi: 10.1016/s0378-1119(99)00516-8.

Tetsuro Yoshida, Kimihiko Kato, Hideki Horibe, Mitsutoshi Oguri, Michio Fukuda, Kei Satoh, Yukitoshi Aoyagi, Shoji Shinkai, Yoshinori Nozawa, and Yoshiji Yamada. Association of a genetic variant of BTN2A1 with chronic kidney disease in Japanese individuals. *Nephrology (Carlton)*, 16(7):642–8, Sep 2011a. doi: 10.1111/j.1440-1797.2011.01470.x.

Tetsuro Yoshida, Kimihiko Kato, Mitsutoshi Oguri, Hideki Horibe, Toshiki Kawamiya, Kiyoshi Yokoi, Tetsuo Fujimaki, Sachiro Watanabe, Kei Satoh, Yukitoshi Aoyagi, Masashi Tanaka, Hiroto Yoshida, Shoji Shinkai, Yoshinori Nozawa, and Yoshiji Yamada. Association of polymorphisms of BTN2A1 and ILF3 with myocardial infarction in japanese individuals with different lipid profiles. *Mol Med Rep*, 4(3):511–8, 2011b. doi: 10.3892/mmr.2011.441.

Irfan Zaidi, Hama Diallo, Solomon Conteh, Yvette Robbins, Jacqueline Kolasny, Sachy Orr-Gonzalez, Dariyen Carter, Brandi Butler, Lynn Lambert, Elizabeth Brickley, Robert Morrison, Mahamadou Sissoko, Sara A Healy, B Kim Lee Sim, Ogobara K Doumbo, Stephen L Hoffman, and Patrick E Duffy. $\gamma\delta$ T cells are required for the induction of sterile immunity during irradiated sporozoite vaccinations. *J Immunol*, 199(11):3781–3788, 12 2017. doi: 10.4049/jimmunol.1700314.

Dirk M Zajonc, M D Max Crispin, Thomas A Bowden, David C Young, Tan-Yun Cheng, Jingdan Hu, Catherine E Costello, Pauline M Rudd, Raymond A Dwek, Marvin J Miller, Michael B Brenner, D Branch Moody, and Ian A Wilson. Molecular mechanism of lipopeptide presentation by CD1a. *Immunity*, 22(2):209 219, Feb 2005. ISSN 1074-7613. doi: 10.1016/j.immuni.2004.12.009.

Xun Zeng, Yu-Ling Wei, Jun Huang, Evan W Newell, Hongxiang Yu, Brian A Kidd, Michael S Kuhns, Ray W Waters, Mark M Davis, Casey T Weaver, and Yueh-hsiu Chien. $\gamma\delta$ T cells recognize a microbial encoded B cell antigen to initiate a rapid antigen-specific interleukin-17 response. *Immunity*, 37(3):524–34, Sep 2012. doi: 10.1016/j.immuni.2012.06.011.

Ibrahim Zgani, Chantal Menut, Michel Seman, Valerie Gallois, Virginie Laffont, Jeanine Liautard, Jean-Pierre Liautard, Marc Criton, and Jean-Louis Montero. Synthesis of prenyl pyrophosphonates as new potent phosphoantigens inducing selective activation of human Vγ9Vδ2 T lymphocytes. *J Med Chem*, 47(18):4600–12, Aug 2004. doi: 10.1021/jm049861z.

Huiyuan Zhang, Hongbo Hu, Xinxin Jiang, Hongbin He, Lianxian Cui, and Wei He. Membrane HSP70: the molecule triggering $\gamma\delta$ T cells in the early stage of tumorigenesis. *Immunol Invest*, 34(4):453–68, 2005. doi: 10.1080/08820130500265349.

Jiang Zhang, Marie Marotel, Sébastien Fauteux-Daniel, Anne-Laure Mathieu, Sébastien Viel, Antoine Marçais, and Thierry Walzer. T-bet and eomes govern differentiation and function of mouse and human nk cells and ilc1. *Eur J Immunol*, 48(5):738–750, 05 2018. doi: 10.1002/eji.201747299.

Li Zhang, Niyun Jin, Maki Nakayama, Rebecca L O'Brien, George S Eisenbarth, and Willi K Born. Gamma delta T cell receptors confer autonomous responsiveness to the insulin-peptide B:9-23. *J Autoimmun*, 34(4):478–84, Jun 2010. doi: 10.1016/j.jaut.2009.12.008.

Tong Zhang, Amorette Barber, and Charles L Sentman. Generation of antitumor responses by genetic modification of primary human T cells with a chimeric NKG2D receptor. *Cancer Res*, 66(11):5927–33, Jun 2006. doi: 10.1158/0008-5472.CAN-06-0130.

Alessandra Zingoni, Rosa Molfetta, Cinzia Fionda, Alessandra Soriani, Rossella Paolini, Marco Cippitelli, Cristina Cerboni, and Angela Santoni. NKG2D and its ligands: "one for all, all for one". *Front Immunol*, 9:476, Mar 2018. doi: 10.3389/fimmu.2018.00476.

Curriculum Vitae

Marc Rigau

Education

2017–Present	**PhD** - Boomerang Program - University of Melbourne and *Rheinische Friedrich-Wilhelms-Universität Bonn*.
2015–16	**MSc Biology** - Ludwig-Maximilians-Universität, Munich, Germany.
2014–15	**Erasmus-Program** - The Arctic University of Norway, Tromsø, Norway.
2011–15	**BS in Biology** - Universidad de Navarra, Iruña, Spain.
2013–14	**Research training** - Universidad de Navarra, Iruña, Spain; Topic: "*Phenotype determination of the hypothalamic cell targets of striatofugal axons from the nucleus accumbens in the rat brain*."
2002–04	**Electromechanical technician training** - *Institut d'Educació Secondaria La Garrotxa*, 17800 Olot, Spain.

Employment

Mar-Apr 2018	**The Florey Institute of Neuroscience and Mental Health**, Melbourne, Australia. Animal technician.
Jun-Aug 2017	**Peter Doherty Institute for Infection and Immunity** - Melbourne, Australia. Research assistant.
Apr-Sep 2016	***Max-Planck-Institut für Ornithologie*** - Seewiesen, Germany. MSc Biology practicum.
2006-11	**Fruits Secs Cortal S.L.** - Industrial maintenance and production manager.
2003-05	**Tallers Mecànics Colomer S.L.** - Industrial Mechanic.
Feb-Aug 2002	**Camòs i Fills S.L.** - Security systems.

Languages

Catalan and Spanish bilingual; English advanced (CAE; score 185; 2017); German basic (currently A2.2 in the CEFR); Norwegian elementary.

Software

Research

LaTeX Free software system for writing scientific documents (mathematics, statistics, chemistry, biology, computer science, engineering, physics, economics, etc.). Leslie Lamport, 1984. LaTeX Project Public License.

R Programming language and free software environment for statistical computing and graphics supported. Ross Ihaka and Robert Gentleman, University of Auckland, 1993. GNU GPL License.

ASReml Statistical software package for fitting linear mixed models using restricted maximum likelihood. VSNI, UK.

ArcGIS Geographic information system software for working with maps and geographic information. Environmental Systems Research Institute (Esri), 1999.

FlowJo Software package for analysing flow cytometry data. FlowJo LLC,1996.

CLC Genomics Workbench Software for cloud-based bioinformatics workflow execution. CLC Bio, 2020.

PyMOL Open source molecular visualisation system. Warren Lyford DeLano, 2000. Phyton License.

Operative Systems

macOS Graphical operating systems developed and marketed by Apple Inc since 2001.

Windows Graphical operating system families developed and marketed by Microsoft Inc.

Office Technology

Apple Inc. Numbers, Keynote, and Pages as a main IT software products (spreadsheets, presentations, and edition, respectively).

Microsoft Inc Excel, Powerpoint, and Word as a main IT software products (spreadsheets, presentations, and edition, respectively).

Publications

Oct 2020	Adam P. Uldrich, Marc Rigau, Dale I. Godfrey. Immune recognition of phosphoantigen–butyrophilin molecular complexes by $\gamma\delta$ T cells. *Immunological Reviews*, Oct 2020. doi: 10.1111/imr.12923 [in press]
Jan 2020	Marc Rigau, Simone Ostrouska, Thomas S. Fulford, Darryl N. Johnson, Katherine Woods, Zheng Ruan, Hamish E. McWilliam, Christopher Hudson, Candani Tutuka, Adam K. Wheatley, Stephen J. Kent, Jose A. Villadangos, Bhupinder Pal, Andrew Hammet, Anne M. Verhagen, Gino Vairo, Eugene Maraskovsky, Con Panousis, Nicholas A. Gherardin, Jonathan Cebon, Dale I. Godfrey, Andreas Behren, Adam P. Uldrich. Butyrophilin 2A1 is essential for phosphoantigen reactivity by $\gamma\delta$ T cells. *Science*, Jan 2020. doi: 10.1126/science.aay5516

Patents

Dec 2020 **International Patent** entitled "*Method of inhibiting or activating gamma delta T cells*"; Andreas Behren, Jonathan Cebon, Marc Rigau, Thomas S. Fulford, Dale I. Godfrey, Andrew Hammet, Simone Ostrouska, Con Panousis, Adam P. Uldrich; Number WO 2020/257871 A1.

Appendix A

Generation, Titration, and Validation of Reagents

A.1 Production of Soluble Vγ9Vδ2 T-cell Receptor and Butyrophilin Fluorescent Probes

Constructs for mammalian or bacterial cell culture expression systems were adapted to contain DNA sequences encoding for respective TCR clonotypes or BTN protein. These were genetically modified to insert a pice of DNA containing either a mutation for alanine scan, a site-directed mutagenesis to produce a BTN truncated protein, or a section gene that encoded for a fluorescent reporter protein. To confirm the correct genetic insertion, cloned constructed plasmids were run on an electrophoresis gel and subsequently sequenced in the Sanger method for verification. The clones containing correct sequences were transfected on desired cell types and the expression of the plasmid confirmed by the fluorescence reporter protein or antibody-labeled detection of the surface expression molecule by flow cytometry.

A.2 Prevention from Secondary Antibody Cross-reactivity

In some experiments, primary purified unconjugated antibodies were detected with a conjugated solid-absorbed secondary goat anti-mouse IgG labelled antibodies. Thus, we confirmed the absence of secondary goat anti-mouse secondary antibody cross-reactivity (Fig. A.3 a). Additionally, we prevented nonspecific binding of primary monoclonal antibodies to human Fc receptors. Two comercial available brands (Beckon Dickinson and Miltenyi Biotec) were evaluated (Fig. A.3 b) and titrated to determine its most adequate dilution for use in our experiments with human cells (Fig. A.3 c).

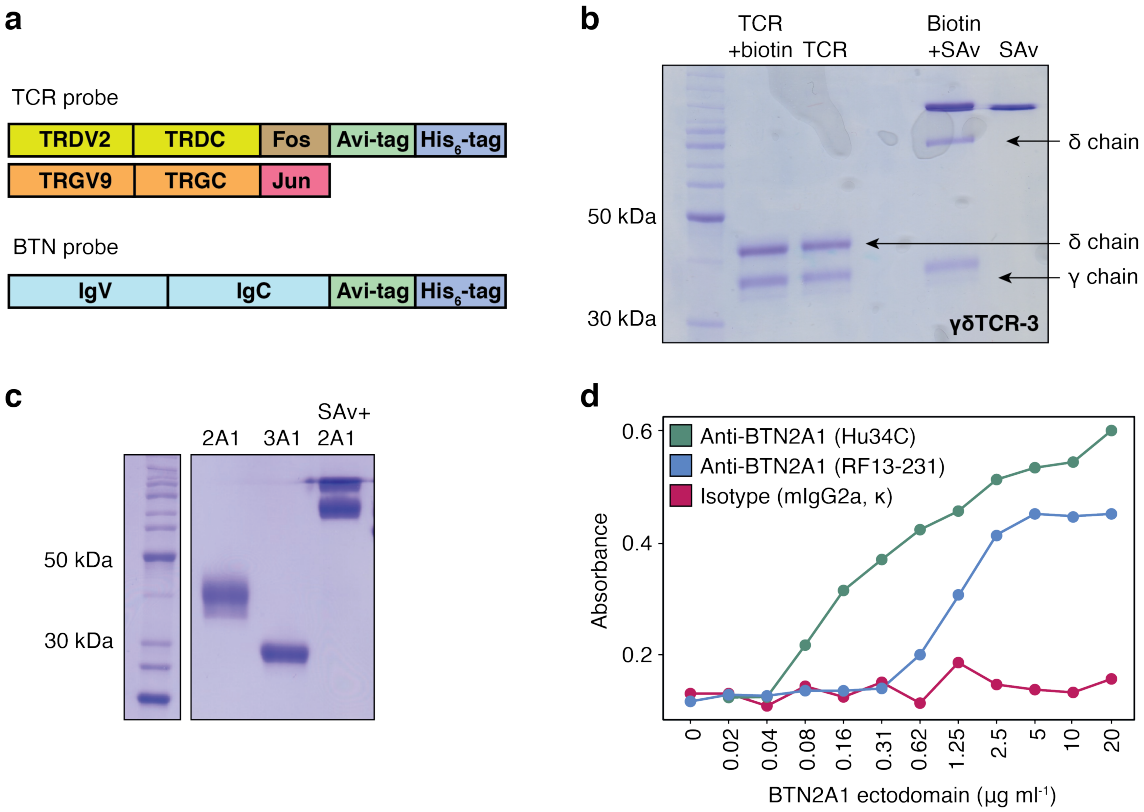

Figure A.1: *In (a) design of soluble $\gamma\delta$ TCR and BTN constructs containing full-length ectodomains where Fos and Jun are leucine zippers that join both $\gamma\delta$ TCR chains and like BTN2A1 ectodomain composed of IgV and IgC regions (Q29–S245) were fused to a carbosyl-terminal linker (GTGSGSGG), followed by Avi (biotin ligase) and His6 tags (LNDIFEAQKIEWHEHHHHHH). SDS–PAGE analysis of (b) denatured soluble biotinylated and unbiotinylated Vγ9Vδ2 TCR clone 3, either alone or mixed with undenatured native streptavidin (SAv), showing incorporation of the biotinylated TCR δ-chain into a complex with native streptavidin by a protein molecular weight marker and (c) biotinylated BTN2A1 and respective control ectodomains produced in HEK-293T cells by a molecular weight marker. Right-hand lane contains denatured BTN2A1–biotin complexed with undenatured native streptavidin (SAv); (d) ELISA of plate-bound BTN2A1 ectodomain reactivity to anti-BTN2A1 clones Hu34C (green) and RF13-231 (blue), compared to mouse BM4 isotype control (red).*

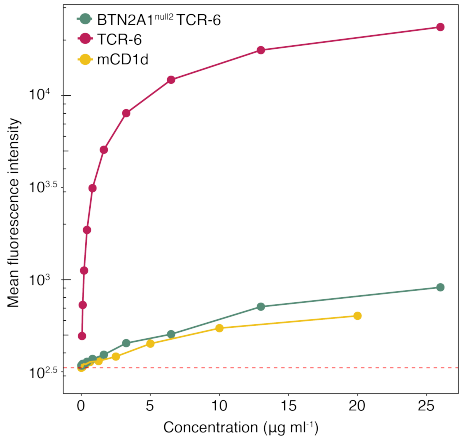

Figure A.2: *Titration of tetramer TCR-6 in LM-MEL-62 and respective* BTN2A1^{null2}*. A control mouse CD1d*α*-GalCer conjugate to streptavidin-PE was included, which sets the dashed baseline.*

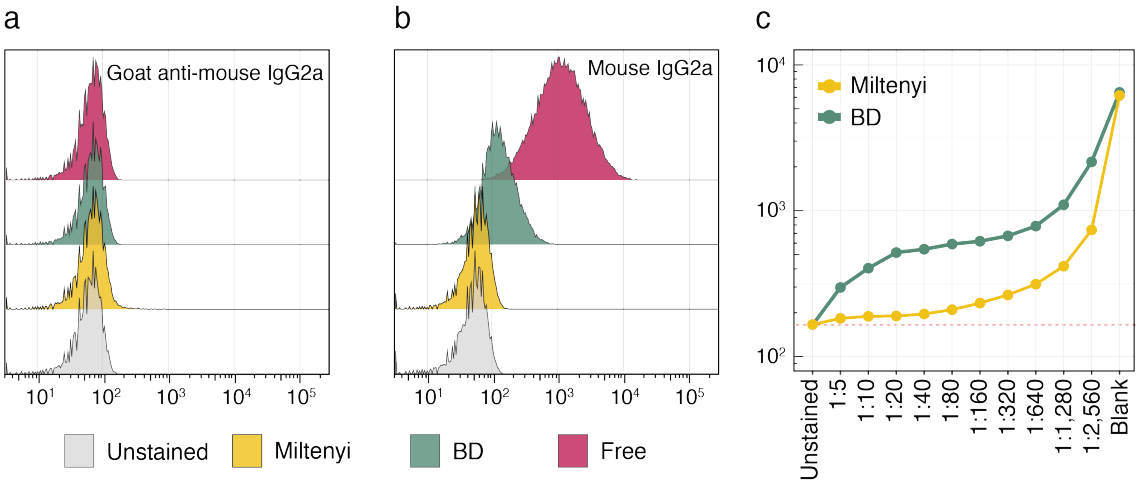

Figure A.3: *Antibody unspecificity controls for (a) goat anti-mouse polyclonal secondary antibody (conjugated to AF-647) targeting unspecific surface protein was confirmed absent; (b) mouse IgG2a isotype control (conjugated to PE) was used to evaluate efficiency of 1:10 diluted Becton Dickinson (BD) or Miltenyi Biotec (Miltenyi Biotec) Fc-receptor blocking agents (c) Fc-receptor blocking agents were titrated; experiments were treated with Fc-block for 20 min at 4 ℃ before subsequent staining of (a-b) 100 k or (c) 1 M human THP-1 monocytic leukemia cells.*

A.3 Generation of Monoclonal Antibodies

A.3.1 Cloning and Elution Profiles of anti-BTN3A Antibodies

Antibody clone variable sequences against BTN3A protein members were obtained from the Palakodeti et al. (2012) entry in the protein data bank website (Berman et al., 2000, last access 2020) and optimised for a mammalian expression system (Table. A.1). After antibody expression, the monoclonal antibody clones 20.1 and 103.2 were purified and run in an electrophoresis gels (Fig. A.4) and elution profiles (Fig. A.5) for verification of the purified and consolidated final product.

Table A.1: *Codon-optimised of clones 20.1 and 103.2 anti-human BTN3A monoclonal antibody construct details for the IGKV15-103 light and IGHV1S81*02 *heavy chains including somatic hypermutations (single chain fusion sequences from PDB codes 4F9L [20.1] and 4F9P [103.2]). Cloning of light chain variable domain into high copy number Kanamycin-resistance in DH5alpha vector containing existing mouse IGKC domain with AgeI (ACCGGT)/BsiWI (CGTACG) and heavy chain variable domain cloned into vector containing existing mouse IGHG1 constant domains with AgeI (ACCGGT)/SalI (GTCGAC).*

Clone	*Chain*	*Sequence*
20.1	Heavy	GTCCACAGCCAGGTGCAGCTCCAAGAATCTGGCGCCGAGCTTGTGAAACCTGGCGCCTCTGTGAAGCTGAGCTGTAAAGCCAGCGGCTACACCTTCACACGGTACT ACCTGTACTGGGTCAAGCAGAGGCCTGGACAGGGCCTCGAATGGATCGGCGAGATCAACCCTAACAACGGCGGCACCAAGTTCAACGAGAAGTTCAAGAGCAAGG CCACACTGACCGTGGACAAGAGCAGCCGGACAACCTACATCCAGCTGAGCAGCCTGACCAGCGAGGATAGCGCCGTGTACTACTGCTCCAGAGAGGACGACTACG ACGGCACCCCTGACGCCATGGATTATTGGGGACAGGGCACAGCCGTGACCGTTTCTGCAGCGTCGACCACCCCTCCCTCCGTGTACCCTCTCGCTCCTGGGAGCG CTGCCCAACAAACAGCATGGTGACCCTGGGCTGCCTCGTCAAGGGATACTTTCCCGAACCCGTGACCGTCACCTGGAACAGCGGAAGCCTGTCCTCCGGCGTGCAT ACATTCCCTGCTGTGCTCCAGAGCGACCTGTATACACTCTCCAGCAGCGTGACAGTCCCCTCCAGCACCTGGCCTAGCGAGACCGTGACATGCAACGTGGCTCACC CCGCCAGCTCCACCAAGGTGGACAAAAAGATCGTCCCCAGGGATTGTGGCTGCAAACCCTGTATCTGCACCGTGCCTGAAGTCTCCTCCGTCTTTATCTTCCCCCCC AAGCCTAAGGACGTCCTGACCATCACCCTCACCCCTAAGGTCACCTGCGTCGTGGTCGATATCTCCAAAGATGACCCCGAGGTGCAGTTCAGCTGGTTCGTGGACG ATGTGGAAGTCCACACCGCCCAGACCCAACCCAGGGAGGAGCAGTTCAACTCCACCTTCAGGTCCGTGAGCGAGCTGCCCATTATGCACCAGGACTGGCTCAACG GAAAGGAATTCAAGTGTAGAGTCAACAGCGCTGCCTTCCCCGCCCCCATCGAAAAGACAATCTCCAAGACCAAGGGCAGGCCTAAAGCTCCTCAGGTCTACACCAT CCCCCCCCCCAAGGAGCAGATGGCCAAGGACAAGGTGAGCCTCACCTGCATGATCACAGACTTCTTCCCCGAGGATATCACCGTGGAGTGGCAGTGGAATGGCCA GCCCGCCGAGAACTATAAGAACACCCAGCCCATTATGGACACCGACGGCAGCTATTTCGTCTATAGCAAGCTGAACGTCCAGAAGTCCAATTGGGAAGCCGGCAAC ACCTTTACCTGCTCCGTGCTGCATGAGGGCCTGCACAATCACCACACCGAGAAGAGCCTGAGCCACTCCCCCGGCAAGTGATGAGGATCCAGATCT
20.1	Light	ACCACCATGGGATGGTCATGTATCATCCTTTTTCTAGTAGCAACTGCAACCGGTGTCCACAGCGACATCGTGCTGACACAGAGCCCTTCTAGCCTGTCTGCCAGCCT GGGCGACACCATCACCATTACATGTCACGCCAGCCAGAACATCAACCTGTGGCTGAGCTGGTATCAGCAGAGGCCCGGCAACATCCCCAAGCTGCTGATCTACAGA GCCAGCAACCTGCACACAGGCGTGCCCAGCAGATTTTCTGGCAGCGGATCTGCCACCGGCTTCACCCTGACCATATCTAGCCTGCAGCCTGAGGATATCGCCACCT ACTACTGTCAGCAGGGCCACAGCTACCCCTACACATTTGGCGGCGGAACAAAGCTGGACATCAAGCGTACGGATGCTGCACCAACCGTGAGCATTTTCCCCCCTTC TAGTGAACAGCTGACTAGTGGCGGAGCTTCAGTGGTCTGTTTCCTGAACAACTTCTACCCTAAGGACATCAACGTGAAGTGGAAAATTGATGGGTCCGAGAGGCAGA ACGGCGTCCTGAATTCTTGGACAGACCAGGATAGTAAGGACTCAACTTATAGCATGTCAAGCACTCTGACCCTGACAAAAGATGAGTACGAAAGACATAATTCCTATA CATGTGAGGCAACCCATAAAACTTCAACTAGCCCTATTGTCAAATCTTTCAACAGGAACGAGTGTTGATGAGGATCCAGATCT

Continued on next page.

Table A.1. *Continued from previous page.*

Clone	*Chain*	*Sequence*
103.2	Heavy	ATGGGATGGTCATGTATCATCCTTTTTCTAGTAGCAACTGCAACCGGTGTCCACAGCCAGGTGCAGCTTCAGCAATCTGGCGCCGAGGTTGTCAGACCTGGCACCAG CGTGAAGGTGTCCTGTAAAGCCAGCGGCTACGCCTTCACCAGCTACCTGATCCACTGGATTAAGCAGCGGCCTGGACAGGGCCTGGAGTGGATCGGAGTGATCAAT CCCAGAAGCGGCGACAGCCACTACAACGAGAAGTTCAAGGACCGGACCACACTGACCGCCGATCAGTCTAGCAGCACCGCCTACATGCAGCTGAGCAGCCTGACC TCTGATGACAGCGCCGTGTACTTCTGCGCCAGATCCGATTACGGCGCCTATTGGGGACAGGGCACACTGGTCACAGTTTCTGCAGCGTCGACCACCCCTCCCTCCG TGTACCCTCTCGCTCCTGGGAGCGCTGCCCAAACAAACAGCATGGTGACCCTGGGCTGCCTCGTCAAGGGATACTTTCCCGAACCCGTGACCGTCACCTGGAACAG CGGAAGCCTGTCCTCCGGCGTGCATACATTCCCTGCTGTGCTCCAGAGCGACCTGTATACACTCTCCAGCAGCGTGACAGTCCCCTCCAGCACCTGGCCTAGCGAG ACCGTGACATGCAACGTGGCTCACCCCGCCAGCTCCACCAAGGTGGACAAAAAGATCGTCCCCAGGGATTGTGGCTGCAAACCCTGTATCTGCACCGTGCCTGAAG TCTCCTCCGTCTTTATCTTCCCCCCCAAGCCTAAGGACGTCCTGACCATCACCCTCACCCCTAAGGTCACCTGCGTCGTGGTCGATATCTCCAAAGATGACCCCGAG GTGCAGTTCAGCTGGTTCGTGGACGATGTGGAAGTCCACACCGCCCAGACCCAACCCAGGGAGGAGCAGTTCAACTCCACCTTCAGGTCCGTGAGCGAGCTGCCC ATTATGCACCAGGACTGGCTCAACGGAAAGGAATTCAAGTGTAGAGTCAACAGCGCTGCCTTCCCCGCCCCCATCGAAAAGACAATCTCCAAGACCAAGGGCAGGC CTAAAGCTCCTCAGGTCTACACCATCCCCCCCCCCAAGGAGCAGATGGCCAAGGACAAGGTGAGCCTCACCTGCATGATCACAGACTTCTTCCCCGAGGATATCAC CGTGGAGTGGCAGTGGAATGGCCAGCCCGCCGAGAACTATAAGAACACCCAGCCCATTATGGACACCGACGGCAGCTATTTCGTCTATAGCAAGCTGAACGTCCAG AAGTCCAATTGGGAAGCCGGCAACACCTTTACCTGCTCCGTGCTGCATGAGGGCCTGCACAATCACCACACCGAGAAGAGCCTGAGCCACTCCCCCGGCAAGTGAT GAGGATCCAGATCT
103.2	Light	ACCACCATGGGatggtcatgtatCaTCCTTTTTCTAGTAGCAACTGCAACCGGTGTCCACAGCGACATCGTGCTGACACAGAGCCCTGTGACACTGAGCGTGACACCTGGC GATAGCGTGTCCCTGAGCTGTAGAGCCAGCCAGAGCATCAGCAACAACCTGCACTGGTACAGACAGAAGTCCCACGAGAGCCCCAGACTGCTGATTAAGTACGCCA GCCAGTCCATCTTCGGCATCCCCAGCAGATTTTCTGGCAGCGGCTCTGGCACCGAGTTCACCCTGAGCATCAACAGCGTGGAAACCGAGGACTTCGGAATCTACTT CTGCCAGCAGTCCAACAGCTGGCCCCACACATTTGGCACCGGCACCAAGCTGGAACTGAAGCGTACGGATGCTGCACCAACCGTGAGCATTTTCCCCCCTTCTAGT GAACAGCTGACTAGTGGCGGAGCTTCAGTGGTCTGTTTCCTGAACAACTTCTACCCTAAGGACATCAACGTGAAGTGGAAAATTGATGGGTCCGAGAGGCAGAACG GCGTCCTGAATTCTTGGACAGACCAGGATAGTAAGGACTCAACTTATAGCATGTCAAGCACTCTGACCCTGACAAAAGATGAGTACGAAAGACATAATTCCTATACAT GTGAgGCAACCCATAAAACTTCAACTAGCCCTATTGTCAAATCTTTCAACAGGAACGAGTGTTGATGAgGATCCAGATCT

Continued on next page.

Table A.1. *Continued from previous page.*

Clone	*Chain*	*Sequence*
pCMV	Vector	TCGCGCGTTTCGGTGATGACGGTGAAAACCTCTGACACATGCAGCTCCCGGAGACGGTCACAGCTTGTCTGTAAGCGGATGCCGGGAGCAGACAAGCCCGTCAGG GCGCGTCAGCGGGTGTTGGCGGGTGTCGGGGCTGGCTTAACTATGCGGCATCAGAGCAGATTGTACTGAGAGTGCACCATATGCGGTGTGAAATACCGCACAGAT GCGTAAGGAGAAAATACCGCATCAGATTGGCTATTGGCCATTGCATACGTTGTATCCATATCATAATATGTACATTTATATTGGCTCATGTCCAACATTACCGCCATGT TGACATTGATTATTGACTAGTTATTAATAGTAATCAATTACGGGGTCATTAGTTCATAGCCCATATATGGAGTTCCGCGTTACATAACTTACGGTAAATGGCCCGCCTG GCTGACCGCCCAACGACCCCCGCCCATTGACGTCAATAATGACGTATGTTCCCATAGTAACGCCAATAGGGACTTTCCATTGACGTCAATGGGTGGAGTATTTACGG TAAACTGCCCACTTGGCAGTACATCAAGTGTATCATATGCCAAGTACGCCCCCTATTGACGTCAATGACGGTAAATGGCCCGCCTGGCATTATGCCCAGTACATGAC CTTATGGGACTTTCCTACTTGGCAGTACATCTACGTATTAGTCATCGCTATTACCATGGTGATGCGGTTTTGGCAGTACATCAATGGGCGTGGATAGCGGTTTGACTC ACGGGGATTTCCAAGTCTCCACCCCATTGACGTCAATGGGAGTTTGTTTTGGCACCAAAATCAACGGGACTTTCCAAAATGTCGTAACAACTCCGCCCCATTGACGCA AATGGGCGGTAGGCGTGTACGGTGGGAGGTCTATATAAGCAGAGCTCGTTTAGTGAACCGTCAGATCGCCTGGAGACGCCATCCACGCTGTTTTGACCTCCATAGA AGACACCGGGACCGATCCAGCCTCCATCGGCTCGCATCTCTCCTTCACGCGCCCGCCGCCCTACCTGAGGCCGCCATCCACGCCGGTTGAGTCGCGTTCTGCCGC CTCCCGCCTGTGGTGCCTCCTGAACTGCGTCCGCCGTCTAGGTAAGTTTAAAGCTCAGGTCGAGACCGGGCCTTTGTCCGGCGCTCCCTTGGAGCCTACCTAGACT CAGCCGGCTCTCCACGCTTTGCCTGACCCTGCTTGCTCAACTCTAGTTAACGGTGGAGGGCAGTGTAGTCTGAGCAGTACTCGTTGCTGCCGCGCGCGCCACCAGA CATAATAGCTGACAGACTAACAGACTGTTCCTTTCCATGGGTCTTTTCTGCAGTCACCGTCCTCGACACGTGTGATCAGATATCGCGGCCGCTCTAGA

Continued on next page.

Table A.1. *Continued from previous page.*

Clone	*Chain*	*Sequence*
mAb	Insert	GGATCCAGATCTGCTGTGCCTTCTAGTTGCCAGCCATCTGTTGTTTGCCCCTCCCCCGTGCCTTCCTTGACCCTGGAAGGTGCCACTCCCACTGTCCTTTCCTAATAA AATGAGGAAATTGCATCGCATTGTCTGAGTAGGTGTCATTCTATTCTGGGGGGTGGGGTGGGGCAGGACAGCAAGGGGGAGGATTGGGAAGACAATAGCAGGCAT GCTGGGGATGCGGTGGGCTCTATGGGTACCCAGGTGCTGAAGAATTGACCCGGTTCCTCCTGGGCCAGAAAGAAGCAGGCACATCCCCTTCTCTGTGACACACCCT GTCCACGCCCCTGGTTCTTAGTTCCAGCCCCACTCATAGGACACTCATAGCTCAGGAGGGCTCCGCCTTCAATCCCACCCGCTAAAGTACTTGGAGCGGTCTCTCCC TCCCTCATCAGCCCACCAAACCAAACCTAGCCTCCAAGAGTGGGAAGAAATTAAAGCAAGATAGGCTATTAAGTGCAGAGGGAGAGAAAATGCCTCCAACATGTGAG GAAGTAATGAGAGAAATCATAGAATTTTAAGGCCATGATTTAAGGCCATCATGGCCTTAATCTTCCGCTTCCTCGCTCACTGACTCGCTGCGCTCGGTCGTTCGGCTG CGGCGAGCGGTATCAGCTCACTCAAAGGCGGTAATACGGTTATCCACAGAATCAGGGGATAACGCAGGAAAGAACATGTGAGCAAAAGGCCAGCAAAAGGCCAGG AACCGTAAAAAGGCCGCGTTGCTGGCGTTTTTCCATAGGCTCCGCCCCCCTGACGAGCATCACAAAAATCGACGCTCAAGTCAGAGGTGGCGAAACCCGACAGGAC TATAAAGATACCAGGCGTTTCCCCCTGGAAGCTCCCTCGTGCGCTCTCCTGTTCCGACCCTGCCGCTTACCGGATACCTGTCCGCCTTTCTCCCTTCGGGAAGCGTG GCGCTTTCTCATAGCTCACGCTGTAGGTATCTCAGTTCGGTGTAGGTCGTTCGCTCCAAGCTGGGCTGTGTGCACGAACCCCCCGTTCAGCCCGACCGCTGCGCCT TATCCGGTAACTATCGTCTTGAGTCCAACCCGGTAAGACACGACTTATCGCCACTGGCAGCAGCCACTGGTAACAGGATTAGCAGAGCGAGGTATGTAGGCGGTGC TACAGAGTTCTTGAAGTGGTGGCCTAACTACGGCTACACTAGAAGAACAGTATTTGGTATCTGCGCTCTGCTGAAGCCAGTTACCTTCGGAAAAAGAGTTGGTAGCTC TTGATCCGGCAAACAAACCACCGCTGGTAGCGGTGGTTTTTTTGTTTGCAAGCAGCAGATTACGCGCAGAAAAAAAGGATCTCAAGAAGATCCTTTGATCTTTTCTAC GGGGTCTGACGCTCAGTGGAACGAAAACTCACGTTAAGGGATTTTGGTCATGAGATTATCAAAAAGGATCTTCACCTAGATCCTTTTAAATTAAAAATGAAGTTTTAAA TCAATCTAAAGTATATATGAGTAAACTTGGTCTGACAGTTACCAATGCTTAATCAGTGAGGCACCTATCTCAGCGATCTGTCTATTTCGTTCATCCATAGTTGCCTGAC TCGGGGGGGGGGGGGCGCTGAGGTCTGCCTCGTGAAGAAGGTGTTGCTGACTCATACCAGGCCTGAATCGCCCCATCATCCAGCCAGAAAGTGAGGGAGCCACGG TTGATGAGAGCTTTGTTGTAGGTGGACCAGTTGGTGATTTTGAACTTTTGCTTTGCCACGGAACGGTCTGCGTTGTCGGGAAGATGCGTGATCTGATCCTTCAACTCA GCAAAAGTTCGATTTATTCAACAAAGCCGCCGTCCCGTCAAGTCAGCGTAATGCTCTGCCAGTGTTACAACCAATTAACCAATTCTGATTAGAAAAACTCATCGAGCAT CAAATGAAACTGCAATTTATTCATATCAGGATTATCAATACCATATTTTTGAAAAAGCCGTTTCTGTAATGAAGGAGAAAACTCACCGAGGCAGTTCCATAGGATGGCA AGATCCTGGTATCGGTCTGCGATTCCGACTCGTCCAACATCAATACAACCTATTAATTTCCCCTCGTCAAAAATAAGGTTATCAAGTGAGAAATCACCATGAGTGACGA CTGAATCCGGTGAGAATGGCAAAAGCTTATGCATTTCTTTCCAGACTTGTTCAACAGGCCAGCCATTACGCTCGTCATCAAAATCACTCGCATCAACCAAACCGTTATT CATTCGTGATTGCGCCTGAGCGAGACGAAATACGCGATCGCTGTTAAAAGGACAATTACAAACAGGAATCGAATGCAACCGGCGCAGGAACACTGCCAGCGCATCA ACAATATTTTCACCTGAATCAGGATATTCTTCTAATACCTGGAATGCTGTTTTCCCGGGGATCGCAGTGGTGAGTAACCATGCATCATCAGGAGTACGGATAAAATGC TTGATGGTCGGAAGAGGCATAAATTCCGTCAGCCAGTTTAGTCTGACCATCTCATCTGTAACATCATTGGCAACGCTACCTTTGCCATGTTTCAGAAACAACTCTGGC GCATCGGGCTTCCCATACAATCGATAGATTGTCGCACCTGATTGCCCGACATTATCGCGAGCCCATTTATACCCATATAAATCAGCATCCATGTTGGAATTTAATCGC GGCCTCGAGCAAGACGTTTCCCGTTGAATATGGCTCATAACACCCCTTGTATTACTGTTTATGTAAGCAGACAGTTTTATTGTTCATGATGATATATTTTTATCTTGTGC AATGTAACATCAGAGATTTTGAGACACAACGTGGCTTTCCCCCCCCCCCCATTATTGAAGCATTTATCAGGGTTATTGTCTCATGAGCGGATACATATTTGAATGTATT TAGAAAAATAAACAAATAGGGGTTCCGCGCACATTTCCCCGAAAAGTGCCACCTGACGTCTAAGAAACCATTATTATCATGACATTAACCTATAAAAATAGGCGTATCA CGAGGCCCTTTCGTC

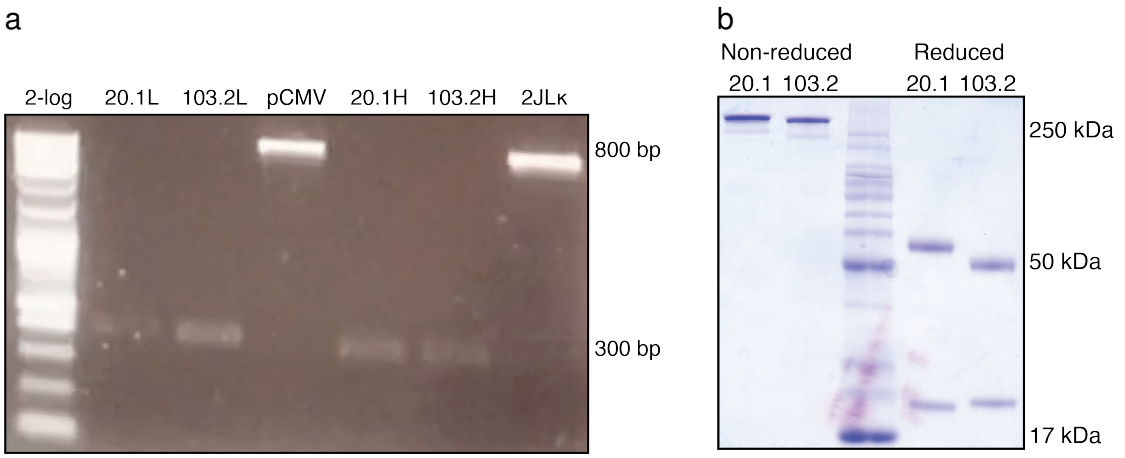

Figure A.4: *Scans of (a) purified digested light, heavy, and vector DNA products by a 2-Log DNA ladder; and (b) SDS-PAGE of purified anti-BTN3A monoclonal antibodies by a blue prestained protein standard ladder (NEB) under normal (non-reduced) and 100* mM *1,4-dithiothreitol (DTT) treated (reduced) conditions.*

A.3.2 Generation of anti-BTN2A1 Monoclonal Antibodies

CSL generated a panel of a mouse-human hybrid anti-human BTN2A1-reactive monoclonal antibodies in a phage display library screen where same purified phage was used for subsequentround of panning. Positive clones were tested by ELISA for binding to BTN2A1 immobilised in a microplate (Fig. A.6). Sequencing of positive clones revealed a total of 52 individual antibody clones, of which 45 were then sub-cloned into a mammalian expression vector for expression in Expi293F cells (Thermo Fisher) and purification on MabSelect SuRe resin (GE Lifesciences) as full-length IgG molecules which comprised a human IgG4 Fab region and murine IgG2a Fc region. Isotype control clone BM4 contained the same Fc region, except for a mouse Fab region with irrelevant specificity. The accessible panel was scanned for varying degrees of cross-reactivity to BTN2A2 (87 % ectodomain homology) and to BTN3A1 (45 % ectodomain homology) by overexpressing these human proteins on mouse fibroblast 3T3 cells. Specificity to human BTN2A1 was also confirmed in *BTN2A1*$^{-/-}$ melanocyte lines (Fig. A.6).

Antibody clones RF13-231, RF13-259, and matched isotype control (clone BM4, produced by CSL) were conjugated in-house to AF647 via amine coupling kit (Thermo Fisher).

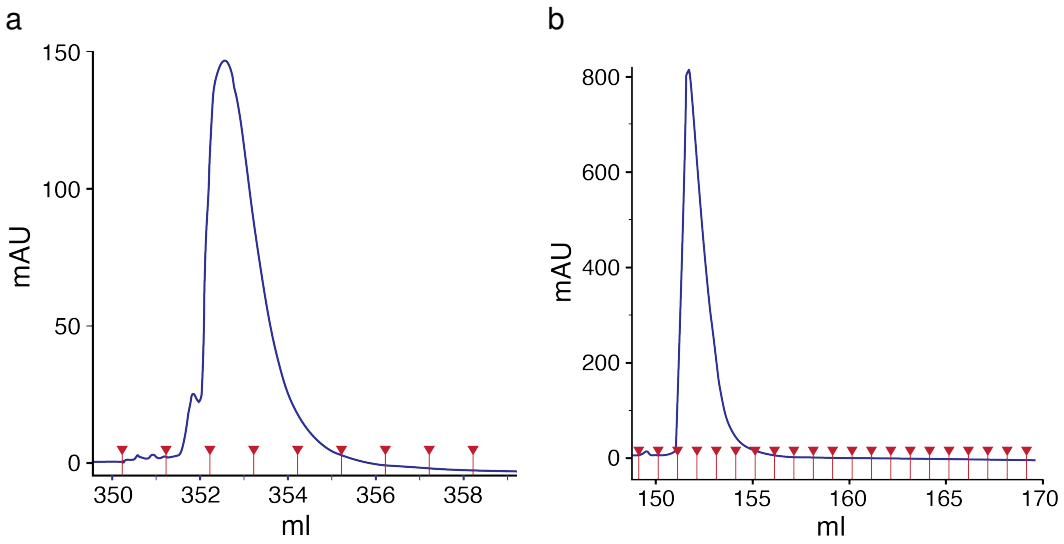

Figure A.5: *Elution profiles of monoclonal antibody clones (a) 20.1 and (b) 103.2;* x *axis indicates* ml *of eluted protien,* y *axis absorbance (*mAU*), and each* ml *of collected fractions is within red intervals.*

A.4 Validation of CRISPR/Cas9-mediated Knockout Cell Lines

Melanoma LM-MEL-62 and -75 CRISPR/Cas9 Knockout lines for *BTN2A1* or all three *BTN3A* members were provided by the ONJC who cloned 5'-TCACAAAGGTGGTTCT TCCT (*BTN2A1*^{null1}) and 5'-CAATAGATGCATACGGCAAT (*BTN2A1*^{null2}) into GeneArt® CRISPR Nuclease Vector Kit (Life Technologies). For BTN3A1-knockout lines they use a BTN3A1 CRISPR/Cas9 KO Plasmid kit (sc-404202, Santa Cruz Biotechnology) containing three specific guiding sequences (5'-GGCACTTACGAGATGCATAC, 5'-GAGAGACAT TCAGCCTATAA, 5'-ACCATCAGAAGTTCCCTCCT). They sequence-verified each vector by Sanger sequencing before transfection and stained with anti-BTN2A1 (clone Hu34C) or anti-BTN3A1 (clone 103.2) for sorting the negative population. Here, the absence of these surface membrane proteins was validated once more in a flow cytometry analyser using RF13-231 and RF13-259 antibody clones for *BTN2A1*^{null} knockouts or an in-house produced 103.2 for *BTN3A1*^{null}. Note, LM-MEL-62 have two knockout lines each corresponding to an independent guide RNA for the CRISPR/Cas9 experiment, and despite detecting a slight fluorescent signal this was later confirmed negative using a more specific monoclonal antibody RF13-259.

Besides, melanoma LM-MEL-62 was knockout for BTN3A2 with CRISPR/Cas9 KO Plasmid kit (sc-416698, Santa Cruz Biotechnology) with a pool of three different plasmids each containing a guide (5'-GCCACTCACGAGTCAAGTAC, 5'-ACTTACCCAC-TTCAGCTCCA, 5'-TAATCTTCACGTCGAAGTGA); LM-MEL-62 and -75 were knockout with for BTN2A2 using a kit (sc-417653, Santa Cruz Biotechnology) containing

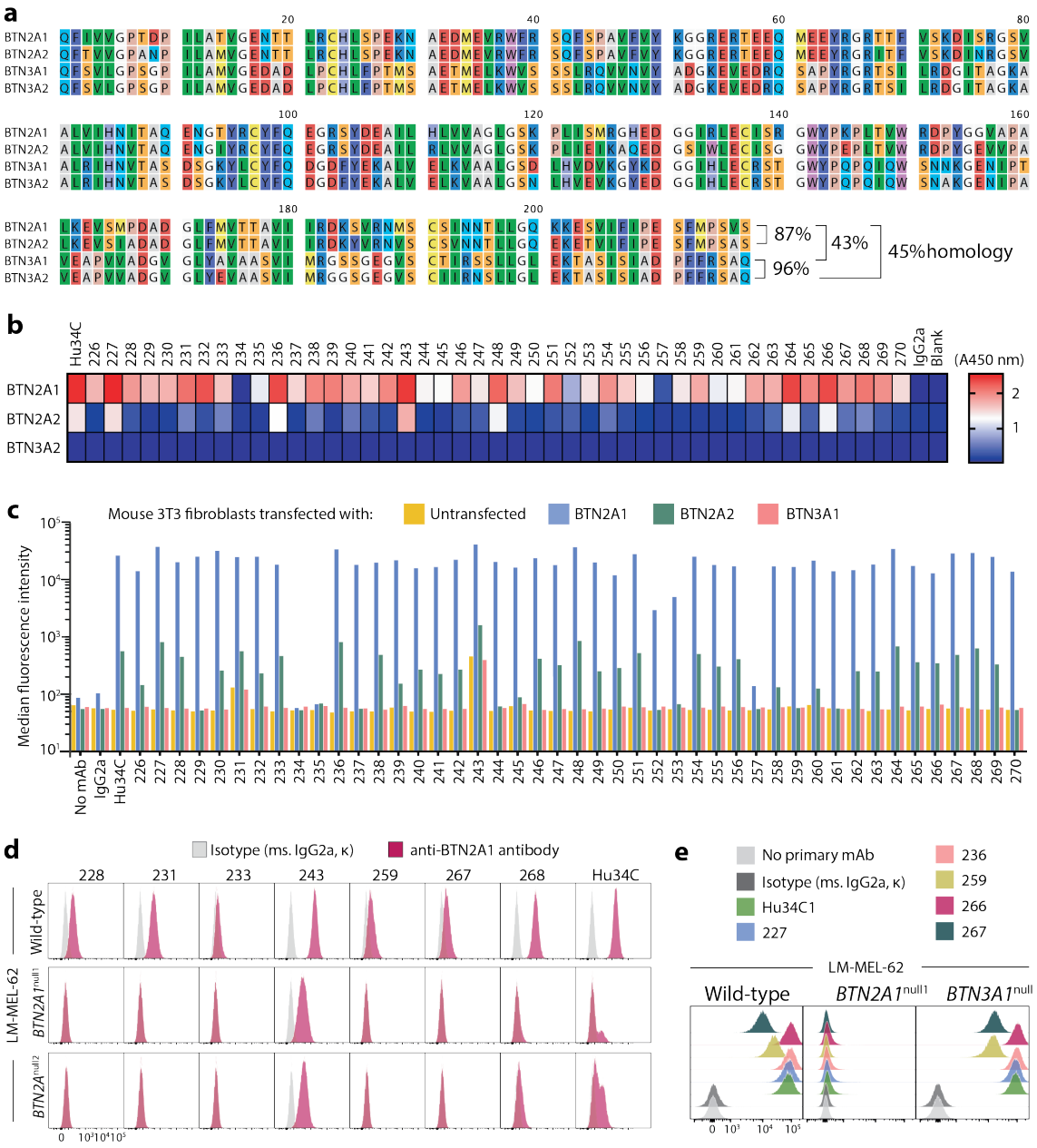

Figure A.6: *Anti-BTN2A1 cross-reactivity to close members; (a) alignment of BTN2A1, BTN2A2, BTN3A1, and BTN3A2 ectodomains in RasMol colour scheme; (b) reactivity to plate-bound BTN2A1, BTN2A2, or BTN3A2 ectodomains by ELISA, where heat maps depicts relative absorbance; (c) screen to mouse NIH-3T3 cells transfected with full length human BTN2A1 (blue), BTN2A2 (green), BTN3A1 (pink), or untransfected cells (yellow). Data averaged from two independent experiments; (d) Reactivity of selected clones (red) or isotype control (mouse IgG2aκ, clone BM4, gray) to LM-MEL-62 parental (WT),* BTN2A1^{null1} *and* BTN2A1^{null2} *cells, using a BV421-conjugated secondary polyclonal antibody, over isotype control; (e) Reactivity of selected clones to LM-MEL-62 parental (WT),* BTN2A1^{null1} *and* BTN2A1^{null} *cells using a PE-conjugated secondary polyclonal antibody.*

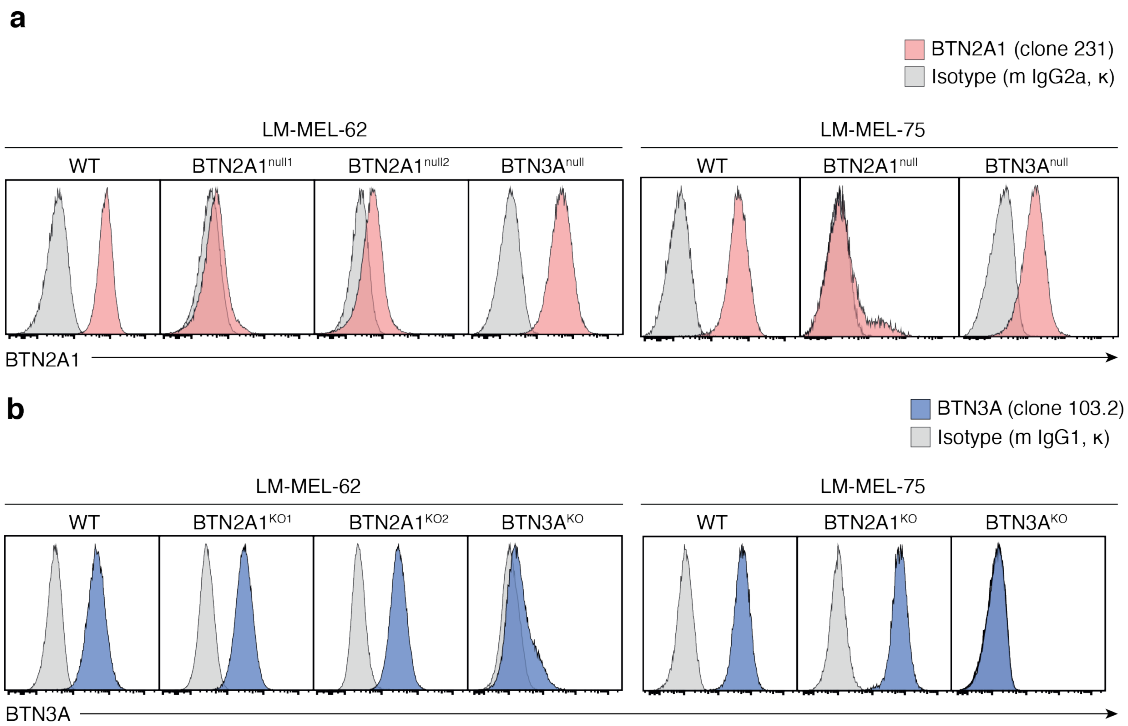

Figure A.7: *Melanoma LM-MEL-62 and -75 CRISPR/Cas9 Knockout lines for (a)* BTN2A1 *or (b) all three* BTN3A *members were confirmed by flow cytometry using specific monoclonal antibodies against these respective proteins.*

three plasmids with guiding sequences (5'-TAAGCCCCTCATTGAAATCA, 5'-GACAG-TCATGGACACCATCC, 5'-TGAGGCCATCCTACGCCTCG). Nonetheless, the absence of surface targeted protein could not be confirmed due to the lack of reliable monoclonal antibodies against these butyrophilins.

A.5 Assessment of Förster Resonance Energy Transfer

FRET were conducted from using monoclonal antibody conjugates to detect co-localisation at the surface membrane of cells or producing full-length protein constructs with an attached fluorophore at the carboxyl-terminal domain of respective proteins.

A.5.1 Monoclonal Antibody Fluorophore Experiments

The detection of FRET occurs if two fluorophore molecules are within a very close distance from each other. The use of antibodies to experiment this effect may constrain the results due the fact the antibody size and its mode of binding to its target may alter the real distance between the two protein targets to be evaluated. For this reason, we have tested a few different possible combinations between antibodies that

target our proteins of interest. Figure A.9 captures the results from a different combinations tested across five tumour cell lines that possess both BTN members on their surface plasma membranes. The antibody clone 20.1 against BTN3A members produces a weaker signal compared to clone 103.2, and it is unable to donate enough energy to the acceptor AF647 fluorophore on BTN2A1 protein. Some antibody clones targeting BTN2A1 emit a signal resulting form accepting energy from PE fluorophore in antibody clone 103.2 with clone RF13-259 being the most clear of all four tested clones. Clone Hu34C produced a weak signal in the FRET 670/30 yellow detection sensor in cell lines LM-MEL-75, Ramos, and RPMI-8226, whereas in LM-MEL-62 and THP-1 signal is not detected –note this clone cross-reacts to BTN2A2. Clone RF13-231 has a similar effect than Hu34C but the detected signal is increased. Lastly, the clone RF13-267 has a signal barely detectable and only observed in Ramos and RPMI-8226 lines.

Transfected mouse fibroblast NIH-3T3 and Chinese hamster ovary CHO-K1 cell lines transfected with different human BTN members were checked for successful expression protein expression on the surface membrane by direct specific monoclonal antibody staining followed by a flow cytometry detection. A BTN2A1$^{\text{PILR}\beta}$ was detected with less intensity than the full length protein (Fig. A.10 .a). The independent emission spectrum resulting a donor or receptor fluorophore was confirmed absent of spilling over into the FRET detection channel (Fig. A.10 .b).

A.5.2 Intracellular Fluorescent Protein Constructs

Fluorescent cyan (mTurquoise2) or yellow (mVenus) fluorescent proteins were attached at BTN carboxyl-terminal expression sequences for flow cytometry experiments (Fig. A.8 a-c). The codon-optimised sequences were engineered for a carboxyl-terminal fluorescent-tagged protein mammalian expression system (Fig. A.8 d). Expression of these constructs was confirmed with flow cytometry analysis, and the levels of surface expressed protein comparable to wild-type protein expression detected by plasmid co-expression of GFP (Fig. A.8 e). Respective detection of FRET signal in the 530/30-violet channel diminished or was absent in pre-treatments with a series of monoclonal antibodies with affinity for BTN2A members (Fig. A.11).

A.6 Site-directed Mutagenesis

We engineered mutated protein products by inducing precise changes or deletions to the double stranded plasmid DNA with site-directed mutagenesis. That allowed to

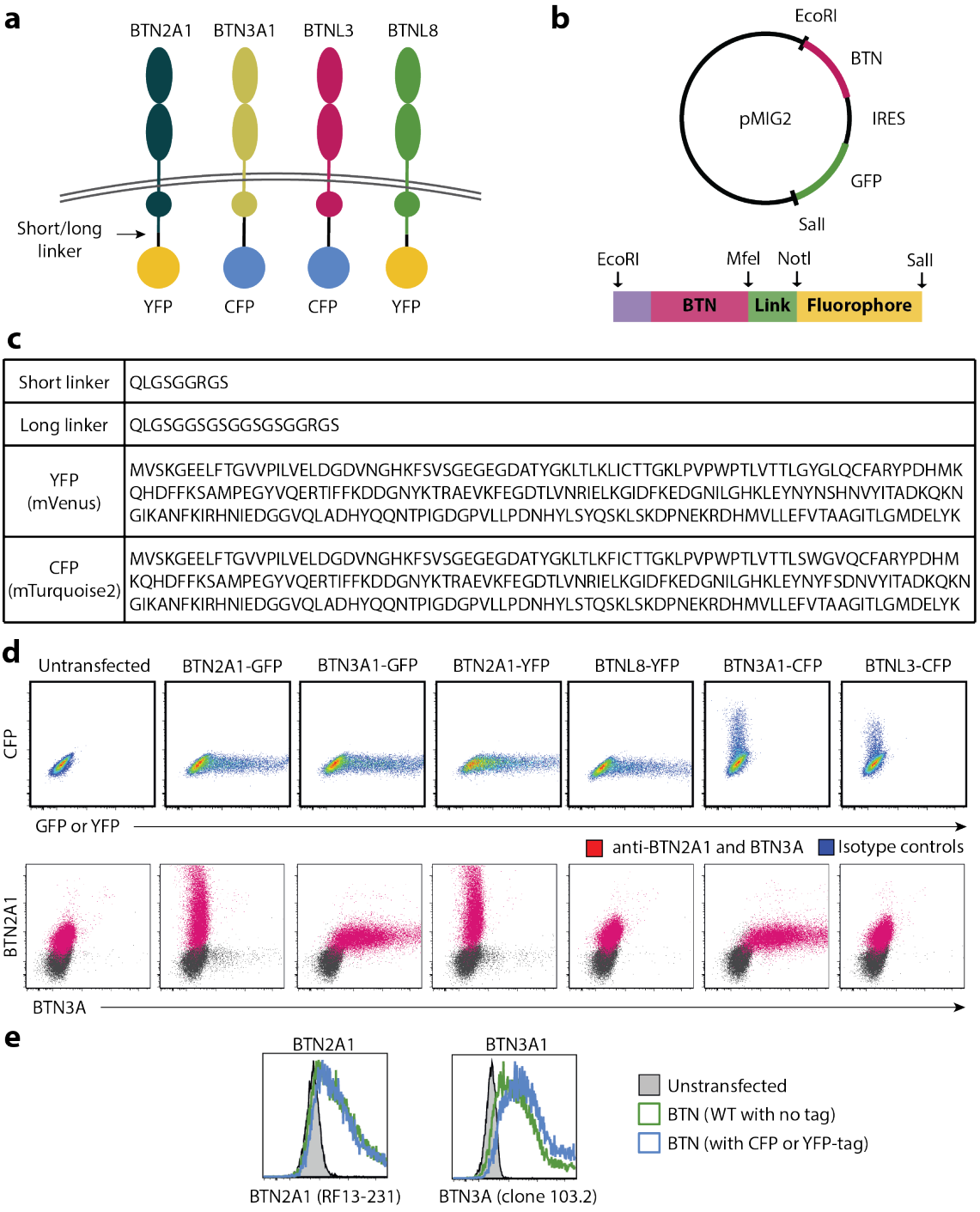

Figure A.8: *Generation of intracellular fluorescent tagged proteins. (a) Representation of BTN proteins with either a long or short carboxyl-terminal flexible linker coupled to cyan or yellow fluorescent protein (C/YFP). (b) Construct design. (c) Codon-optimised amino acid sequences. (d) Expression of BTN constructs (above) and antibodies targeting surface BTN2A1 (RF13-231) or BTN3A (clone 103.2) (red) overlaid to isotype controls (IgG1 and IgG2a; grey) on mouse fibroblast (NIH-3T3) cells. (e) Dotplots showing equal expression of BTN2A1 (left) and BTN3A1 (right) surface protein on NIH-3T3 cells transfected with wild-type BTN (green) or CFP/YFP-tagged BTN molecules (blue).*

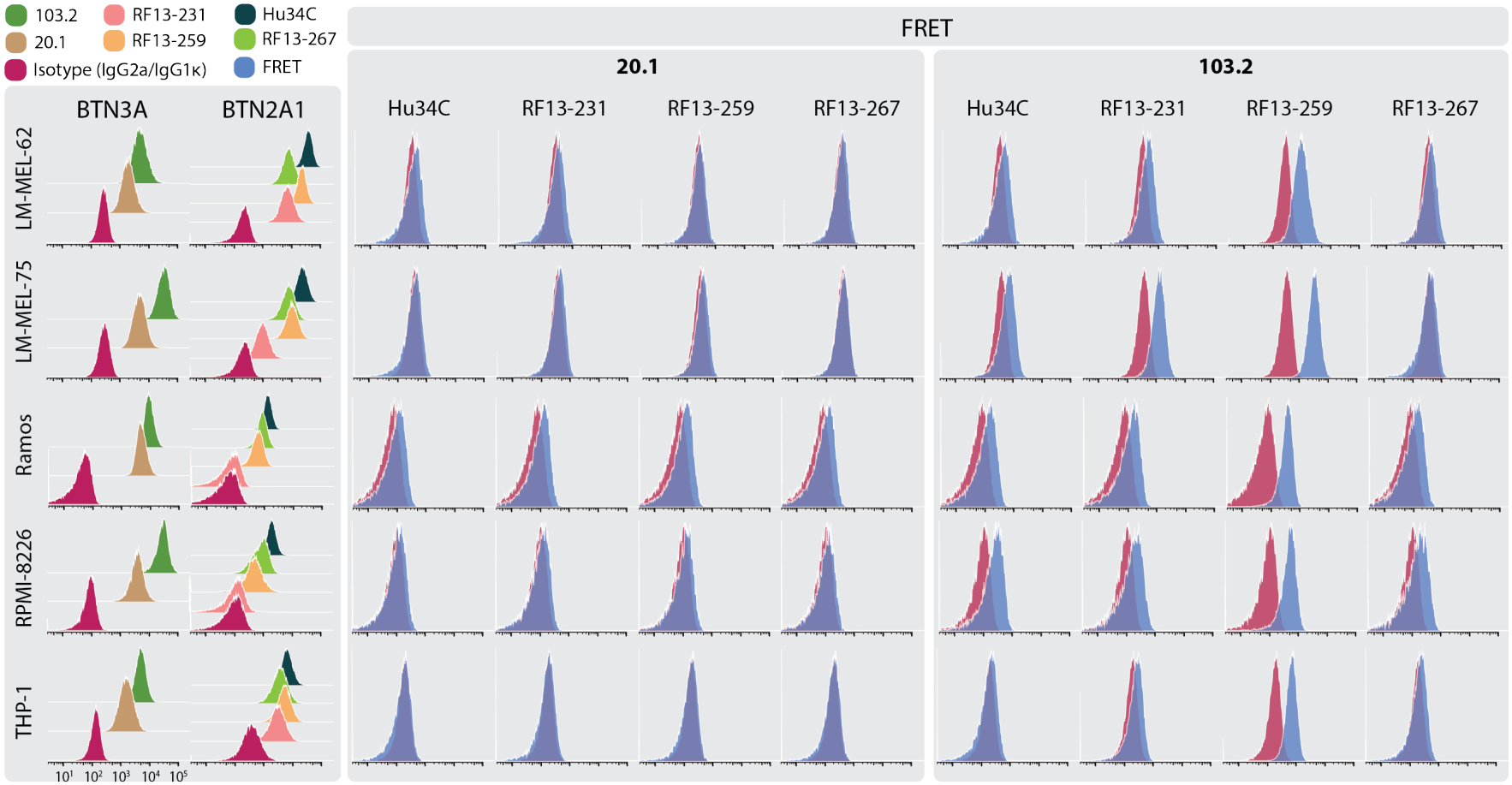

Figure A.9: *Assessing the best monoclonal antibody combination pair for FRET experiments analysing BTN2A1 and BTN3A1 cooperation on the surface of the cell membrane. Human melanoma LM-MEL-62 and -75, B-cell Burkitt's lymphoma Ramos and RPMI-8226, and monocytic THP-1 established cell lines were assessed for expression of BTN3A members (Clones 20.1 and 103.2 conjugated to PE) or BTN2A1 (clones RF13-231, -259, -267, and Hu34C conjugated to AF647) independently and in combination to determinate a wave-length signal on the 670/30 yellow detection channel resulting from a Förster resonance energy transfer effect.*

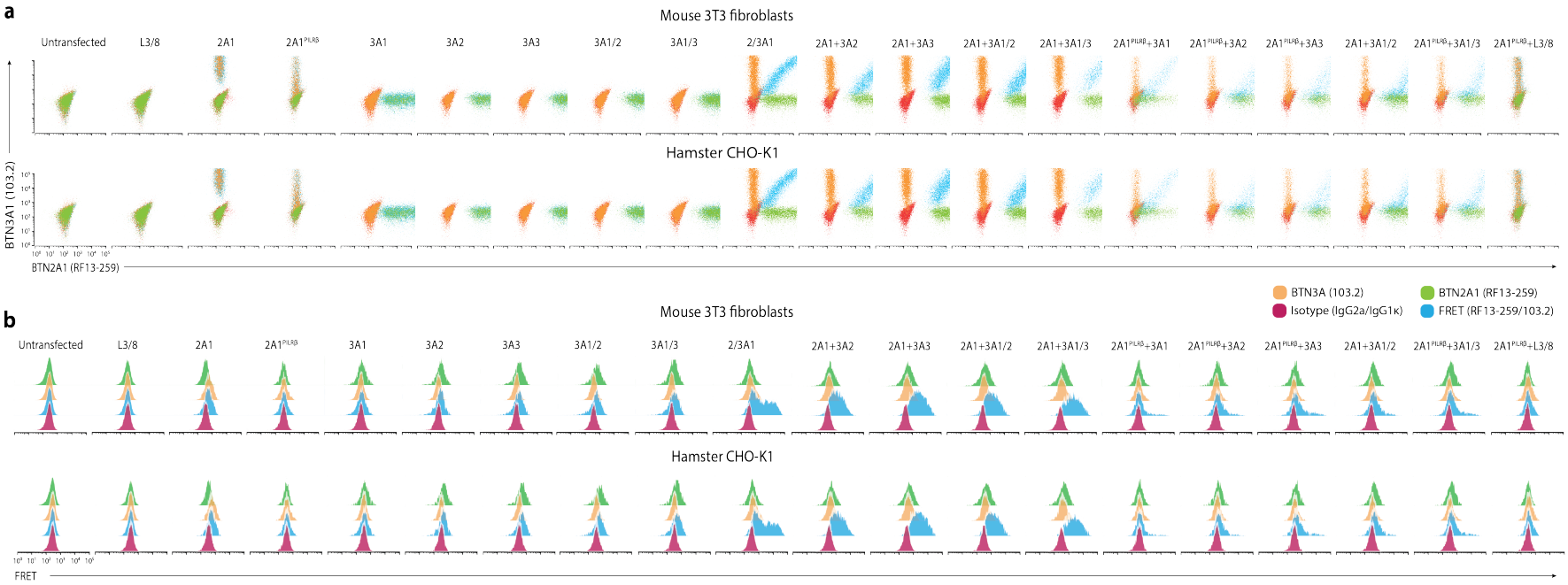

Figure A.10: *Association of BTN2A1 and BTN3A on the surface of mouse fibroblast 3T3 or Chinese hamster ovary CHO-K1 cell lines detected by FRET. Fluorophore-antibody conjugates (Clone 103.2 and RF13-259 carrying a PE or an AF647 fluorophores, respectively) corroborate in (a) the successful surface expression of BTN transfected members on rodent cells independently, and their combination in (b) detected the transfer of energy from PE to AF647 in antibody fluorophores when BTN2A1 was co-expressed with any member of the BTN3A family. Single antibody tests were added for comparison and ensure single fluorophore signal is absence in the FRET readout channel.*

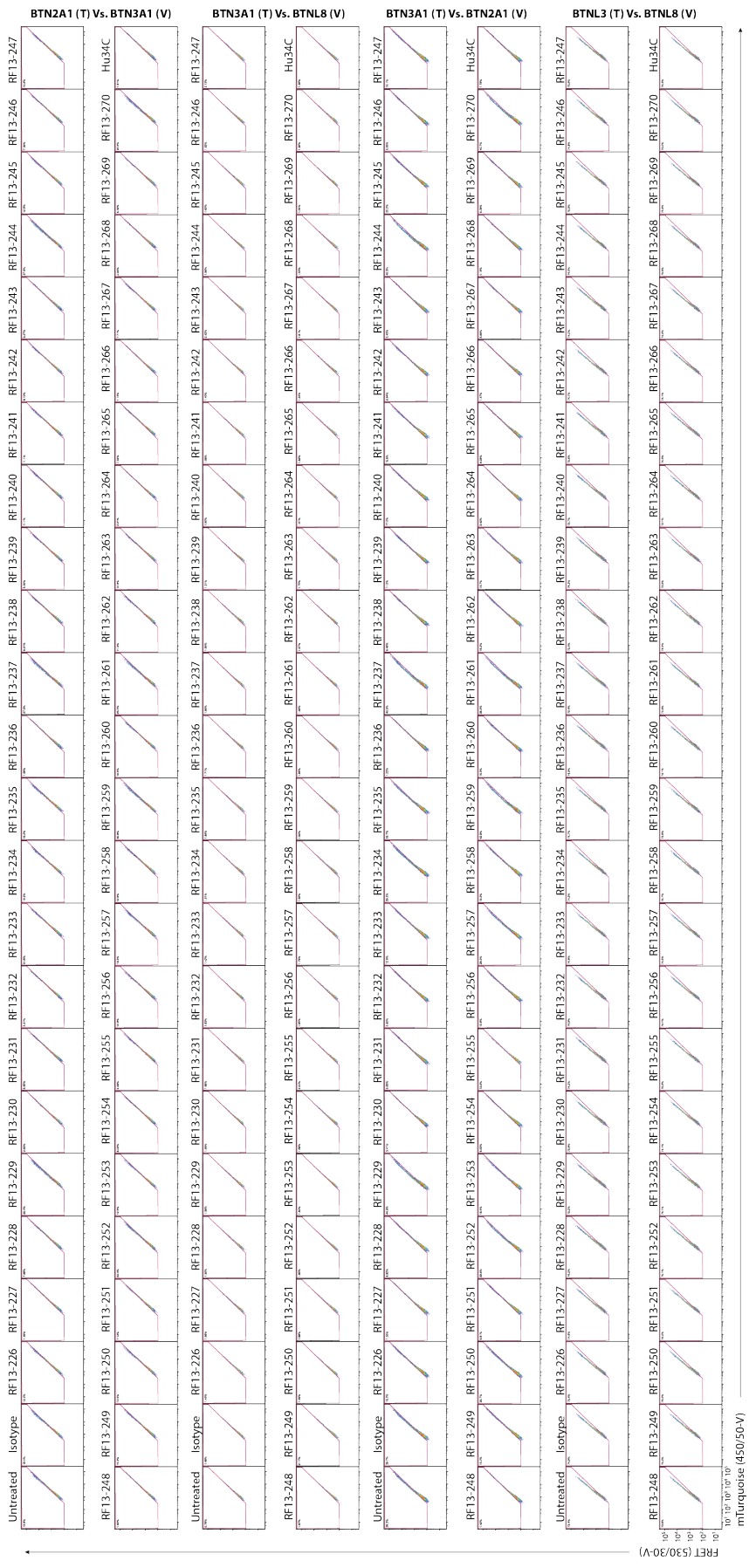

Figure A.11: *Treatment with a series of specific monoclonal antibodies against human BTN2 members or specific for BTN2A1 in murine transfected cells with fluorescent-intracellular BTN-pair constructs designed for detection of FRET disrupts this signal as the readout in the 530/30-violet channel swift off towards the 450/50-violet detection of the mTurquoise fluorophore.*

introduce specific nucleotide substitutions and change the amino acid coding codon in the targeted wild-type protein of interest.

A.6.1 Alanine Scanning Method of the G115 T-Cell Receptor

Site-directed mutagenesis was used to create specific, targeted substitutions in double stranded plasmid DNA encoding for a $\gamma\delta$TCR prototype clone G115. Induced mutations were incorporated into the plasmid by inverse PCR with standard primers. Back-to-back 5' primers were designed to prevent primer overlapping and produce non-nicked plasmids, which allows exponential amplification and yields more desired product. The products were next transfected into E. coli strain DH5α for cloning, sequencing, and selection of the successfully incorporated mutations. Table A.2 show the sequences for the selected primers. All TCR-G115 mutant clones were validated by Sanger-sequencing and their expression was monitored by detecting the plasmid expression of GFP and protein surface expression confirmed by labelling the CD3ϵ region of the TCR complex structure (Fig A.12).

A.6.2 Generating a Truncated BTN2A1 Protein

A truncated BTN2A1 protein was constructed by inducing site-directed mutagenesis in a wild-type BTN2A1 plasmid. The raw data resulting from coculturing mouse fibroblast antigen-presenting cells and random donor purified-expanded Vδ2 T cells show the respective lymphocyte activation response (Fig. A.16).

A.7 Transcript Expression of BTN Molecules

We quantified the levels of transcribed *BTN* genes in human $\gamma\delta$ T cells or melanoma tumour lines in a quantitative real-time PCR instrument. The quantification of *BTN* gene products was relative to the average expression of four reference genes (*ACTB*, *B2M*, *GAPDH*, and *18S*), which are considered to have relatively stable transcription rate. Primers used to amplify these genes are reported in Table A.3.

A.8 Glycosylation Effects on BTN2A1

The glycosylation effect in BTN2A1 protein when binding to monocyte-derived DC or Vγ9Vδ2 TCR clone G115 expressed in Jurkat cells (Fig. A.15 a-b). The same BTN2A1 partially deglycosylated or wild-type protein affinity comparison on donor-purified V$\delta2^+$ T cells in-vitro (Fig. A.15 c).

Table A.2: *Primers used for PCR and site-directed mutagenesis substituting the target amino acid residue for an alanine amino acid in the $\gamma\delta$ TCR-G115 prototype clone in a pHLsec vector.*

Purpose	*Name*	*Sequence (5' → 3')*
Single-cell PCR round 1	TRDV2 External	TGGGCAGGAGTCATGTClAG
Single-cell PCR round 1	TRDC Rev1	GCAGGATCAAACTCTGTTATCTTC
Single-cell PCR round 1	TRGV9 External	GGCTCTGTGTGTATATGGTGC
Single-cell PCR round 1	TRGC Rev1	CTGACGATACATCTGTGTTCTTTG
Single-cell PCR round 2	TRDV2 Fwd soluble	ATACCGGTGCCATTGAGTTGGTGCCT
Single-cell PCR round 2	TRDC Rev soluble	TGTTCCGGATATCCTTGGGGTAGAATTCCTTCA
Single-cell PCR round 2	TRDV9 Fwd soluble	ATACCGGTGCAGGTCACCTAGAGCAAC
Single-cell PCR round 2	TRDC Rev soluble	CAGCAATTGAAGGAAGAAAAATAGTGGGCTTG
Site-directed mutagenesis	E28A δ Fwd	ATGAAGGGCGCAGCCATCGGC
Site-directed mutagenesis	E28A δ Rev	GCTACACCGCAGTGTGGC
Site-directed mutagenesis	R51A δ Fwd	CTTCATCTACGCAGAGAAGGACATCTACGG
Site-directed mutagenesis	R51A δ Rev	GTCATGGTGTTGCCCTGG
Site-directed mutagenesis	L97A δ Fwd	CTGTGACACAGCTGGAATGGGCGGCGAG
Site-directed mutagenesis	L97A δ Rev	GCGCAGTAGTAGCTGCCC
Site-directed mutagenesis	E5A γ Fwd	GGACATCTGGCACAGCCCCAG
Site-directed mutagenesis	E5A γ Rev	AGCGCCATACACACACAG
Site-directed mutagenesis	R20A γ Fwd	CAAGACCGCCGCACTGGAATGC
Site-directed mutagenesis	R20A γ Rev	CTCAGTGTCTTGGTGCTG
Site-directed mutagenesis	E22A γ Fwd	GCCAGACTGGCATGCGTGGTG
Site-directed mutagenesis	E22A γ Rev	GGTCTTGCTCAGTGTCTTGG
Site-directed mutagenesis	T29A γ Fwd	GTCCGGCATCGCAATCAGCGC
Site-directed mutagenesis	T29A γ Rev	ACCACGCATTCCAGTCTGG
Site-directed mutagenesis	Y54A γ Fwd	GTCCATCAGCGCCGATGGCACC
Site-directed mutagenesis	Y54A γ Rev	ACCAGGAACTGGATCACTTC
Site-directed mutagenesis	T57A γ Fwd	CTACGATGGCGCCGTGCGGAA
Site-directed mutagenesis	T57A γ Rev	CTGATGGACACCAGGAACTGG
Site-directed mutagenesis	K60A γ Fwd	CACCGTGCGGGCAGAGAGCGGC
Site-directed mutagenesis	K60A γ Rev	CCATCGTAGCTGATGGACAC
Site-directed mutagenesis	S62A γ Fwd	GCGGAAAGAGGCCGGCATCCCTTC
Site-directed mutagenesis	S62A γ Rev	ACGGTGCCATCGTAGCTG
Site-directed mutagenesis	S66A γ Fwd	CGGCATCCCTGCTGGCAAGTT
Site-directed mutagenesis	S66A γ Rev	CTCTCTTTCCGCACGGTG
Site-directed mutagenesis	E70A γ Fwd	GGCAAGTTCGCGGTGGACAGAATC
Site-directed mutagenesis	E70A γ Rev	AGAAGGGATGCCGCTCTC
Site-directed mutagenesis	E76A γ Fwd	AGAATCCCCGCGACAAGCACC
Site-directed mutagenesis	E76A γ Rev	GTCCACCTCGAACTTGCC
Site-directed mutagenesis	H85A γ Fwd	ACTGACCATCGCCAACGTGGAAAAGCAG
Site-directed mutagenesis	H85A γ Rev	GTGCTGGTGCTTGTCTCG
Site-directed mutagenesis	N86A γ Fwd	GACCATCCACGCCGTGGAAAAGCAG
Site-directed mutagenesis	N86A γ Rev	AGTGTGCTGGTGCTTGTC
Site-directed mutagenesis	E88A γ Fwd	CACAACGTGGCAAAGCAGGATATC
Site-directed mutagenesis	E88A γ Rev	GATGGTCAGTGTGCTGGT
Site-directed mutagenesis	Q90A γ Fwd	CGTGGAAAAGGCGGATATCGCC
Site-directed mutagenesis	Q90A γ Rev	TTGTGGATGGTCAGTGTG
Site-directed mutagenesis	K108A γ Fwd	AGAGCTGGGCGCGAAAATCAAGGTGTTCG
Site-directed mutagenesis	K108A γ Rev	TGTTGGGCTTCCCACAGG

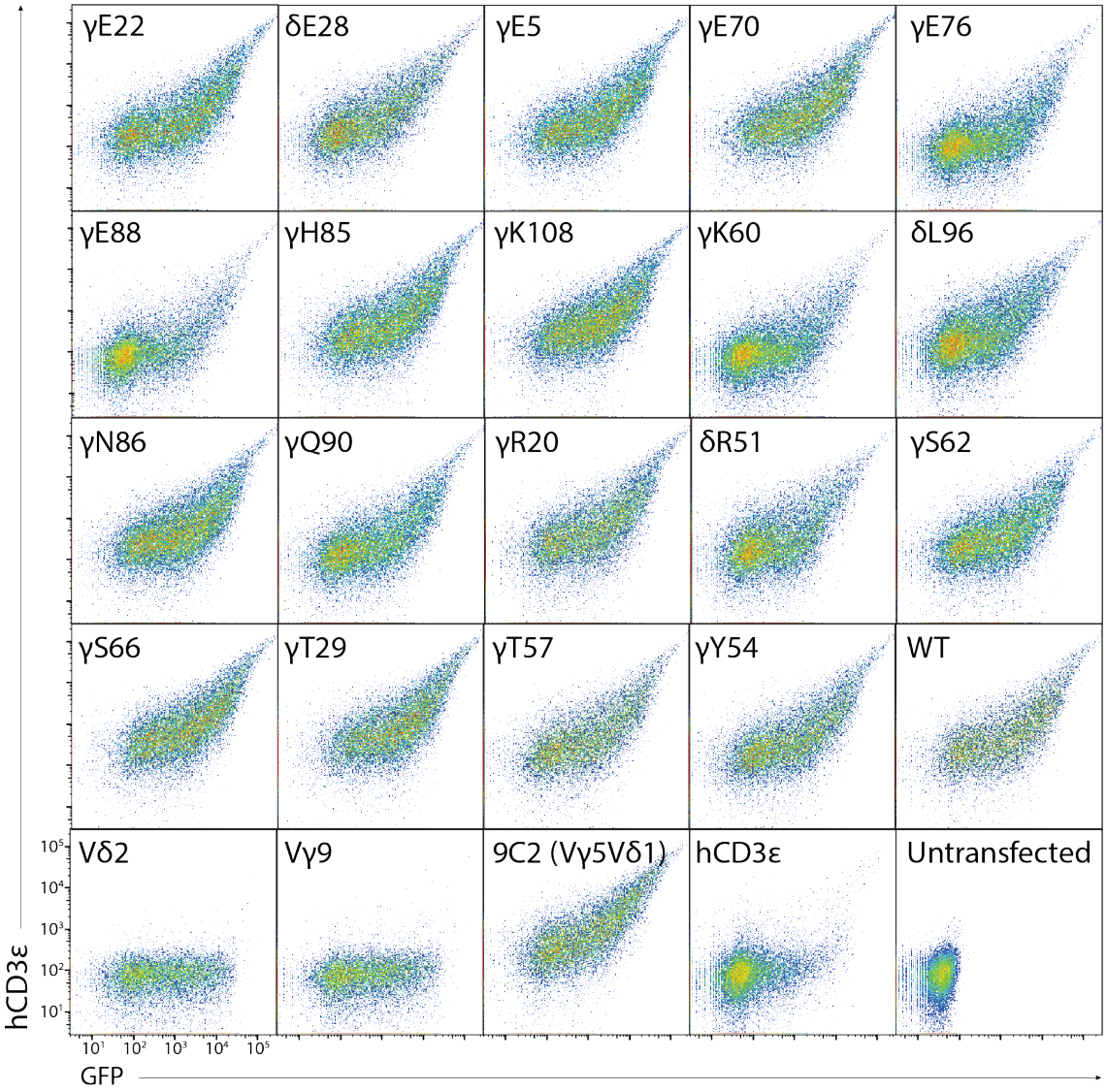

Figure A.12: *Efficiency of mutant $\gamma\delta$TCR transfectants in human HEK-293 cells using FuGENE^{TM} following the online Promega protocol. Average percentage of transfectant cells is 70 %.*

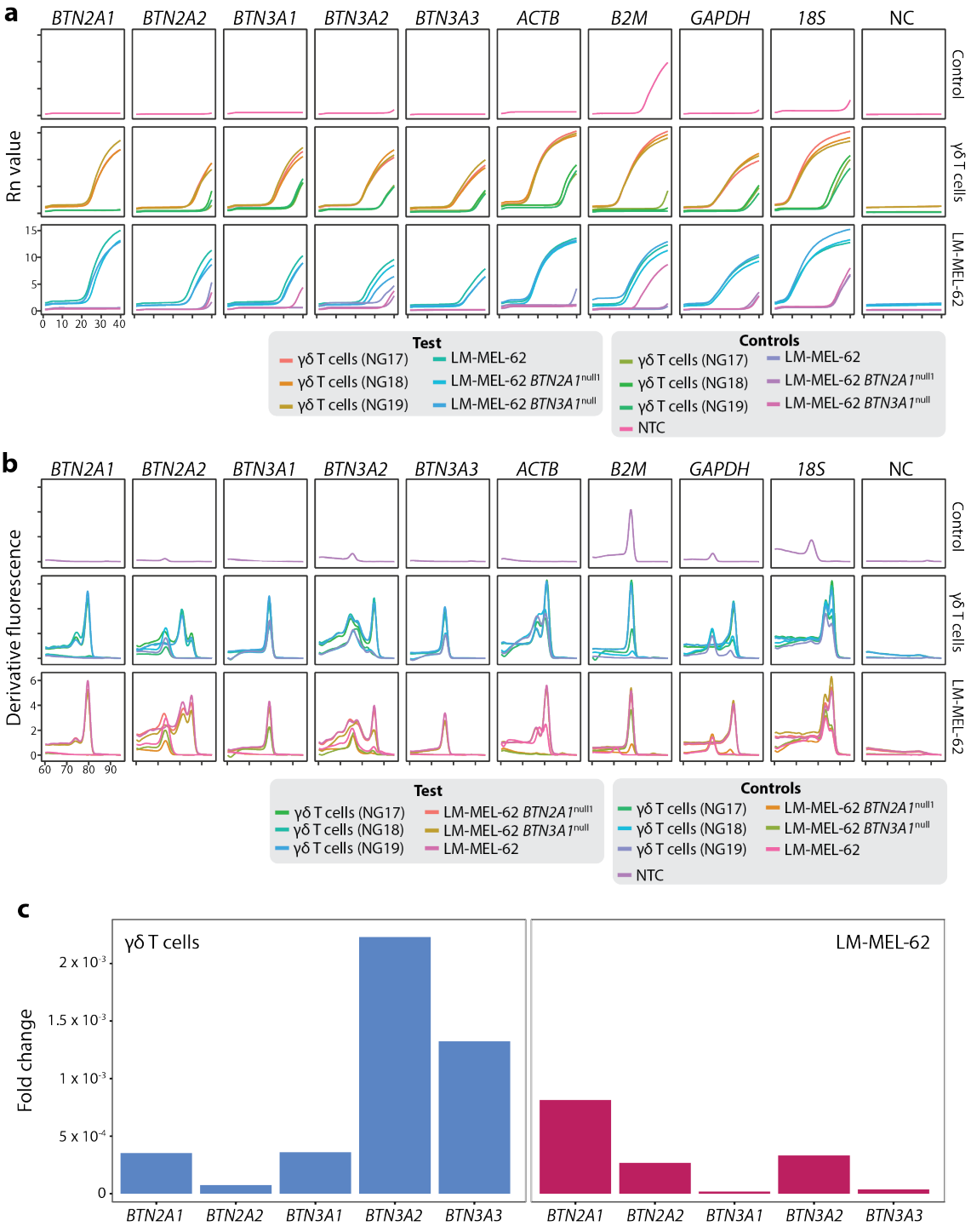

Figure A.13: *Estimated transcription profile of BTN molecules in $\gamma\delta$ T cells and melanoma LM-MEL-62 cell line detected in QuantStudio 7 Flex Real-Time qPCR (60 ℃, 10 ng template). (a) Rn values; (b) melting curves; (c) fold-change transcripts to reference genes* ACTB, B2M, GAPCH, *and* 18S *computed in the $2^{\Delta Cq}$ method. Data shown the average between three random $\gamma\delta$ T cell donors and three LM-MEL-62 cell lines. —CRISPR/Cas9 knockout gene engineering mutilates the transcript, while gene expression is maintained.*

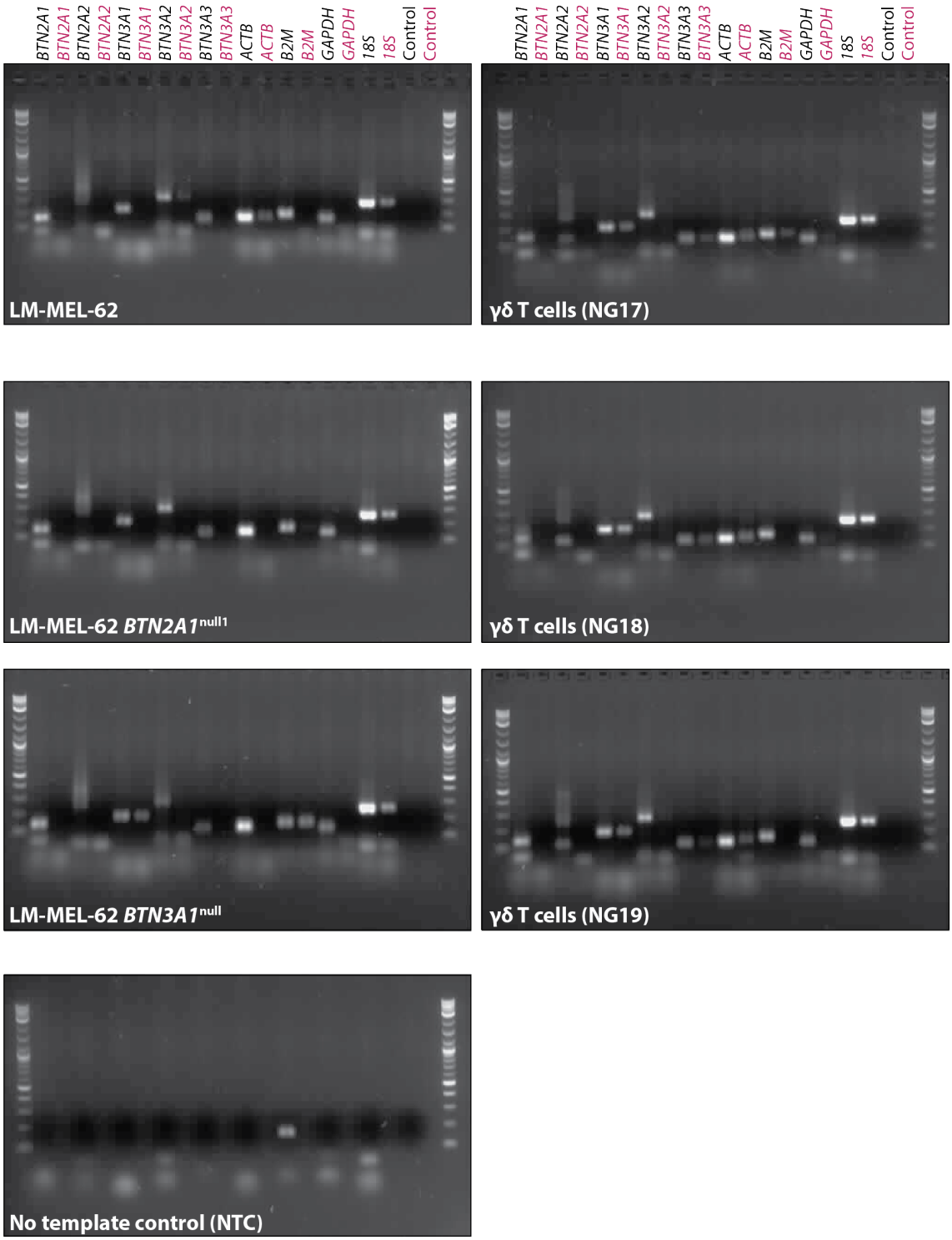

Figure A.14: *Electrophoresis gels post real-time qPCR (1.5 % agarose gel). Lanes containing the cDNA template (black typed) or respective non-reverse transcriptase control (red).*

Table A.3: *Primer sequences and respective characteristics used in the real-time qPCR.*

Name	*Sequence (5' → 3')*	*Scale* (nmol)	*Purification*	*Tm (5.5* mM, ℃)
qh2A1_2_F	GTCCTGCTCTATCAACAACACC	25	STD	63.7
qh2A1_2_R	ACGGCAATGGGTATCATCAG	25	STD	63.2
qh2A2_1_F	CCAGATACCGAGTCCGCAAC	25	STD	65.1
qh2A2_1_R	GACAGATGGCAGCGTAATGT	25	STD	63.6
qh3A1_F	GTGACCGGCTTACAGGGATA	25	STD	64.2
qh3A1_R	AAGCACATGCCAGGTAGAGG	25	STD	65.1
qh3A2_F	AGACCATCCTGGCTAACACG	25	STD	64.7
qh3A2_R	CACATTGATTCTGCCCACTG	25	STD	62.3
qh3A3_F	ATTCCTCACAATAACCAGATAGCC	25	STD	63.5
qh3A3_R	TCCCCTCTGAAAATCACAGC	25	STD	63.1
qhACTB_F	CTGGAACGGTGAAGGTGACA	25	STD	65
qhACTB_R	AAGGGACTTCCTGTAACAATGCA	25	STD	65.4
qhB2M_F	CTATCCAGCGTACTCCAAAG	25	STD	60.6
qhB2M_R	ACAAGTCTGAATGCTCCACT	25	STD	62.6
qhGAPDH_F	CTTTGTCAAGCTCATTTCCTGG	25	STD	62.8
qhGAPDH_R	TCTTCCTCTTGTGCTCTTGC	25	STD	63.2
qh18S_F	CAGCCACCCGAGATTGAGCA	25	STD	67.4
qh18S_R	TAGTAGCGACGGGCGGTGTG	25	STD	68.7

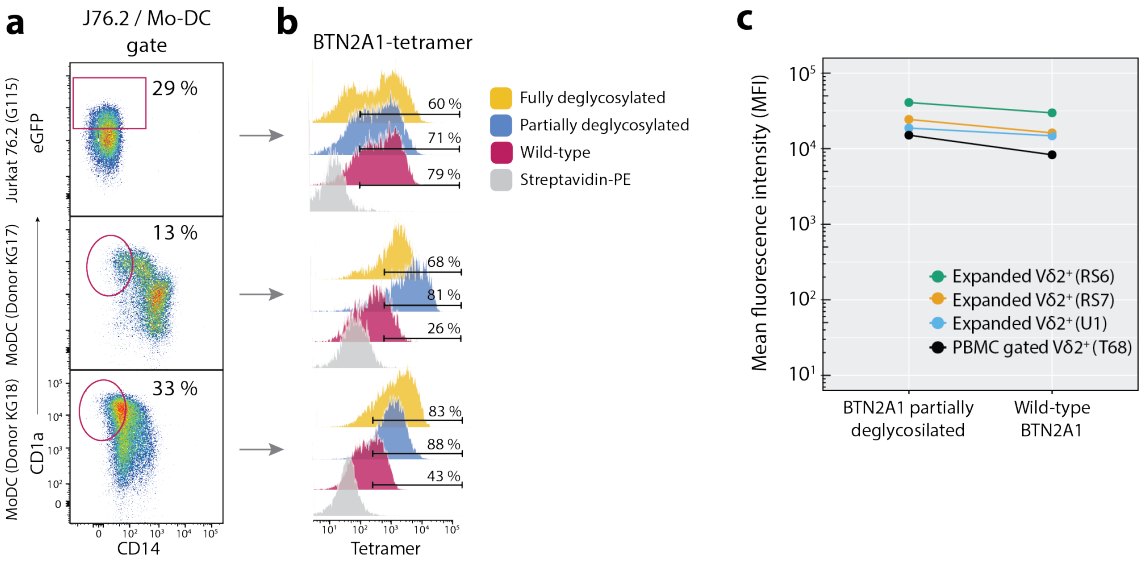

Figure A.15: *Deglycosylated BTN2A1 binds more efficiently than wild-type glycosylated protein to monocyte-derived DCs. (a) Flow cytometry gating strategy to assess Jurkat cells expressing a Vγ9Vδ2 TCR clone G115 control sample and monocyte-derived DCs which have high expression of CD1a marker and lost CD14. (b) Histograms depict the number of cells bond to a BTN2A1-tetramer PE fluorescent probe in a glycosylated, partially deglycosylated (produced in HEK-293 or Expi293T cells deficient for* GnTI*, or fully glycosylated (partially deglycosylated protein treated with Endoglycosidase H). (c) Binding of either wild-type or partially deglycosylated BTN2A1-tetramer PE fluorescent protein to four random donor-purified Vδ2$^+$ T cells.*

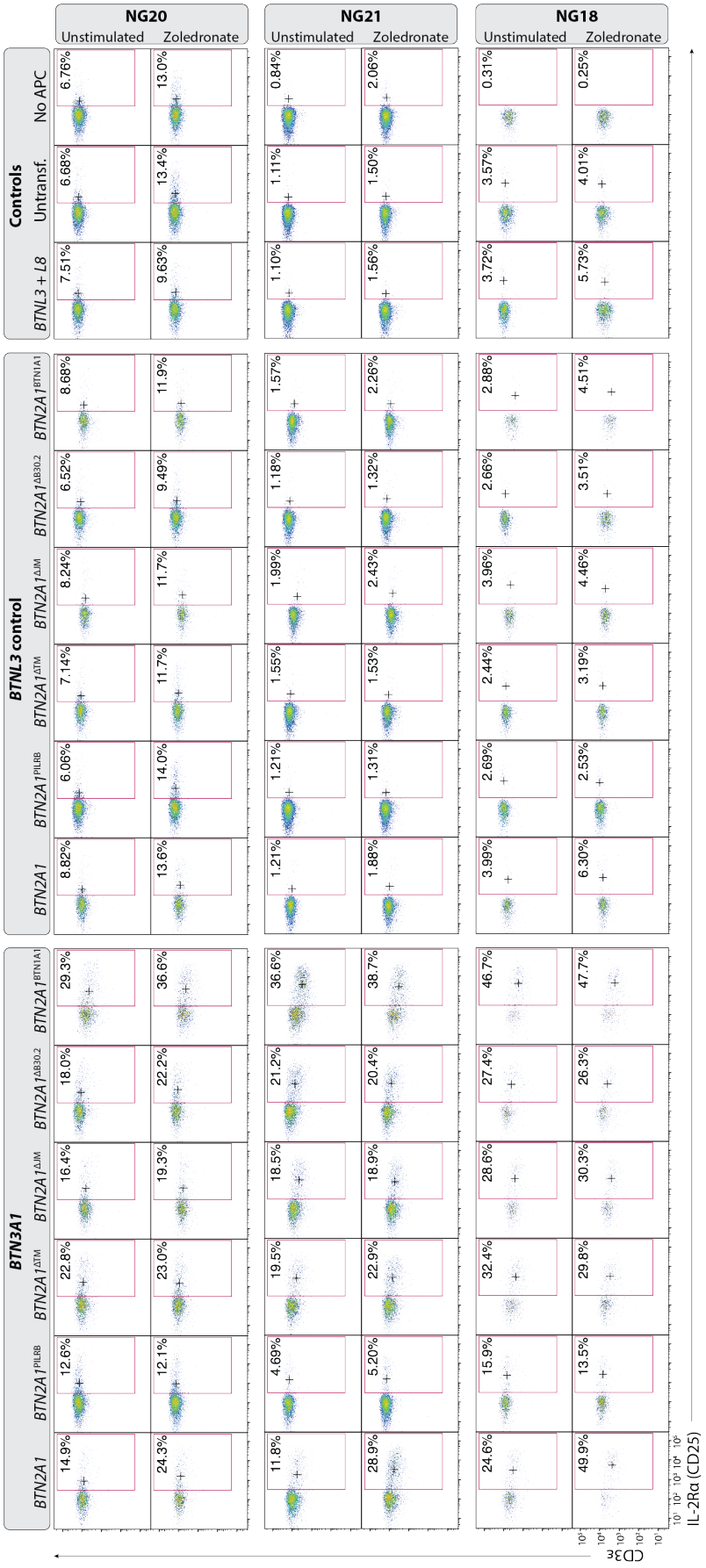

Figure A.16: *The intracellular domain of BTN2A1 is important for γδ T-cell response to phosphorylated antigens induced by zoledronate treatment. Truncated* BTN2A1 *was transfected into mouse fibroblast NIH-3T3 antigen-presenting cells and subsequently stimulated overnight with 4* µM *zoledronate drug to evaluate the upregulation of CD25 activation lymphocyte marker and internalisation of the TCR (CD3ϵ) in fresh isolated and expanded Vδ2^{+} T cells. Showing three random donors (NG18, NG20, NG21) of a total of eight tested.*

Appendix B

Data Collection

B.1 Collection of Raw Datasets

This section collects a series of raw datasets supporting data shown in the results chapter.

The phenotypic profile of surface transmembrane BTN3A and BTN2A1 proteins in twenty human tumour lines with respective affinity for six phosphoantigen-reactive TCR clonotypes (Fig. B.2).

Data collection showing dot-plot and histograms from an experiment assay were we assessed donor-purified expanded Vδ2 T-cell signalling response to plate bound BTN protein under different conditions (Fig. B.3).

BTN2A1 boosts reactivity to CD1c/d TCR-reactive expressed in reporter cell lines. Mouse fibroblast cells were transfected with respective genes (Fig. B.1) and cocultured with SKW3 or Jurkat reporter cells (Fig. B.4).

B.2 Commercial Antibody List

The list of antibodies used in this work are noted in Table. B.1, in the exception of CSL-produced antibodies against BTN2A1.

B.3 Record of Mycoplasma Tests

Mycoplasma contamination in cell cultures has been assessed using the Myco-Alert™ Mycoplasma Detection Kit with a luminometer CLARIOstar®. Table B.2 shows the results from each test performed during the course of this work. Additional mycoplasma test by PCR tests were performed on renal carcinoma cell lines 786-O and Caki-1 on the 27th August 2020.

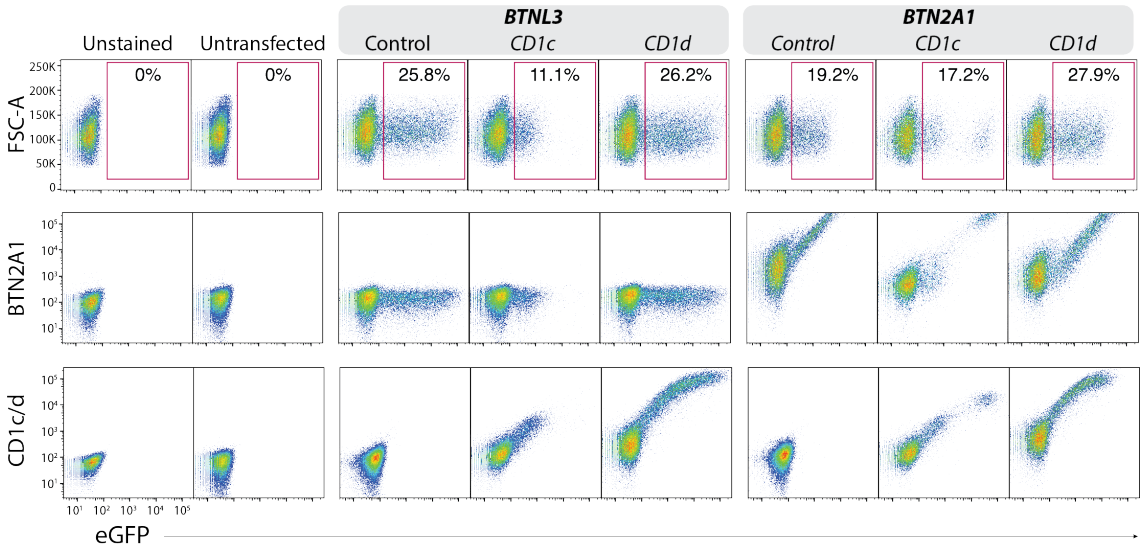

Figure B.1: *Transfection efficiency of mouse fibroblasts (NIH-3T3) cells with* CD1c *or* CD1d *lipid-presenting molecules together with* BTN2A1 *or* BTNL3 *controls.*

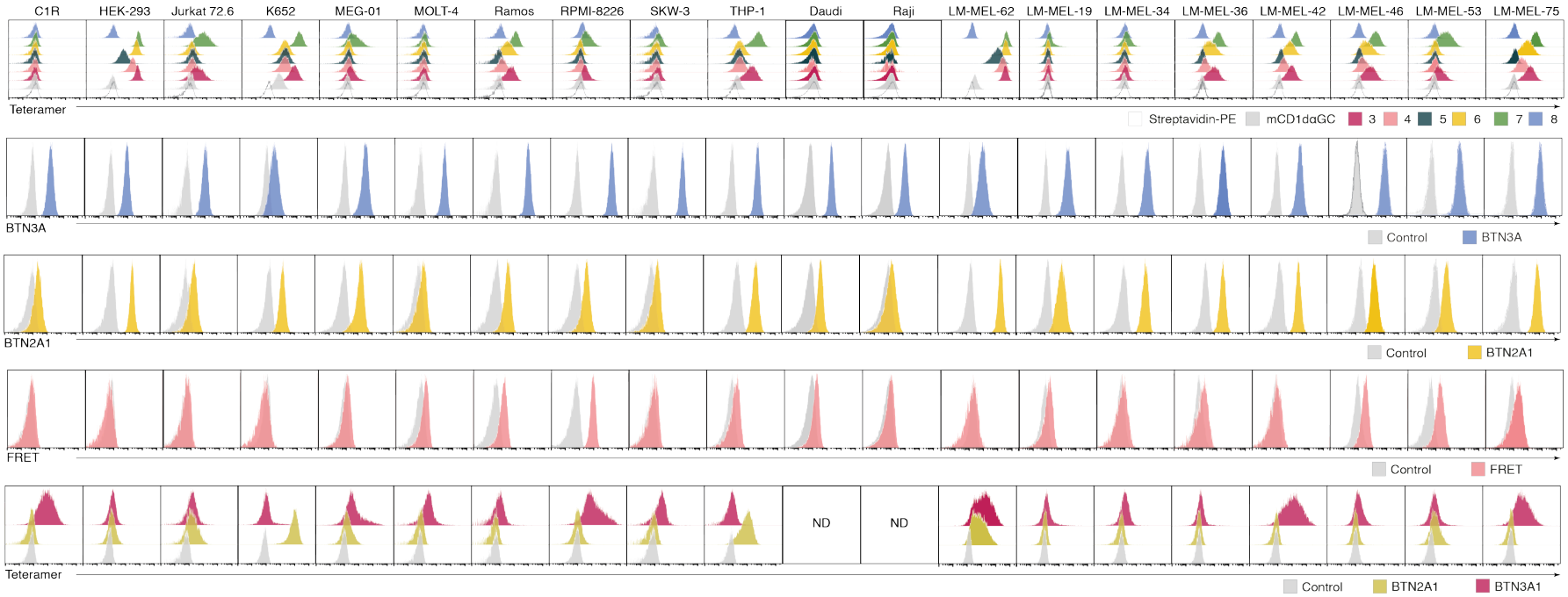

Figure B.2: *A panel of twenty human tumour cell lines screened; from top to bottom each of the six tetramer Vγ9Vδ2 TCR clones (3–8) and tetramerised mouse CD1dα-GalCer control (C) or streptavidin-PE conjugate (S) alone; anti-BTN3A (103.2 in PE) overlaps its respective isotype IgG1 control; BTN2A1 (RF13-231 in AF647) overlaps an isotype IgG2a/BM4 control; the FRET channel overlaps isotype controls IgG1 and IgG2a/BM4; and BTN2A1 or BTN3A1 tetramerised extracellular domains versus streptavidin-PE control. All x axis are $\log_{10}$ scale. Representative of at least two experiments each. Not done (ND).*

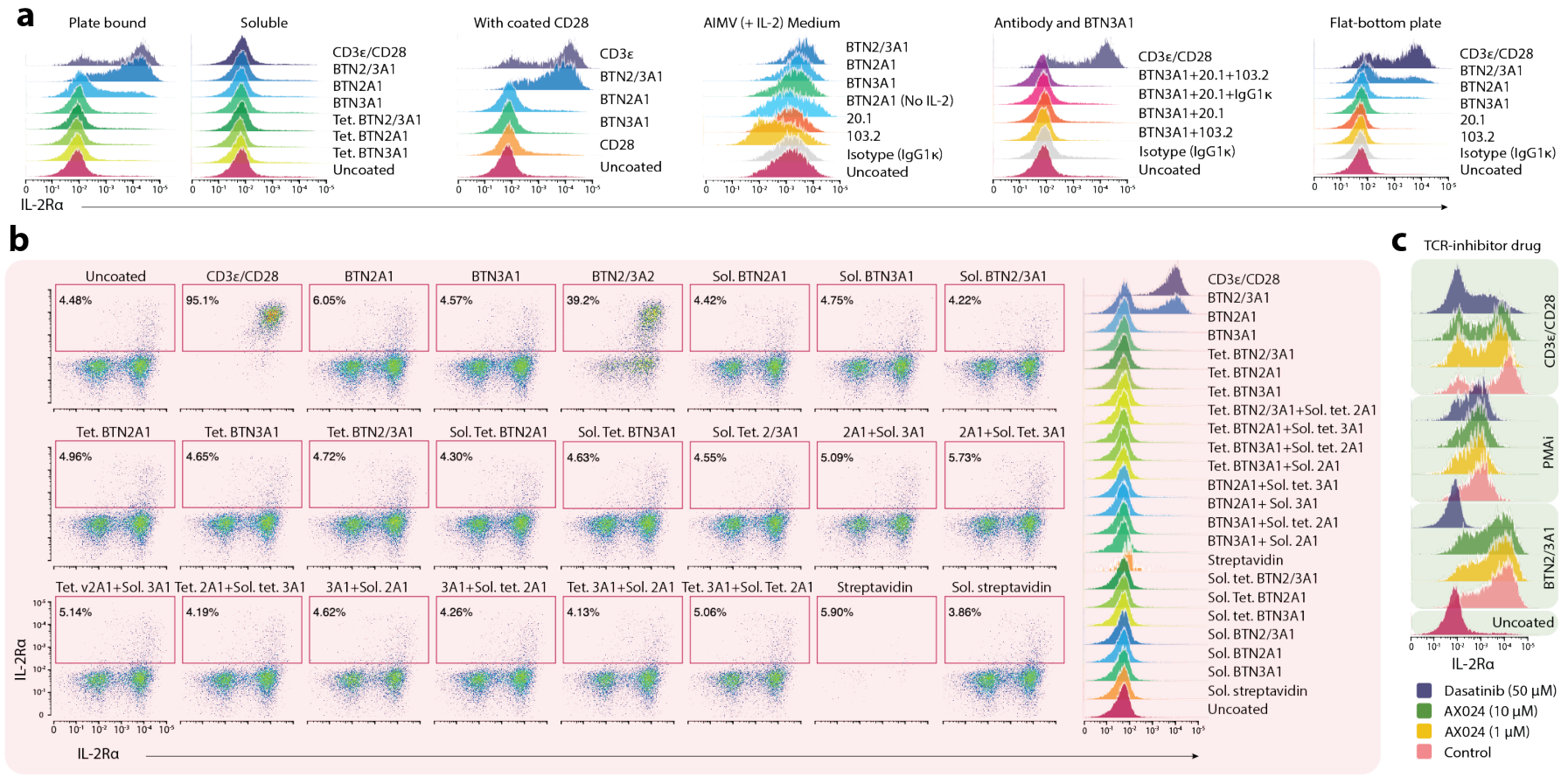

Figure B.3: *Donor-purified expanded Vδ2^{+} T-cell signalling response as they up-regulated the activation marker CD25 to immobilised BTN2A1 and BTN3A1 ectodomains combined. (a) histograms depicting the number of cells responding to plate-bound protein, soluble protein, under the presence of agonist antibody against the co-stimulatory CD28 receptor, with AIM-V serum-free medium, immobilised BTN3A1 together with functional antibody combinations, and assessment of the use of a flat-bottom plate compared to default round-bottom; (b) alternate combinatory between BTN2A1 or BTN3A1 soluble or tetramer immobilised protein; (c) the effect of AX-024 and Dasatinib TCR-inhibitory signalling pathways in immobilised BTN2/3A1 protein and mitogenic PMA or agonist CD3ϵ and CD28 antibodies.*

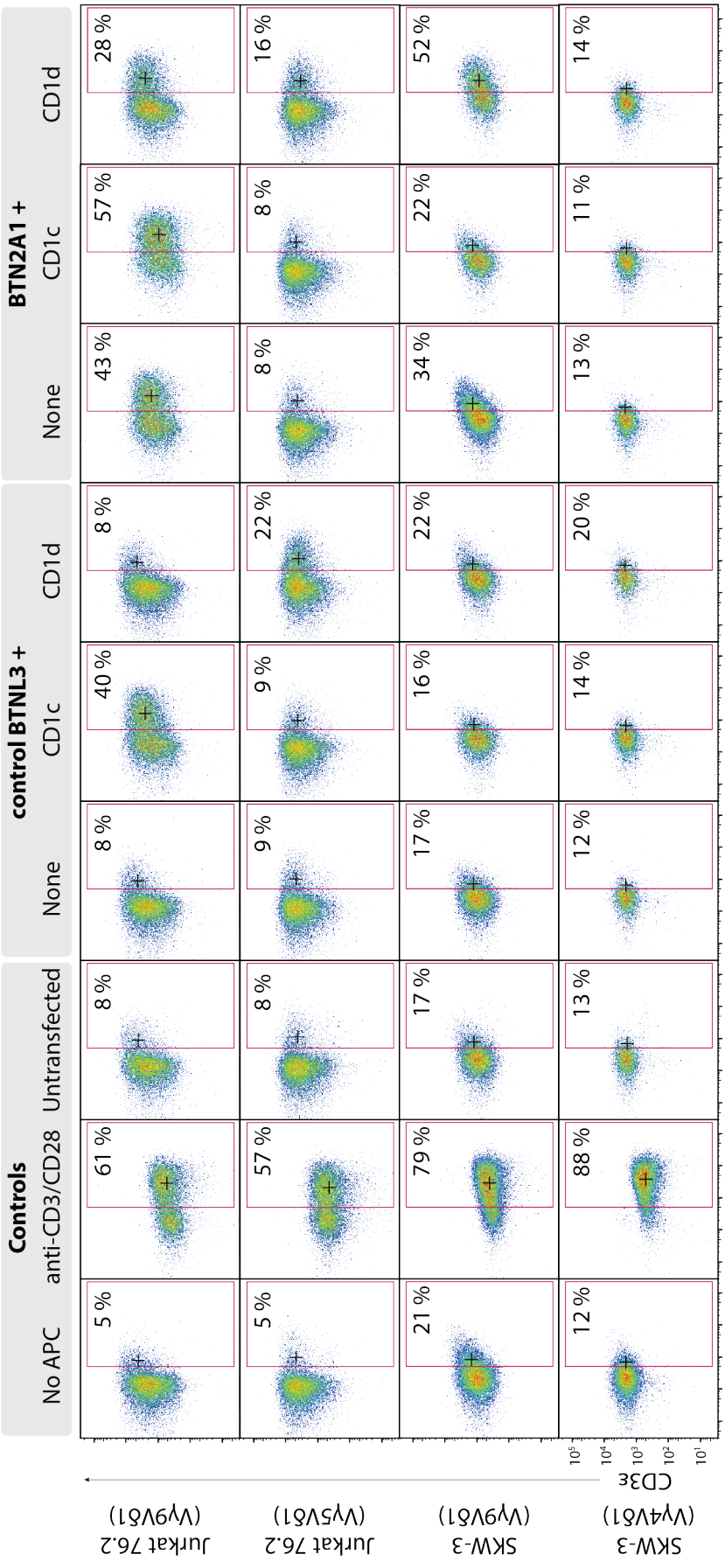

Figure B.4: *The BTN2A1-Vγ9 interaction favours CD1c/d-reactivity by lymphocyte-reporter cells bearing the Vγ9-chain on their TCR. Antigen-presenting mouse fibroblast (NHI-3T3) cells transfected with CD1c/d and BTN2A1 or control BTNL3 were cocultured overnight with respective lymphocyte (Jurkat 76.2 or SKW-3) reporter cells. Expression of surface CD3ε estimates and activation cell marker CD69. One of two experiments each with a technical replicate.*

Table B.1: *General information regarding the most important reagents used in this work except for antibodies against BTN2A1.*

Target	*Target species*	*Source species*	*Clone name*	*Fluorochrome*	*Manufacturer*	*Concentration*
Fc receptor block	Human	Unknown	N.A.	None	Miltenyi Biotec	1:40
Fc receptor block	Mouse	Rat	2.4G2	None	In-house	1:50
7-AAD	Mouse/human	N.A	N.A	Dye	Sigma	3 µg ml^{-1}
Live/dead marker	Mouse/human	N.A.	N.A	Dye	ThermoFisher	1:1,000
CD3ϵ	Human	Mouse	UCHT1	APC	BD-Pharmingen	1:50
CD3ϵ	Human	Mouse	UCHT1	BUV395	BD-Pharmingen	1:100
CD3ϵ	Human	Mouse	OKT3	-	In-house	1:100
pan-$\gamma\delta$TCR	Human	Mouse	11F2	PE-Cy7	BD-Pharmingen	1:50
CD19	Human	Mouse	SJ25C1	APC-Cy7	BD-Pharmingen	1:100
CD4	Human	Mouse	RPA-T4	FITC	BD-Pharmingen	1:20
CD8α	Human	Mouse	SK1	APC/PE	BD-Pharmingen	1:200
CD56	Human	Mouse	HCD56	BV605	BioLegend	1:100
TCR Vδ1	Human	Mouse	TS8.2	FITC	Invitrogen	1:200
TCR Vδ2	Human	Mouse	B6	BV711	BioLegend	1:400
TCR Vγ9	Human	Mouse	B3	APC	BioLegend	1:400
CD14	Human	Mouse	M5E2	BUV805	BD-Pharmingen	1:400
CD45	Human	Mouse	HI30	AF700	BioLegend	1:150
CD25	Human	Mouse	M-A251	PE	BD-Pharmingen	1:50
CD69	Human	Mouse	FN50	PE-Cy7	BD-Pharmingen	1:100
CD69	Human	Mouse	FN50	PE	BD-Pharmingen	1:50
IFN-γ	Human			PerCP-Cy5.5		
Isotype control IgG1,κ	N.A.	Mouse	MOPC-21	Unconjugated, PE	BioLegend	10 µg ml^{-1}
Isotype control IgG2a,κ	N.A.	Human–mouse hybrid	BM4	Unconjugated or AF647	In house	2 µg ml^{-1}
BTN2A1	Human	Human–mouse hybrid	See Supp. Fig. 4B	Unconjugated or AF647	In house	2 µg ml^{-1}
BTN3A1/3A2/3A3	Human	Mouse	20.1	Unconjugated or PE	In house	2 µg ml^{-1}
BTN3A1/3A2/3A3	Human	Mouse	103.2	Unconjugated or PE	In house	0.3 µg ml^{-1}
Immunoglobulin	Mouse	Goat	polyclonal	BV421 or PE	BioLegend	
5-OP (in-house tetramer)	Human		N.A.	BV421	In-house	1:300
$\gamma\delta$TCR tetramers	Human	Human	3, 4, 5, 6, 7	PE	In-house	5 µg ml^{-1}
BTN2A1ec tetramer	Human	Human	N.A.	PE	In-house	5 µg ml^{-1}

Table B.2: *The ratio between read B and A is used to determinate whether a cell culture is contaminated by mycoplasma. Results are based on* < 0.9 *is negative for mycoplasma;* $0.9 - 1.2$ *is borderline and the cell line must be cultured for further 48 h and the supernatant retested;* > 1.2 *mycoplasma contamination.*

Date	*Cell line*	*Ratio*	*Contamination*
1 Jun 2018	Positive control	54.439	Positive
1 Jun 2018	Negative control	0.200	Negative
1 Jun 2018	Media RPMI	0.723	Negative
1 Jun 2018	Media 1:10	0.209	Negative
1 Jun 2018	LM-Mel62-wt	0.442	Negative
1 Jun 2018	LM-Mel62-KD2	0.490	Negative
1 Jun 2018	LM-Mel62-KD4	0.520	Negative
1 Jun 2018	C1R-wt	0.680	Negative
1 Jun 2018	C1R-BTN3A1	0.512	Negative
1 Jun 2018	C1R-BTN3A2	0.491	Negative
1 Jun 2018	C1R-BTN3A3	0.581	Negative
1 Jun 2018	RPMI-8226	0.704	Negative
1 Jun 2018	MOLT-04	0.774	Negative
1 Jun 2018	Jurkat-76.2-wt	0.669	Negative
1 Jun 2018	JRT3-T3.5	0.691	Negative
1 Jun 2018	MEG-01	0.387	Negative
1 Jun 2018	K562	0.747	Negative
1 Jun 2018	THP-1	0.599	Negative
1 Jun 2018	Ramos	0.434	Negative
1 Jun 2018	SKW-3	0.735	Negative
6 Jun 2018	Positive control	9.553	Positive
6 Jun 2018	Negative control	0.125	Negative
6 Jun 2018	RMPI media	0.486	Negative
6 Jun 2018	DMEM media	0.521	Negative
6 Jun 2018	C1R-wt	0.356	Negative
6 Jun 2018	C1R-BTN3A1	0.429	Negative
6 Jun 2018	C1R-BTN3A2	0.412	Negative
6 Jun 2018	C1R-BTN3A3	0.387	Negative
6 Jun 2018	Jurkat	0.418	Negative
6 Jun 2018	JRT3-T3.5	0.381	Negative
6 Jun 2018	HLPC water	0.096	Negative

Continued on next page.

Table B.2. *Continued from previous page.*

Date	*Cell line*	*Ratio*	*Contamination*
6 Jun 2018	THP-1	0.468	Negative
6 Jun 2018	K562	0.396	Negative
6 Jun 2018	SKW-3	0.505	Negative
6 Jun 2018	Ramos	0.410	Negative
6 Jun 2018	RPMI-8226	0.433	Negative
6 Jun 2018	Meg-01	0.598	Negative
6 Jun 2018	Molt-04	0.457	Negative
6 Jun 2018	293T	0.419	Negative
27 Jul 2018	Positive control	38.291	Positive
27 Jul 2018	Negative control	0.188	Negative
27 Jul 2018	HPLC Water	0.069	Negative
27 Jul 2018	Media RPMI	0.395	Negative
27 Jul 2018	Media DMEM	0.551	Negative
27 Jul 2018	Media Expi	0.395	Negative
27 Jul 2018	Expi293	0.473	Negative
27 Jul 2018	GNTI (23/7/18)	0.760	Negative
27 Jul 2018	GNTI (26/7/18)	0.700	Negative
27 Jul 2018	LM-MEL-19	0.461	Negative
27 Jul 2018	LM-MEL-34	0.718	Negative
27 Jul 2018	LM-MEL-36	0.557	Negative
27 Jul 2018	LM-MEL-42	0.456	Negative
27 Jul 2018	LM-MEL-46	0.507	Negative
27 Jul 2018	LM-MEL-53	0.500	Negative
27 Jul 2018	LM-MEL-75	0.579	Negative
27 Jul 2018	LM-MEL-62 (New Batch)	0.504	Negative
27 Jul 2018	LM-MEL-62	0.480	Negative
27 Jul 2018	LM-MEL-62 *BTN2A1*^{null1}	0.567	Negative
27 Jul 2018	LM-MEL-62 *BTN2A1*^{null2}	0.431	Negative
27 Jul 2018	C1R	0.543	Negative
27 Jul 2018	C1R (BTN3A1)	0.496	Negative
27 Jul 2018	C1R (BTN3A2)	0.591	Negative
27 Jul 2018	C1R (BTN3A3)	0.408	Negative
27 Jul 2018	Jurkat 76.2	0.318	Negative
27 Jul 2018	Jurkat 76.2 (9C2)	0.309	Negative

Continued on next page.

Table B.2. *Continued from previous page.*

Date	*Cell line*	*Ratio*	*Contamination*
27 Jul 2018	THP-1	0.406	Negative
27 Jul 2018	K562	0.368	Negative
27 Jul 2018	Ramos	0.478	Negative
27 Jul 2018	Meg-01	0.254	Negative
27 Jul 2018	SKW-3	0.399	Negative
27 Jul 2018	JRT3-T3.5 (G115) [Sorted]	0.472	Negative
27 Jul 2018	Jurkat 76.2 (G115) [Sorted]	0.350	Negative
27 Jul 2018	JRT3-T3.5 (G115) [Presort]	0.434	Negative
6 Nov 2018	Positive control	27.516	Positive
6 Nov 2018	Negative control	0.184	Negative
6 Nov 2018	Baxter Water	0.141	Negative
6 Nov 2018	Mel-62	0.527	Negative
6 Nov 2018	KD2	0.525	Negative
6 Nov 2018	293T	0.659	Negative
6 Nov 2018	Unsorted K562 (Replica 1)	0.334	Negative
6 Nov 2018	Unsorted K562 (Replica 2)	0.388	Negative
6 Nov 2018	Unsorted K562 (Replica 3)	0.400	Negative
6 Nov 2018	Unsorted K562 (Replica 4)	0.351	Negative
6 Nov 2018	Low K562 (Replica 1)	0.569	Negative
6 Nov 2018	Low K562 (Replica 2)	0.458	Negative
6 Nov 2018	Low K562 (Replica 3)	0.555	Negative
6 Nov 2018	Low K562 (Replica 4)	0.489	Negative
6 Nov 2018	K562 (Replica 1)	0.538	Negative
6 Nov 2018	K562 (Replica 2)	0.438	Negative
6 Nov 2018	K562 (Replica 3)	0.538	Negative
6 Nov 2018	K562 (Replica 4)	0.530	Negative
6 Nov 2018	Low LM-MEL-62 (Replica 1)	0.551	Negative
6 Nov 2018	Low LM-MEL-62 (Replica 2)	0.500	Negative
6 Nov 2018	Low LM-MEL-62 (Replica 3)	0.497	Negative
6 Nov 2018	Low LM-MEL-62 (Replica 4)	0.470	Negative
6 Nov 2018	High LM-MEL-62 (Replica 1)	0.632	Negative
6 Nov 2018	High LM-MEL-62 (Replica 2)	0.468	Negative
6 Nov 2018	High LM-MEL-62 (Replica 3)	0.632	Negative
6 Nov 2018	High LM-MEL-62 (Replica 4)	0.527	Negative

Continued on next page.

Table B.2. *Continued from previous page.*

Date	*Cell line*	*Ratio*	*Contamination*
25 Dec 2018	Positive control	28.720	Positive
25 Dec 2018	Negative control	0.110	Negative
25 Dec 2018	Baxter Water	0.120	Negative
25 Dec 2018	Media gdT cell	0.607	Negative
25 Dec 2018	Media DMEM	0.594	Negative
25 Dec 2018	Media RPMI 1640	0.553	Negative
25 Dec 2018	Jurkat 76.2 (Parental)	0.548	Negative
25 Dec 2018	SKW-3 (Parental)	0.545	Negative
25 Dec 2018	J.RT3-T3.5 (Parental)	0.449	Negative
25 Dec 2018	Jurkat 9C2	0.420	Negative
25 Dec 2018	SKW-3 NKT	0.460	Negative
25 Dec 2018	Jurkat 76.2 TCR-3	0.429	Negative
25 Dec 2018	J.RT3-T3.5 G115	0.501	Negative
25 Dec 2018	Jurkat 76.2 TCR-6	0.541	Negative
25 Dec 2018	Jurkat 76.2 G115	0.578	Negative
25 Dec 2018	SKW-3 G115	0.567	Negative
25 Dec 2018	SKW-3 TCR-3	0.471	Negative
25 Dec 2018	Pre-enriched Vd2+ RS6	0.830	Negative
25 Dec 2018	Low LM-MEL-62 (Replica 1)	0.575	Negative
25 Dec 2018	Low LM-MEL-62 (Replica 2)	0.436	Negative
25 Dec 2018	Low LM-MEL-62 (Replica 3)	0.427	Negative
25 Dec 2018	Low LM-MEL-62 (Replica 4)	0.572	Negative
25 Dec 2018	High LM-MEL-62 (Replica 1)	0.777	Negative
25 Dec 2018	High LM-MEL-62 (Replica 2)	0.655	Negative
25 Dec 2018	High LM-MEL-62 (Replica 3)	0.656	Negative
25 Dec 2018	High LM-MEL-62 (Replica 4)	0.563	Negative
25 Dec 2018	Human HEK-293T	0.603	Negative
25 Dec 2018	Hamster CHO-K1	0.703	Negative
25 Dec 2018	Mouse NIH-3T3	0.599	Negative
25 Dec 2018	RPMI-8226	0.513	Negative
25 Dec 2018	THP-1	0.649	Negative
25 Dec 2018	C1R	0.577	Negative
25 Dec 2018	Ramos	0.545	Negative
25 Dec 2018	Meg-01	0.543	Negative

Continued on next page.

Table B.2. *Continued from previous page.*

Date	*Cell line*	*Ratio*	*Contamination*
25 Dec 2018	Molt-04	0.696	Negative
25 Dec 2018	SKW-3	0.548	Negative
25 Dec 2018	Jurkat 76.2	0.559	Negative
25 Dec 2018	K562	0.551	Negative
25 Dec 2018	LM-MEL-62	0.646	Negative
25 Dec 2018	LM-MEL-62 *BTN2A1*^{null1}	0.783	Negative
25 Dec 2018	LM-MEL-62 *BTN2A1*^{null2}	0.546	Negative
25 Dec 2018	LM-MEL-19	0.642	Negative
25 Dec 2018	LM-MEL-34	0.531	Negative
25 Dec 2018	LM-MEL-36	0.702	Negative
25 Dec 2018	LM-MEL-42	0.743	Negative
25 Dec 2018	LM-MEL-46	0.677	Negative
25 Dec 2018	LM-MEL-53	0.526	Negative
25 Dec 2018	LM-MEL-75	0.631	Negative
21 Feb 2019	Positive control	1.408	Positive
21 Feb 2019	Negative control	0.166	Negative
21 Feb 2019	Media gdT cell	0.650	Negative
21 Feb 2019	Media DMEM	0.881	Negative
21 Feb 2019	Media RPMI 1640	0.675	Negative
21 Feb 2019	C1R	0.599	Negative
21 Feb 2019	Pre-enriched Vd2+ G23	0.541	Negative
21 Feb 2019	Pre-enriched Vd2+ G24	0.668	Negative
21 Feb 2019	Pre-enriched Vd2+ G25	0.523	Negative
21 Feb 2019	Pre-enriched Vd2+ G26	0.921	Negative
21 Feb 2019	Pre-enriched Vd2+ MJ1	0.592	Negative
21 Feb 2019	Pre-enriched Vd2+ MJ1	0.536	Negative
21 Feb 2019	Pre-enriched Vd2+ MJ4	0.776	Negative
21 Feb 2019	Total gdT cells MJ1	0.479	Negative
21 Feb 2019	Total gdT cells MJ4	0.666	Negative
21 Feb 2019	Total gdT cells G18	0.434	Negative
21 Feb 2019	Low LM-MEL-62 (Replica 1)	0.515	Negative
21 Feb 2019	Low LM-MEL-62 (Replica 2)	0.681	Negative
21 Feb 2019	Low LM-MEL-62 (Replica 3)	0.599	Negative
21 Feb 2019	Low LM-MEL-62 (Replica 4)	0.611	Negative

Continued on next page.

Table B.2. *Continued from previous page.*

Date	*Cell line*	*Ratio*	*Contamination*
21 Feb 2019	Human HEK-293T-T75	0.335	Negative
21 Feb 2019	Human HEK-293T-T185	0.443	Negative
21 Feb 2019	Hamster CHO-K1	0.320	Negative
21 Feb 2019	Mouse NIH-3T3	0.440	Negative
21 Feb 2019	Expi293T Parental	0.288	Negative
21 Feb 2019	Expi293T Subset	0.348	Negative
21 Feb 2019	LM-MEL-62	0.640	Negative
21 Feb 2019	LM-MEL-62 KO2	0.624	Negative
21 Feb 2019	LM-MEL-62 KO4	0.356	Negative
21 Feb 2019	LM-MEL-62 KO3A1	0.624	Negative
21 Feb 2019	LM-MEL-62 KO3A2	0.559	Negative
21 Feb 2019	LM-MEL-62 KO2A2	0.410	Negative
21 Feb 2019	LM-MEL-75	0.559	Negative
21 Feb 2019	LM-MEL-75 KO3A1	0.541	Negative
21 Feb 2019	LM-MEL-75 KO2A1	0.445	Negative
21 Feb 2019	LM-MEL-75 KO2A2	0.410	Negative
21 Feb 2019	LM-MEL-19	0.345	Negative
21 Feb 2019	LM-MEL-34	0.319	Negative
21 Feb 2019	LM-MEL-42	0.277	Negative
21 Feb 2019	LM-MEL-53	0.333	Negative
11 Jul 2019	Positive	43.154	Positive
11 Jul 2019	Negative	0.194	Negative
11 Jul 2019	Baxter water	0.253	Negative
11 Jul 2019	cRPMI	0.725	Negative
11 Jul 2019	$\gamma\delta$ T-cell media	0.718	Negative
11 Jul 2019	Total $\gamma\delta$ T-cells (G28)	0.713	Negative
11 Jul 2019	JRT G115	0.500	Negative
11 Jul 2019	JRT Parent	0.501	Negative
11 Jul 2019	JRT 9C2	0.517	Negative
11 Jul 2019	JRT G115	0.605	Negative
11 Jul 2019	JRT E5	0.511	Negative
11 Jul 2019	JRT R20	0.611	Negative
11 Jul 2019	JRT E22	0.713	Negative
11 Jul 2019	JRT E28	0.789	Negative

Continued on next page.

Table B.2. *Continued from previous page.*

Date	*Cell line*	*Ratio*	*Contamination*
11 Jul 2019	JRT T29	0.407	Negative
11 Jul 2019	JRT R51	0.662	Negative
11 Jul 2019	JRT Y54	0.585	Negative
11 Jul 2019	JRT T57	0.678	Negative
11 Jul 2019	JRT K60	0.500	Negative
11 Jul 2019	JRT S62	0.648	Negative
11 Jul 2019	JRT S66	0.407	Negative
11 Jul 2019	JRT E70	0.573	Negative
11 Jul 2019	JRT E76	0.556	Negative
11 Jul 2019	JRT H85	0.584	Negative
11 Jul 2019	JRT N86	0.586	Negative
11 Jul 2019	JRT E88	0.468	Negative
11 Jul 2019	JRT Q90	0.454	Negative
11 Jul 2019	JRT L97	0.636	Negative
11 Jul 2019	JRT K108	0.598	Negative
11 Jul 2019	K562	0.454	Negative
11 Jul 2019	LM-MEL-62	0.632	Negative
11 Jul 2019	LM-MEL-62 *BTN2A1*^{null2}	0.685	Negative
11 Jul 2019	LM-MEL-62 *BTN3A1*^{null}	0.516	Negative
11 Jul 2019	LM-MEL-75	0.485	Negative
11 Jul 2019	LM-MEL-75 *BTN2A1*^{null2}	0.641	Negative
11 Jul 2019	LM-MEL-75 *BTN3A1*^{null}	0.567	Negative
27 Aug 2020	Positive	-	Positive
27 Aug 2020	Negative	-	Negative
27 Aug 2020	cRPMI	-	Negative
27 Aug 2020	786-0	-	Negative
27 Aug 2020	CaKi-1	-	Negative
13 Oct 2020	Positive	-	Positive
13 Oct 2020	Negative	-	Negative
13 Oct 2020	cDMEM	-	Negative
13 Oct 2020	Mouse L-Wnt3a	-	Negative